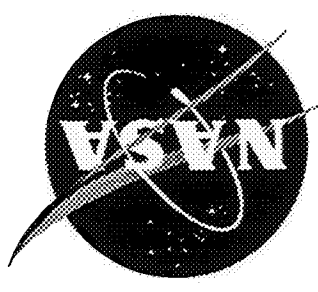NASA CONTRACTOR REPORT 191538

ENVIRONMENT ENHANCED FATIGUE CRACK
PROPAGATION IN METALS: INPUTS TO FRACTURE
MECHANICS LIFE PREDICTION MODELS

Richard P. Gangloff and Sang-Shik Kim
University of Virginia
Charlottesville, VA

National Aeronautics and
Space Administration

LANGLEY RESEARCH CENTER
Hampton, Virginia 23681-0001

EXECUTIVE SUMMARY

The fatigue crack growth resistance of metallic alloys and structures is generally reduced by concomitant exposure to a wide range of aggressive environments. Notable examples are nickel-based superalloys in high pressure hydrogen gas, high strength alloy steels in water vapor and titanium or aluminum alloys in aqueous chloride. Despite substantial advances over the last 30 years, the fracture mechanics approach for damage tolerant fatigue life prediction has not been adequately developed to define deleterious environmental effects for use in computerized codes such as NASA FLAGRO.

The objective of this report is to review and critically evaluate both environment-enhanced fatigue crack propagation (FCP) data and the predictive capabilities of crack growth rate models to broadly extend laboratory data. This information provides the necessary foundation for incorporating environmental effects in NASA FLAGRO and will better enable predictions of aerospace component fatigue lives.

This review presents extensive literature data on "stress corrosion cracking" (more accurately monotonic load environmental cracking) and "corrosion fatigue" (more accurately environmental fatigue cracking). The linear elastic fracture mechanics approach, based on stress intensity range (ΔK) similitude with macroscopic crack propagation thresholds (ΔK_{TH}) and growth rates (da/dN), provides the basis for these data. The results of laboratory experiments demonstrate that gases (viz., H_2 or H_2O) and electrolytes (e.g., NaCl and H_2O) enhance FCP rates in aerospace alloys including: C-Mn and heat treated alloy steels, aluminum alloys, nickel-based superalloys and titanium alloys. Environment causes purely time-dependent fatigue cracking above the monotonic load cracking threshold (K_{IEAC}) and promotes cycle-time dependent cracking below K_{IEAC} where cyclic deformation is uniquely damaging. Crack growth in nickel based superalloys in elevated temperature oxidizing environments is phenomenologically similar to lower temperature "corrosion fatigue".

While mechanistic understanding is qualitative, environmental effects on FCP can be rationalized based on either an environmental hydrogen production/embrittlement mechanism, or on electrochemical film formation with repeated rupture and transient anodic dissolution. For many aerospace alloys and environments, so-called Hydrogen Environment Embrittlement is the suspected failure mechanism. This process provides a framework for understanding the effects of variables on environmental fatigue crack growth. Electrochemical dissolution models are similarly useful for considering environmental effects on cracking.

The magnitude of environment enhanced FCP kinetics is determined by the synergistic interaction of a plethora of mechanical, microstructural and chemical variables. Environment activity (e.g., H_2, H_2O or O_2 pressure in addition to temperature and electrode potential), stress intensity range and mean level, and loading frequency are critical. Stress ratio (R) effects are qualitatively understood based on crack closure, but not based on intrinsic damage processes. The complex and multifaceted dependence of da/dN on ΔK and the dominant effect of fatigue loading time (viz., frequency and hold time), are particularly important.

Environmental effects generally increase with decreasing frequency or increasing hold time; the exact dependence is determined by rate limiting mass transport and reaction processes. Environment enhanced fatigue crack growth models must be capable of predicting the effects of these critical variables in order to accurately scale laboratory data to component service conditions. For example, it is crucial to be able to extrapolate short term (of order weeks) laboratory data to predict long term (of order years) component cracking behavior.

The fracture mechanics stress intensity range correlates environmental fatigue crack propagation rates independent of load magnitude, crack size and geometry. Stress intensity-based similitude is, however, complicated by the effects of crack closure, small crack size and loading spectra. Several crack closure and small crack mechanisms are unique to external environments, and are not well understood based on data and modeling for FCP in moist air. Such complications to similitude must be considered in fatigue life prediction.

Approaches to predict da/dN-ΔK for environmental situations; including empirical interpolative equations, linear superposition of mechanical fatigue and time-based environmental cracking, and mechanism-based models; are presented. For several technologies, successes have been reported in evaluating the environmental fatigue contribution and were incorporated in fracture mechanics life prediction models. Considerable uncertainties are, however, associated with these models. The linear superposition analysis is emphasized; material-environment systems that are severely environment-sensitive should be adequately described by this method. Direct and indirect methods exist to define time-based crack growth rates for use in linear superposition predictions of da/dN. This approach is effective, but only for those cases where K_{IEAC} is on the order of stress intensity levels typical of components in service. Empirical curve-fit models require an extensive environmental crack growth rate data base, are costly to develop, and are effective for interpolations but not predictions of FCP data. Mechanism based models for broad predictions of cycle-time dependent da/dN versus ΔK, and other variables such as frequency or hold time, are in an infant state.

Substantial work is required in order to effectively incorporate environmental effects in fatigue life prediction codes. For example, research is necessary in the areas of near-threshold environmental fatigue behavior, advanced alloy and composite cracking, experimental methods development, fundamental damage mechanism models, da/dN-ΔK modeling, crack closure, and small crack effects on similitude. The challenge to NASA is acute because of the wide range of materials and complex environments that are relevant to aerospace applications.

Specific recommendations for incorporating environmental effects on FCP in NASA FLAGRO include cataloging the data contained in this report, adapting a linear superposition computer program as a FLAGRO module, testing the linear superposition approach for a relevant material/environment system, experimentally defining the "below K_{IEAC}" behavior of a relevant material/environment system, and continuing to develop fundamental models of environment sensitive crack closure and intrinsic damage mechanisms.

FOREWORD

This final report resulted from a program commissioned in September of 1989 by Dr. Royce G. Forman of the NASA Lyndon B. Johnson Space Center, and supported by funding from the George C. Marshall Space Flight Center. The statement of work, LESC-N-2585, is entitled *Formulation of Models Describing Environmental Effects on Fatigue Crack Propagation for Inclusion in the NASA/FLAGRO Program*. Dr. Forman has served a technical monitor and Dr. V. Shivakumar of Lockheed Engineering and Sciences Company in Houston has been the program administrator. Professor Richard P. Gangloff has conducted the work as a consultant to NASA. An interim report was published in 1990.[1]

The challenge to incorporate environmental effects on fatigue crack propagation into NASA FLAGRO is immense, owing to the complexity of environmental cracking and to the broad range of material-environment systems that are of interest to NASA. Accordingly, in January of 1991, the NASA-Langley Research Center initiated funding of an ongoing research project at the University of Virginia and aimed at incorporating environmental effects into fracture mechanics fatigue life prediction methods. This research is being supervised by Professor Gangloff and Dr. Sang-Shik Kim, and conducted in conjunction with the NASA-UVa Light Aerospace Alloy and Structures Technology Program monitored by Mr. Dennis L. Dicus under Grant NAG-1-745. A graduate student and three undergraduates are currently working on this program, with emphasis on environmental cracking in aluminum and titanium alloys. Drs. Robert S. Piascik and James C. Newman of the Mechanics of Materials Branch at Langley are the technical project monitors. This final report was completed with NASA-LaRC support supplementing the original funding from Marshall SFC.

---

[1]R.P. Gangloff, "Hydrogen Environment Enhanced Fatigue Crack Propagation in Metals", in <u>Advanced Earth-To-Orbit Propulsion Technology</u>, R.J. Richmond and S.T. Wu, eds., NASA CP 3092, Vol. III, Washington, DC, pp. 483-510 (1990).

TABLE OF CONTENTS

PRECEDING PAGE BLANK NOT FILMED

I. INTRODUCTION

A.   The Fracture Mechanics Method for Component Fatigue Life Prediction

The fracture mechanics approach for predicting damage tolerant fatigue life of metallic alloy components has been extensively researched and developed over the past three decades [1-10].   This methodology is critical because structural alloys and components contain inhomogeneities or flaws which effectively eliminate fatigue crack nucleation life.   The damage tolerant fracture mechanics approach currently utilizes short-term empirical laboratory data to predict the fatigue life of a component through the similitude concept.   Fatigue damage mechanism based models will ultimately augment or replace these empirical data.

Fig. 1 illustrates the fracture mechanics description of fatigue crack propagation (FCP) which is traceable to the seminal work of Paris and coworkers for the case of structural metallic alloys in moist air environments [11].   Subcritical fatigue crack propagation is measured in precracked laboratory specimens according to standardized methods [12]. Fatigue crack length (a) versus load cycles (N) data are analyzed to yield a material property; averaged macroscopic fatigue crack growth rate (da/dN) as a function of the applied stress intensity range, ΔK. ΔK is the difference between the applied maximum (K_{max}) and minimum (ΔK_{MIN}) stress intensity levels in a single load cycle.   Paris experimentally demonstrated the principle of similitude; that is, equal fatigue crack growth rates are produced for equal applied stress intensity ranges, independent of load, crack size and component or specimen geometry [11].   Wei and coworkers extended this concept to describe corrosion fatigue crack propagation in aggressive gas and liquid environments [13,14].   The similitude principle enables integration of laboratory da/dN-ΔK data to predict component fatigue behavior, in terms of either applied stress range ($\Delta \sigma$) versus total life (N_f) or crack length (a) versus applied load cycles (N), for any initial defect size and component configuration.   Such computation are performed by integrating the da/dN versus ΔK growth rate law in conjunction with the component stress intensity solution, and with the initial and final flaw sizes as limits of the integration.

Over the last 20 years, extensive research studies have enabled the fracture mechanics approach to account for near-threshold fatigue cracking [1], small crack effects [6], crack closure [15], spectrum loading [16] and the behavior of anisotropic advanced materials [17]. This method has been successfully incorporated into computerized life prediction codes for

1

(ASTM E647-88)

Material
Environment

$\text{LOG } da/dN$

$\frac{da}{dN} \propto \Delta K^{2-4}$

ΔK_{th}

$\text{LOG } \Delta K$

$+$

$$\Delta K_{COMPONENT} = f \text{ (Loading, Flaw size , Geometry)}$$

$$N, N_f = \int_{a_{INIT}}^{a_{LIM}} \text{(Crack Growth Law)}(\Delta K_{COMPONENT}) \, da$$

$\Delta \sigma$

N_f

$\Delta \sigma_1$

a

N
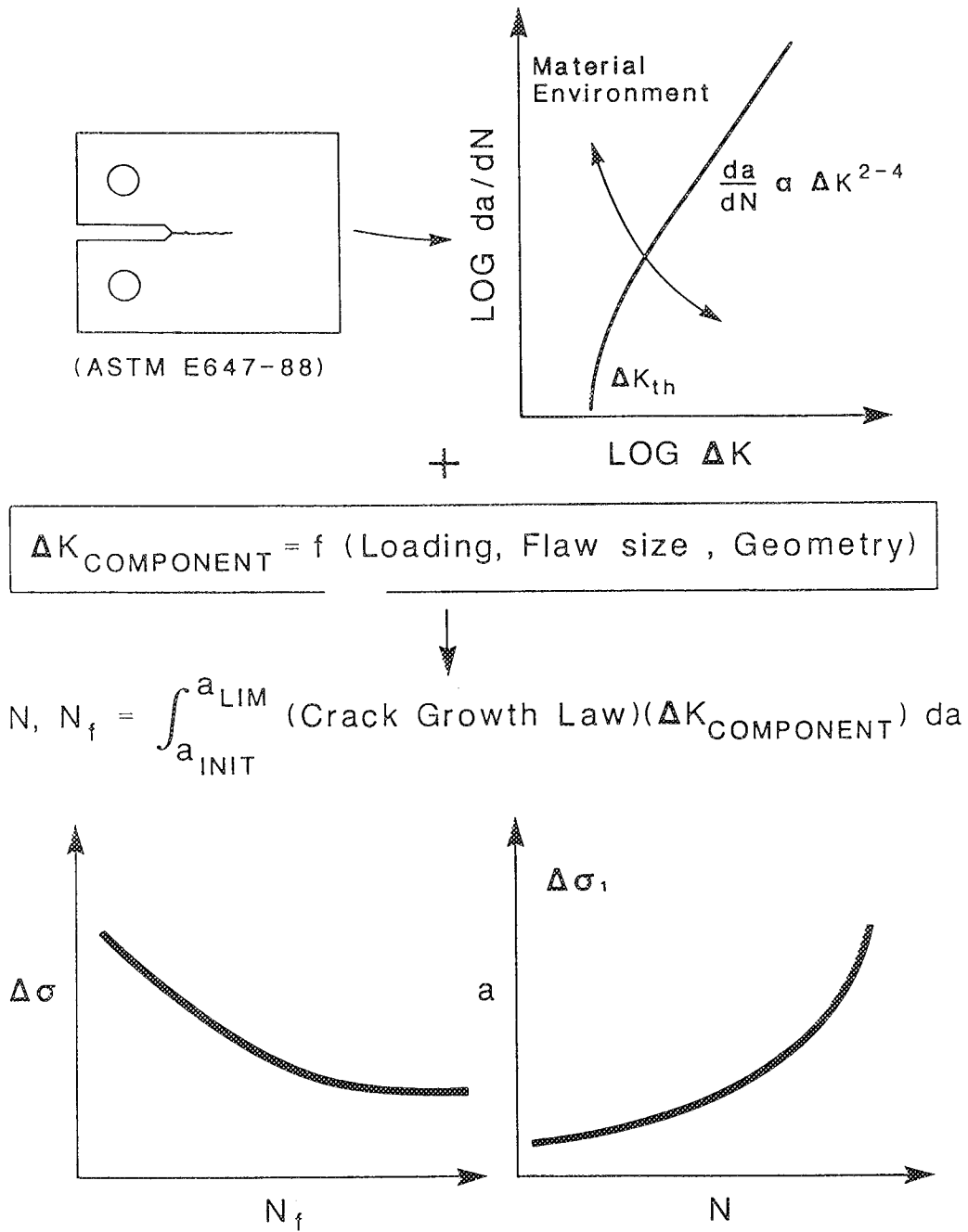
Fig. 1   Fracture mechanics approach to fatigue crack growth: material characterization and component life prediction [11].

aerospace components, such as NASA FLAGRO [18-21]. The NASA FLAGRO fatigue damage tolerance computer code provides an automated procedure for calculating the fatigue life of cyclically loaded structures with initial crack-like defects [19]. This state-of-the-art life code includes libraries of stress intensity solutions for various geometries and an extensive tabulation of materials property data in the form of da/dN versus ΔK and R where R is the stress ratio (K_{min}/K_{max}). In FLAGRO crack growth rate data are described by a modified Forman equation:

$$da/dN = \{C(1 - R)^m \Delta K^n [\Delta K - \Delta K_{TH}]^p\}/[(1-R)K_c - \Delta K]^q \qquad (1)$$

where R: stress ratio

ΔK: stress intensity factor range

K_c: critical stress intensity factor for fracture

C: growth rate constant

ΔK_{TH}: fatigue threshold stress intensity factor range

m, n, p, and q: exponent constants.

Equation 1 gives good accuracy, versatility, and can be fit to data using standard least squares methods [22]. The constants may be derived by either including a consideration of crack closure or by disregarding it. The crack closure analysis is based on Newman's equation expressed in the form:

$$\Delta K_2 = \{[1-(S_o/S_{max})1(1-R_2)]/[1-(S_o/S_{max})2(1-R_1)]\}\Delta K_1 \qquad (2)$$

where ΔK_1 is a baseline or known ΔK value corresponding to a da/dN for $R = R_1$ ($R_1 = 0$ in NASA/FLAGRO). The ΔK_2 variable is the ΔK value that gives the same da/dN at a different R value. S_o and S_{max} are the crack opening stress and the maximum cyclic stress, respectively. An example of a FLAGRO fit to material behavior is given in Fig. 2 for an aerospace steel, 300 M. The data and growth rate model in FLAGRO have, however, focused on FCP in moist air.

Considering the fact that rates of fatigue crack propagation in most structural alloys are significantly accelerated by the presence of deleterious environments, particularly those capable of producing atomic hydrogen through reactions with a metal [23-33], it is of crucial importance to understand and incorporate complex environment-alloy interactions into the life prediction method for aerospace components. An extreme example of environmentally enhanced da/dN in a high strength tempered martensitic steel is shown in Fig. 3 [31]. Due

3
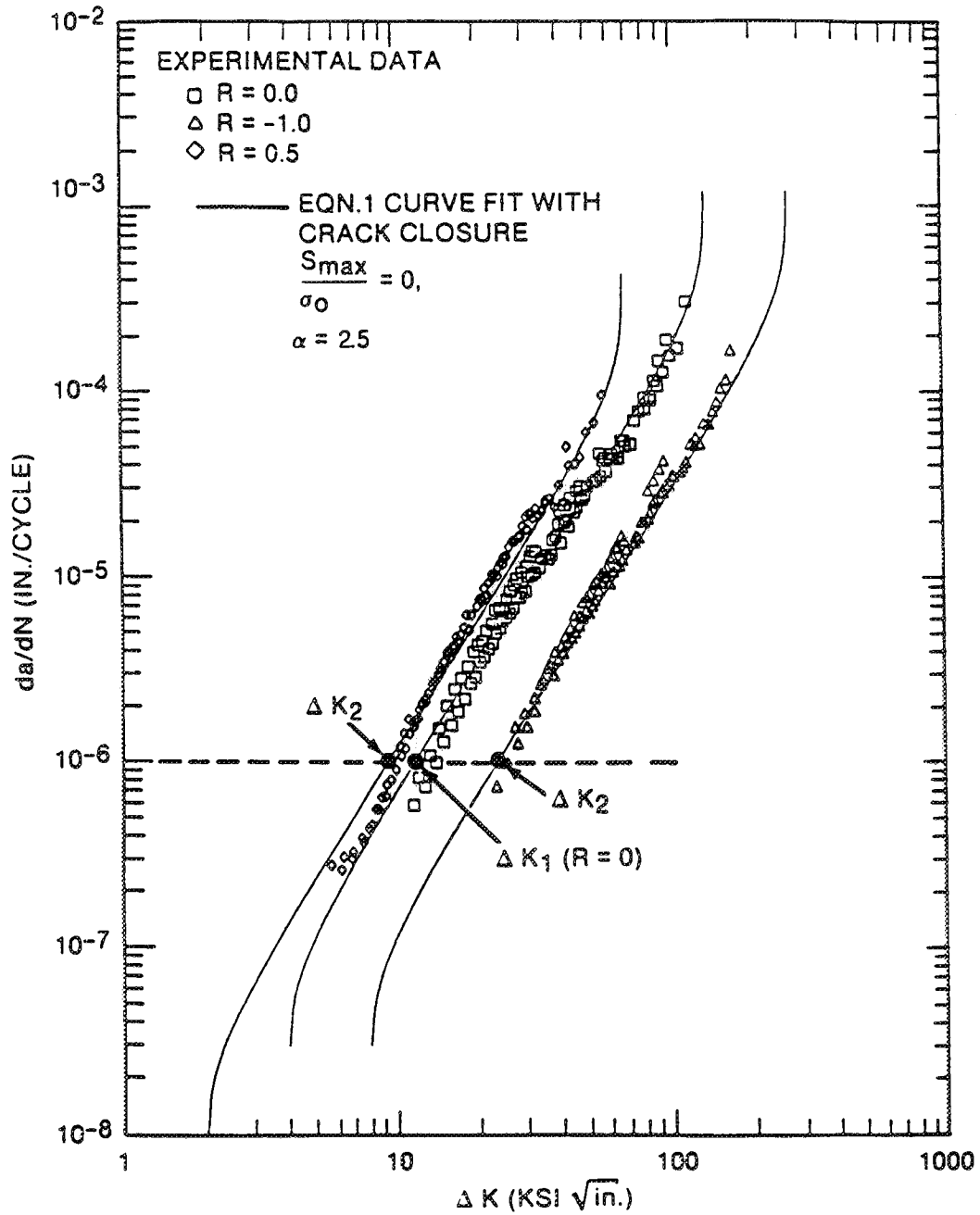
Fig. 2   The modified Forman equation (Equation 1), including crack closure, fit to crack growth rate data for 300 M steel [19].

4
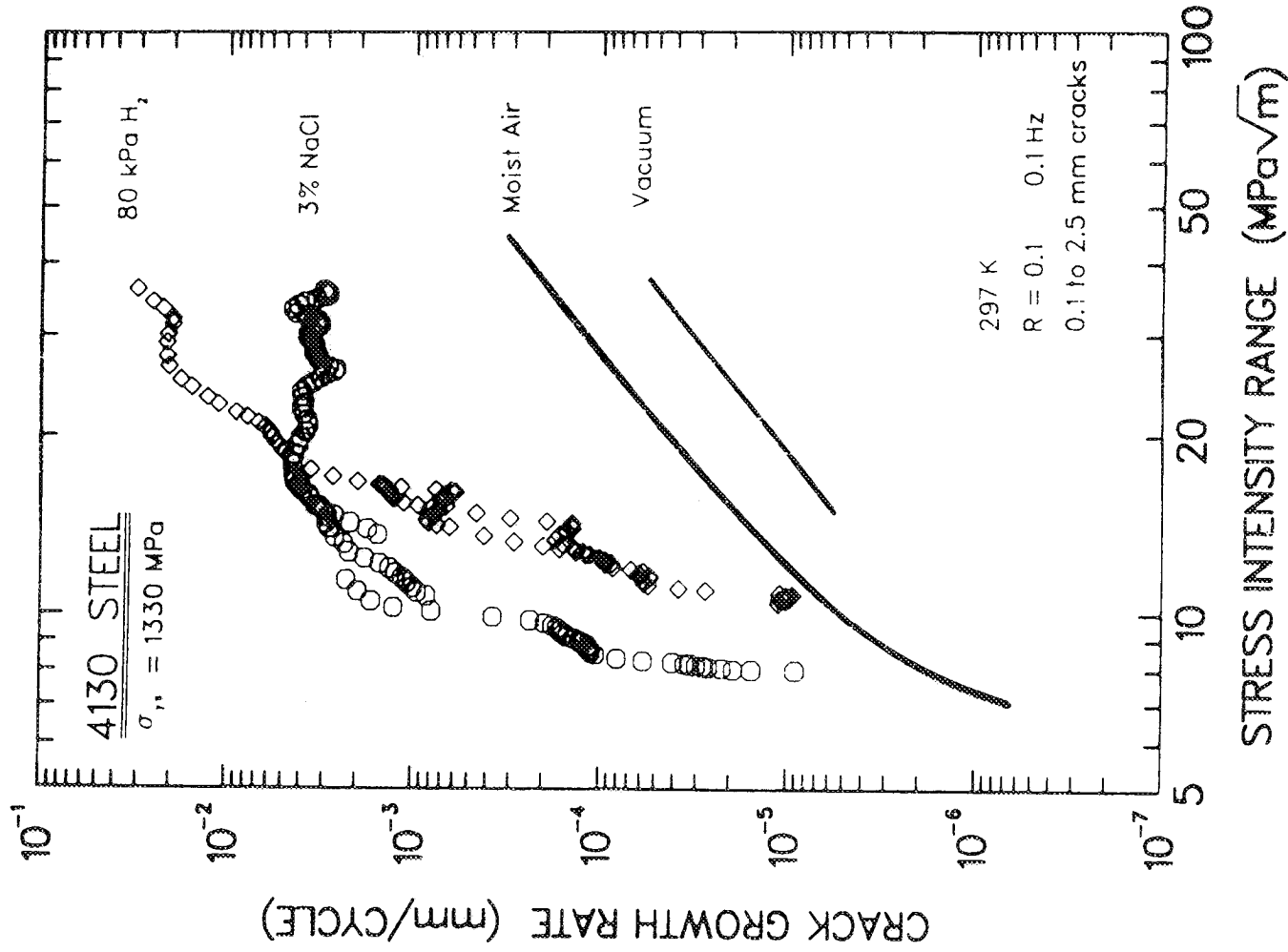
Fig. 3   Effect of various environments on fatigue crack propagation rates for 4130 steel.

to the complexity of the problem, however, environmental effects have not been systematically incorporated into fatigue life prediction codes.

B.   Environmental Effects on FCP Kinetics

The extent of the environmental enhancement of fatigue crack propagation rates is determined by the interactions of a myriad of variables [23-33].   Over the past 20 years, research efforts have aimed to characterize and quantitatively explain the effects of environment chemistry variables (viz., temperature; gas pressure and impurity content; electrolyte pH, potential, conductivity, and halogen or sulfide ion content).   Mechanical and metallurgical variables; including mean stress, loading frequency, crack geometry and size, wave shape, material strength, alloy composition and microstructure; also significantly alter the environmental fatigue crack propagation (EFCP) kinetics. The most important factors that influence EFCP are presented in Table 1 for aerospace aluminum alloys.

The need exists to generate laboratory data and predictive models for $da/dN-\Delta K$ as a means of extrapolating from existing inert environment and environment-sensitive crack growth kinetics data, and for incorporation into damage-tolerant remaining-life prediction codes such as FLAGRO.   Quantitative estimates of the flaw tolerance of structures in aerospace applications must account for a plethora of variables that interactively affect environmental FCP kinetics and which do not normally influence fatigue in benign environments. The time-dependent nature of EFCP must be appraised to describe the long life performance of load-bearing components based on necessarily short-term $da/dN-\Delta K$ data. Our understanding of fatigue mechanisms, necessary to incorporate environmental effects into life prediction methods, is limited [13,31,34-40]. Accordingly, environmental $da/dN-\Delta K$ data are decidedly more complex to incorporate into life prediction models.

C.   Objectives

The objective of this review and analysis is to provide a basis for enhancing the predictive capability of damage tolerance fatigue life prediction codes by incorporating environmental effects on FCP behavior. As a first step, fatigue crack growth rate data, available for implementation into various fracture mechanics-based fatigue life prediction methods such as NASA FLAGRO, are summarized. Emphasis is placed on alloy-environment

MECHANICAL, ENVIRONMENT CHEMISTRY AND METALLURGICAL VARIABLES AFFECTING ENVIRONMENTAL FATIGUE IN ALUMINUM ALLOYS	
STRESS INTENSITY RANGE	MEAN STRESS
CRACK SIZE AND SHAPE	SPECIMEN THICKNESS
LOADING FREQUENCY	SPECIMEN ORIENTATION
LOADING SEQUENCE	LOADING WAVEFORM
SOLUTION Cl^-, H^+, O_2, S^{-2}	WATER VAPOR PRESSURE
ELECTRODE POTENTIAL	OXYGEN CONTAMINATION
ALLOY MICROSTRUCTURE	ALLOY COMPOSITION
GRAIN/SUBGRAIN SIZE	ALLOY YIELD STRENGTH
SLIP MORPHOLOGY	ALLOY TEXTURE
PRECIPITATES	TEMPERATURE

Table 1   Variables that affect environmental fatigue crack propagation rates for aluminum alloys. After Gangloff [31].

systems which are relevant to aerospace components. These include: (1) alloy steels in hydrogen producing gases and electrolytes, (2) precipitation hardened aluminum alloys in water vapor and aqueous chloride, (3) titanium alloys in halogen bearing electrolytes, (4) precipitation hardened nickel based superalloys in hydrogen gas and elevated temperature moist air, and (5) stainless and ferritic steels in high purity water at elevated temperatures. The effects of important variables are illustrated.

The models that are currently available to predict environment sensitive da/dN behavior are summarized and critiqued. Approaches in this regard include empirical curve-fitting, linear superposition of monotonic load environmental cracking and inert environment FCP, and mechanism based modeling. To facilitate linear superposition modeling, sustained load environmental crack growth rate kinetics are summarized for aerospace alloys.

Appropriate model material-environment systems for evaluating and further developing environmental FCP models are suggested. Deficiencies in understanding and directions for research and engineering are identified.

II. OVERVIEW OF ENVIRONMENTAL CRACKING MECHANISMS

A primary aim of research on mechanisms of inert environment mechanical fatigue crack propagation, and environmental FCP, is to develop models that predict the ΔK dependence of da/dN from the basic principles of crack tip stress and strain, alloy microstructure, and localized fatigue damage accumulation. Successful models will enable the broad extrapolation of limited laboratory FCP data for incorporation into codes such as FLAGRO. While a wide variety of models have been proposed, none are at the point in development of contributing to the life prediction mission. Mechanistic understanding is none-the-less important for qualitative assessments of the importance and effects of variables on da/dN-ΔK, particularly for environmental FCP.

A. Mechanical Fatigue Crack Propagation

Fatigue crack propagation rates in metals are primarily governed by the alternating stress intensity factor, ΔK. The parameter K can be defined for any loading systems, crack geometry and opening mode, and uniquely characterizes the elastic stress and strain distributions associated with the crack tip. In 1961 Paris first proposed that stress intensity described FCP as follows:

$$da/dN = A(\Delta K)^m \qquad (3)$$

where A and m are material-dependent constants that also depend on loading frequency, environment and mean stress [11]. It was later realized that FCP kinetics are divided into three different stages, as indicated in Fig. 4, after a classification by Forsyth [41].

1. Near-threshold Fatigue Crack Propagation Regime

At low values of ΔK, the relationship between log (da/dN) and log (ΔK) exhibits a substantial slope increase, such that the value of da/dN possibly decreases to zero (experimentally, to 10^{-10} m/cycle or less) below a "threshold" value, ΔK_{TH}. Values of ΔK_{TH} and da/dN in the near-threshold region effectively control the high-cycle fatigue behavior of many components. The reason for this is that, first of all, most real structures contain defects from which fatigue cracks may readily initiate after few load cycles, making crack propagation life-controlling. Secondly, the nature of the growth rate dependence implies that a crack will grow relatively slowly in the initial stages and rapidly accelerate as its length and applied ΔK increase.

Several theoretical models for ΔK_{TH} have been proposed based on: (1) a Griffith-type energy balance [42,43], (2) dislocation dynamics [44,45], and (3) crack-tip plasticity [46-48]. While the predictive success of the energy balance models, first suggested by Purushothaman and Tien, was significant, the formulation contains significant errors in the assumed stress/strain conditions in the plastic zone [42]. More sophisticated models based on the behavior of dislocations in the region ahead of the crack tip were later developed by Yokobori, Mura and Weertman [45]. The dislocation dynamics model requires input of many material parameters which can often only be approximately estimated and which critically affect the resulting predictions. Several models were derived based on the distribution and magnitude of crack-tip plasticity, without dealing directly with the behavior of dislocations. As an example, Beevers assumed that ΔK_{TH} is related to a lower bound value of the crack tip opening displacement which results in the following relationship [47]:

$$\Delta K_{TH} \, \alpha \, \sqrt{\sigma_o E l} \qquad (4)$$

where σ_o is yield strength, E is Young's modulus and l is a microstructural size scale such as grain size. The prediction that the threshold increases with increasing flow strength is generally inconsistent with experimental observations. Starke and coworkers developed a more detailed model of ΔK_{TH} which coupled the crack tip strain field, averaged over a microstructurally significant distance, with a Coffin-Manson failure criterion with linear damage summation [48]. The threshold stress intensity in this model corresponds to the crack tip strain range below which persistent slip bands cannot form.

2. Power-Law Fatigue Crack Propagation Regime

Within a limited range of crack growth rates, typically 10^{-9} to 10^{-6} m/cycle, log (da/dN) linearly increases with increasing log (ΔK) with a slope, m, as given in Equation 3. This linear (or Paris) crack growth regime has been the target of extensive research and a multitude of theories over the last three decades. Proposed models can be classified into the following two groups.

(a) Crack Opening Displacement

This type of model is based on the assumption that the amount of crack growth per load cycle is proportional to the crack tip opening displacement (CTOD) [49-51]. The physical basis for these models evolves from experimental correlations of striation spacings with crack growth rates and from actual crack tip opening shapes from blunting on loading
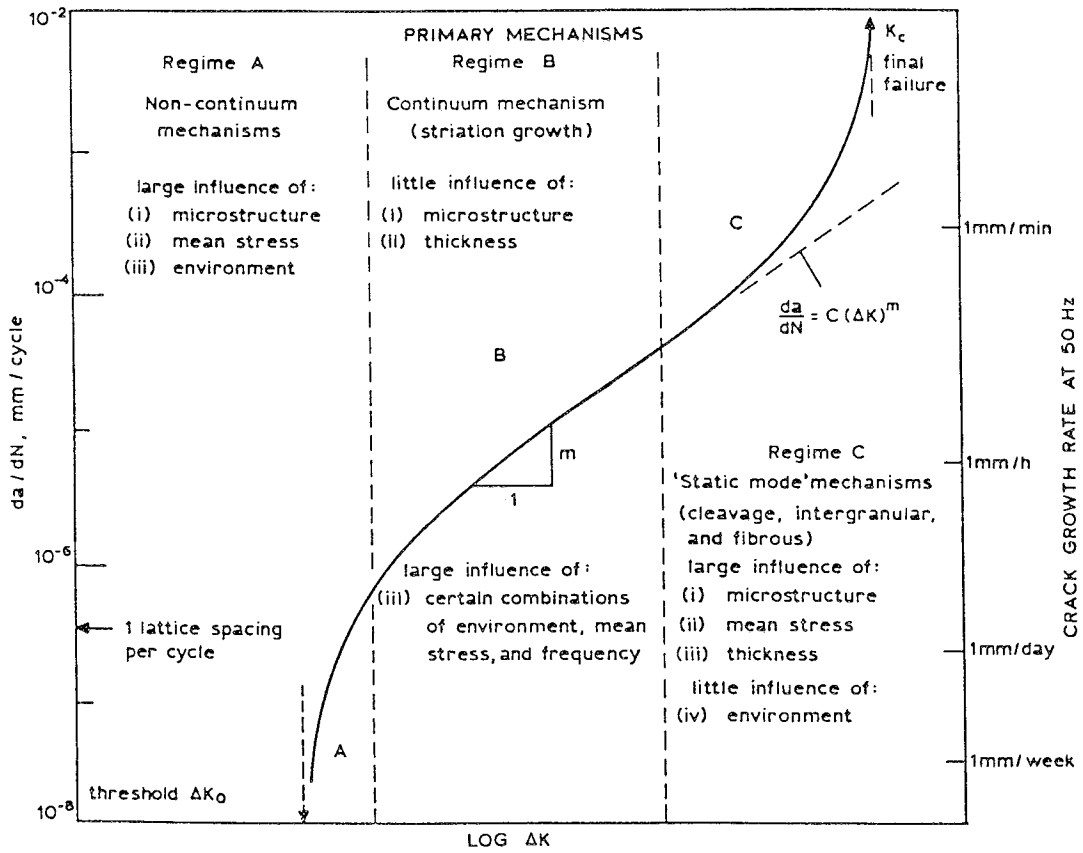
Fig. 4   Schematic variation of fatigue crack propagation rate as a function of stress intensity range, ΔK. After Forsythe [41].

and buckling during unloading. The fatigue crack growth rate is expressed as:

$$da/dN = \beta \; CTOD = \gamma \; (\Delta K^2/E\sigma_o) \qquad (5)$$

where β and γ are constants that depend on the specific model. This equation predicts a Paris exponent (m) of 2, which is reasonable for many alloys but which is far from being universally observed. The inverse proportionality of crack growth rates with yield strength is not observed. Crack growth rates are often only a small portion of the CTOD. Further modifications are necessary to derive quantitative FCP relationships that compare favorably with the experimental crack growth rates.

(b) Damage Accumulation

Damage accumulation models postulate that crack growth discontinuously occurs over a distance, Δa, when the damage accumulated during ΔN load cycles exceeds a critical value in a small process zone ahead of the crack tip. Several approaches have been proposed in this regard [48,52-55]. A damage accumulation model was first proposed by McClintock [52], who predicted crack growth in proportion to the square of the plastic zone size, or to the fourth power of ΔK. More detailed models have been proposed by Majumdar and Morrow as well as by Chakrabrotty and Starke, employing reasonable crack tip strain distributions over microstructurally meaningful distances and a material dependent fatigue damage criterion [54-55]. These approaches do not result in a simple expression for the ΔK dependence of da/dN, and must be numerically solved based on input of specific material strength, cyclic work hardening, smooth specimen fatigue stress-life and microstructure properties.

An energy balance approach was also utilized to model Paris regime crack growth, without detailing the mechanisms involved in fatigue damage [56,57]. Such models essentially compute the plastic work done per unit distance of crack growth, U, which is equal to $D_c\sigma_o$. D_c is the critical value of the accumulated displacement that must be exceeded for crack advance to occur after ΔN cycles.

3. High Fatigue Crack Propagation Rate Regime

At high values of ΔK, crack growth rates are higher than predicted by extrapolation of the Paris relationship. The reason for this behavior is that monotonic, or "static" modes of fracture are produced by the high portions of the applied loading cycle. The importance of these monotonic modes, with respect to the overall value of crack growth rate, depends on the value of K_{max} in the cycle and the magnitude of the static growth mode.

12

Forman developed a model for crack growth rate in this regime, although it is more often used to model mean stress effects [58].

$$da/dN = C\Delta K^m/[(1-R)K_c-\Delta K] \tag{6}$$

where K_c is the critical fracture toughness for the specimen or component thickness of interest. Equation 6 predicts the sharp upturn in the da/dN versus ΔK curve as K_c is approached. In this region plasticity influences crack growth rate because the plastic zone size becomes large compared to the dimensions of the crack and specimen. Therefore, this problem should be analyzed by the elastic-plastic fracture approach rather than by linear-elastic fracture mechanics. When the plastic zone is on the order of the specimen thickness, plane stress "slant" fracture modes also affect FCP. In many engineering situations, this regime may be ignored because high ΔK da/dN values do not significantly affect the total fatigue crack propagation life.

B. Hydrogen Environment Embrittlement

While there is no single unifying mechanism governing environmental FCP in metals, several common concepts have been proposed, and are useful for understanding and categorizing da/dN-ΔK data. Among these, the hydrogen environment embrittlement (HEE) mechanism is commonly invoked to explain the enhancement in fatigue crack growth rates in alloys and aggressive environments that are relevant to aerospace applications [33,59-66]. Hydrogen embrittlement as a dominant mechanism has been effectively argued for several systems, including ferritic/martensitic steels in gases and electrolytes [13,34-36,40,67-70], titanium alloys in hydrogen gas and aqueous chloride solution [71-73], precipitation-hardened aluminum alloys in water vapor and halogen-bearing solutions [13,40,74-77], and nickel based superalloys in H_2 [78-82]. Quantitative models of da/dN versus ΔK, governed by hydrogen embrittlement, have not been fully developed.

1. Hydrogen Production, Transport and Trapping

For hydrogen environment enhanced fatigue crack propagation, atomic hydrogen is typically produced on clean metallic crack surfaces by one of three the transport and reaction sequences indicated in Fig. 5 [68]. Specific cases include high strength steels or nickel based alloys in gaseous hydrogen, aluminum alloys in water vapor, and aluminum alloys, titanium alloys or ferritic/martensitic alloy steels in chloride bearing electrolytes [31].

13

GASEOUS HYDROGEN | WATER VAPOR | ELECTROLYTE

$\sigma_Y , \Delta\epsilon_p$

C_H ⑤

⑦

$C_{H\sigma}$

① ②→④ ⑥

$\vdash \delta \dashv$

GASEOUS HYDROGEN	WATER VAPOR	ELECTROLYTE
(1) MOLECULAR TRANSPORT	MOLECULAR TRANSPORT	OXYGEN DEPLETION
(2) PHYSICAL ADSORPTION H_2	PHYSICAL ADSORPTION H_2O	CATION DISSOLUTION, HYDROLYSIS
(3) H_2 MIGRATION, DISSOCIATION TO ATOMIC H	CHEMICAL REACTION TO $Fe_xO_Y \cdot H_2O$; H	H^+ REDUCTION TO H
(4) CHEMICAL ADSORPTION		WATER REDUCTION TO H

(5) SOLUTION TO LATTICE, TRAP SITES

(6) BULK DIFFUSION TO FPZ

(7) ENHANCED FATIGUE DAMAGE

Fig. 5   Mass transport, chemical/electrochemical reaction and mechanical embrittlement processes necessary for hydrogen environment enhanced fatigue crack propagation in alloys [68].

Atomic hydrogen on crack surfaces, derived from the various reaction sources, can move in the crack-tip plastic zone to the point of fatigue damage, either by diffusion or dislocation transport with appreciable mobilities [83,84]. Absorbed hydrogen causes embrittlement in front of the crack tip and, consequently, increases fatigue crack propagation rates. Hydrogen is often segregated or "trapped" at various microstructural trap sites such as grain or phase boundaries; such traps are either reversible or irreversible [85,86]. Reversible traps act as a hydrogen source by exchanging hydrogen with stronger traps. Trapping is detrimental if cracking occurs at such sites, but is beneficial if broadly distributed traps reduce hydrogen transport kinetics and accumulation at fatigue damage sites. Little is known about the specific mechanisms for hydrogen enhanced fatigue damage (#7) within the crack tip process zone and presumably common to each environment.

It is commonly recognized that crack growth rate depends on the amount of hydrogen produced per load cycle and is limited by one or more of the slow steps (#1 to #6) in the transport and surface reaction sequence in Fig. 5. A variety of simple models to predict da/dN have been developed based on this chemical concept [13]. Quantitative HEE models for corrosion fatigue are largely classed as either hydrogen production-based [69,75,87-90] or hydrogen diffusion-based [89,91-93]. A detailed discussion on quantitative HEE models is given in the section "Quantitative Crack Growth Rate Models". Broadly predictive HEE models of da/dN-ΔK are limited [68].

2. Hydrogen Embrittlement Failure Mechanisms

Although the atomistic processes are debatable, it is generally postulated that hydrogen, diffused in the crack tip plastic zone to the point of fatigue damage, embrittles the metal via: (1) bond decohesion [94-96], (2) hydride formation [97-99], or (3) hydrogen-enhanced localized plasticity [100-103].

(a) Bond Decohesion

The decohesion mechanism was originally suggested by Troiano [94] and advanced by Oriani [95,96]. The basic postulates of the decohesion mechanism are that brittle fracture occurs when the local stress ahead of the crack tip exceeds the atomic bond strength, and that the presence of hydrogen decreases the atomic bond strength. This model is advocated as a hydrogen embrittlement mechanism for high-strength steels and aluminum alloys.

(b) Hydride Formation

The idea of a hydrogen-rich phase formed and cleaved in front of the crack tip was first postulated as a cause of embrittlement by Westlake [98]. Thermodynamically, applied tensile stress reduces the hydride chemical potential at the crack tip and atomic hydrogen diffuses to this region. Once the brittle hydride precipitates, it cleaves with microcracking arrested at the hydride-matrix interface at which point the microcrack is blunted by deformation in the ductile matrix. This process repeats and brittle fracture propagates by repeated stress-induced hydride formation and cleavage. Convincing demonstration of stress-induced hydride formation as a leading hydrogen embrittlement mechanism was reported for α and α/β-titanium alloys [104]. The hydride model appears to be applicable to the hydrogen embrittlement of other hydride formers; particularly V, Nb, Zr and Mg-Al alloys. It is, however, difficult to extend this model to those systems where there is no evidence for hydride formation such as high-strength steels, austenitic stainless steels and some aluminum alloys.

(c) Hydrogen-enhanced Localized Plasticity (HELP)

Locally enhanced plasticity, due to the presence of hydrogen at the crack tip, was first suggested by Beachem for steels [100]. Recently, Birnbaum and coworkers observed that the resistance to dislocation motion due to obstacles, and hence the stress for plastic deformation, was decreased by the presence of hydrogen in solid solution. Thus, the flow stress is decreased in the regions of high hydrogen concentration at the crack tip, slip localization occurs and promotes macroscopically brittle fracture [101,103]. That the HELP mechanism is a feasible hydrogen embrittlement process was demonstrated for several pure metals and alloys including aluminum, Inconel 718, precipitation-hardened 7075 and 304 stainless steel. The detailed mechanism by which hydrogen-induced slip localization leads to local fracture in macroscopically cracked specimens under substantial plane strain constraint, and cyclic loading, is not completely understood.

(d) Effect of Cyclic Loading

HEE is significantly accelerated by cyclic loading. Several hypotheses qualitatively explain the uniquely damaging effect of cyclic plastic deformation:

oo   Fatigue crack convective mixing provides deleterious species from the bulk environment to the crack surface;

16

oo   Loading and unloading produce a sufficiently high crack tip strain rate to enhance film rupture, hydrogen production and hydrogen entry efficiency,

oo   Cyclic plasticity continuously transports atomic hydrogen from the crack surface-environment interface to strong trapping sites within the embrittlement process zone,

oo   cyclic deformation produces crack tip dislocation cell/slip band structures that are "embrittled" by trapped hydrogen,

oo   High normal stress is maintained within the crack tip field because of continued crack tip sharpening by cyclic unloading.

The quantitative explanation of cyclic plastic deformation on hydrogen embrittlement process is, however, limited. No model has been developed to quantify these explanations, and to predict da/dN as a function of ΔK, chemical and microstructural variables.

C.   Corrosion Fatigue by Film Rupture, Transient Dissolution and Repassivation

Corrosion (environmental) fatigue cracking in some systems, particularly for carbon and stainless steels exposed to high-temperature water environments [36,38,105,106], can be attributed to electrochemical reaction damage at ruptures in an otherwise protective crack surface passive film. Fig. 6 schematically illustrates the elements of the slip-dissolution (or film-rupture) model for environmentally enhanced fatigue crack propagation. While controversial, film-rupture models have been applied to the aluminum-aqueous chloride system [76,107].

Film rupture models for both monotonic and cyclic load environmental cracking are based on a sequence of passive film rupture at the crack tip, oxidation and progressive repassivation of the exposed metal, and a new rupture of the freshly formed film after a critical fracture strain is accumulated. This model was applied to predict the service life of ferritic and stainless steels in high-purity water over a temperature range of 300 to 600 K [106,108]. This model hypothesizes that, once the protective film is ruptured at the straining crack tip, the crack growth increment due to an environmental effect is controlled by both the rate of decay of the oxidation charge density during repassivation and the frequency of oxide rupture at the strained crack tip. The latter is controlled by the crack tip surface strain rate for static, monotonic or cyclic loading. Da/dN$_{cf}$ is specifically related to the oxidation charge

density passed between oxide rupture events, Q_f, and the strain rate at the crack tip, $\dot{\epsilon}_{ct}$, by Faraday's Law [38,105,106,109]:

$$da/dN_{CF} = 1/f \; (M/\rho ZF) \; Q_f \; (\dot{\epsilon}_{ct}/\epsilon_f) \qquad (7)$$

where M and ρ are the atomic weight and density of the dissolving metal, Z is the number of electrons involved in oxidation, F is Faraday's constant, and ϵ_f is the fracture strain of the oxide at the crack tip. Charge density passed per rupture event is given by:

$$Q_f = \int_0^{t_f \; = \; \epsilon_f/\dot{\epsilon}_\alpha} i(t) \; dt \qquad (8)$$

where i(t) is the transient current associated with dissolution during reformation of the crack tip passive film.

Significant successes have been reported in predicting da/dN versus ΔK with Equation 8 [38,105]. As an example, Fig. 7 shows excellent agreement between predictions and measurements of time-based crack growth rates, for either monotonic or cyclic loading [106]. On balance, however, controversy surrounds determinations of the adjustable parameters involved in this model.

D. Elevated Temperature Cracking in Nickel Based Superalloys

Extensive research over the past ten years has been aimed at the fatigue crack propagation behavior of high strength nickel based superalloys in elevated temperature moist air. The application for this work has been the development of damage tolerant alloys and fracture mechanics design methods for turbine disk components in military and commercial aircraft engines. For high strength disk alloys, elevated temperature environmental effects can be strong, similar to the data presented for structural alloys in room temperature gases and electrolytes. The fracture mechanics approach is relevant so long as time dependent plasticity is limited to a hundreds-of-micron sized process zone at the crack tip. This is in fact the case, at least for important alloys such as IN 718 at temperatures up to 600°C.

The effect of elevated temperature moist air on fatigue crack propagation in high strength precipitation hardened nickel based superalloys is phenomenologically similar to low temperature EFCP in Fe, Al and Ni based alloys in hydrogen producing environments [110-115]. Floreen and Kane studied the effects of fourteen different gaseous environments on FCP rates in Inconel 718 at 650°C, and concluded that fatigue crack growth rates in this alloy
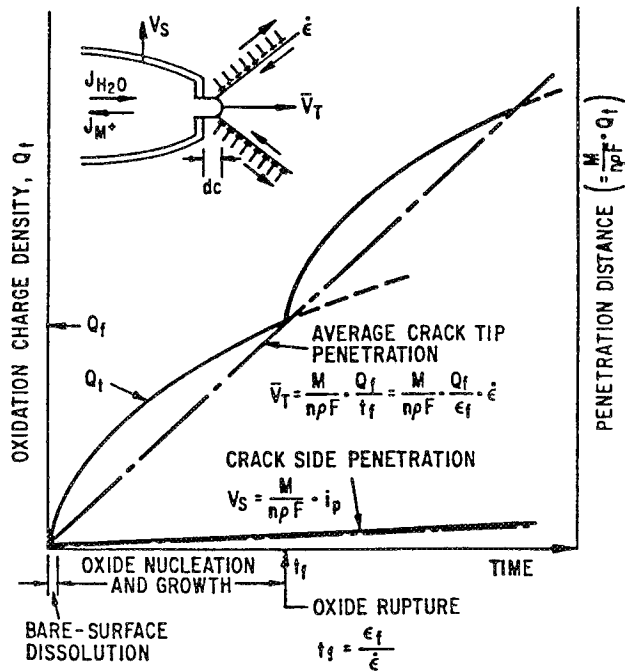
Fig. 6   Schematic illustration of the elements of the film-rupture model for environmentally assisted crack propagation. After Ford [38,105,106].
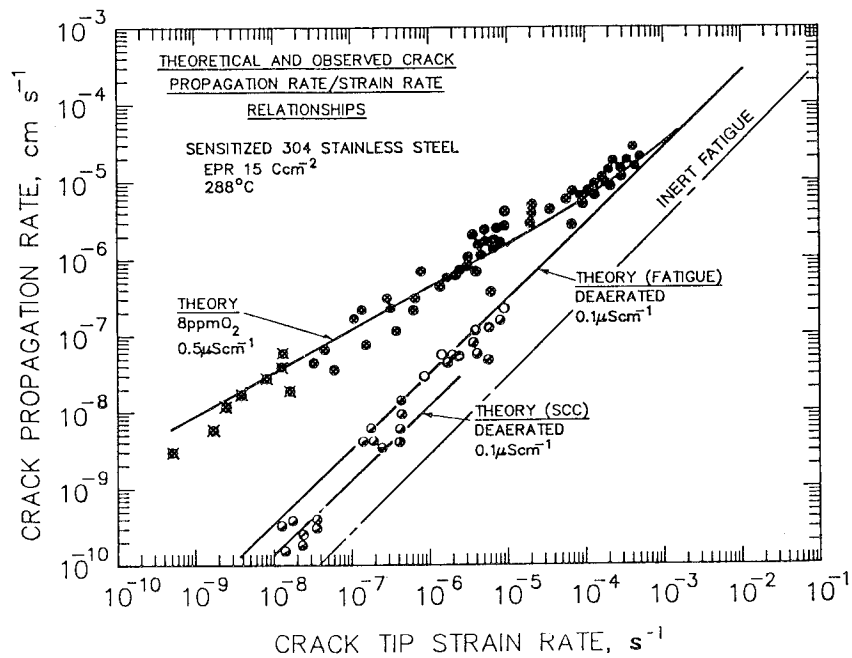
Fig. 7   Film-rupture model predictions compared to measurements of time-based crack growth rates versus crack-tip strain rate for monotonic and cyclic loading of 304 stainless steel in high-temperature water. After Ford and Andresen [106].

are significantly accelerated by the presence of oxygen [116]. The inclusion of a hold time in the fatigue cycle increases crack growth rates substantially for superalloys in the moist air environment, while little increase is observed for FCP in vacuum [117]. This phenomena suggests that the time dependence of the environmental interaction is attributed to the oxygen diffusion within the crack tip process zone. While the mechanism for oxygen enhanced crack growth at elevated temperature has not been established, diffusion of oxygen along grain boundaries and/or intersecting slip planes, and oxygen-induced reduction in crack tip plasticity, are often cited [117,118]. These notions have not been incorporated into a predictive model for da/dN versus ΔK.

III. FATIGUE CRACK PROPAGATION IN AEROSPACE ALLOY-INERT/BENIGN ENVIRONMENT SYSTEMS

A. Introduction

In order to enhance existing fatigue prediction codes to quantitatively evaluate environmental effects on component fatigue crack propagation life, it is necessary to proceed in four steps: (a) define FCP data for aerospace alloys in an "inert" reference environment, (b) assess the environmental cracking resistance of alloys under simple sustained load, (c) determine environmental effects on da/dN versus ΔK, and (d) define the effects of important metallurgical, mechanical and chemical variables on da/dN versus ΔK growth rate laws. The next four Chapters, III through VI, present this information for alloys that are often used in aerospace structural applications; namely steels, aluminum alloys, titanium alloys, and nickel based superalloys. Since the literature is massive, a restricted number of references are included.

Care was taken in selecting the following results because literature data are often affected by one or more extrinsic contribution, particularly crack closure. Premature contact between mating crack faces, even during the tensile portion of the fatigue cycle, is often observed in metals. The consequence of crack closure is to significantly reduce the actual stress intensity factor range experienced by the crack tip from a nominal value of ΔK to an effective value defined as $\Delta K_{eff} = K_{max} - K_{cl}$, where K_{cl} is the stress intensity value at which two fracture surfaces first come into contact during the unloading portion of the fatigue cycle. The magnitude of crack closure level depends on microstructure, stress ratio, stress intensity range and environment. The detailed aspects of crack closure are discussed in the section "Factors Complicating Life Prediction".

As a basis for consideration of environmental effects on FCP, it is necessary to establish the behavior of structural alloys in a suitable reference environment. Contaminant-free vacuum or inert gases (viz., helium, argon or nitrogen) provide an absolute reference for environmental effects on mechanical fatigue. Even though aggressive relative to vacuum for all alloys, moist air is often considered as a useful environment for comparison since data are typically available and are often incorporated into existing life prediction codes.

Crack growth rates in structural alloys, exposed to benign environments at room temperature, are described by well established material property laws based on stress intensity range ($\Delta K = K_{max} - K_{min}$) and the associated similitude concept. These laws are reasonably

21

independent of variables such as frequency, stress ratio, and microstructure. Results are presented in Figs. 8 through 14 for: (a) all materials in vacuum, (b) steels in moist air and vacuum, (c) 7000 series aluminum alloys in moist air and vacuum, (d) nickel based superalloys in moist air at elevated temperatures and (e) titanium alloys in moist air and argon. These results are based on analyses of extensive data bases, perhaps on the order of 1000 crack growth rate experiments.

The data in Figs. 8 through 14 provide a basis for examination of environmental effects. Inert environment fatigue data need to be carefully interpreted, since those factors which compromise stress intensity similitude (viz., crack closure, small/short crack size and large scale yielding) are not well defined by the data in Figs. 8 to 14. For example, the extreme crack closure contributions due to tortuous crack microstructures as encountered for aluminum or titanium alloys, particularly at low stress ratios and in the near-threshold stress intensity regime, may not be well defined by the data in Figs. 8 to 14. Stress ratio and microstructure effects can be large when significant crack closure is present. Such closure effects have not been generally isolated for inert environment FCP data. These issues are beyond the scope of the current analysis which emphasizes the growth of long fatigue cracks at rates above 10^{-6} mm/cycle. This issue is discussed in the section "Factors Complicating Life Prediction".

B.   All Materials in Vacuum (Fig. 8)

Speidel argues that the fatigue crack propagation behavior of a wide variety of materials, stressed in vacuum at 25°C, is well described by a single law given by the following equations for Paris regime (Equation 9) and near-threshold (Equation 10) cracking [119]. Da/dN is in units of m/cycle, ΔK is MPa$\sqrt{m}$ and the modulus of elasticity is MPa.

$$da/dN = 1.7 \times 10^6 \ (\Delta K/E)^{3.5} \qquad (8) \ [119]$$

$$\Delta K_{TH} = 2.7 \times 10^{-5} \ E \ (m^{1/2}) \qquad (9) \ [119]$$

These equations are plotted in Fig. 8 along with the specific data that were measured by Speidel with a common laboratory procedure; specific alloys, polymers and ceramics are identified in the original paper [119]. Speidel points out that metallurgical and environmental embrittlement phenomena, often interacting with high stress ratio and slow loading frequency, will exacerbate crack growth rates compared to the values shown in Fig. 8. Crack closure

22
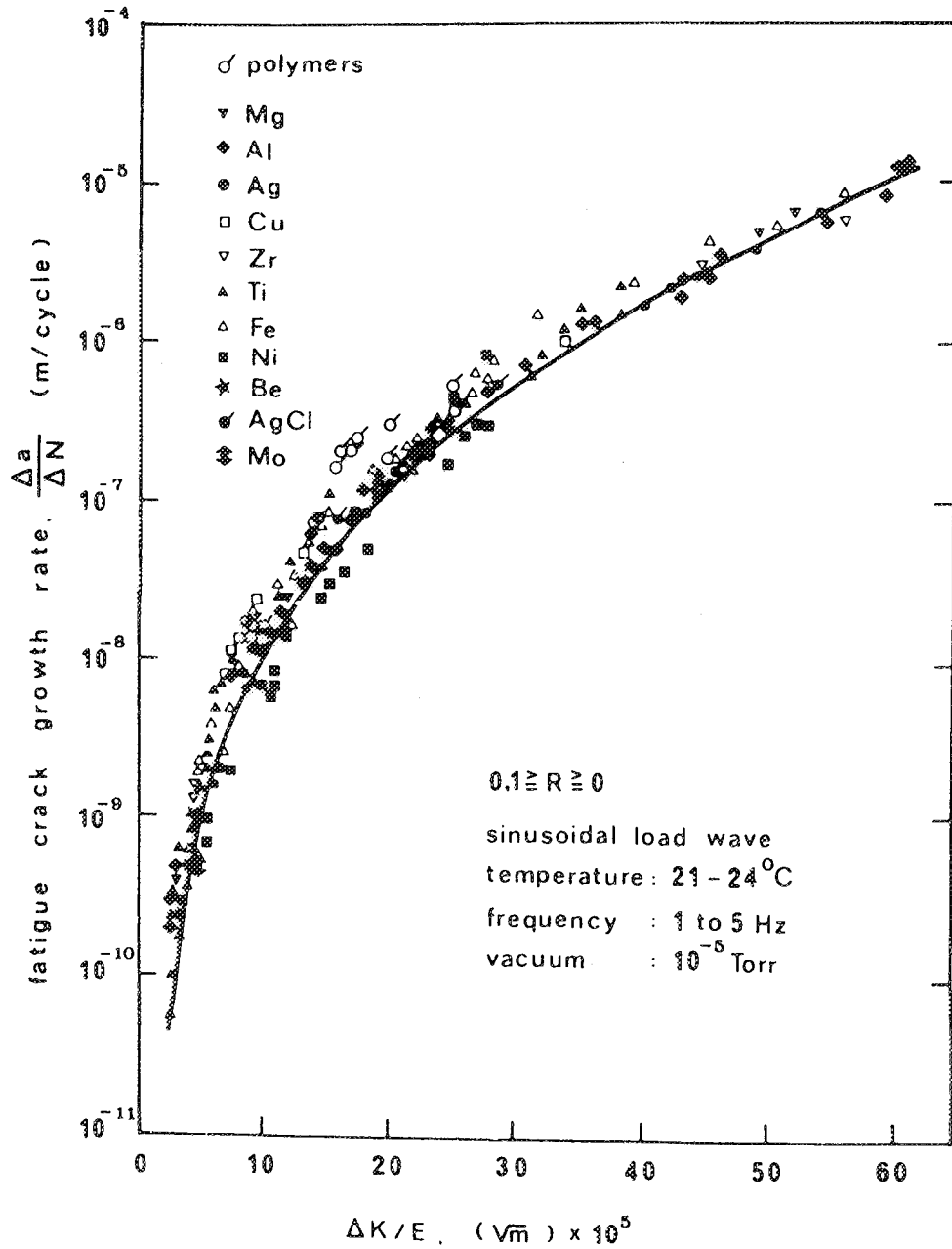
Fig. 8   Modulus normalized stress intensity range correlation of fatigue crack propagation rate for a variety of structural materials stressed in vacuum at 25°C. After Speidel [119].

effects were not well understood at the time of Speidel's work and may have affected the correlation shown in Fig. 8. This issue was recently considered for closure-free, inert environment FCP in aluminum alloys [120].

C. Steels in Moist Air and Vacuum (Fig. 9)

Considering moist air as a benign environment, the fatigue crack propagation behavior of a wide variety of ferritic and martensitic steels is well established. Only mean stress, expressed in terms of stress ratio ($R = K_{min}/K_{max}$), and monotonic yield strength (σ_{ys}) influence FCP, with the effects being small in the moderate ΔK power law regime, but significant for near-threshold (ΔK_{TH}) crack propagation. The mechanical and microstructural effects in the near-threshold region are generally attributed to a crack closure mechanism, with roughness-induced closure being most prominent for this benign environment.

Albrecht, Bertini, and Scott et al. independently analyzed an extensive moist air fatigue crack propagation data base by least squares statistics and reported the following relationships for Paris Law crack propagation in structural steels [69,121,122]. Da/dN is mm/cycle and ΔK is MPa$\sqrt{m}$.

1. Normalized C-Mn Steels ($\sigma_{ys} < 500$ MPa)

Yazdani and Albrecht reported:

$$da/dN = 1.54 \times 10^{-9} (\Delta K/(1-0.23R))^{3.34} \qquad (11) \quad [122]$$

Bertini reported:

$$da/dN = 10^{A+Bm} (\Delta K)^m$$

$$m = (3.53 - 0.91 R)$$

$$A = -3.94 \qquad B = -1.40 \qquad (12) \quad [121]$$

Scott, Thorpe and Silvester reported:

$$da/dN = 5.9 \times 10^{-9} (\Delta K)^{3.15} \text{ for low } \Delta K$$

$$da/dN = 2.8 \times 10^{-8} (\Delta K)^{2.65} \text{ for high } \Delta K \qquad (13) \quad [69]$$

2. Quenched/Tempered HSLA Steels ($\sigma_{ys} = 900$ MPa)

Yazdani and Albrecht reported:

$$da/dN = 2.27 \times 10^{-8} (\Delta K/(1-0.11R))^{2.53} \qquad (14) \quad [122]$$

Barsom and Rolfe presented the following equations based on an analysis of a variety
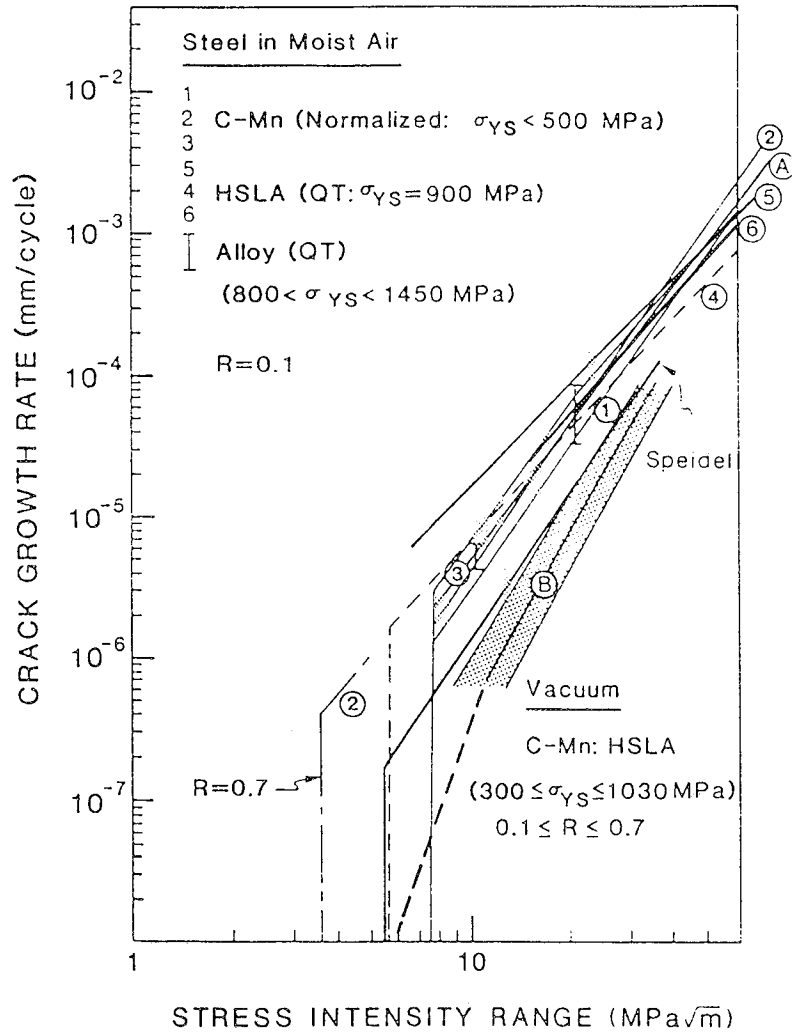
Fig. 9   Fatigue crack propagation kinetics for steels in moist air and vacuum. Curves
1 and 4, Equations 11 and 14, Albrecht [122]; Curve 2, Equation 12, Bertini
[121]; Curve 3, Equation 13, Scott, et al. [69]; Curves 5 and 6, Equations 15
and 16, Rolfe and Barsom [123]. An elastic modulus of 200 GPa was
employed to calculate the vacuum behavior after Speidel [119].

of steels [123]. Mean behavior is described here, however, the authors present results for both upper and lower bounds on the crack growth rate data. In these equations da/dN is in/cycle and ΔK is ksi$\sqrt{}$in.

3. Ferrite-Pearlite C-Mn Steels (200 < σ_{ys} < 550 MPa)

$$da/dN = 2.8 \times 10^{-10} (\Delta K)^{3.00} \qquad (15) \quad [123]$$

4. Martensitic C-Mn and Alloy Steels (550 < σ_{ys} < 2070 MPa)

$$da/dN = 0.47 \times 10^{-8} (\Delta K)^{2.25} \qquad (16) \quad [123]$$

Equations 11 through 16 are plotted in Fig. 9, with each result identified in the caption. For these cases, Paris law crack propagation kinetics are essentially independent of stress ratio, with a slight tendency for higher da/dN with increasing R at fixed ΔK.

Threshold stress intensity range values, ΔK_{TH}, are highly variable, however, the following results are reasonable.

5. Normalized C-Mn Steels (σ_{ys} < 500 MPa)

$$\Delta K_{TH} = 6.0 \text{ to } 9.0 \text{ MPa}\sqrt{}\text{m} \text{ at } R = 0.1 \qquad (17) \quad [124\text{-}126]$$

$$\Delta K_{TH} = 3.0 \text{ to } 4.0 \text{ MPa}\sqrt{}\text{m} \text{ at } R = 0.7 \qquad (18) \quad [124]$$

6. Quenched and Tempered HSLA Steel (σ_{ys} = 900 MPa)

$$\Delta K_{TH} = 5.0 \text{ to } 6.0 \text{ MPa}\sqrt{}\text{m} \text{ at } R = 0.1 \qquad (19) \quad [125,127]$$

$$\Delta K_{TH} = 3.5 \text{ MPa}\sqrt{}\text{m} \text{ at } R = 0.7 \qquad (20) \quad [127]$$

The R dependence of ΔK_{TH} is empirically described by [128]:

$$\Delta K_{TH} \text{ at any } R = \Delta K^{\circ}_{TH} (1\text{-}R)^{t} \qquad (21) \quad [128]$$

where for normalized C-Mn steel, ΔK°_{TH} (threshold ΔK for R = 0) equals 10.8 MPa$\sqrt{}$m and t is 0.64 [92]. Alternately, Barsom and Rolfe argue that ΔK_{TH} varies with R for a wide variety of martensitic and ferrite-pearlite steels according to:

$$\Delta K_{TH} = 7.0 (1.0 - 0.85R) \text{ (MPa}\sqrt{}\text{m)} \qquad (22) \quad [123]$$

This equation provides a lower bound on threshold which is consistent with extensive data. A number of theoretical models for ΔK_{TH} have been proposed based on an energy balance, dislocation dynamics, and crack-tip plasticity [42-47]. A brief review of these models is given in the section "Overview of Environmental Cracking Mechanisms".

The fatigue behavior of steels in high vacuum is represented in Fig. 9 by the power law line and threshold stress intensity value reported by Speidel, Equations 9 and 10 with E equal to 200 GPa, and by the scatter band. The band for vacuum describes the bounds of

26

data for low strength C-Mn (1020 and BS4360:43A) and high strength quenched and tempered (Q1N, A537 and 4340) steels [92,129-133]. Monotonic yield strength varied from 300 MPa to 1030 MPa for these steels. The strength and microstructure of the steel do not appear to influence Paris regime fatigue crack propagation in vacuum. Vacuum FCP behavior can be represented by an average power law relationship from the middle of the band in Fig. 9. These rates are lower than the values predicted by the Speidel relationships. The slow rates of FCP in this inert environment, relative to moist air, are apparent; the latter is an embrittling environment.

For use in life prediction modeling, lines A and B in Fig. 9 represent the average crack growth rate behavior for steels in moist air and vacuum, respectively. These lines are represented by the following equations with ΔK in MPa$\sqrt{m}$ and da/dN in mm/cycle:

$$\text{Steels in Moist Air (Line A):} \quad da/dN = 4.08 \times 10^{-9} \, \Delta K^{3.11} \tag{23}$$

$$\text{Steels in Vacuum (Line B):} \quad da/dN = 9.48 \times 10^{-12} \, \Delta K^{4.52} \tag{24}$$

D. Aluminum Alloys in Moist Air and Vacuum (Figs. 10 and 11)

The FCP behavior of aluminum alloys, particularly in the Al-Li-X composition group, can be complicated by a significant contribution of extrinsic crack closure. The similitude concept is no longer applicable, as discussed in Chapter VIII on "Factors Complicating Life Prediction.

Intrinsic fatigue crack growth in aluminum alloys in moist air and vacuum is relatively insensitive to microstructure and stress ratio, and provides a reasonable basis for comparisons of environmental effects [120]. Crack closure effects are minimized at moderate to high stress intensity range levels, and for all ΔK at high mean stress (typically, for R $>$ 0.7). Conversely roughness-induced crack closure affects low stress ratio near-threshold FCP, particularly for tortuous crack path precipitation hardened aluminum alloys that deform by localized planar slip.

The intrinsic fatigue crack propagation behavior of high strength aluminum alloys exposed to moist air at 25°C is summarized in Fig. 10. Low ΔK ($<$ 6 MPa$\sqrt{m}$) data are exclusively for high stress ratios with R above 0.75 to minimize closure. For ΔK levels above about 6 MPa$\sqrt{m}$, Paris behavior is observed for a variety of alloys, as indicated by the shaded band reported by Clark [134]. For the indicated materials, the monotonic yield strength
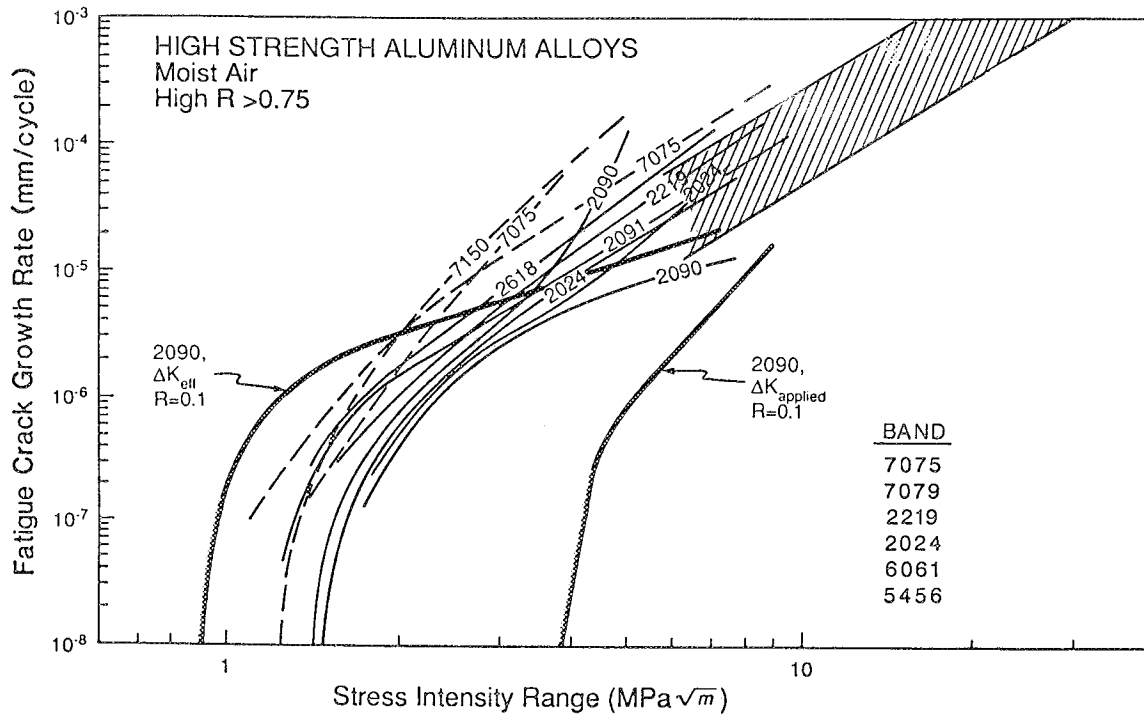
Fig. 10   Fatigue crack propagation behavior for high strength precipitation hardened aluminum alloys in moist air. Crack growth rate data were reported by Piascik [136] and Clark [134].

varies from 250 to 450 MPa. This shaded band contains data obtained at low stress ratios between R equalling 0 and 0.1, and at various loading frequencies between 1 and 30 Hz. Within this band, it is likely that crack growth rates increase with increasing R at any fixed ΔK. Frequency should have no resolvable effect on da/dN for the moist air environment. The upper and lower bounds of the data within the shaded band are given by the following equations, with da/dN in in/cycle and ΔK as ksi√/in.

$$da/dN = 1.5 \times 10^{-8} (\Delta K)^{3.0} \qquad (25) \quad [134]$$

$$da/dN = 0.25 \times 10^{-8} (\Delta K)^{3.0} \qquad (26) \quad [134]$$

Piascik and Gangloff employed an experimental method based on decreasing ΔK and increasing R at constant K_{max} to minimize the contribution of crack closure to EFCP [135,136]. The data obtained by this method for Al-Li-Cu alloys are reasonably consistent with the high ΔK, low R data in the shaded band. As a lower bound, ΔK_{TH} for many of the alloys approaches 1.3 MPa√/m.

Some advanced aluminum alloys, such as Al-Li alloy 2090, exhibit excellent and unique fatigue crack propagation resistance due to enhanced crack path tortuosity and resultant roughness-induced crack closure, as shown in Fig. 10. The intrinsic fatigue crack growth behavior of such materials can be given by either an effective stress intensity range approach ($\Delta K_{eff} = K_{max} - K_{cl}$) or by high mean stress results. Uncertainties are associated with each analysis (see "Factors Complicating Life Prediction").

Moist air is an aggressive environment for aluminum alloys, as indicated by the results in Fig. 11. Here, moist air data from Fig. 10 are compared to the "all material-modulus normalized" result (E = 85 GPa) from Speidel [119], and to specific data for alloys 7075 and 2090 tested in ultrahigh purity vacuum [135]. The modulus based result was obtained for low R of about 0.1, while the data for 2090 and 7075 were obtained by a constant K_{max} method where R increases from 0.1 at the highest ΔK examined to 0.9 near threshold. Work by Piascik indicates that similar low fatigue crack growth rates are produced in high strength aluminum alloys exposed to highly purified inert gases such as helium, argon and nitrogen [135]. There are no literature data to indicate a contradictory conclusion on the effects of physically adsorbed inert molecules, however, contamination limits the amount of definitive data.
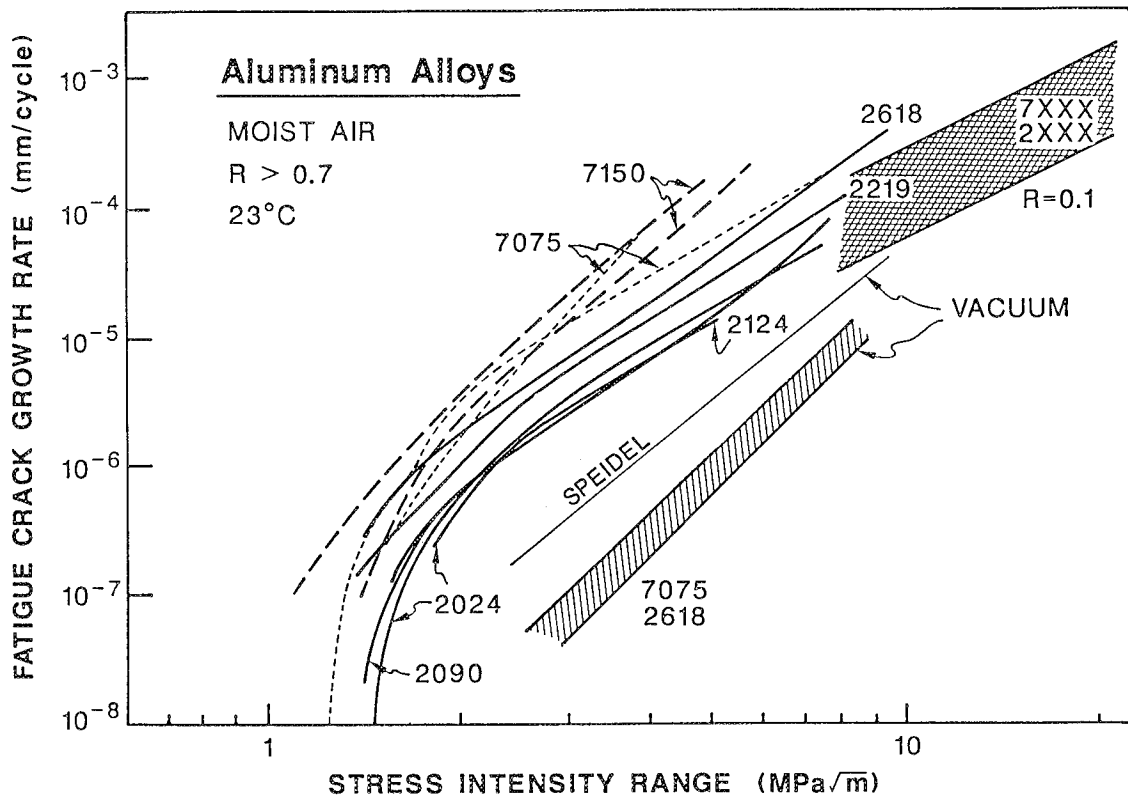
Fig. 11   Fatigue crack propagation behavior for high strength precipitation hardened aluminum alloys in ultrahigh purity inert vacuum. An elastic modulus of 85 GPa was employed to calculate the vacuum behavior after Speidel [119]. Crack growth rate data were reported by Piascik [135] and Clark [134].

Fatigue crack growth behavior in vacuum or other presumably inert gases must be interpreted with caution. Small amounts of water vapor, and perhaps oxygen, contamination can have large accelerating effects on crack growth rate. Water vapor in a vacuum system enhances growth rates above values typical of moist air because of an inhibiting effect of oxygen in the latter [135]. The critical level of water vapor approaches sub-part-per-million, particularly at high stress ratio, low loading frequency and perhaps near-threshold where crack advance may be discontinuous over many hundreds of load cycles. The data in Fig. 11 represent a high quality inert environment; reports of fatigue cracks growing faster in "vacuum" or "inert helium" compared to air are most likely explainable by contamination effects. In the least such claims must be supported by rigorous experimentation.

Comparing Figs. 10 and 11, 2000 series alloys exhibit superior fatigue crack growth resistance compared to 7000 series alloys, but only for moist air. This behavior is most likely due to the relative sensitivities of each class of alloys to hydrogen embrittlement from moist air. 2000 series alloys are less adversely affected by HEE.

E.   Nickel Based Superalloys in Moist Air   (Figs. 12 and 13)

A detailed literature search has not been conducted for fatigue crack propagation in high strength, precipitation hardened nickel based superalloys exposed to moist air. It is likely that a substantial amount of data exist and could be compiled if necessary.

Example data are presented in Figs. 12 and 13 for Inconel 718 in moist air at temperatures between 4 and 825 K [110,137]. The monotonic yield strength of this material is probably between 1100 and 1300 MPa. Results in Fig. 12 were obtained at high frequency (20 Hz), while the data in Fig. 13 are for low frequency (0.33 Hz); load cycling was continuous in both cases.

For high frequency 20 Hz loading in moist air, Paris regime crack growth rates increase mildly with increasing temperature for each data set. Comparison of the data for elevated temperature indicates that crack growth rates increase with decreasing loading frequency. Interestingly, the threshold stress intensity range increases with increasing temperature for low frequency cycling (Fig. 13), but declines with increasing temperature for fast frequency loading (Fig. 12). The origin of this difference, be it experimental variability or reflective of a frequency effect on fatigue damage, is not clear. Van Stone demonstrated
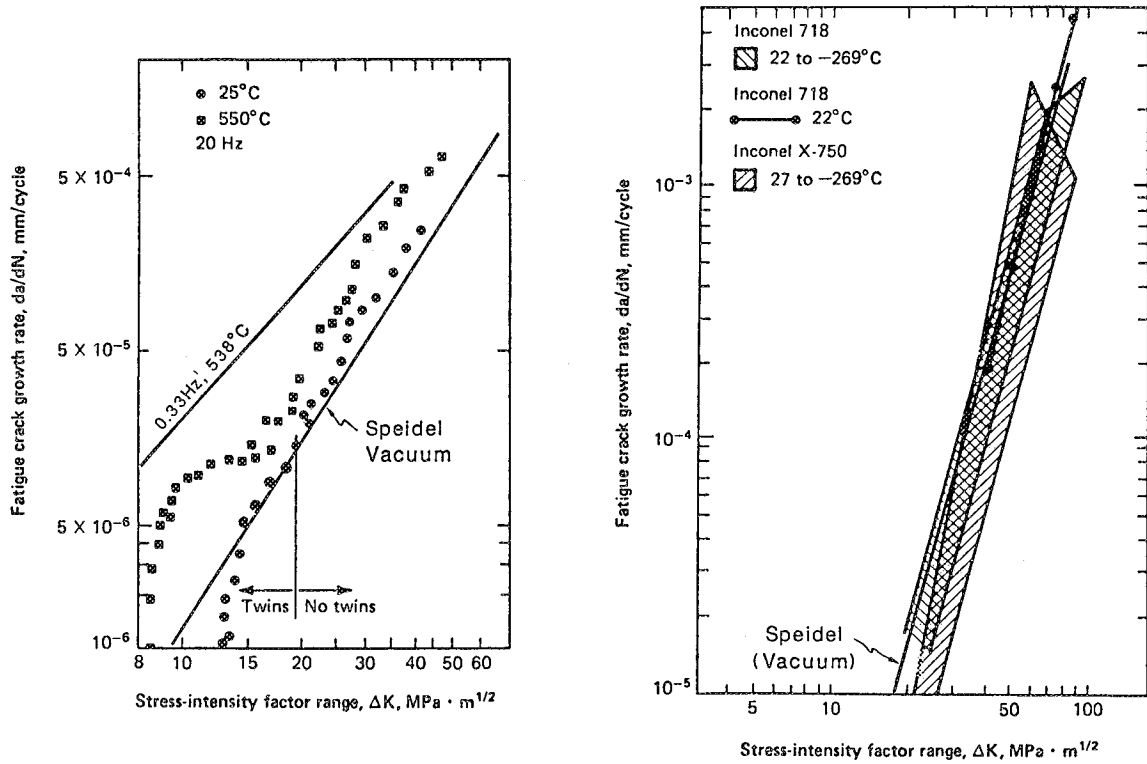
Fig. 12   Fatigue crack propagation in precipitation hardened high strength nickel based superalloys in moist air. An elastic modulus of 206 GPa was employed to calculate the vacuum behavior after Speidel [119]. Crack growth rate data were reported by Antolovich and Campbell [137].
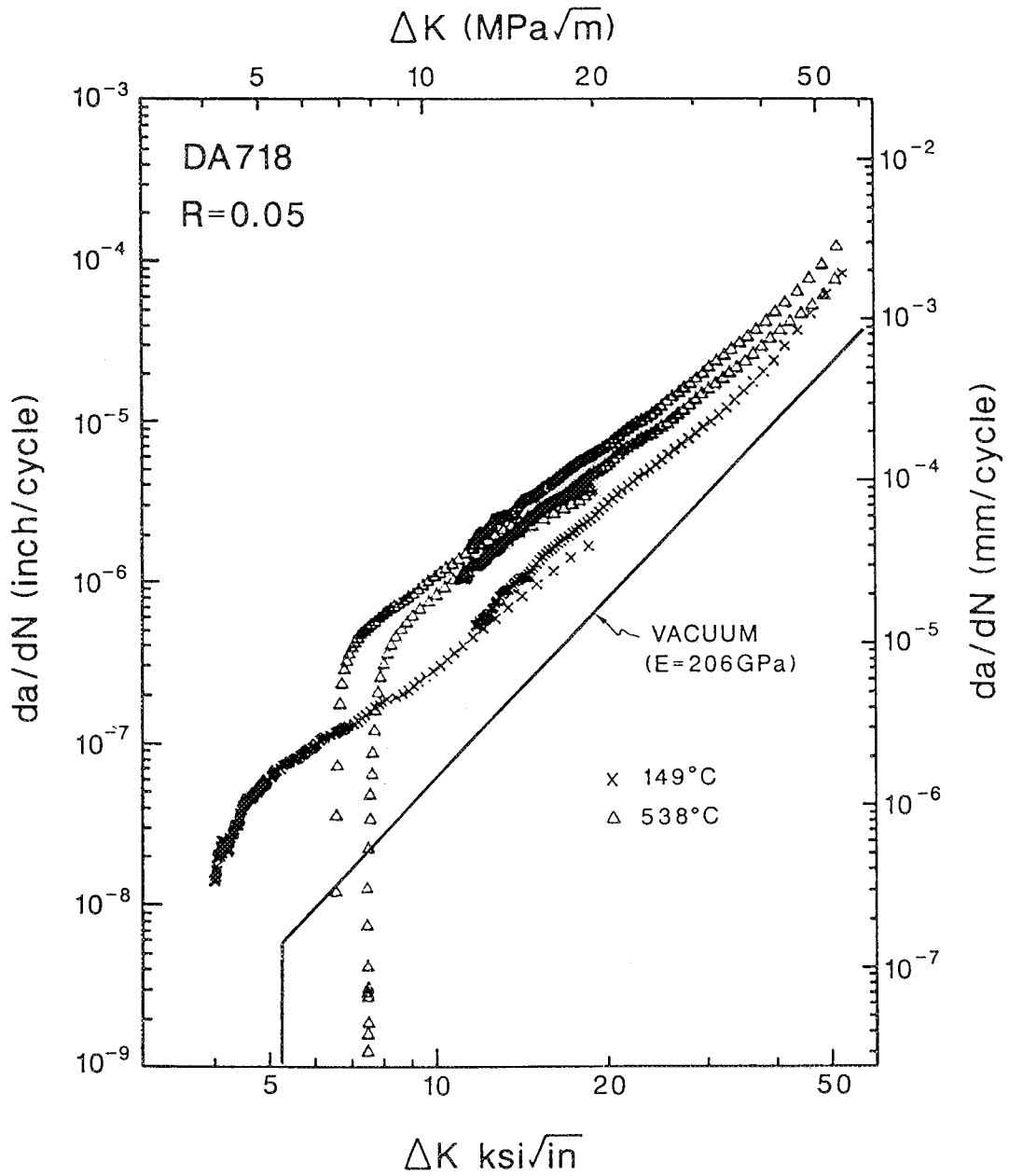
Fig. 13   Fatigue crack propagation in Inconel 718 in moist air at two temperatures. An elastic modulus of 206 GPa was employed to calculate the vacuum behavior after Speidel [119]. Crack growth rate data were reported by Van Stone [110].

that the temperature sensitivity of ΔK_{TH} is not due to oxide induced crack closure because the crack growth response of IN 718 at high mean stress is similar to that presented for low R in Fig. 13 [110]. The role of closure in Fig. 12 is not clear. A more extensive literature search is required to clarify the issues implied in Figs. 12 and 13.

Moist air is aggressive compared to vacuum, as indicated by the comparison with the modulus normalized result from Fig. 8 using an assumed modulus of 206 GPa. While the effect is minimal at 25°C, a substantial difference between air and vacuum behavior is observed for the elevated temperatures, Fig. 13.

F.   Titanium Alloys in Moist Air and Argon   (Fig. 14)

Fatigue crack growth rate data for titanium alloys have not been systematically reviewed. Typical results are presented in Fig. 14. The behavior predicted by the modulus normalization approach (Fig. 8 and Equation 9 with E = 120 GPa) is indicated by the solid line. Specific data were reported by Bucci for Ti-8 wt%Al-1Mo-1V cycled in either argon or aqueous NaCl at 25°C [138]. The latter case is considered in an ensuing section. The data for the argon environment are in reasonable agreement with the modulus normalization for low R of 0.05 and are independent of loading frequency. Increased R to 0.5 produced higher FCP rates for Ti-8-1-1 in the argon environment, compared to the data for R = 0.05 in Fig. 14 [138]. The purity of the argon environment, particularly the degree of water vapor contamination, is unclear; growth rates may reflect the aggressive action of trace H_2O, as discussed for aluminum alloys. The Speidel line may provide a reasonable indication of the FCP behavior of α/β-titanium alloys in inert vacuum.

For ΔK levels above about 6 MPa√m, Paris behavior is observed for a variety of titanium alloys in moist air, as indicated by the shaded band reported by Clark [134]. For the indicated materials, the monotonic yield strength varies from 790 to 1040 MPa. This band contains data obtained at low stress ratio between R = 0 and 0.1 and at various loading frequencies between 1 and 30 Hz. Within this band, it is likely that crack growth rates increase mildly with increasing R at any fixed ΔK. Frequency should have no resolvable effect on da/dN for the moist air environment. The upper bound and mean of the data are
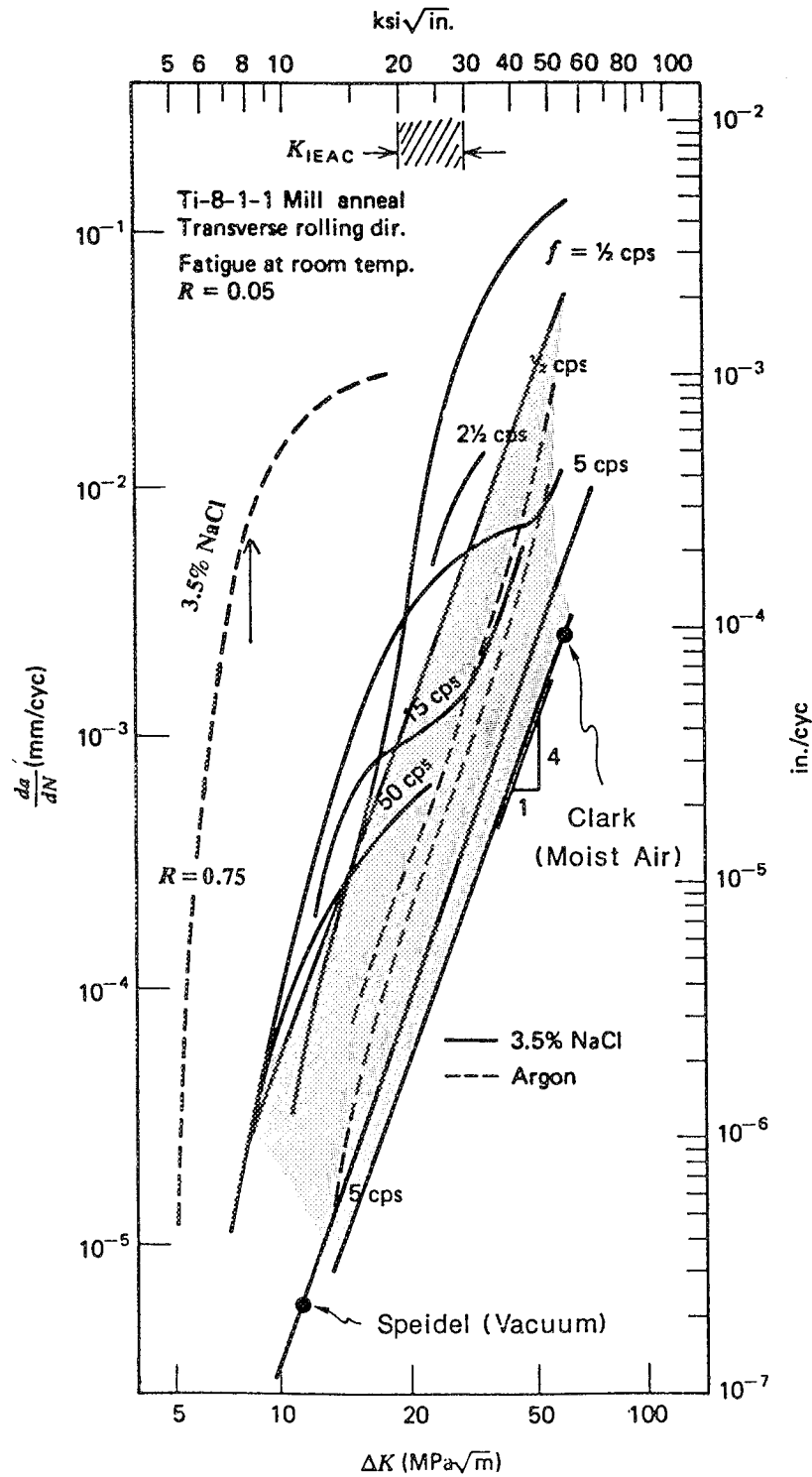
Fig. 14   Fatigue crack propagation behavior for titanium alloys in argon and moist air; after Hertzberg [139]. A modulus of 120 GPa was employed in the modulus normalization calculation [119]. Crack growth rate data were reported by Bucci [138] and Clark [134].

35

given by the following equations, with da/dN in in/cycle and ΔK as ksi$\sqrt{in}$.

$$da/dN = 2.0 \times 10^{-10} (\Delta K)^{4.0} \qquad (27) \quad [134]$$

$$da/dN = 0.40 \times 10^{-10} (\Delta K)^{4.0} \qquad (28) \quad [134]$$

IV. MONOTONIC LOAD ENVIRONMENTAL CRACKING

A. Introduction

Monotonic load environmental cracking processes include stress corrosion cracking (SCC), hydrogen environment embrittlement (HEE) and liquid metal embrittlement (LME), with SCC often employed as a generic descriptor of this failure mode. Each of these cracking modes can occur in a precracked fracture mechanics specimen subjected to constant applied load (increasing K with crack extension), constant displacement (decreasing K with crack extension), as well as constantly increasing load or load-line displacement at a fixed rate (increasing K with load/displacement and crack extension).

Aerospace alloys based on Al, Ti, Ni, and Fe are susceptible to monotonic load environmental crack propagation (MECP) [23,24,30,33,140-142]. As an example, high strength steels fail by stress corrosion cracking, most probably due to hydrogen embrittlement, in a variety of hydrogen producing environments including H_2 [33,68,143-145]. The degree of embrittlement increases with increasing yield strength and hydrogen environment activity, and is maximized near ambient temperature. Aluminum alloys, particularly the high-strength precipitation-hardened series, are sensitive to SCC in moist air and aqueous solutions with various halogen ions [146,147]. Susceptibility strongly depends on alloy aging characteristics, where slight-overaging provides a beneficial effect; and on crack orientation, where precracks parallel to major planes of thermomechanical extrusion, forging or rolling are particularly prone to SCC. Despite good corrosion characteristics, nickel based superalloys are sensitive to SCC in a number of environments including high pressure H_2, pure water in certain stress-microstructure combinations, and sodium hydroxide solutions [79,80,148]. Titanium alloys are vulnerable to SCC in aqueous chloride, alcohols and methanol-hydrochloric acid solutions [149-151].

Apart from being an important individual failure mode, monotonic load cracking is critical to environmental fatigue crack propagation in aerospace alloys. Monotonic load data indicate alloy/environment systems that will be susceptible to EFCP. Often, MECP is a prime contributor to the time-dependent component of environment enhanced fatigue crack growth rates, as modeled by linear superposition. FCP behavior is significantly influenced when K values in fatigue deformation exceed the threshold for monotonic load crack growth to occur. Therefore, it is important to understand and quantify the contribution of monotonic

load cracking to EFCP. In many cases EFCP extends well beyond the domain where an alloy is susceptible to monotonic load cracking. Accordingly, MECP data must be employed as one of many inputs to the environmental fatigue life prediction problem.

The objective of this chapter is to provide the basis in monotonic load environmental crack propagation that is necessary to categorize, understand and model EFCP. The general aspects of monotonic load environmental cracking are reviewed. Susceptible alloy-environment systems are identified, with emphasis on those relevant to the aerospace applications. Environmental and metallurgical variables that affect monotonic load crack growth kinetics are assessed for specific alloy-environment systems.

B.   LEFM Approach to Monotonic Load Environmental Cracking

Classic SCC studies did not isolate the sequential nucleation and growth stages of cracking; smooth specimens were typically employed to generate applied stress or strain versus total time to failure for an aggressive environment. Since the pioneering work of Brown [149,152], the linear elastic fracture mechanics approach was successfully adopted to characterize MECP [153-155]. The LEFM approach determines the relationship between the macroscopic and time-based crack propagation rate, da/dt or v, as a function of applied opening mode stress intensity factor, K_I. Such data can be directly employed for alloy selection and for damage tolerant life prediction, analogous to the LEFM approach to FCP illustrated in Fig. 1, and based on the concept of K similitude. Equal MECP rates should be realized for equal applied K, comparing a laboratory specimen and a structural component.

Numerous experiments on alloys in a variety of environments show that da/dt versus K relationships for conditions of constant material and environmental variables have the general form illustrated in Fig. 15 [24,156]. The curve is composed of three distinct regions of crack growth behavior designated as Stages I, II, and III. In Stages I and III, crack growth rates strongly depend on applied stress intensity. At intermediate K levels within Stage II, crack growth rate is often independent of stress intensity, giving a so-called plateau appearance. Alternately, Stage II da/dt may increase as a mild power-law function of K. The Stage I crack growth rate dependence on applied K is attributed to the combined chemical and mechanical driving forces for cracking, while Stage II crack growth is controlled by a rate limiting mass transport or chemical/electrochemical reaction process in the solution filling the
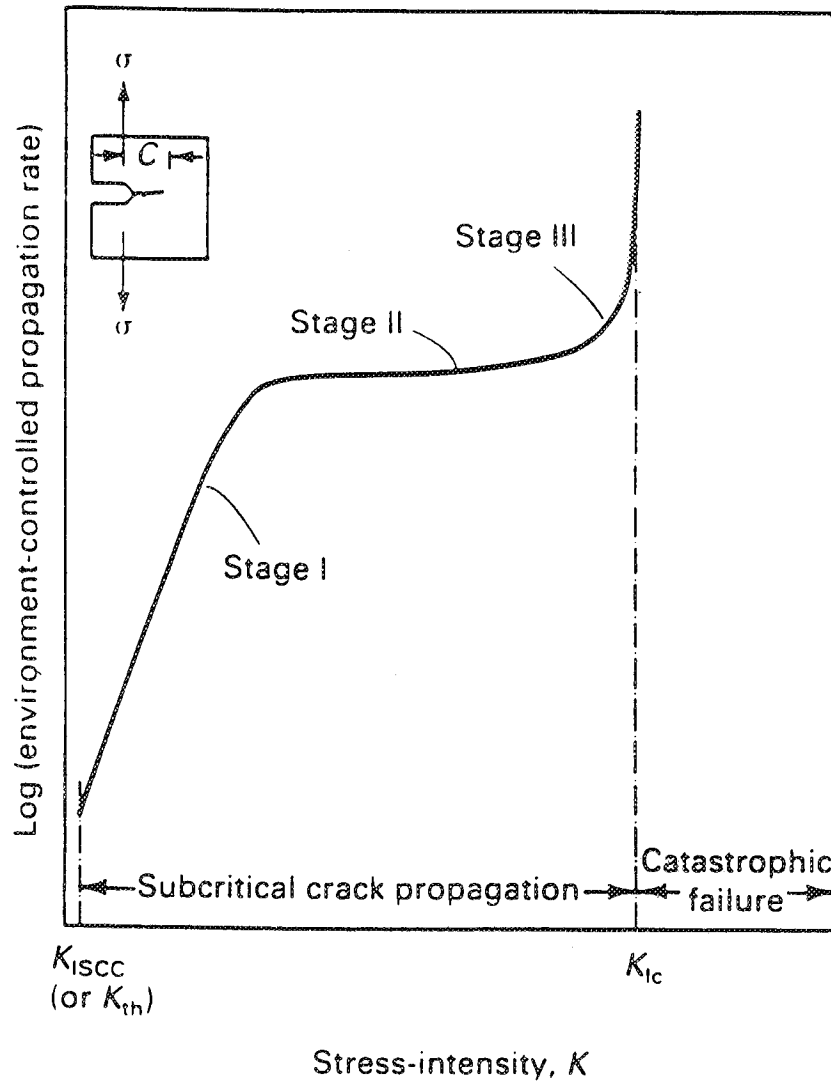
Fig. 15   The general form of the subcritical MECP rate versus stress intensity factor relationship [24].

crack, on the straining crack tip surface, or within the crack tip process zone. Region III results from predominantly mechanical separation.

Data of the type illustrated in Fig. 15 establish that MECP is governed by apparent threshold behavior. The highest value of stress intensity factor, in plane strain and at which subcritical crack growth does not occur in a material monotonically loaded in an aggressive environment, is called K_{ISCC} (or more recently, K_{TH} or K_{IEAC}). Experimental determination of K_{IEAC} depends on test time and the specific fracture mechanics method, be it rising load or crack arrest. Several problems hinder the measurement of an MECP threshold; including the lack of a published ASTM Standard Method, prolonged nonsteady state incubation times prior to crack growth at any K, and the large number of variables that affect K_{IEAC}. High-strength steels and titanium alloys exhibit a well-defined K_{IEAC} after a reasonable test period [140]. K_{IEAC} values for high-strength aluminum alloys, particularly in nonsusceptible crack orientations, and for lower strength ferritic and stainless steels tend to decrease with increasing test time [146]. For such cases, on the order of 5000 hours are necessary to determine a reasonable threshold. A first standardized method for K_{IEAC} determination is currently being balloted by the ASTM Committee E24 on Fracture Mechanics [157].

C. Stress Corrosion Cracking Failure Mechanisms

Many detailed mechanisms for monotonic load environmental cracking have been postulated for specific metal-environment combinations [140,158-161]. As pointed out by Staehle [161], however, a general mechanism for "stress corrosion cracking" is an unreasonable and unattainable goal; one or more specific processes appear to operate under specific metallurgical and environmental conditions. Proposed MECP models are basically in three groups and mirror the mechanisms put forth in Chapter II for environmental FCP. A reasonable view is that a common chemo-mechanical mechanism exists for MECP and EFCP, with cyclic plastic strain in the latter uniquely affecting the damage mechanism.

1. Dissolution Models

The film rupture mechanism for MECP postulates that metal at the crack tip is protected by a passive surface film. Loading causes crack tip plastic deformation which ruptures the film and permits rapid anodic dissolution of the exposed substrate; crack tip advance occurs during repassivation after the film rupture, and the entire sequence is repeated

[76,107,161,162]. Nondeforming crack walls remain protected by the passive film to maintain a sharp crack tip. This mechanism is analogous to the film rupture model for environmental fatigue crack growth, illustrated in Fig. 6, with the crack tip strain rate central to each phenomena [38,105,106].

In the slip dissolution model, crack tip slip ruptures the surface oxide film and dissolution occurs along an active path to advance the crack. This model was originally proposed to account for SCC in precipitation hardened aluminum alloys. In such alloys compounds such as $MgZn_2$, which are anodic with respect to their surroundings along a grain boundary, dissolve preferentially and the applied stress tears remaining ligaments of near-grain boundary material.

An essential aspect of dissolution models concerns the kinetics of the repassivation process [163]. If repassivation takes place too rapidly, corrosion is insufficient for an increment of crack growth. If repassivation takes place too slowly, then excessive corrosion creates a blunt fissure or deep pit rather than a sharp crack.

2. Adsorption Model

This model hypothesizes that atomic species adsorb and interact with strained bonds at the crack tip to reduce bond strength and permit brittle fracture at low stress [164,165]. While often advocated as an LME mechanism, the applicability of this model to MECP is questioned. There is no direct evidence of reduced bond strength induced by adsorbed species in metals. Many atoms or molecules (e.g., O_2) strongly chemisorb on clean metal surfaces, but do not promote brittle crack advance. Moreover, this model does not explain the impact of extensive highly localized crack tip plasticity on crack growth. The adsorption concept has not been developed into a quantitative model of da/dt as a function of K.

3. Hydrogen Embrittlement Model

Monotonic load crack growth in many material-environment systems may proceed by the hydrogen embrittlement process represented in Fig. 5 [68]. Identical mass transport, chemical/electrochemical reaction and process zone embrittlement steps are likely involved in both MECP and EFCP by hydrogen environment embrittlement. A variety of quantitative da/dt versus K models have been developed based on these ideas, as discussed elsewhere [13,34,35,68,95,96,143,145,166-170]. These models, particularly those for K_{IEAC}, are the most developed predictive descriptions of MECP. Such models indicate the effects of a

41

variety of variables on K_{IEAC}, however, each contains unknown adjustable parameters which preclude precise predictions of absolute threshold values.

D. Relationship between MECP and EFCP

If stress intensity levels in the fatigue load cycle exceed K_{IEAC}, and if da/dt is significant when converted to an increment of crack advance per fatigue load cycle, then MECP will contribute and possibly dominate rates of environmental fatigue crack propagation. As an example, the 7079-T651/NaCl system is characterized by a K_{IEAC} value of 4 MPa/m with a substantial sustained load crack growth rate (da/dt $\approx$ 2 x 10^{-2} mm/sec). The fatigue crack growth rate for Al 7079 in aqueous NaCl solution will be significantly influenced by monotonic load cracking when K_{max} exceeds 4 MPa/m. Da/dN in this alloy is time-dependent and depends on stress ratio, each effect is accurately predicted by the simple superposition of da/dt-K data with inert environment da/dN-ΔK. In contrast Stage II stress corrosion crack velocities for other 7000 series aluminum alloys are approximately 4 x 10^{-5} mm/sec. Even if such velocities apply throughout the fatigue stressing cycle, linear superposition does not sufficiently account for the observed rates of EFCP. A detailed discussion of the superposition model and its implication regarding the relationship between corrosion fatigue and stress corrosion cracking is given in the section "Quantitative Crack Growth Rate Models".

Environment enhanced fatigue crack growth response was originally characterized by three general patterns of behavior, as illustrated in Fig. 16 [171]. Each form of da/dN versus ΔK for EFCP is understood based on K_{IEAC} for monotonic load environmental cracking. The simplest behavior, Type B, represents those alloy/environment systems where there is substantial environment-enhanced monotonic load crack growth during fatigue; that is EFCP only occurs at those ΔK and R values where K_{max} exceeds K_{IEAC} and where da/dt is relatively high. For such cases, da/dN for the environment substantially exceeds fatigue crack propagation rates for the same alloy in benign or inert environments. Da/dN for the aggressive environment increases with increasing R at any ΔK above the K_{IEAC} criterion, and with decreasing loading frequency where EFCP is purely time-dependent.

Figure 17 provides an excellent example of Type B corrosion fatigue crack growth in high strength 4340 steel in distilled water [119]. This high strength steel is susceptible to
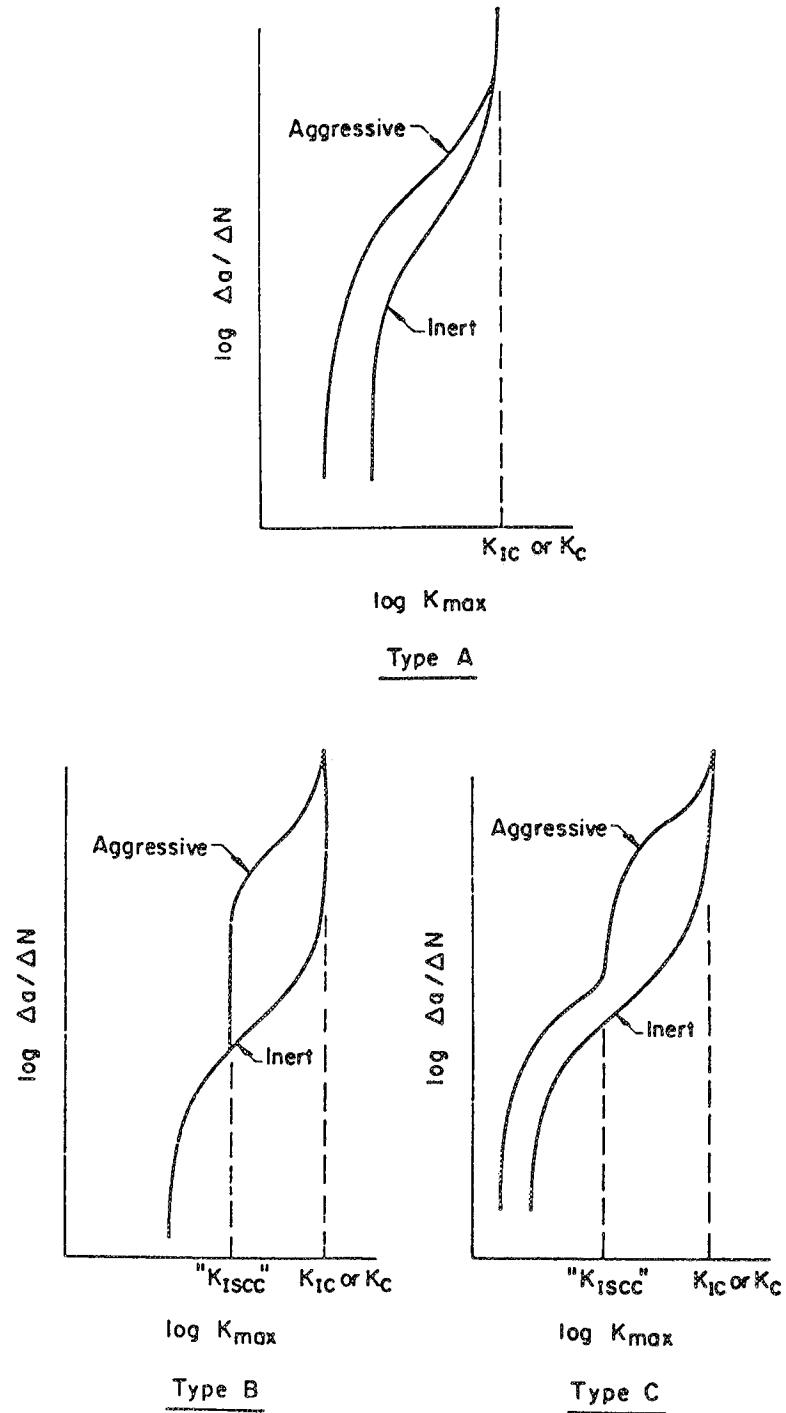
Fig. 16   Schematic representations of the types of environmental fatigue crack propagation rate behavior. After McEvily and Wei [171].

SCC in the distilled water environment with a K_{IEAC} value of 18 MPa/m and an average Stage II crack growth rate of 10^{-2} mm/sec. At ΔK greater than 10 to 12 MPa/m for R = 0, da/dN is strongly enhanced by the environment and increases with decreasing frequency. The steep increase in da/dN with increasing ΔK in this region, and that da/dN is proportional to the inverse of loading frequency and thus directly proportional to the time per load cycle, are indicative of Type B EFCP. Note that the onset of the strong frequency dependent environmental effect on da/dN occurs at K_{max} values somewhat less than K_{IEAC}, indicated by the vertical arrow. Either the threshold for MECP (18 MPa/m) was not precisely determined for this lot of steel, or the environmental effect on FCP was truly exacerbated by cyclic loading, as discussed with regard to Types A and C behavior. Note that environment also increases da/dN for ΔK levels between 6 and 10 MPa/m in Fig. 17. Fatigue crack growth in this regime is not frequency sensitive and occurs at K_{max} less than K_{IEAC}.

A critical aspect of environmental FCP is that environment can substantially enhance da/dN at ΔK and K_{max} levels well below K_{IEAC} [67]. Materials that are essentially immune to MECP can be prone to environment enhanced FCP. These cases are illustrated by Types A and C response in Figure 15. While Type B behavior is common for high strength, SCC prone alloy/environment systems, Types A and C behavior are a common scenario for low- to moderate-strength alloys that are either immune to SCC or exhibit high K_{IEAC} and low da/dt. An example of Type A behavior is given in Fig. 18, which illustrates the effect of loading frequency on fatigue crack growth rates for 12Ni-5Cr-3Mo steel in aqueous NaCl and at K_{max} levels below K_{IEAC} [67]. In this case crack growth is both time and cycle-dependent and is substantially more difficult to model [13,172]. Realistically, many alloy-environment systems exhibit EFCP behavior that falls between the two extremes (Type C). Indeed, Type C behavior is a combination of the Types A and B.

As extensive data have been collected to characterize environmental effects on FCP, the complexity of the possible relationships between applied ΔK and crack growth rates has become apparent [87]. One or more of the features of the da/dN-ΔK relationship that is schematically illustrated in Fig. 19 may operate for a given material-environment system. When K_{max} exceeds K_{IEAC}, da/dN is substantially enhanced by MECP and is predominantly time dependent; that is da/dN is proportional to reciprocal frequency. The diagnostic for this behavior is the steep rise in da/dN at a single ΔK level and the magnitude of the resulting FCP

44

steel 4340 M

2,5 mm thick plate
austenitized 870°C
tempered 300°C [2h]
TYS 1700 MN/m²
UTS 2000 MN/m²
crack orientation WL
sinusoidal load wave
R = 0 , 23°C

□ 10⁻³ Hz
▩ 10⁻² Hz   } dist.
○ 10⁻¹ Hz   } H₂O
× 1 Hz
⊕ 4 Hz

△ 4 Hz, vacuum
10⁻⁵ Torr

$$\left(\frac{K}{TYS}\right)^2 \approx \frac{B}{2.5}$$
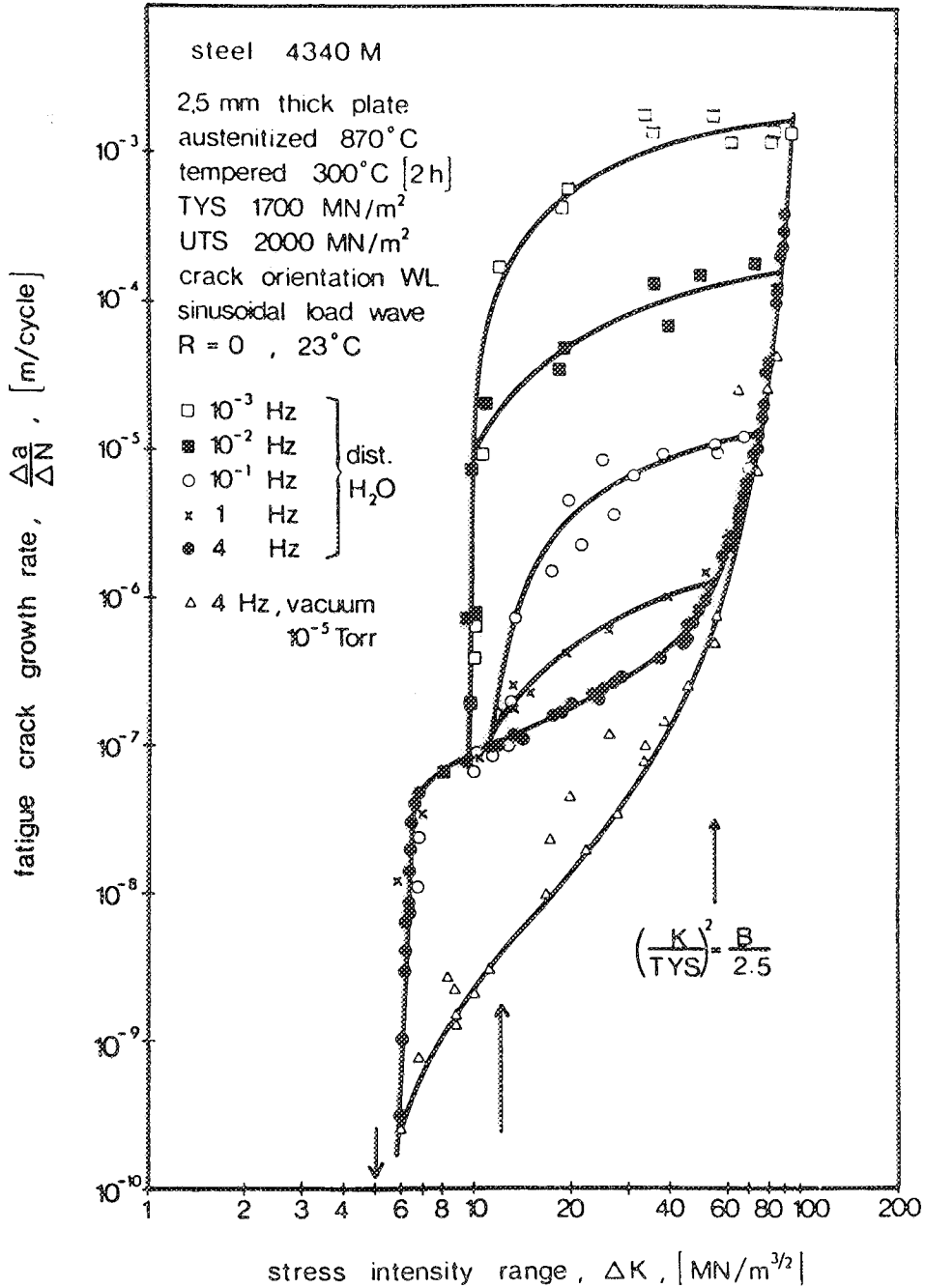
Fig. 17   Effect of cyclic frequency on the corrosion fatigue behavior of high-strength 4340 steel exposed to water or vacuum. After Speidel [119].
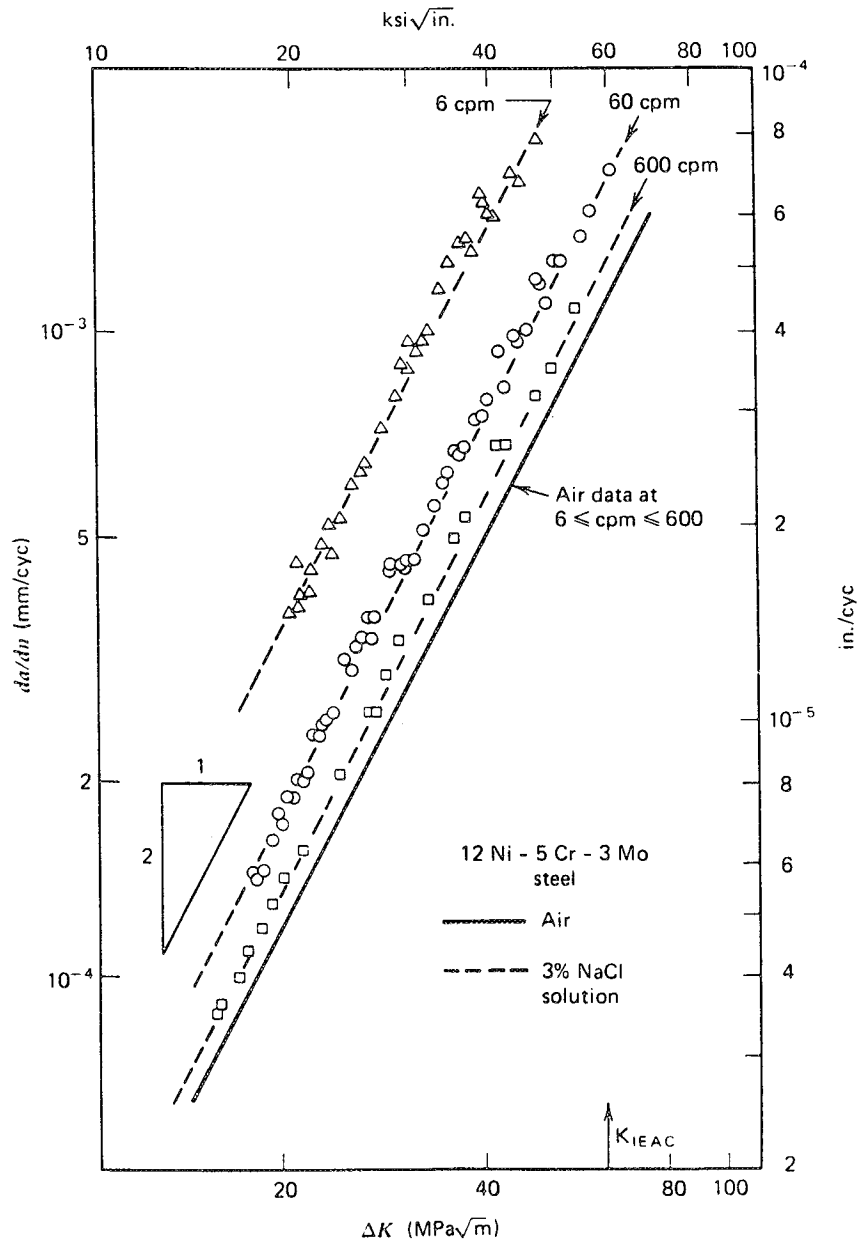
45

Fig. 18   Effect of frequency on fatigue crack growth kinetics (below K_{IEAC}) for 12Ni-5Cr-3Mo steel in aqueous NaCl. After Barsom [67]; reprinted from Hertzberg [139].
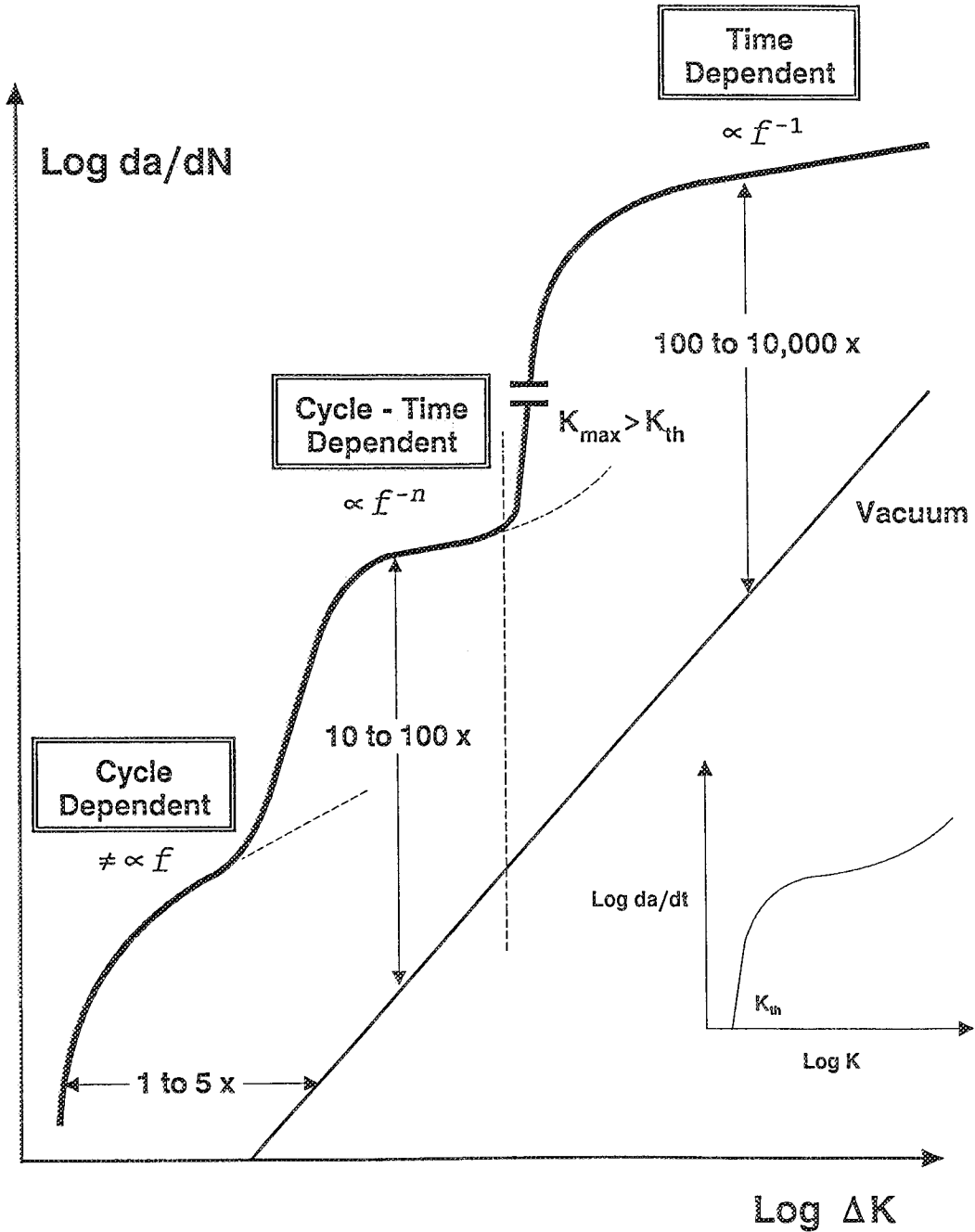
Fig. 19   Schematic illustration of possible environment-induced complexities in da/dN versus ΔK behavior.

rates. When K_{IEAC} is above all K levels in a loading cycle, environment may none-the-less affect da/dN, however, the magnitude of the enhancement is reduced as indicated by the mid-region in Fig. 19. Da/dN for this case depends on frequency raised to a power between 0 and -1, and is time-cycle-dependent. This type of EFCP behavior is often referred to a "cyclic load stress corrosion cracking" based on the notion that K_{IEAC} has been reduced by cyclic plastic deformation during fatigue. This view assumes a mechanism and it is perhaps more reasonable to argue that cyclic deformation has intervened to affect one or more elements of the dissolution or hydrogen mechanism. A final EFCP behavior is sometimes observed for ΔK levels near threshold, as indicated by the low ΔK response in Fig. 19. Here, ΔK_{TH} is lowered and da/dN values are increased by environmental exposure compared to an inert environment reference case such as vacuum. Such environmental enhancements are not influenced by loading frequency; FCP is only cycle-dependent and is often referred to as "true" corrosion fatigue [119,173]. Time-cycle-dependent cracking at low to moderate frequencies can change to purely cycle dependent cracking at higher loading frequencies. Some or all of the complex ΔK and f dependencies of da/dN, represented in Fig. 19, are likely for a given material-environment system. The challenge for life prediction modeling is clear. Accurate growth rate laws must be determined based on some combination of laboratory experimentation and mechanism-based modeling.

E. Alloy-Environment Systems Susceptible to MECP

1. Monotonic Load Environmental Cracking in Steels

Any class of steels, given the right combination of environment, stress intensity, temperature, and environment activity (e.g., gas pressure and purity, electrode potential), is susceptible to monotonic load environmental cracking. Particularly, high-strength steels exhibit an extreme sensitivity to MECP in hydrogen producing environments, including distilled water, aqueous NaCl solution and gaseous hydrogen [33,119,144,145,174,175]. As illustrated in Fig. 17, EFCP behavior in high-strength steels is largely determined by the influence of stress corrosion cracking when K_{max} is above K_{IEAC}.

A literature review established that K_{TH} (or K_{ISCC} or K_{IEAC}), for steels in various gases and electrolytes which are capable of producing atomic hydrogen on crack tip and boldly exposed specimen surfaces, decreases sharply with increasing σ_{ys} and hydrogen environment

activity [145,176]. Lower bounds on K_{IEAC} versus σ_{ys} are presented in Fig. 20 for ferrite-pearlite, bainitic and martensitic steels stressed in five hydrogen producing environments. These lower bounds represent the results of over 500 laboratory determinations of K_{IEAC} and may be employed to assess the nature of the likely environmental effect on da/dN versus ΔK. Very high strength steels (σ_{ys} above 1100 MPa) are severely embrittled by each environment, with a common K_{IEAC} level between 10 and 15 MPa$\sqrt{m}$. Low strength steels can be strongly hydrogen embrittled, but only by very aggressive, sulfur bearing hydrogen environments. Accordingly, environmental fatigue in high strength steels will often be of the "above K_{ISCC}" type, while "sub-K_{IEAC}" will be encountered for low to moderate strength steels in environments such as hydrogen gas. Finally, exceptions exist as illustrated by the data for thermally hydrogen charged Cr-Mo-V pressure vessel steels [145]. Here, severe MECP was caused by either a uniquely sensitive bainitic microstructure, dynamic loading to K_{IEAC}, or high resolution crack length detection [177].

The effects of microstructure and heat treatment on susceptibility to MECP were broadly examined for high-strength steels. Fig. 21 shows the MECP behavior of ultra high-strength AISI 4340 and 300-M steels in distilled water [174]. AISI 4340 steel is a widely used high-strength steel in structural components such as aircraft landing gears. 300-M steel has basically the same composition as that of 4340 steel, but with an enhanced Si content and with about 10 % retained austenite for the case represented in Fig. 21. Both AISI 4340 and 300-M steels are susceptible to cracking with similar K_{IEAC} values of 18 MPa$\sqrt{m}$ in this particular condition. The beneficial effects of Si addition and retained austenite are observed in Stage II growth rates. For example, 300-M showed almost one order of magnitude decrease in da/dt compared to that of 4340 steel. The beneficial roles of silicon and retained austenite on the susceptibility to SCC in ultrahigh strength steels are rationalized in terms of hydrogen embrittlement mechanisms for SCC, and are attributed to a reduction in the diffusivity of hydrogen in iron, consistent with the observation of lower Stage II growth rates. It is not known if similar effects would be operative in EFCP for similar material-environment systems.

Fig. 22 shows da/dt versus stress intensity for: (a) AISI 4340 steel in 3.5% NaCl solution [178], and (b) 12% Cr martensitic stainless steel in distilled water [119]. Fig. 22a clearly demonstrates that increasing tempering temperature decreases strength and,

49
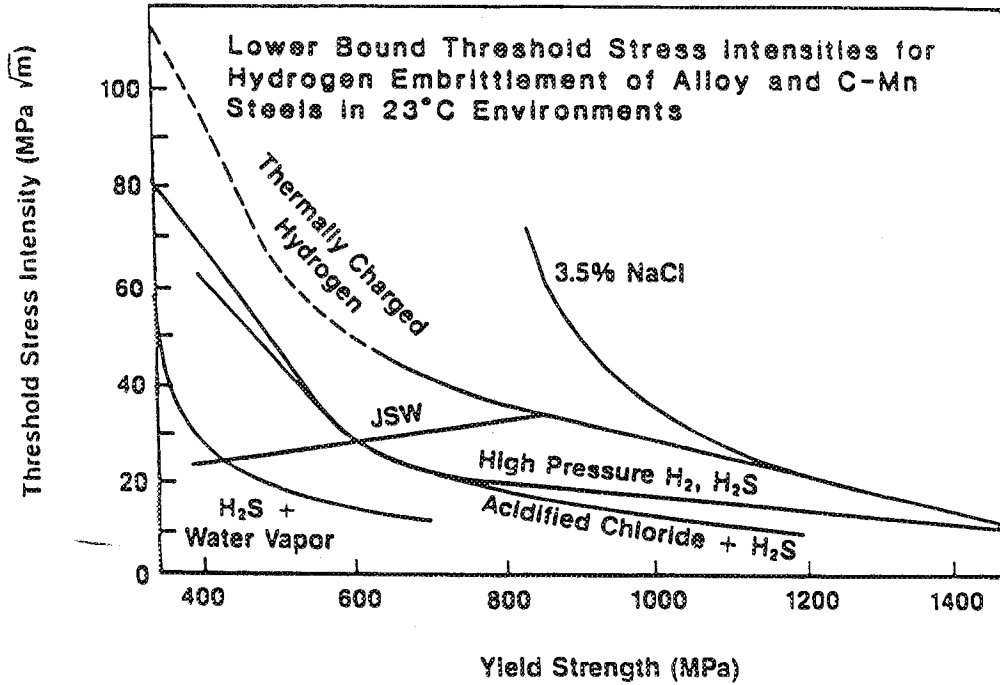
Fig. 20   Lower bounds on K_{TH} versus σ_{ys} for ferrite-pearlite, bainitic and martensitic steels stressed in five hydrogen producing environments. After Gangloff [145].
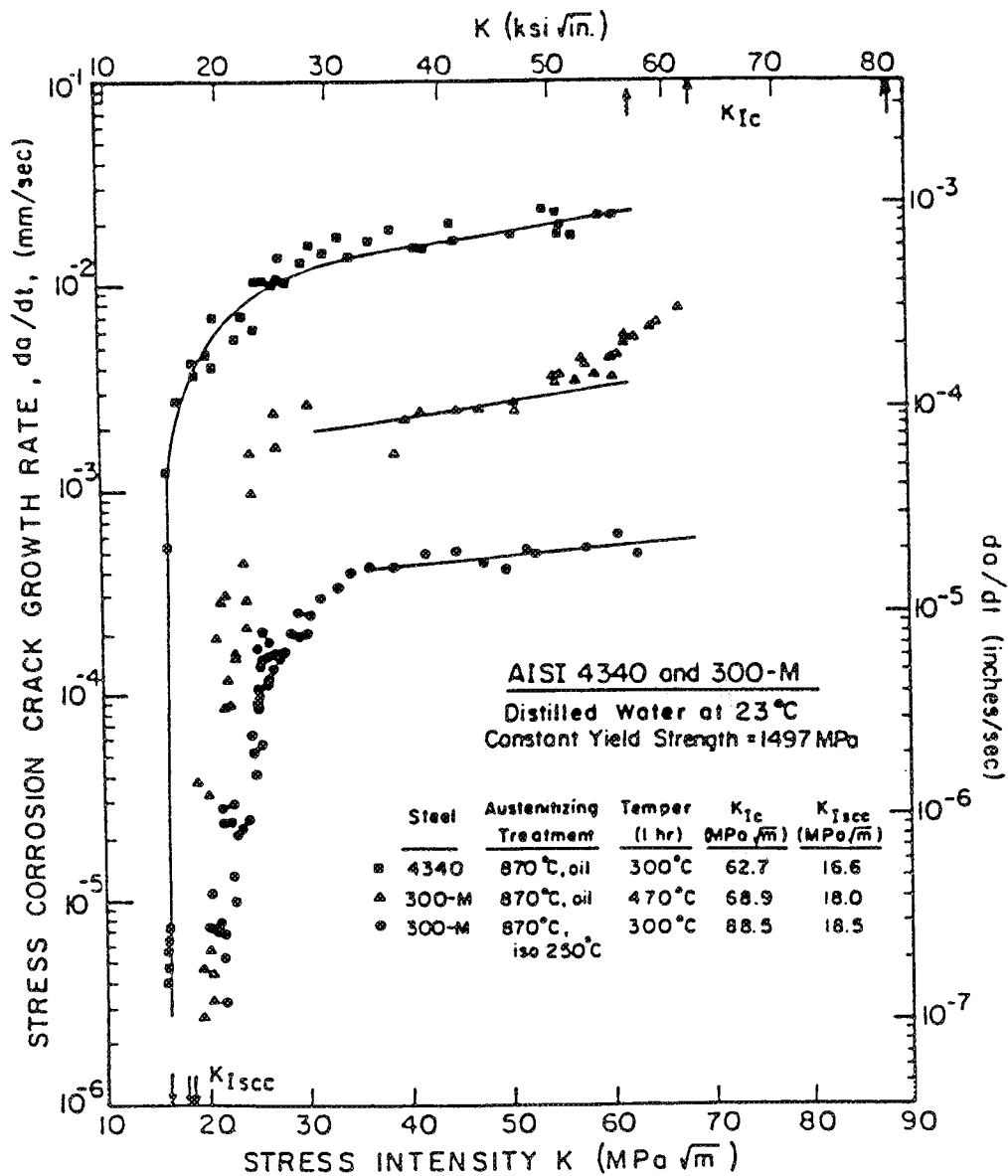
Fig. 21   Environmental crack growth rate (da/dt) versus applied stress intensity for quenched and tempered 4340 and 300-M steels in distilled water at ambient temperature. After Ritchie, et al. [174].

51
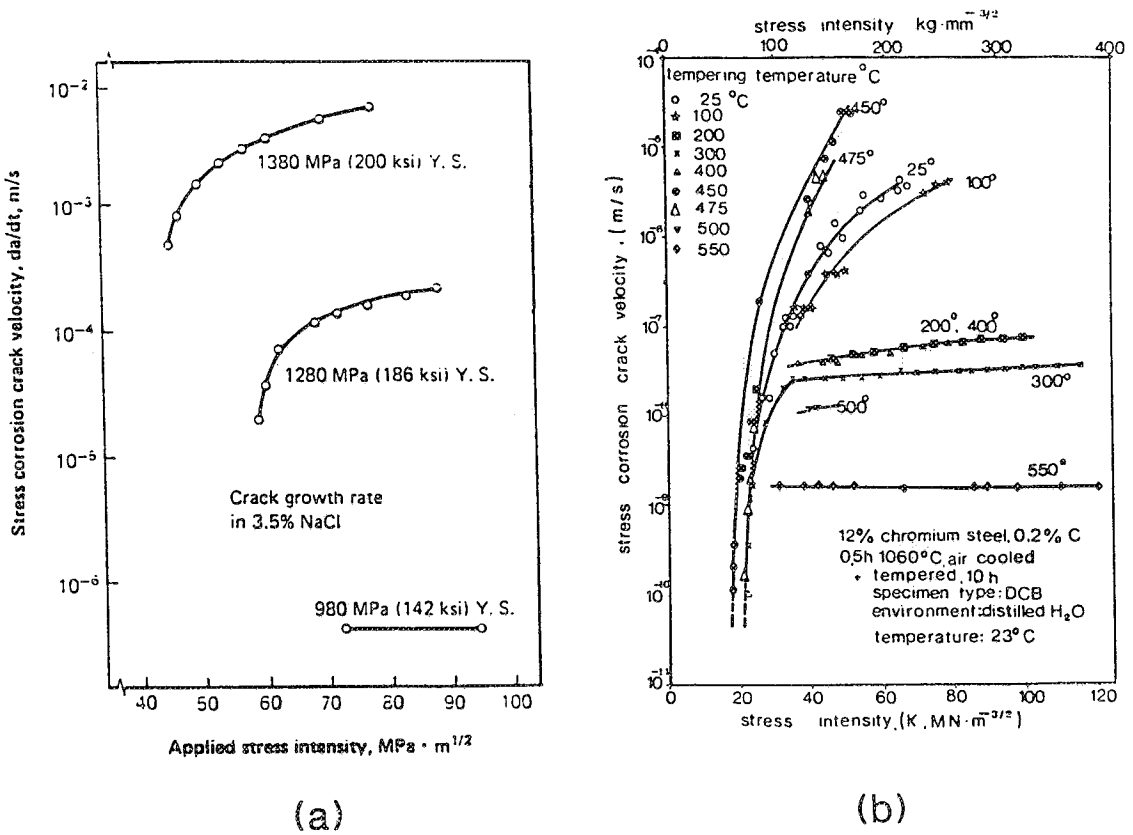
Fig. 22 Effect of tempering temperature on da/dt-K for: (a) 4340 steel in NaCl; after Speidel [119], and (b) 12% Cr martensitic steel in distilled water; after Colangelo et al. [178].

concurrently, decreases the MECP rate for AISI 4340 steel in aqueous NaCl solution. 12% Cr martensitic steel showed a similar trend except at tempering temperatures of 450 and 475°C, as illustrated in Fig. 22b. Alloy steels generally exhibit this behavior; lowering the strength increases the K_{IEAC} value, as shown in Fig. 20.

Fig. 23 demonstrates the effect of H_2 partial pressure (P_{H2}) on K_{IEAC} for high strength (σ_{ys} = 1340 to 1650 MPa) steels stressed at 300 K [145,176]. The inert environment fracture toughness for such steels varies between 60 and 100 MPa√m, while K_{IEAC} values as low as 18 MPa√m are reported. Threshold increases to 38 MPa√m as P_{H2} decreases to 2 kPa.

The effect of temperature on MECP behavior in high-strength steels is complex. Extensive studies on the temperature effect for high-strength steels were performed by Wei et al. [144]. AISI 4340 steel showed three distinct regions of temperature dependence when stressed in high pressure dehumidified hydrogen gas, with intermediate temperatures (50°C to just above 104°C) promoting maximum growth rates. A similar effect of temperature on MECP behavior was observed for 4130 steel (σ_{ys} = 1330 MPa) in hydrogen gas at a pressure of 77.3 kPa [143], as illustrated in Fig. 24. This figure clearly demonstrates that increasing temperature above ambient increases the resistance of alloy steels to HEE. This effect is understood based on competing temperature effects on the elements of the embrittlement mechanism shown in Fig. 5 [13,40,143,145,179,180]. Increasing temperature generally increases rates of chemical and electrochemical reaction to increase the amount of hydrogen available for HEE. On balance, however, increasing temperature retards atomic hydrogen entry by enhancing the rate of atom to H_2 recombination. Increasing temperature also may eliminate hydrogen from deleterious trap sites that would otherwise provide a preferred brittle crack path. Clearly, temperature effects on HEE for both monotonic and cyclic load cracking must be carefully considered in component life prediction.

## 2. Monotonic Load Environmental Cracking in Aluminum Alloys

Comprehensive studies on the SCC behavior of aluminum alloys were summarized by Spiedel [146], McEvily [24] and most recently by Holroyd [147]. It was concluded that aluminum alloys are generally insensitive to MECP in gaseous environments, with the important exception of water vapor. Susceptibility to sustained-load or monotonically increasing-load subcritical cracking in dry gases; including hydrogen, nitrogen, oxygen, air and argon; has not been observed for precipitation hardened aluminum alloys. Fig. 25 clearly

Fig. 23   Effect of H_2 partial pressure (P_{H2}) on K_{IEAC} for high strength (σ_{ys} = 1340 to 1650 MPa) steels stressed at 300 K. After Gangloff [145].
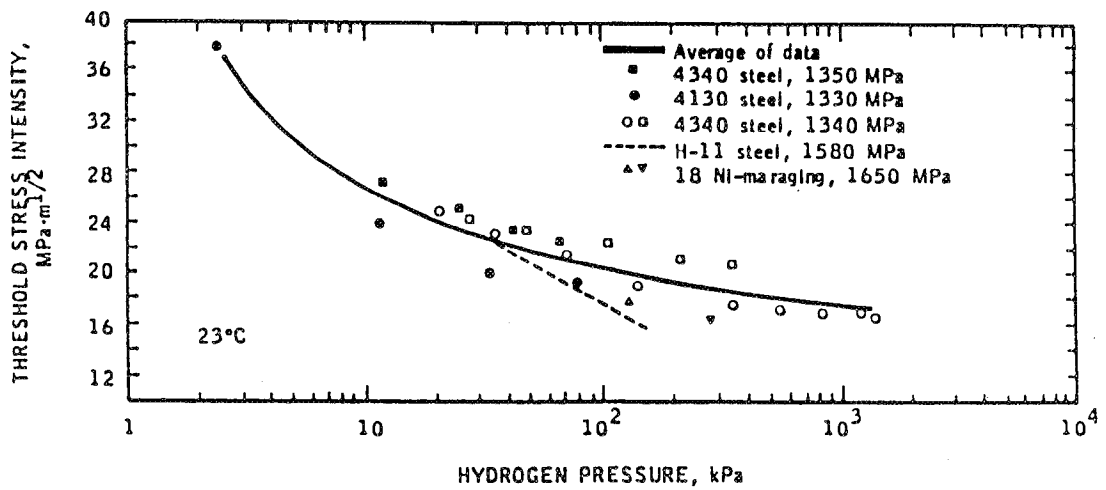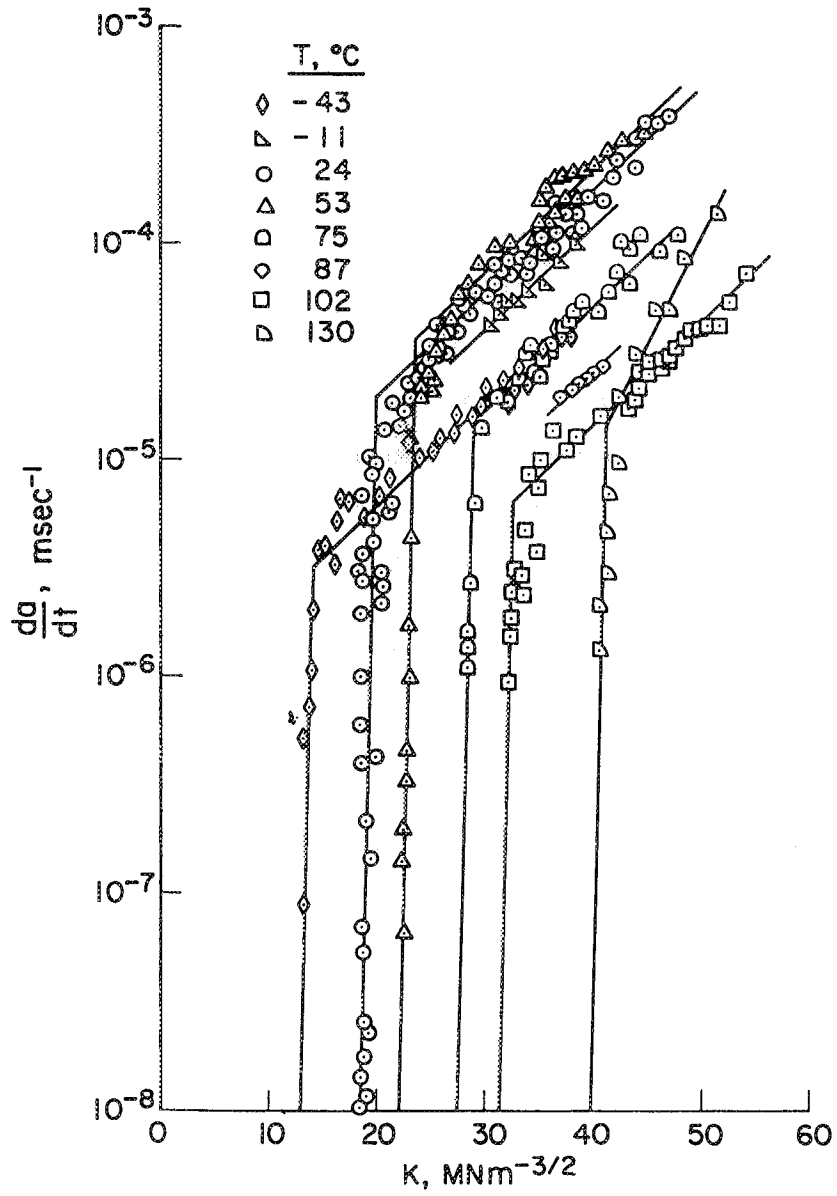
Fig. 24   Effect of temperature on MECP for 4130 steel in gaseous hydrogen at a constant hydrogen pressure of 77.3 kPa.   After Nelson and Williams [143,179].

demonstrates the deleterious effect of moisture on MECP in high-strength aluminum alloys stressed in either wet or dry H_2 [24]. The alloys did not exhibit subcritical crack growth in dry hydrogen, whereas rapid MECP occurred in wet H_2. Similar behavior is reported for aluminum alloys in pure water vapor and the causal mechanism was attributed to HEE as outlined in Fig. 5 [90,98]. H_2 does not readily promote cracking in aluminum alloys because such materials apparently do not catalyze the dissociation of H_2 and the resultant chemical adsorption of atomic hydrogen; atomic hydrogen uptake is insufficient for MECP.

That water vapor promotes the subcritical propagation of cracks in aluminum alloys is further illustrated by the data in Fig. 26 for 7075-T651 in moist air of varying water vapor content [181]. This alloy-environment combination has practical importance since 7075-T651 is the most widely used high-strength aluminum alloy in the aerospace industry. It is apparent that an increase in water content decreases K_{IEAC} values and increases Stage II crack growth rates. With relative humidity approaching 100%, MECP behavior of 7075-T651 is similar to that in aqueous NaCl solution. The extent of MECP at the lower relative humidities in Fig. 26 is reduced and the occurrence of an environmental effect is unclear. The slow growth rates shown in Fig. 26 for humidities below about 10% may have been due to mechanical creep crack growth at the relatively high K levels. It is possible that the effect of water vapor is of less importance for low humidity moist but otherwise pure air. Oxygen in air may compete with H_2O for adsorption sites and thus retard HEE. Aluminum alloys generally exhibit neither substantial sustained load crack growth nor frequency dependent FCP in moist air of relative humidity below about 10%. Such behavior is, in contrast, reported for these alloys in pure but very low pressure water vapor.

The complexity of ambient air environmental exposure is amplified in Fig. 27, a plot representing the effect of outdoor exposure and stress intensity on MECP velocities in several high-strength aluminum alloys; including 7079-T651, 7075-T651, and 7039-T64 [181]. This figure demonstrates that high-strength aluminum alloys are vulnerable to environmental cracking during outdoor exposure. This result is complex to interpret because the specimens were subjected to condensed water, and possible electrochemical action, for a portion of the exposure. Additionally, contamination from sulfur and chloride species may alter the MECP behavior from that expected based on experiments with highly purified water vapor and with distilled water. From a practical perspective, the data in Fig. 27 demonstrate the potential

56
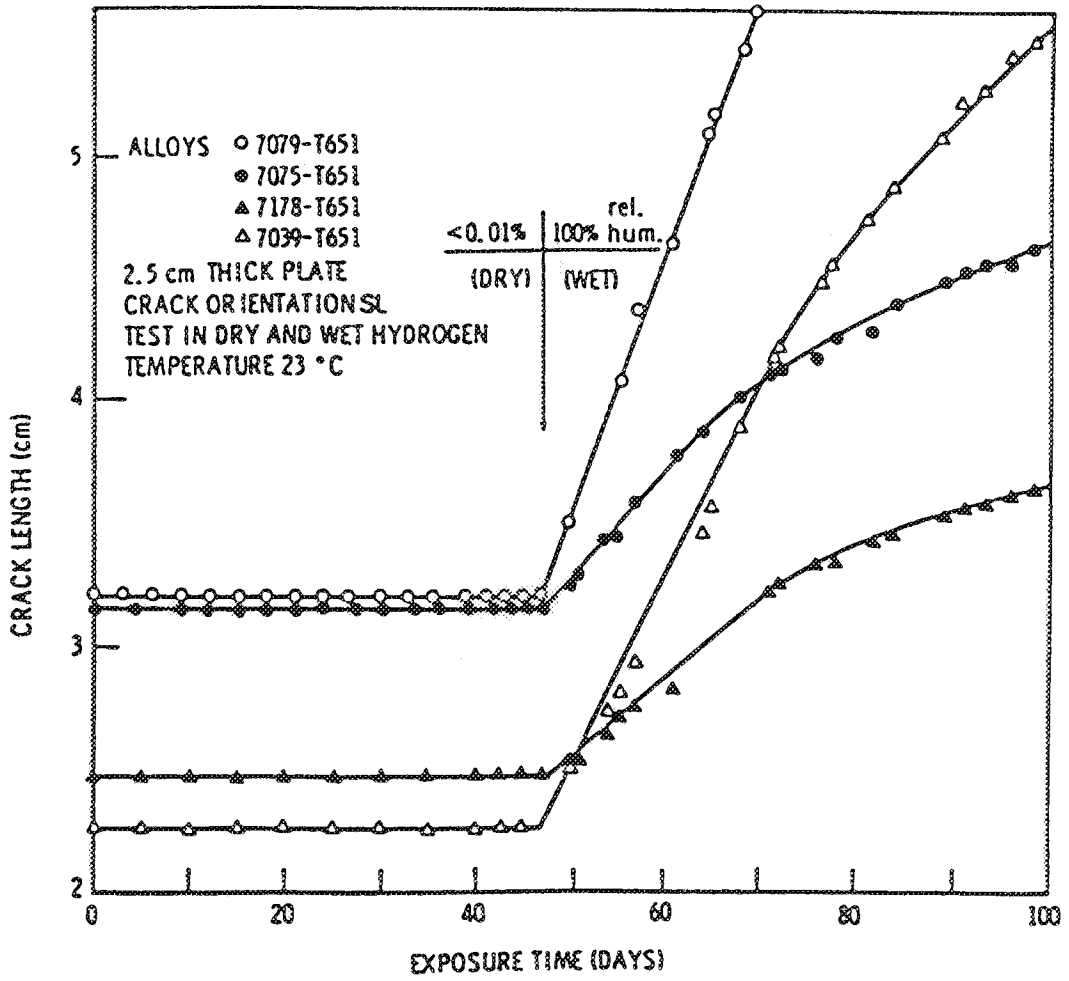
Fig. 25   Effect of moisture on subcritical crack growth in high-strength aluminum alloys
in hydrogen gas [Ref. 24].

57
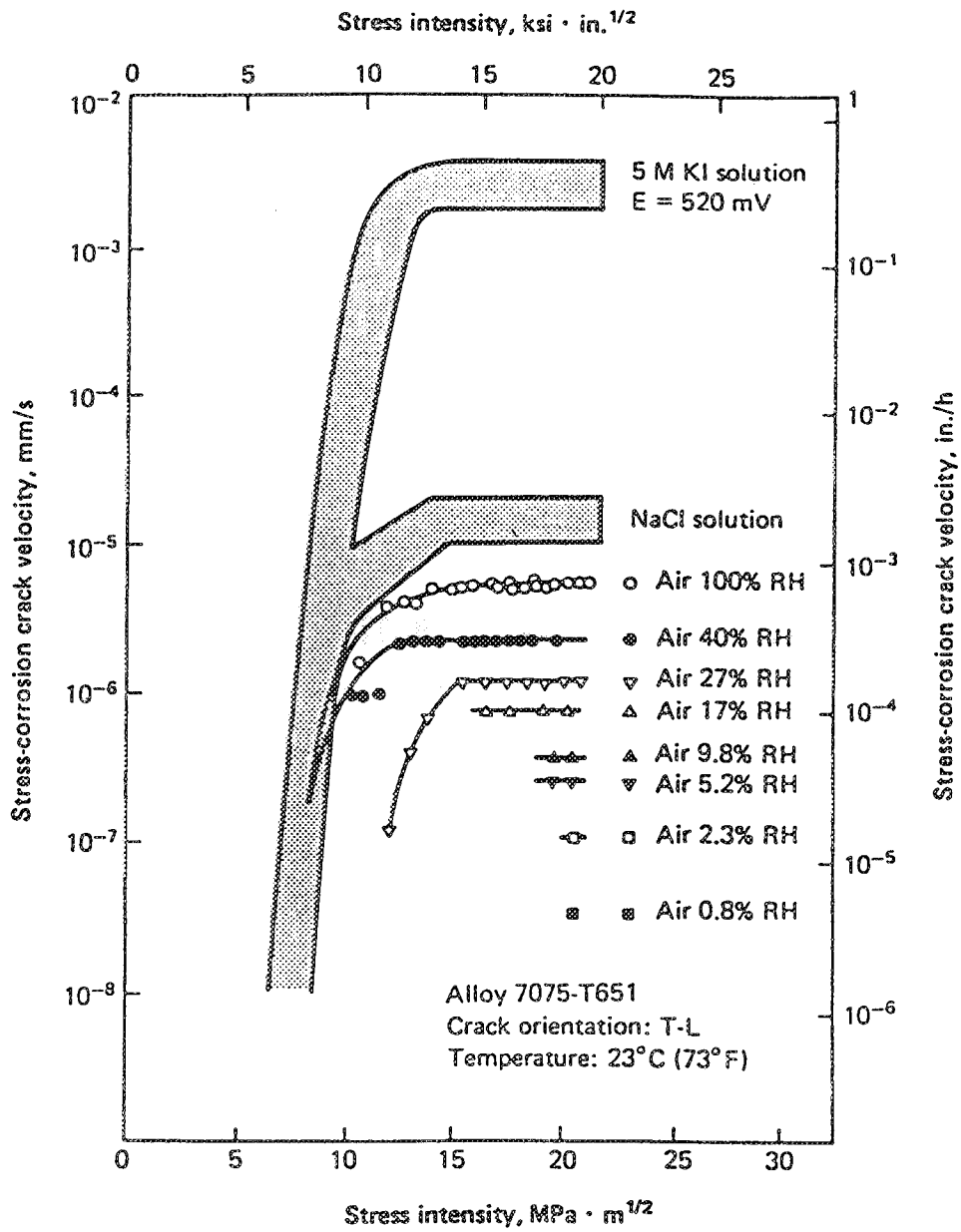
Fig. 26   Effect of humidity and stress intensity on stress corrosion crack velocity in 7075-T651. After Speidel et al. [181].
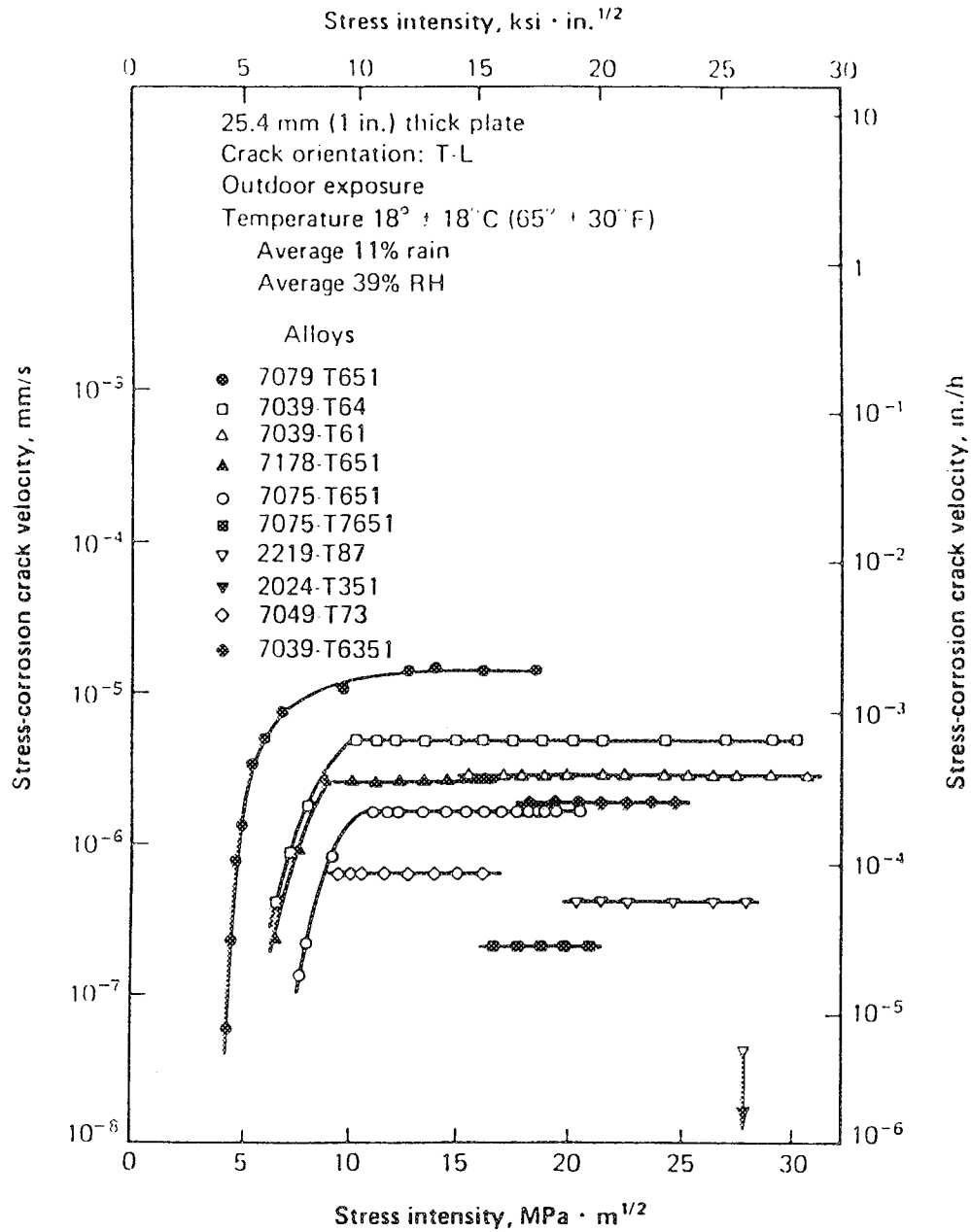
Fig. 27   Effect of outdoor exposure and stress intensity on stress corrosion crack velocity in several high-strength aluminum alloys. After Speidel et al. [181].

for EFCP in precipitation hardened aluminum alloys exposed to complex outdoor environments, including the particularly aggressive sea coast. Alloy 7079-T651 has particularly high susceptibility to SCC for the outdoor exposure conditions in Fig. 26. This result is consistent with the uniquely poor MECP resistance of this alloy [147].

Caution needs to be exercised when determining K_{IEAC} values for aluminum alloys, since crack growth is observed after hundreds of hours of incubation. It is often recommended to define K_{IEAC} as the value where measured crack growth rates are less than 10^{-10} m/s.

Fig. 26 demonstrates that MECP velocity in aluminum alloys is accelerated by continuous and full specimen immersion in aqueous solutions. The magnitude of the enhancement particularly depends on anion concentration, applied electrode potential, temperature and precipitate microstructure. Systematic studies on the effect of various anions on SCC behavior of 7079-T651 were performed by Speidel and results are shown in Fig. 28 [146]. Among the various anions, only Cl^-, Br^-, and I^- accelerated SCC beyond that promoted by distilled water. Considering the ubiquity of these ions in marine environments, it is important to understand the accelerating effect of these specie on MECP and EFCP.

Speidel investigated the effect of electrode potential on SCC growth rates for 7xxx series alloys. A typical result is shown in Fig. 29 [146]. Stage II crack growth rate generally declines with increasingly active potential from values typical of highly anodic polarization (-250 mV in Fig. 29) to modest cathodic polarization (-1000 mV) relative to the free corrosion potential of -635 mV. It is possible that growth rate increases with further increases in cathodic polarization. The observed reduction in growth rates with respect to applied potential was related to reduced hydrogen permeability over the same potential range. While more negative potentials clearly favor hydrogen ion and water reduction, cathodic polarization may also suppress crack tip acidification through cation hydrolysis. The net result could be reduced hydrogen uptake and HEE crack growth rates [31].

SCC behavior in aluminum alloys is sensitive to alloy composition (e.g., 7079-T651 and 2219-T87 in Fig. 27), aging practice (e.g., 7075-T7351 and 7075-T651 in Fig. 27) and crack orientation. Severe MECP is often found for cracks in the SL and TL orientations of thick plate and forgings; most SCC data are specific to these orientations. Smooth specimen experiments do not indicate a correlation between alloy yield strength and susceptibility to
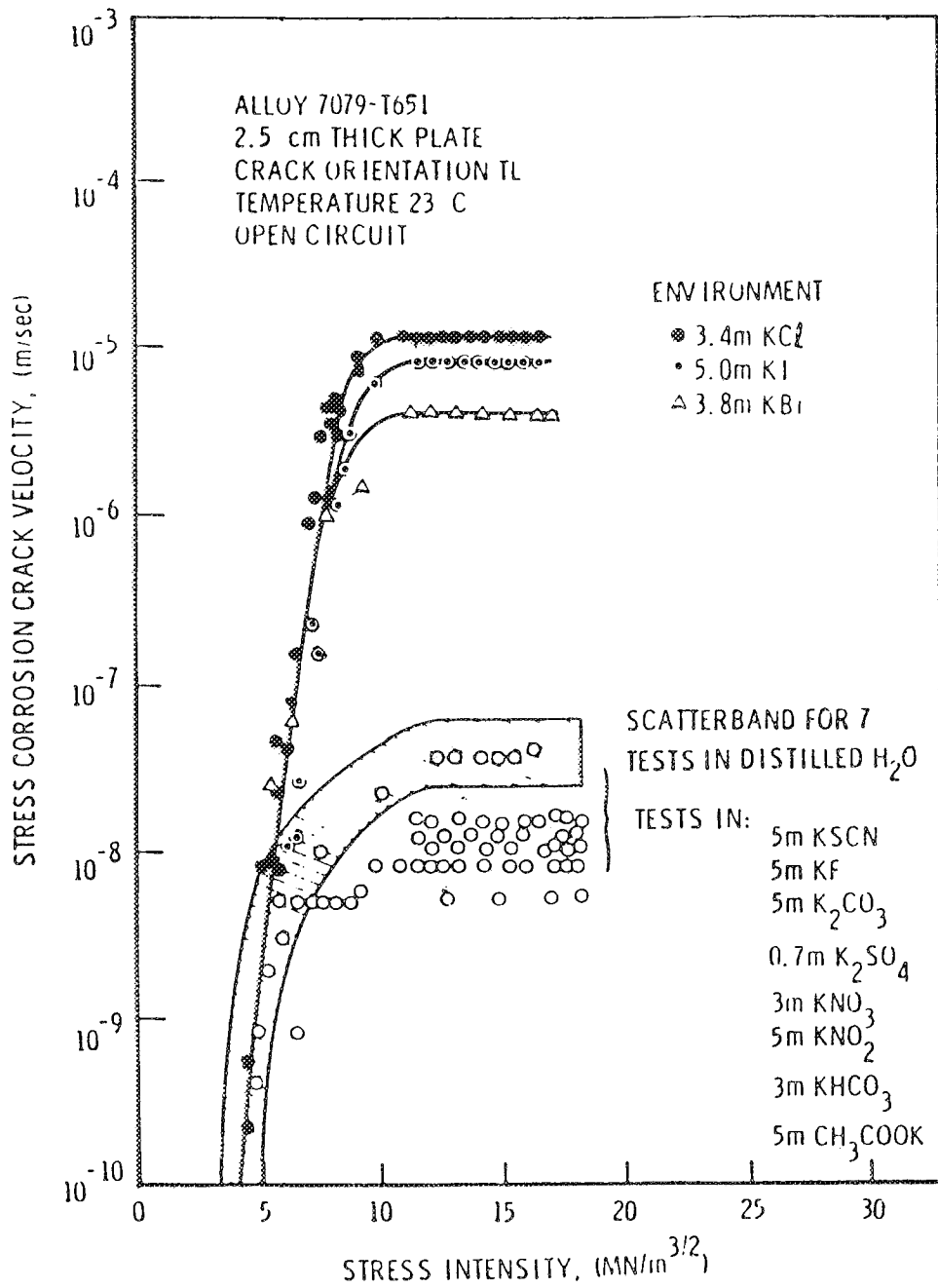
Fig. 28   Effect of various anions on stress corrosion crack velocity for 7079-T651 fully immersed in aqueous solutions. After Speidel [146].
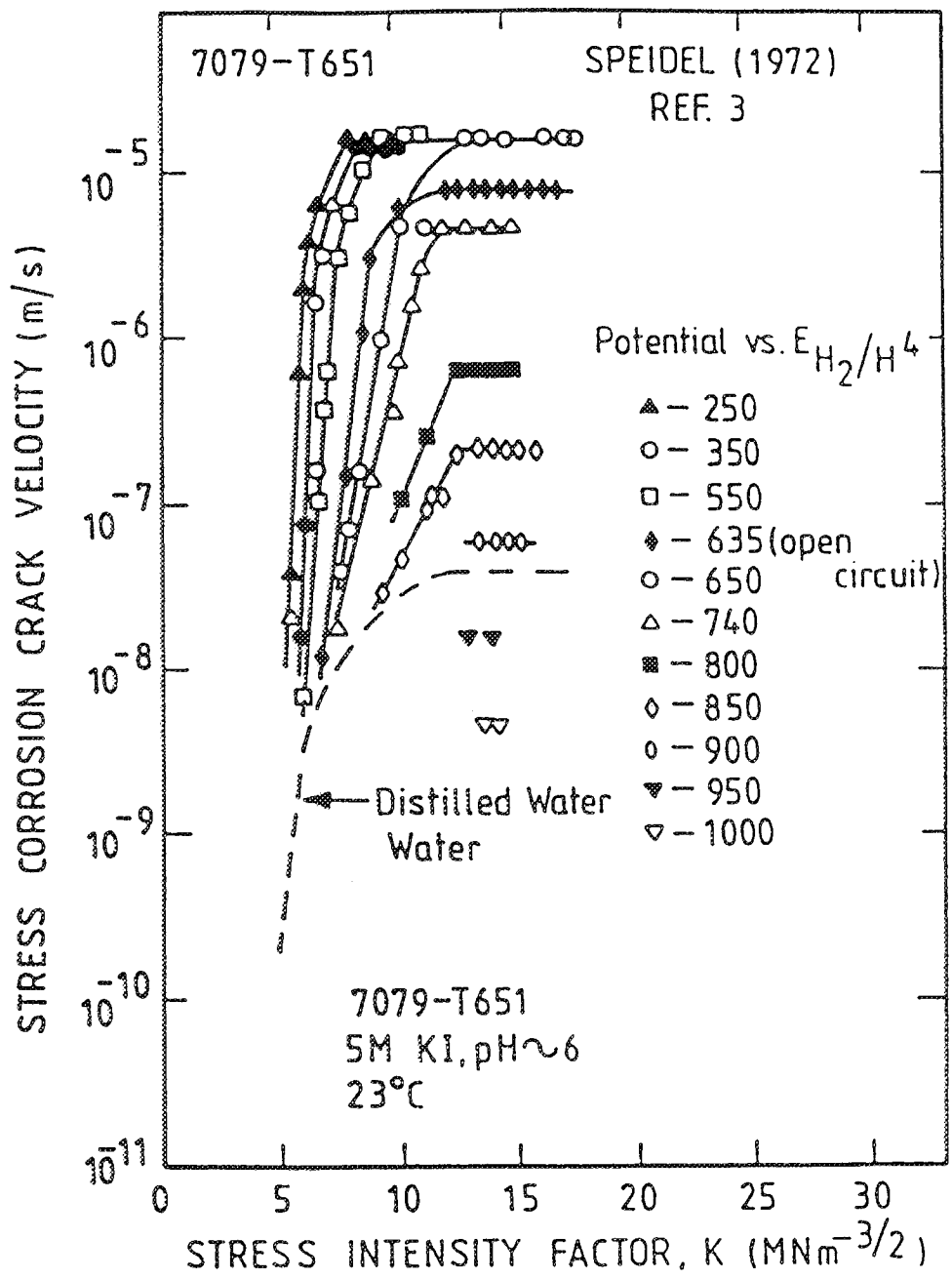
Fig. 29   Effect of electrode potential and stress intensity on stress corrosion crack velocity in a high strength aluminum alloy. After Speidel [146].

environmental cracking [24]. There have been no systematic studies of the effect of this variable on K_{IEAC} or da/dt versus K for aluminum alloys.

Precipitation hardening can cause deleterious reductions of MECP resistance for many aluminum alloys. Maximum susceptibility is often observed before the peak strength is reached during precipitation [147]. Fig. 30 schematically illustrates the variation of strength and stress corrosion resistance during aging of aluminum alloys and is based on virtually thousands of individual stress corrosion cracking data. The beneficial effect of slight overaging for aluminum alloys on stress corrosion cracking is well accepted, however, the precise mechanism is controversial. As a specific example, Fig. 31 demonstrates the effect of overaging on MECP velocity for Al 7178 in aqueous chloride [146]. With 15 hours of overaging at 160°C (-T7651), SCC resistance is increased by more than two orders of magnitude in terms of Stage II da/dt. Care needs to be taken when considering an overaging practice as a practical means to reduce the susceptibility to MECP in aluminum alloys. For example, excessive overaging is necessary to obtain even a slight increase in SCC resistance for copper-lean alloys, such as 7079, which is accompanied with a significant sacrifice in terms of tensile strength and perhaps fracture toughness. On the other hand, slight overaging of 7178 and 7075 can substantially enhance SCC resistance with an acceptable loss of tensile strength [147].

3. Monotonic Load Environmental Cracking in Nickel Base Superalloys

Nickel and iron base superalloys, including IN 718, IN 600, IN 905 and Nimonic 105, are susceptible to monotonic load environmental cracking, particularly in high pressure H_2, distilled water and sodium hydroxide environments [119,182-184]. These alloys are also susceptible to MECP in elevated temperature moist air. Specific subcritical crack growth rate data are presented in Fig. 32 for Nimonic 105 in distilled water [119]. Unlike aluminum alloys and steels, a large body of K_{IEAC} values for various superalloy-environment systems are not available.

Among the nickel base superalloys, precipitation hardened Inconel 718 is widely applied in aerospace industries, particularly in jet engine and hydrogen/oxygen propulsion system components. While there are a large number of experimental data that show that Inconel 718 is significantly embrittled by the presence of gaseous hydrogen, in terms of reduction in tensile properties and K_{IEAC} compared to K_{IC}, crack growth kinetics and the
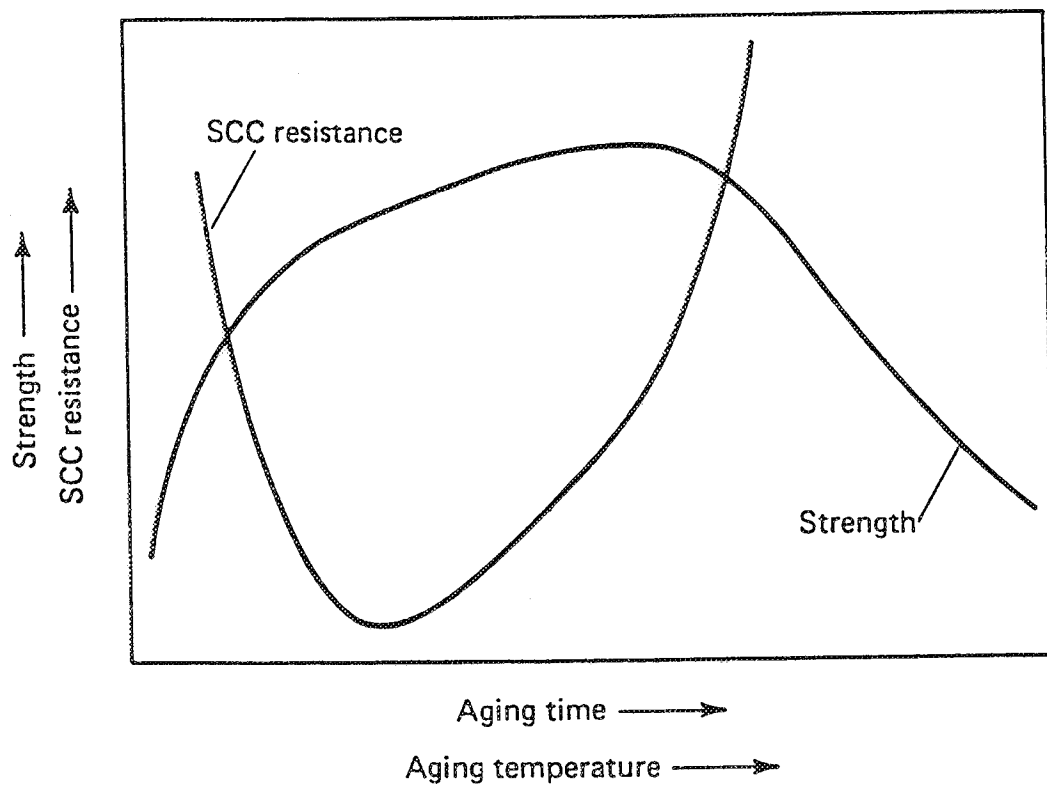
Fig. 30   Variation of strength and stress corrosion resistance during aging of precipitation hardening aluminum alloys. After Holroyd [147].
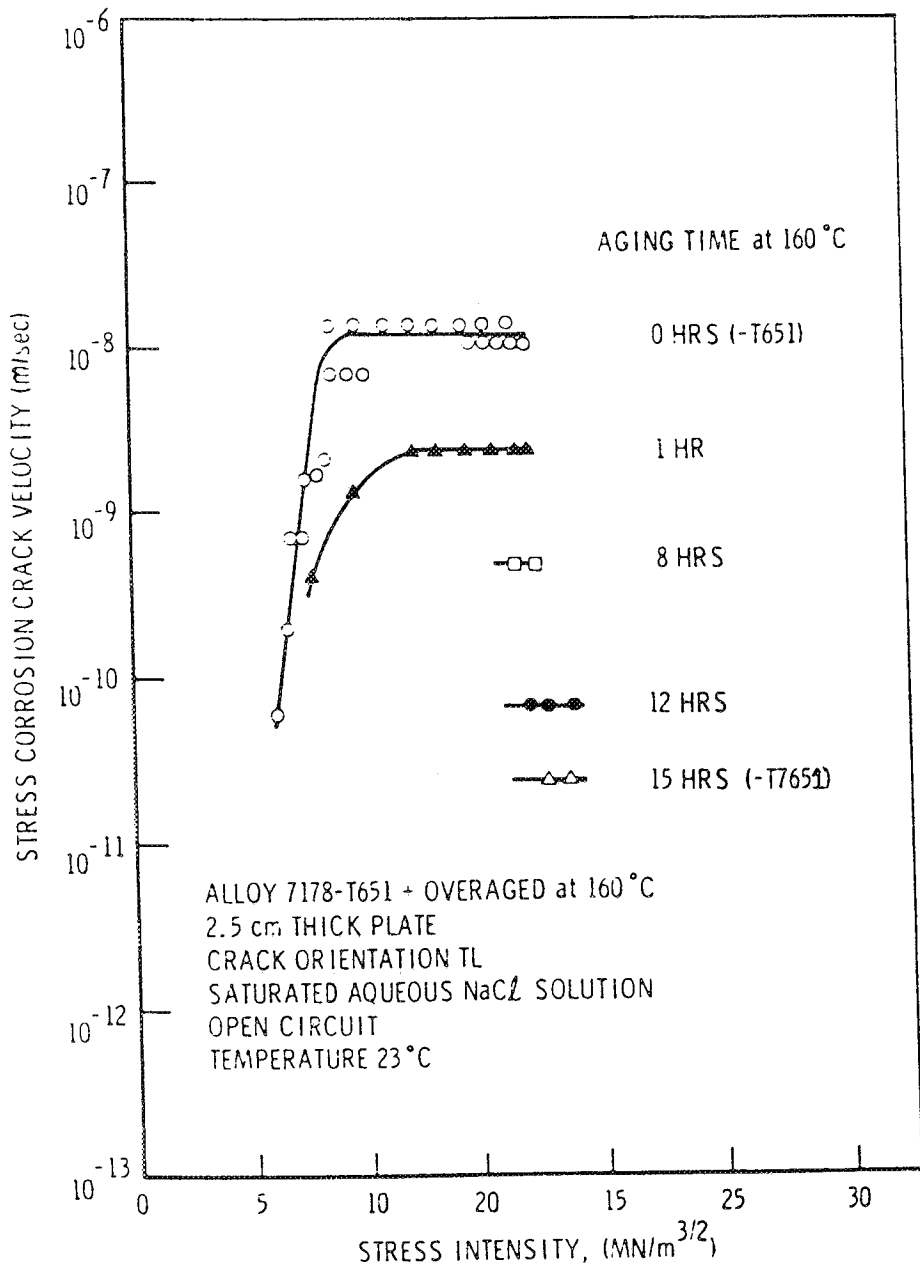
Fig. 31   Effect of overaging on stress corrosion crack velocity in aluminum alloy 7178 exposed to aqueous NaCl. After Speidel [146].
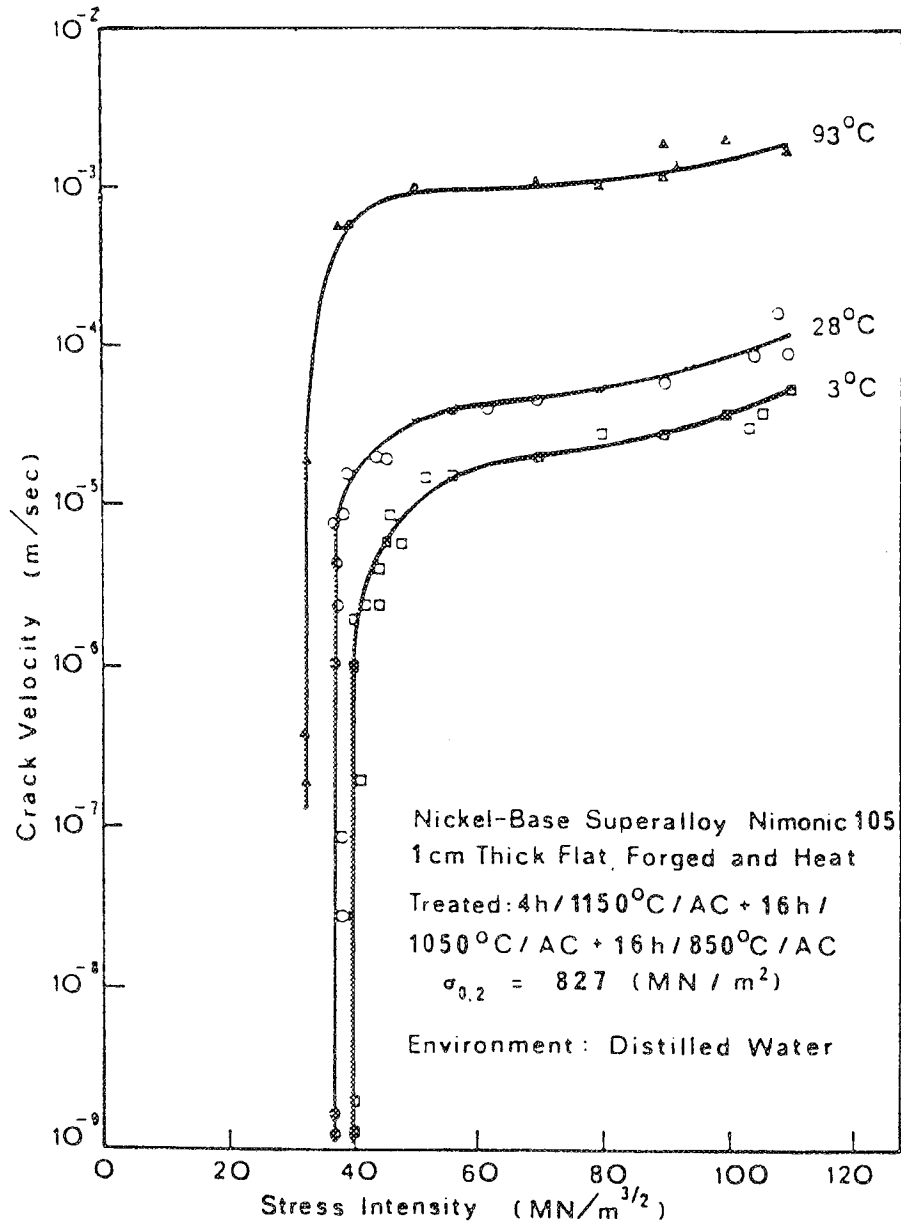
Fig. 32   Effect of stress intensity on stress corrosion crack velocity in Nimonic 105 exposed to distilled water at 300K. After Speidel [119].

MECP behavior for a range of aqueous environments are not well defined [182]. The results of pioneering experiments by Walter and Chandler are presented in Fig. 33 for Inconel 718 in very high pressure hydrogen gas at ambient temperature. Three things are apparent. Inconel 718 is susceptible to MECP in hydrogen gas at stress intensities well below the plane strain fracture toughness of order 125 MPa√m. The susceptibility to monotonic load cracking, as demonstrated by the reduction in K_{IEAC}, increases significantly with increasing hydrogen pressure at ambient temperature. The relationship between da/dt and K is approximated by a simple exponential dependence on K without evidence of Stage I/Stage II plateau behavior.

The effect of hydrogen pressure on K_{IEAC} was systematically studied by Walter et al. for Inconel 718 [182] and by Moody et al. for Inconel 903 [183]. Fig. 34 shows that K_{IEAC} values for both alloys exhibit a similar dependence on hydrogen gas pressure, analogous to the case for steels in Fig. 23. At low pressures, threshold values for both alloys decrease significantly as pressure increases until reaching a lower limiting threshold value at about 20% of K_{IC}. The effect of internally-charged hydrogen on the threshold for monotonic load crack growth was similar for IN 718; increasing predissolved hydrogen content decreased K_{IEAC} [184].

Sustained load environmental cracking of several nickel base superalloys in moist air was intensively studied as a prime contributor to elevated temperature fatigue crack growth behavior [110,111]. Fig. 35 shows MECP rates for IN 718 in moist air and vacuum at 649°C [114]. Crack growth rate at high temperatures is substantially promoted by the moist air environment compared to inert vacuum. This environment-sensitive sustained load crack growth at high temperature is distinguished from classical creep processes which are operative for the vacuum case. In the absence of the deleterious environment, so-called creep crack growth rates decrease by several orders of magnitude. For elevated temperature crack growth, oxygen is often considered as the embrittling species. The effect of temperature on sustained load cracking for Inconel 718 in moist air is demonstrated in Fig. 36 [185,186]. Increasing temperature decreases K_{IEAC} and increases MECP rates. The results in Figs. 35 and 36 indicate that da/dt versus K is described by two stage behavior. While an apparent threshold is suggested, Stage II crack growth rates are not independent of applied K; rather, power-law da/dt-K response is noted.
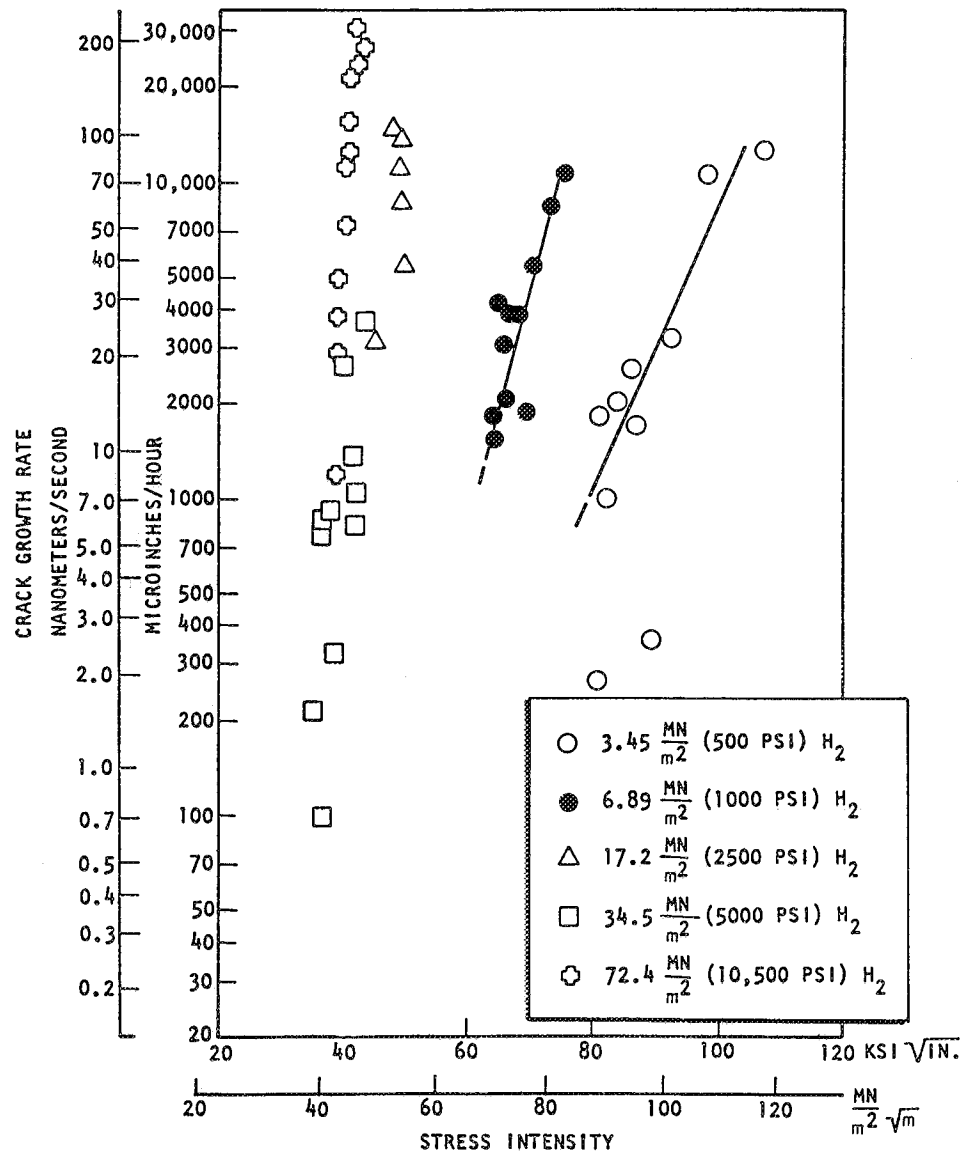
Fig. 33   Effect of hydrogen pressure on monotonic load environmental crack growth in IN 718. After Walter et al. [182].
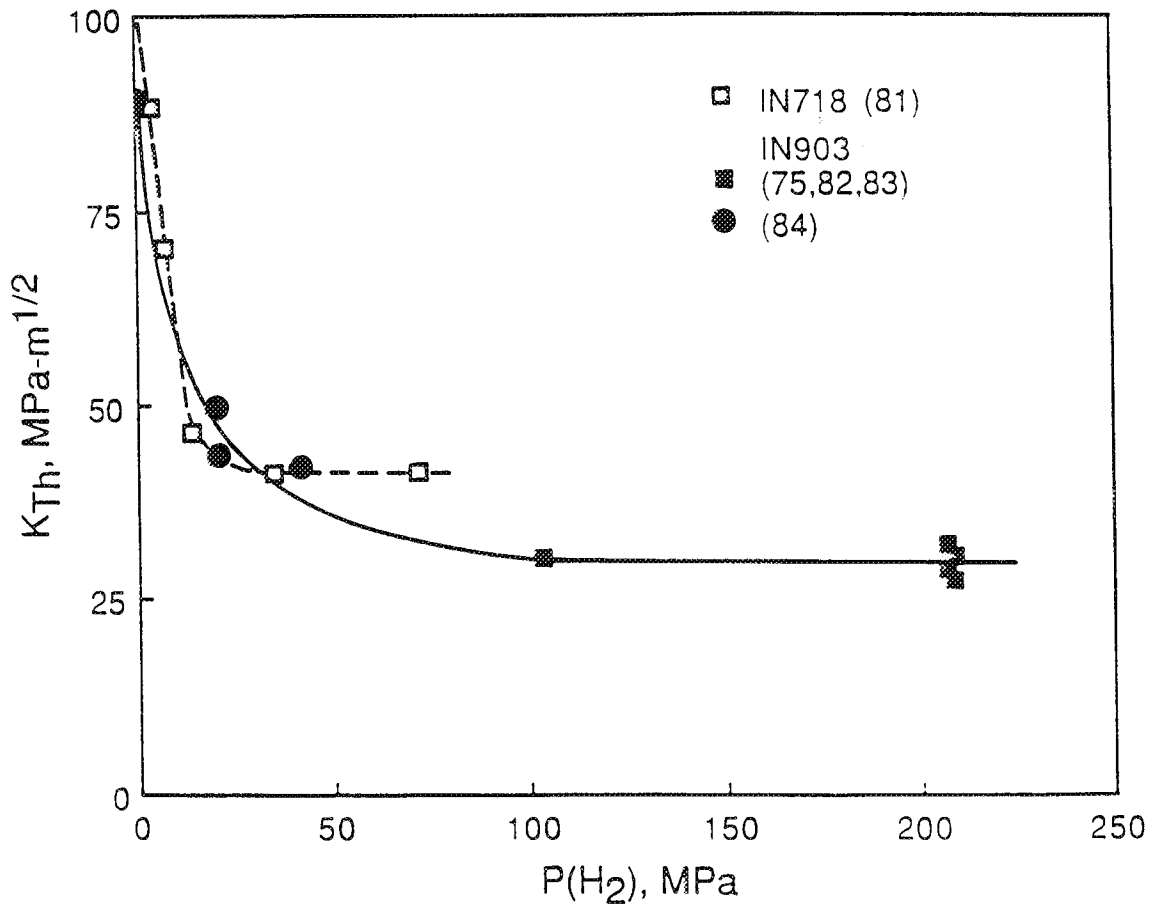
Fig. 34   Effect of hydrogen pressure on the threshold stress intensity for monotonic load
cracking in Inconel 718 and 903 exposed to pure H_2. After Moody et al.
[183].
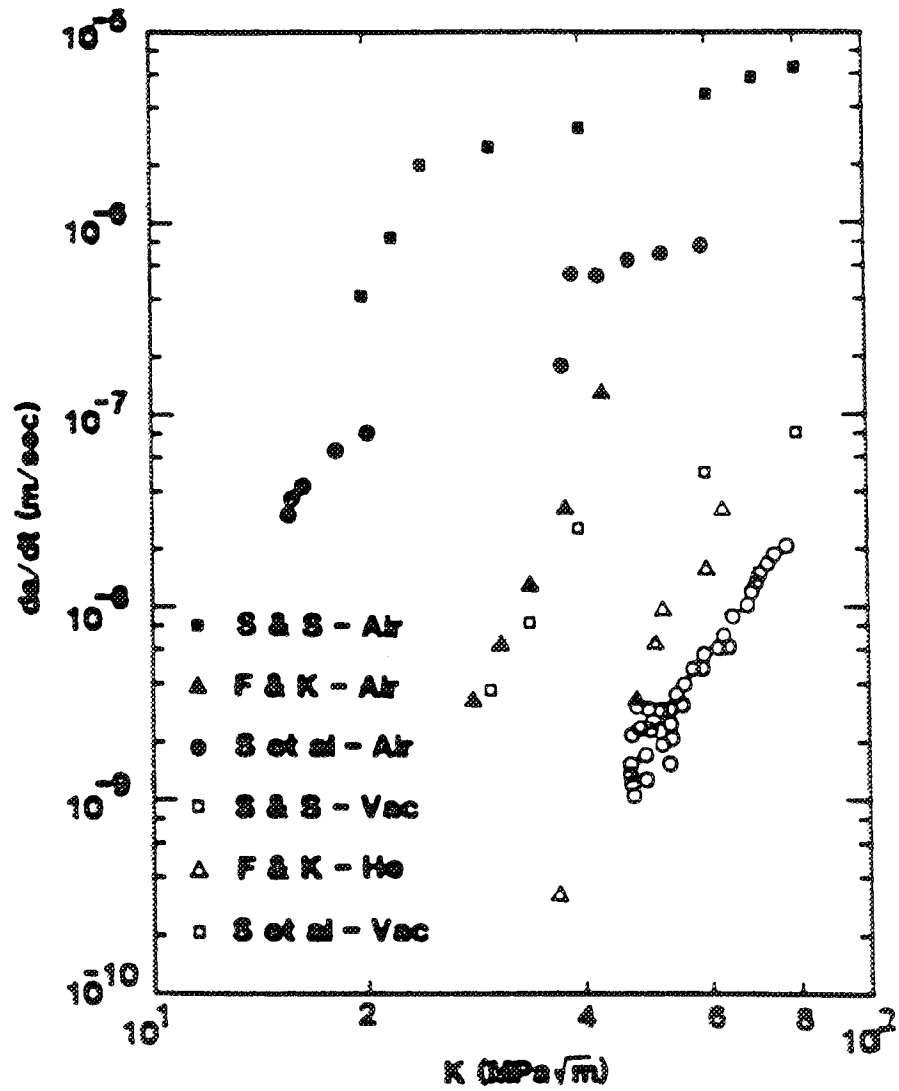
Fig. 35   Effect of the moist air environment on monotonic load subcritical crack propagation rate for IN 718 at 649°C. After Larsen et al. [114].

Fig. 36   Effect of temperature on monotonic load cracking for IN 718 in moist air. The solid line for 649°C represents crack growth in vacuum. After Nicholas et al. [185].
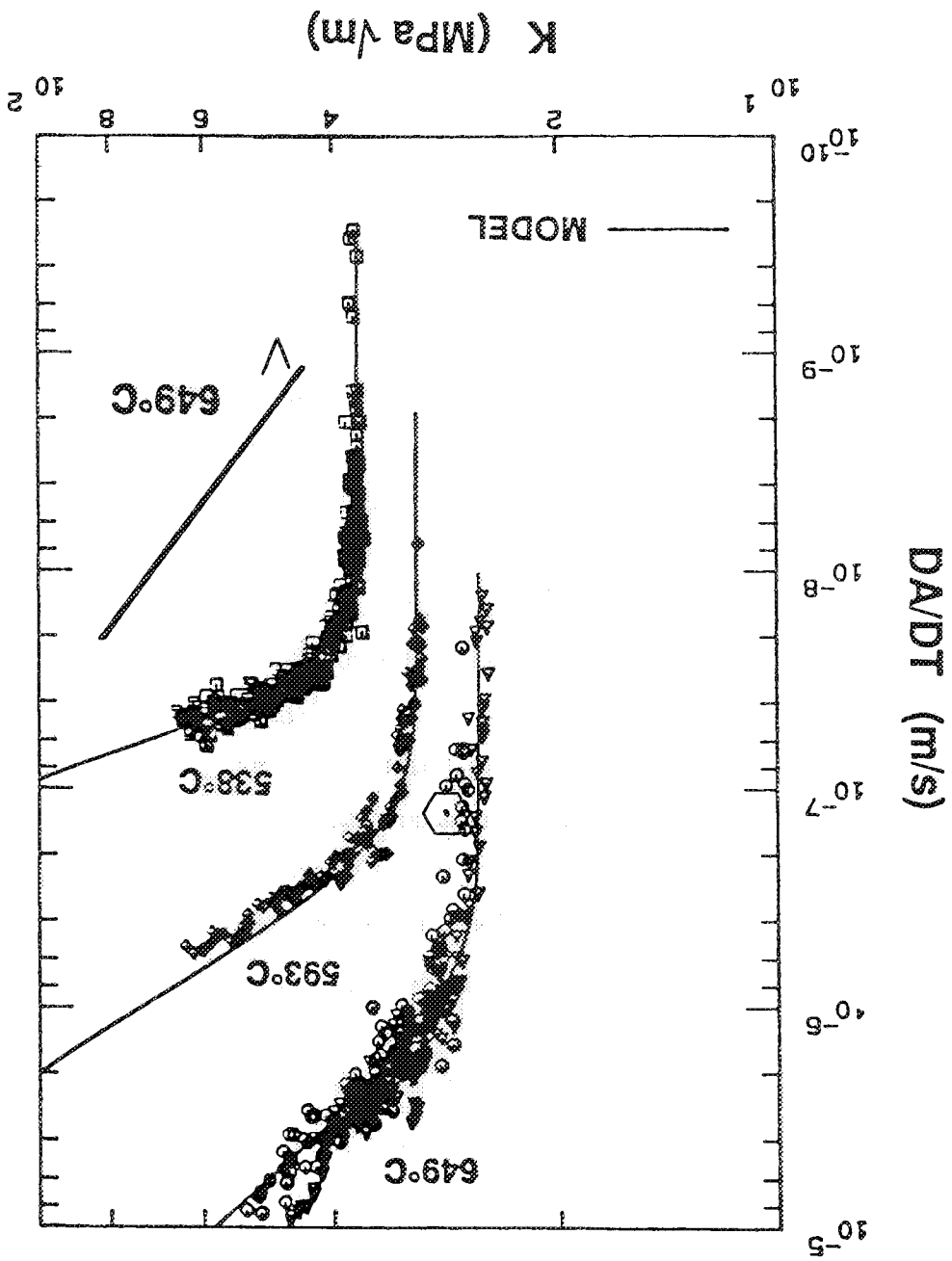
4. Monotonic Load Environmental Cracking in Titanium Alloys

Titanium alloys are susceptible to MECP in a variety of environments including aqueous electrolytes with halogen ions, particularly chloride, alcohols, and methanol-hydrochloric acid solutions [24,187-192]. The susceptibility to environmental cracking in titanium alloys is almost always associated with the high stress concentration and occluded cell electrochemistry typical of precracked specimens, and is not observed with smooth or mildly notched specimens [140]. The relationship between K_{IEAC} and yield strength for various titanium alloys in 3.5 % NaCl solution is given in Fig. 37 [190]. This figure shows that most titanium alloys are susceptible to SCC in aqueous NaCl solution and that the magnitude of susceptibility is largely dependent on alloy composition and microstructure, but not necessarily on yield strength. Few studies were performed on the effect of individual alloying elements on MECP behavior in titanium alloys. Limited data indicate that there is a critical amount of Al for SCC to occur in aqueous solutions, perhaps associated with the deleterious effect of localized slip resulting from long range ordering of aluminum and from precipitation of Ti_3Al. Fig. 38 shows the effect of aluminum on K_{IEAC} for Ti-Al alloys in aqueous KCl [187]. K_{IEAC} for binary titanium alloys decrease with increasing aluminum content.

K_{IEAC} values and Stage II SCC growth rates in titanium alloys change dramatically depending on heat treatment. An example of the change in the degree of sensitivity to SCC with different heat treatment practice and resultant microstructure is demonstrated in Fig. 39 [188]. This figure shows K_{IEAC} values for Ti-8Al-1Mo-1V in three different heat-treatment conditions and for various electrochemical environments. K_{IEAC} changed from 48.3 MPa√m for mill-annealed alloy to 71.4 MPa√m for beta-treated and 63.7 MPa√m for alpha/beta-treated microstructures. The detailed discussion of the effect of each phase on the SCC behavior of titanium alloys is given in Reference 187. Regardless of heat treatment condition, Ti-8Al-1Mo-1V is more susceptible to SCC in methanolic solutions than in aqueous media, perhaps because this species attacks the otherwise passive film on the crack surface.

Fracture mechanics data for three microstructures of Ti-8Al-1Mo-1V tested in 0.6M KCl at -500 mV, distilled water, and laboratory air are given in Fig. 40 [187]. Enhanced MECP rates are observed for environments with Cl⁻ ions. Similar to the SCC behavior for aluminum alloys, halide anions (Cl⁻, Br⁻, and I⁻) accelerate cracking in distilled water.
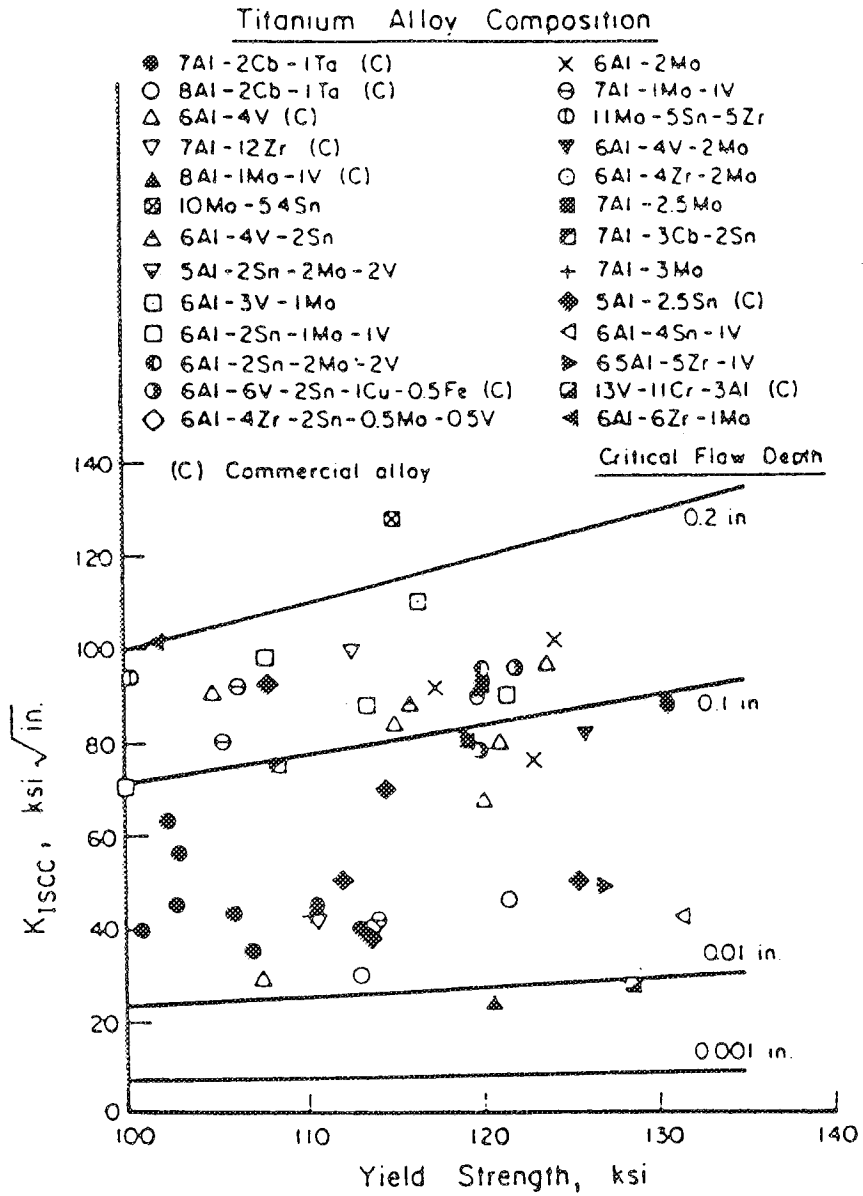
Fig. 37   The effect of yield strength on the threshold stress intensity for MECP in titanium alloys in 3.5% NaCl solution [190].
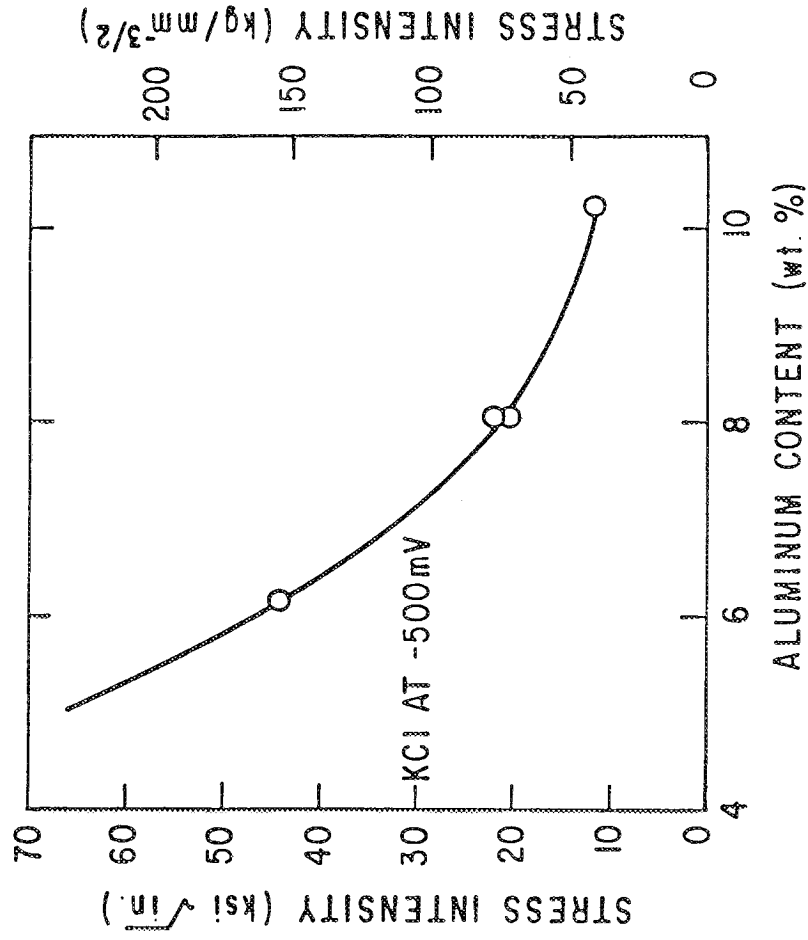
Fig. 38   The effect of aluminum on the threshold stress intensity for stress corrosion cracking of Ti-Al alloys in aqueous KCl. After Feeney and Blackburn [187].

74
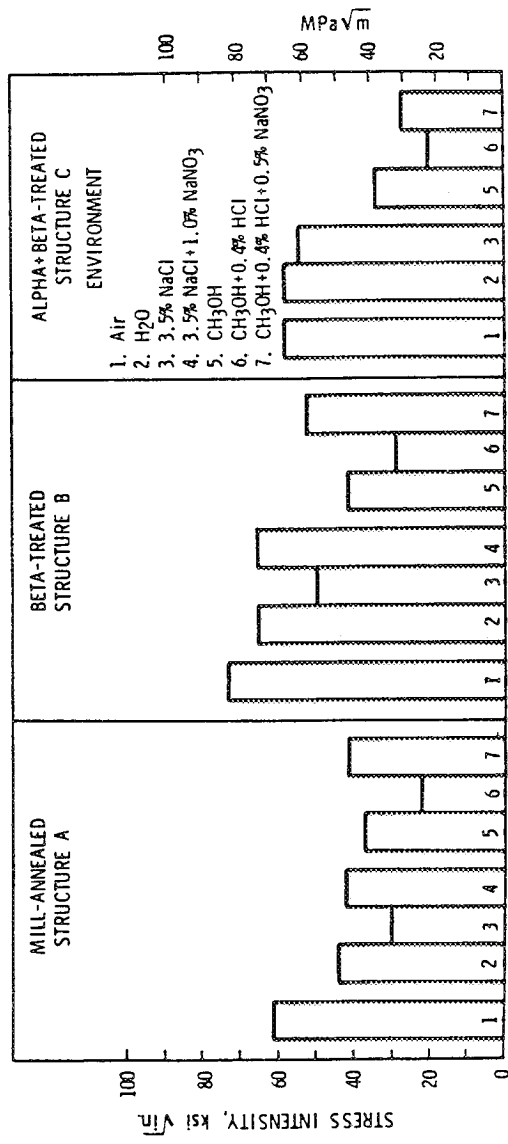
Fig. 39   Effects of heat treatment and solution chemistry on the K_{IEAC} for Ti-8Al-1Mo-1V. After Czyrklis [188].
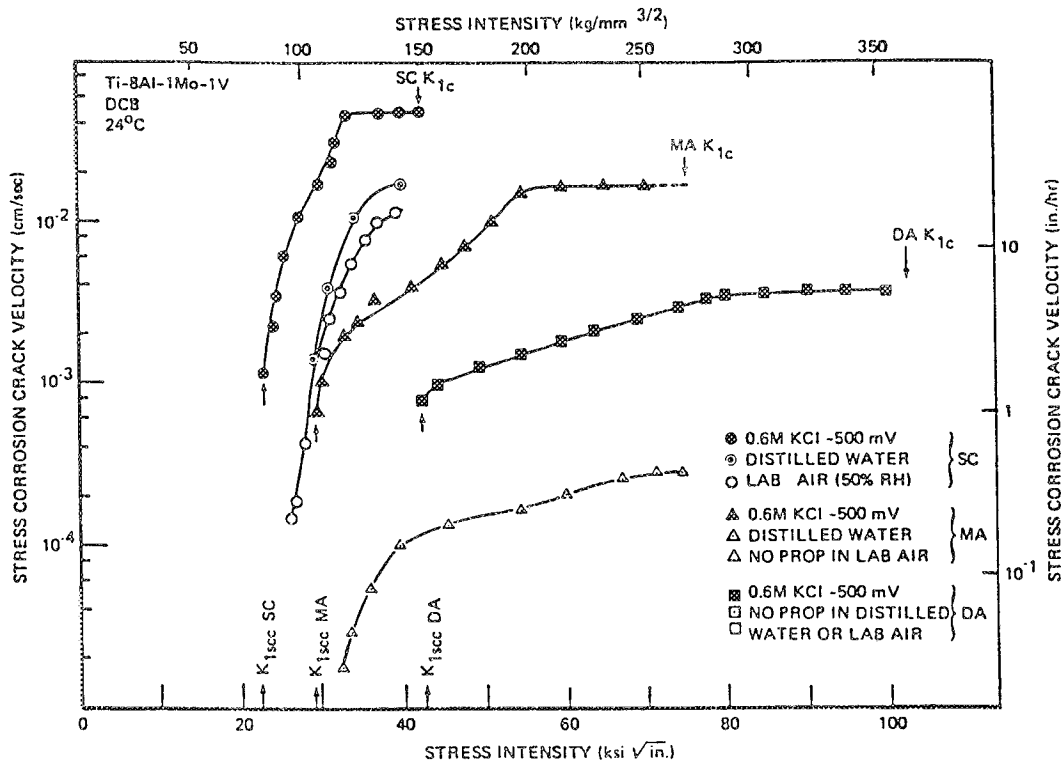
Fig. 40   Stress corrosion crack velocity versus stress intensity relationships for three microstructures of Ti-8Al-1Mo-1V tested in 0.6M KCl at -500 mV, distilled water, and laboratory air. After Feeney and Blackburn [187].

76

Ti-6Al-4V is widely used in aerospace structural applications. Fig. 41 shows the effect of applied electrode potential on MECP velocity for Ti-6Al-4V in KCl solution [189]. K_{IEAC} increased and da/dt decreased with cathodic polarization, and the reverse trend was produced by anodic polarization. Environmental cracking was clearly more severe within increasingly noble applied potential. Stage II crack growth rate increased in a similar manner with anodic polarization for iodine solutions.

F.   Conclusions

In this section the general aspects of monotonic load environmental cracking were reviewed. Examples of fracture mechanics data for MECP in various alloy-environment systems were presented. Widely-used aerospace alloys are often susceptible to environmental cracking, while the magnitude of susceptibility strongly depends on environmental and metallurgical variables. These variables are also likely to affect environmental fatigue crack propagation and are therefore important to the life prediction problem.

Monotonic load cracking will dominate fatigue crack growth rates if K levels in the fatigue cycle exceed K_{IEAC} and if da/dt is significant. Table 2 summarizes K_{IEAC} and corresponding da/dt for selected alloy-environment systems. From these results, EFCP in low-K_{IEAC}, high-da/dt alloy/environment systems such as Al 7079/NaCl solution and AISI 4340/distilled water can be accurately predicted by a simple linear superposition model. Environmental FCP in more resistant alloy/environment systems will only be modeled by more complex empirical curve fitting or mechanism-based approaches, as detailed in Chapter VII on "Quantitative Crack Growth Rate Models".
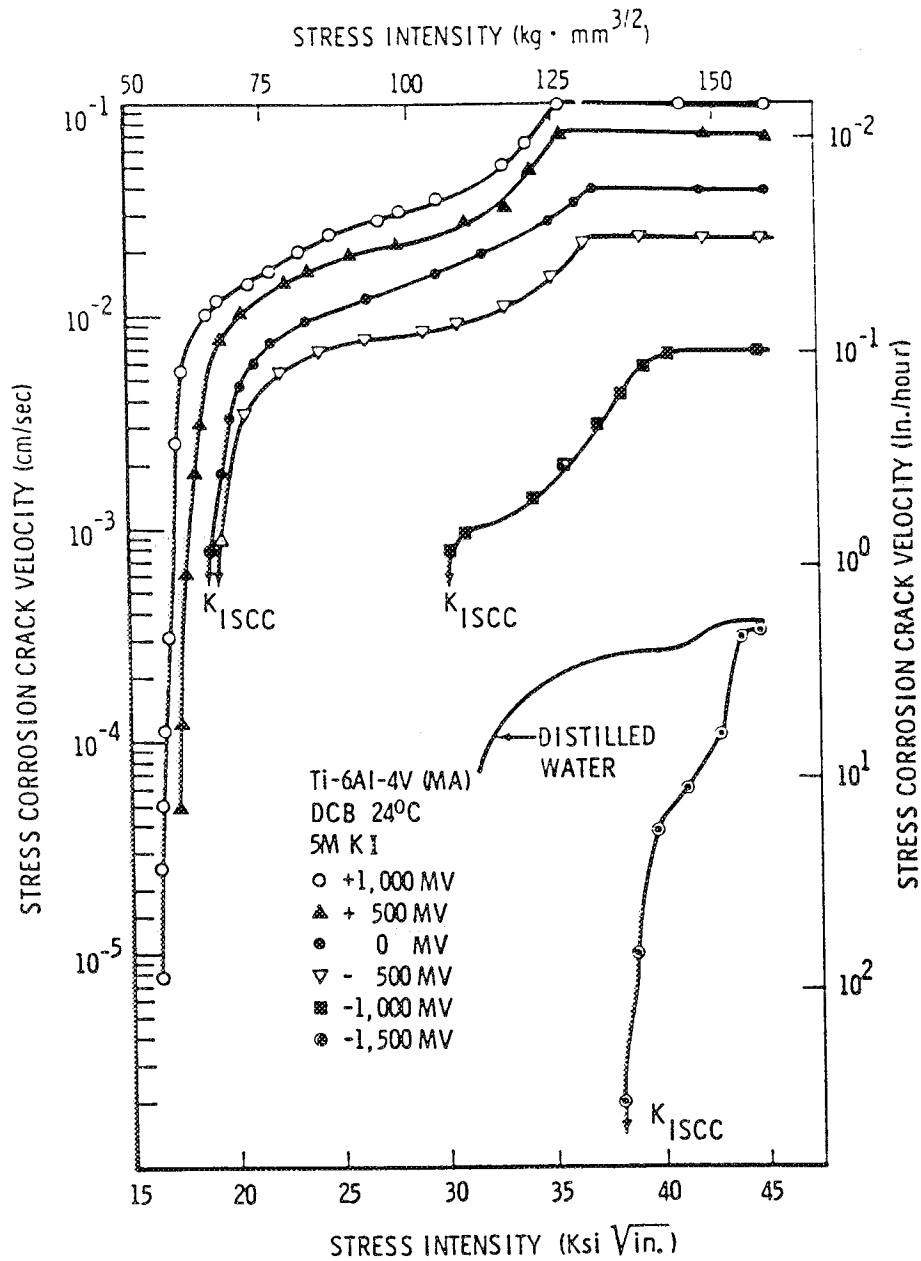
Fig. 41   Crack velocity versus stress intensity relationships for Ti-6Al-4V tested in 5.0
M KI at various electrode potentials. After Blackburn et al. [189].

	K_{th} (MPa/m)	da/dt mm/sec
4340/300M in Distilled Water [temperature]	18	10^{-2}
AA 7079 in NaCl [Cl⁻ concentration]	4	2×10^{-2}
IN718 in High Pressure H_2	30 - 40	—
IN718 at 650°C ●● air ●● vacuum	15 - 25 45	$10^{-4} - 10^{-2}$ $10^{-6} - 10^{-5}$
Ti-8Al-1Mo-1V in NaCl, KI, KCl [electrode potential]	30	10^{-1}
12%Cr Martensitic SS in Water [temper temperature]	20	$10^{-4} - 10^{-2}$
HY130/4340 in NaCl (Low σ_{ys}) [yield strength]	> 75	—
AA 7017, 7075, 2090 in NaCl	6 - 10	4×10^{-5}
Ti-6Al-4V in NaCl	20	10^{-1}
Ti-6Al-6V-2Sn in Methanol/HCl	25	—
Ferritic Steel with Dissolved H [hydrogen content]	25 - 50	$< 10^{-5}$

Table 2 K_{IEAC} values and corresponding crack growth rates for MECP in selected material/environment systems relevant to aerospace applications.

V. ENVIRONMENTAL EFFECTS ON FCP KINETICS

Corrosion fatigue crack propagation results from the synergistic interaction between cyclic plastic deformation and chemical reaction localized within a crack tip process zone. In this review corrosion fatigue and environment enhanced fatigue crack propagation (EFCP) are interchangeably used.

The fracture mechanics method and stress intensity range similitude have been demonstrated to successfully describe environmental fatigue crack propagation as detailed elsewhere [31]. Wei and coworkers first extended the stress intensity similitude concept for environmental fatigue, following from the work of Paris [11,14]. Typical confirming data are presented in Fig. 42a. Caution is, however, required when applying similitude to environmental fatigue. As discussed by Gangloff and indicated in Fig. 42b, stress intensity formulations may not correctly describe the chemical driving force for environmental fatigue, particularly the dependencies on component geometry as well as crack size and opening [31,193,194]. The application of laboratory data to life prediction must be accordingly questioned. At present, it is necessary to consider the occurrence and importance of breakdowns in similitude on a case by case basis. This is dictated because the chemical contribution to fatigue damage is material and environment specific, and is difficult to predict by modeling. This topic is amplified in Chapter VIII on "Factors Complicating Life Prediction".

A wide variety of variables, which have a second order effect on inert environment mechanical fatigue, critically affect fatigue in aggressive gases and liquids. Life prediction through similitude is accordingly complicated. Extensive fracture mechanics based data bases have been developed over the past two decades for the following material-environment systems. A typical application which spawned the crack growth studies is noted in parentheses for each case.

oo C-Mn and alloy steels in hydrogen producing gases and electrolytes. (C-Mn and HSLA steels in offshore platforms for oil and gas production, particularly in the North Sea.)

oo Precipitation hardened aluminum alloys in water vapor and aqueous chloride. (High strength aluminum alloys for aerospace structures.)
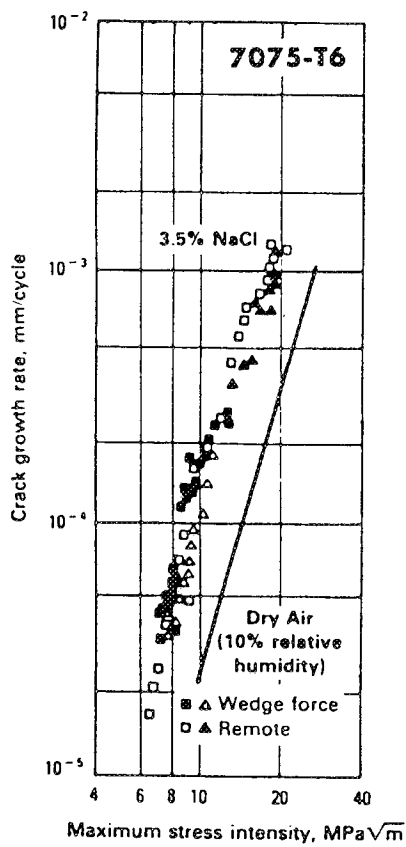
(a)
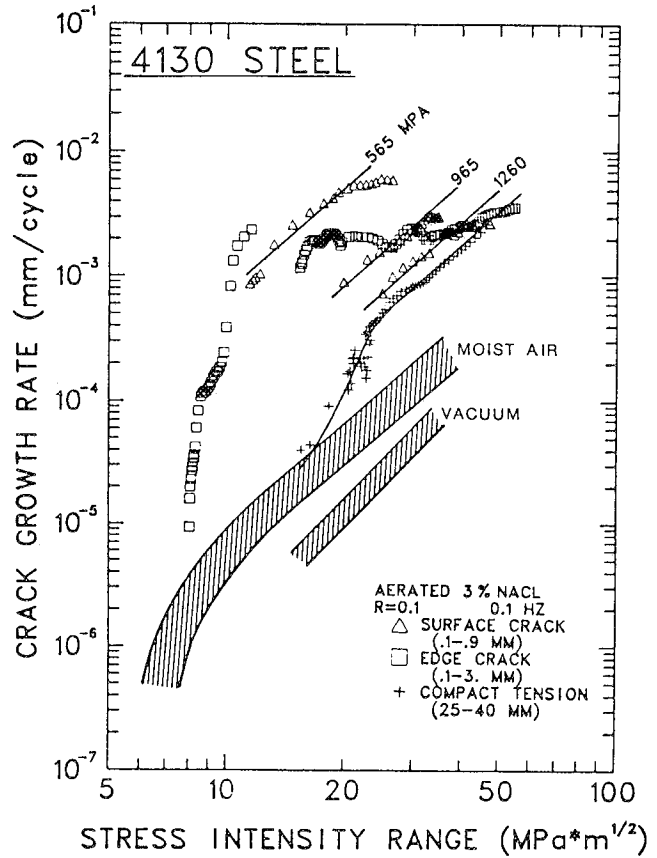
(b)

Fig. 42　　　Effect of specimen geometry and crack size on environmental fatigue crack growth; demonstrating (a) similitude for remote and crack surface loading of an Al alloy in NaCl; after Feeney, McMillan and Wei [14], and (b) a breakdown in similitude for short edge and surface cracks in a steel exposed to aqueous NaCl; after Gangloff [193,194].

oo Titanium alloys in halogen bearing electrolytes.

oo Precipitation hardened nickel based superalloys in hydrogen gas. (Nickel based superalloys in the Space Shuttle Main Engine.)

oo Precipitation hardened nickel based superalloys in elevated temperature moist air. (Nickel based superalloys in jet engine turbine disks.)

oo Stainless and ferritic steels in high purity water at elevated temperatures. (Steels in pressure vessel and piping components of commercial light water nuclear reactor systems.)

With the exception of the last case, data are summarized for each of these material-environment systems.

A. C-Mn and Alloy Steels in Hydrogen Producing Gases and Electrolytes

Ferritic and martensitic steels, ranging from low strength C-Mn (normalized) pearlitic microstructures to high strength quenched and tempered martensitic compositions, are prone to accelerated fatigue crack growth rates in gases and aqueous electrolytes. These environments are capable of producing atomic hydrogen through chemical and electrochemical reactions on clean crack and exposed specimen surfaces as indicated in Fig. 5. Hydrogen environment embrittlement is often maximum near 25°C and declines with both decreasing and increasing temperature. While there is a tendency for an increased environmental effect on fatigue with increasing steel yield strength, certainly above K_{ISCC}, the effect is not as marked as typically encountered for monotonic load hydrogen embrittlement; low strength steels can be severely affected by hydrogen during cyclic loading below K_{ISCC}.

The potency of hydrogen embrittlement during cyclic deformation is illustrated by data for steels in pure hydrogen gas. Results in Figs. 43 and 44 show the EFCP behavior of high (1330 to 1480 MPa) and of moderate (1035 MPa) yield strength martensitic steels cycled in low pressure (50 to 100 kPa) purified hydrogen [131,195]. For the higher strength steels in Fig. 43, (a) crack growth rates are increased by up to three orders of magnitude due to H_2, (b) the Paris regime slope is dramatically increased by hydrogen, (c) oxygen additions mitigate the hydrogen effect, and (d) crack growth rates increase with decreasing frequency. EFCP for the case in Fig. 43 is most likely at stress intensity levels above K_{IEAC} and the
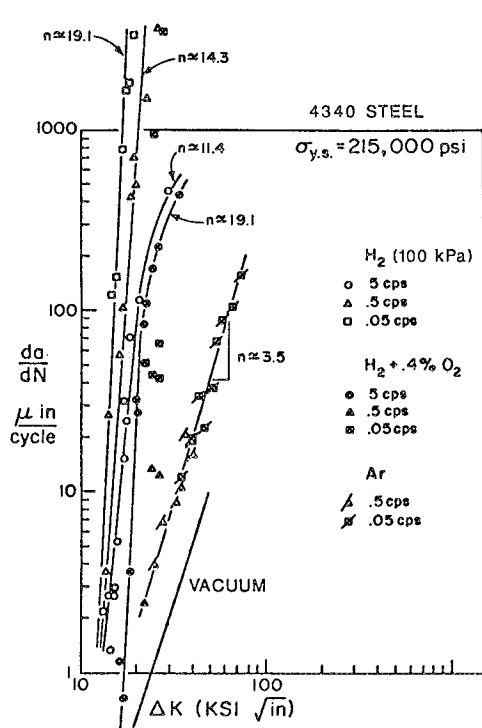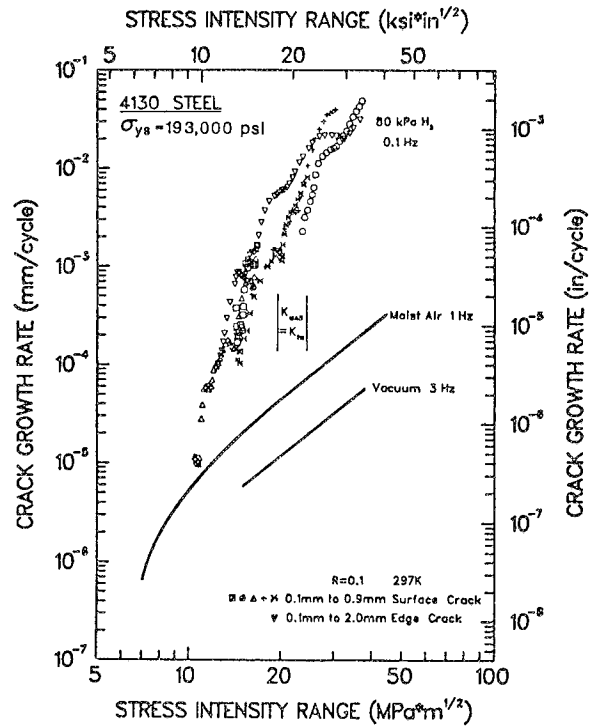
(a)   (b)

Fig. 43   Rates of gaseous hydrogen enhanced fatigue crack propagation in high strength quenched and tempered martensitic steels in 80 to 100 kPa H_2 at 25°C. 4340 (σ_{ys} = 1480 MPa) after Johnson [195], and 4130 (σ_{ys} = 1330 MPa) after Gangloff [131].

(a)

(b)
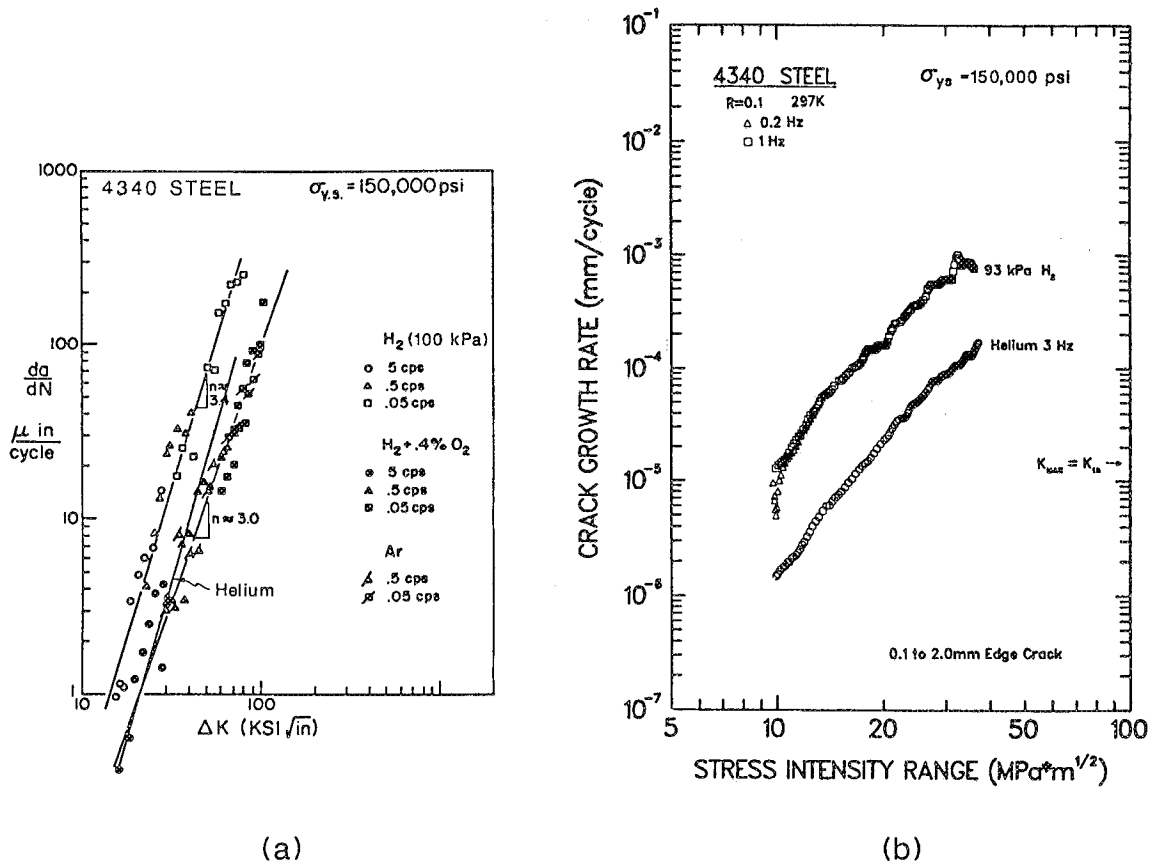
Fig. 44   Rates of gaseous hydrogen enhanced fatigue crack propagation in moderate strength (σ_{ys} = 1030 MPa) quenched and tempered martensitic steels in 90 to 100 kPa H_2 at 25°C. After Johnson [195] and Gangloff [131].

environmental effect is accordingly severe. For the moderate strength steel, Fig. 44, the effect of gaseous hydrogen is measurable, but growth rates are increased by less than an order of magnitude over a wide range of ΔK levels. The Paris exponent is not changed by environment and da/dN is not influenced by loading frequency. These characteristics are typical of cycle-dependent EFCP below K_{IEAC}.

Gaseous hydrogen enhances fatigue crack growth in low to moderate strength C-Mn and alloy steels, however, most data have been obtained at high hydrogen pressures. The damaging effect of low pressure H_2 (90 kPa) was first reported by Nelson for 1020 steel (σ_{ys} = 400 MPa) [129]. A similar result, albeit involving faster fatigue crack growth rates produced for high pressure (6.9 MPa) hydrogen gas, is illustrated by curve 2 in Fig. 45 [197]. Analogous behavior was reported for a moderate strength (σ_{ys} =745 MPa) quenched and tempered alloy steel in very high pressure (52 MPa) gaseous hydrogen [78].

Fig. 45 summarizes the effect of gaseous hydrogen on FCP in steels. Reference growth rate relationships are plotted from Equations 8 and 9 for FCP in vacuum [119], and from Equations 11 [122] and 22 [123] for moist air. The magnitude of the H_2 effect varies by between 5-fold and 10,000-fold increases in da/dN at fixed ΔK and compared to crack growth in vacuum. Curves 1 and 2 define the behavior of very high strength steel (σ_{ys} = 1325 to 1500 MPa from Fig. 43) in low pressure (100 kPa) H_2 [131,195]. Crack growth is largely above K_{IEAC}, and increases in severity with increasing steel yield strength, increasing R and decreasing loading frequency. Curves 3, 4, 5 and 6 define the behavior of lower strength steels (σ_{ys} from 200 to 1030 MPa; for example, from Fig. 44) in low pressure (100 kPa) H_2 [129,131,196]. While data are not definitive, crack growth is less sensitive to yield strength, f and R. Increased hydrogen pressure, for example to 6.9 MPa in curve 7 and between 1 and 100 MPa for interval marker 8, results in increased fatigue crack growth rates [78,197]. H_2 enhanced fatigue in low strength steels progresses below K_{IEAC}; the Paris exponent is unaffected by H_2 for curves 3 to 6, while it is dramatically increased for "above K_{IEAC}" fatigue in high strength steel as indicated in curves 1 and 2. The effects of hydrogen pressure, loading frequency and yield strength on EFCP are considered in Chapter VI on "Variables That Affect Environmental Fatigue Crack Propagation".

The composition of the hydrogen gas environment critically affects the degree of EFCP. As shown in Figs. 43a and 44a, small amounts of O_2 added to the H_2 environment
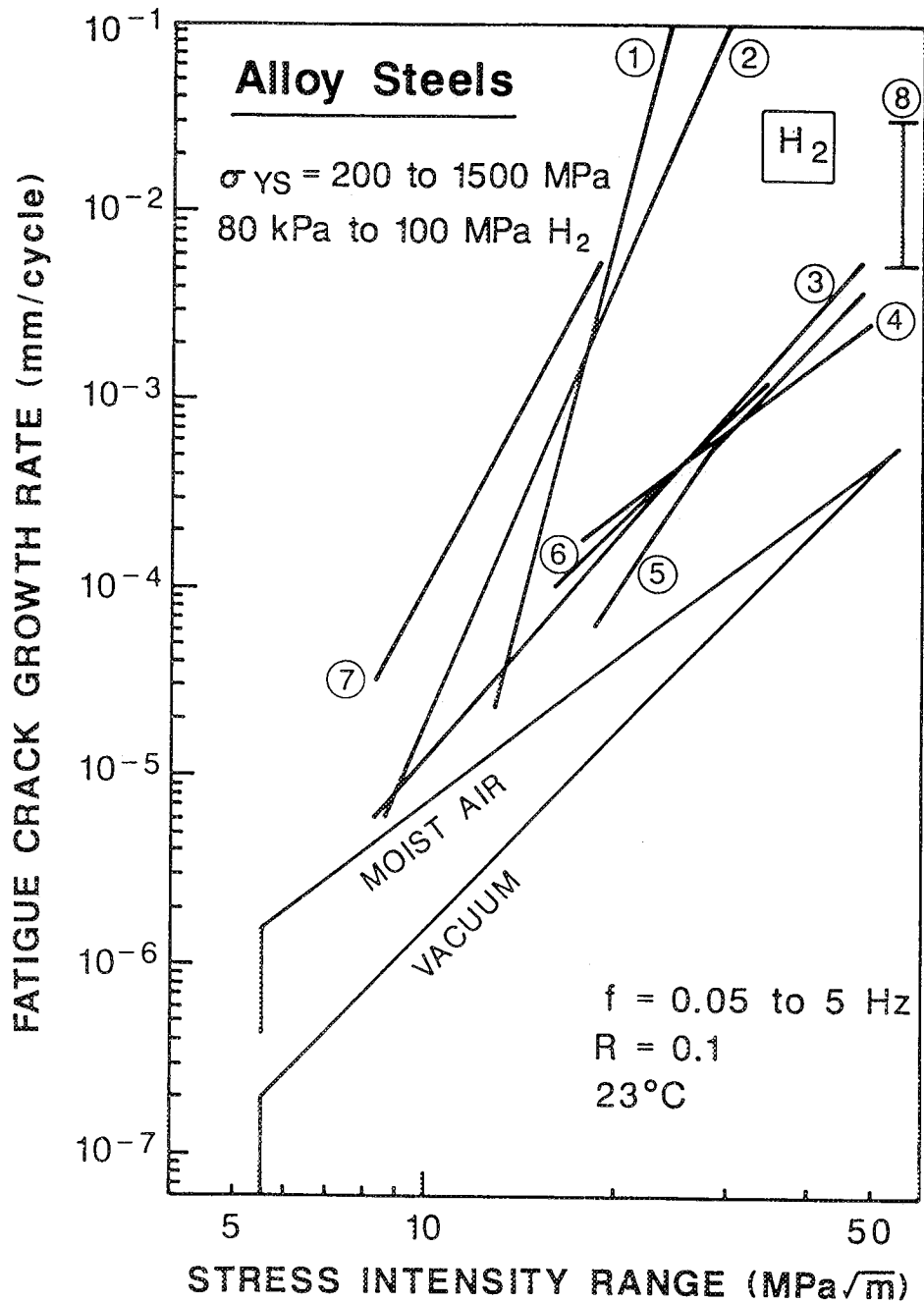
Fig. 45   Gaseous hydrogen enhanced fatigue crack propagation in alloy steels of varying yield strength; both above (curves 1 and 2; low H_2 pressure) and below (curves 3 to 6, 8; low to high pressure H_2) K_{IEAC} [78,129,131,195-197].

reduce the extent of hydrogen embrittlement. Here, oxygen preferentially adsorbs on the crack tip surface and blocks dissociative chemical adsorption of H_2 and subsequent uptake of atomic hydrogen (see Fig. 5). Gaseous hydrocarbons such as ethylene and acetylene are similarly beneficial in mitigating H_2 enhanced fatigue cracking by reducing hydrogen uptake through a chemical reaction-based blocking mechanism, as demonstrated in Fig. 46 [131]. In contrast to the beneficial effects of O_2, C_2H_4 and C_2H_2, Fig. 47 demonstrates the general result that EFCP in steels is exacerbated by exposure to low pressure hydrogen sulfide gas [196]. For moderate strength 2¼Cr-1Mo steel, crack growth rates are increased by well over an order of magnitude for FCP in 670 Pa H_2S compared to the benign environments.

Environmental fatigue is significant for low strength carbon-manganese steels, of normalized ferrite-pearlite microstructures, stressed in a variety of aqueous marine environments. Extensive data are represented in Fig. 48 [198]. Hydrogen environment embrittlement is implicated for these systems, as demonstrated by the two to three order of magnitude increase in da/dN for X42 steel in high pressure, purified hydrogen gas (curve 2) [197]. Considering aqueous environments, seawater produces enhanced fatigue crack growth relative to vacuum and moist air, with the magnitude of the effect increasing from free corrosion (curve 4) to cathodic polarization (curve 3) to H_2S additions at free corrosion (curve 1). The strong effect of H_2S is further evidence for hydrogen environment embrittlement, and is important to marine and other applications where biological reactions produce ionic sulfur bearing products [199,203].

The simple power-law regime of fatigue cracking observed for moist air and vacuum is altered by aqueous environments. A two-slope behavior is shown in Fig. 48, where a strong ΔK dependence of rate at lower stress intensities transforms to a milder dependence at higher ΔK. For cathodic polarization, da/dN values within the latter regime are nearly independent of increasing ΔK; a plateau is sometimes observed.

The amount of data on the effect of hydrogen environments on near-threshold fatigue cracking is not substantial compared to above-Paris regime behavior. For free corrosion, ΔK_{TH} is reduced by seawater exposure, with the effect of stress ratio paralleling that reported for crack growth in benign environments. For cathodic polarization, high R thresholds are probably similar to those reported for free corrosion, but notably, very high ΔK_{TH} values are
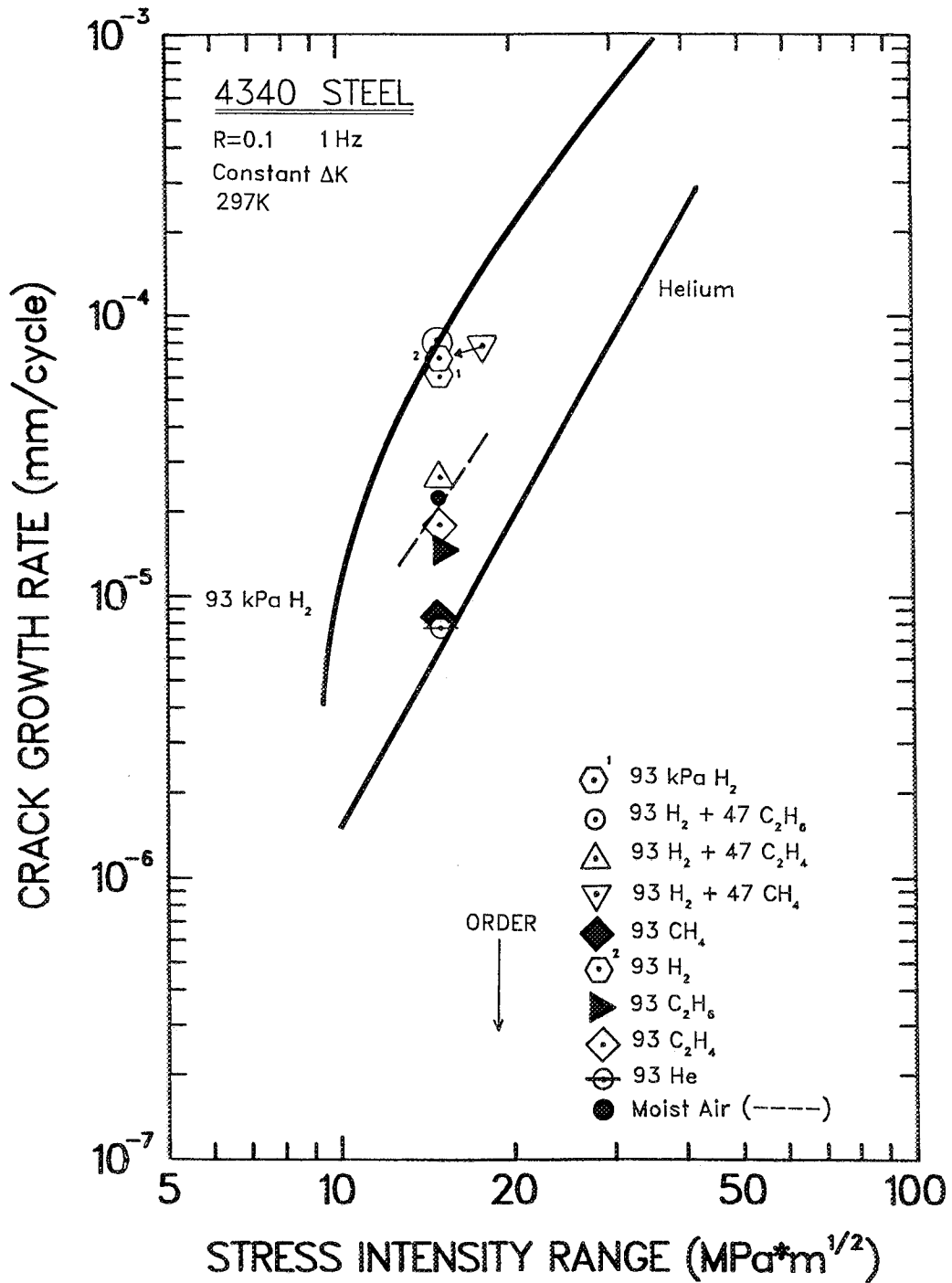
Fig. 46 Fatigue crack propagation rate data for moderate strength 4340 (σ_{ys} = 1030 MPa) steel in hydrogen-hydrocarbon gases at constant ΔK and frequency; after Gangloff [131].

89
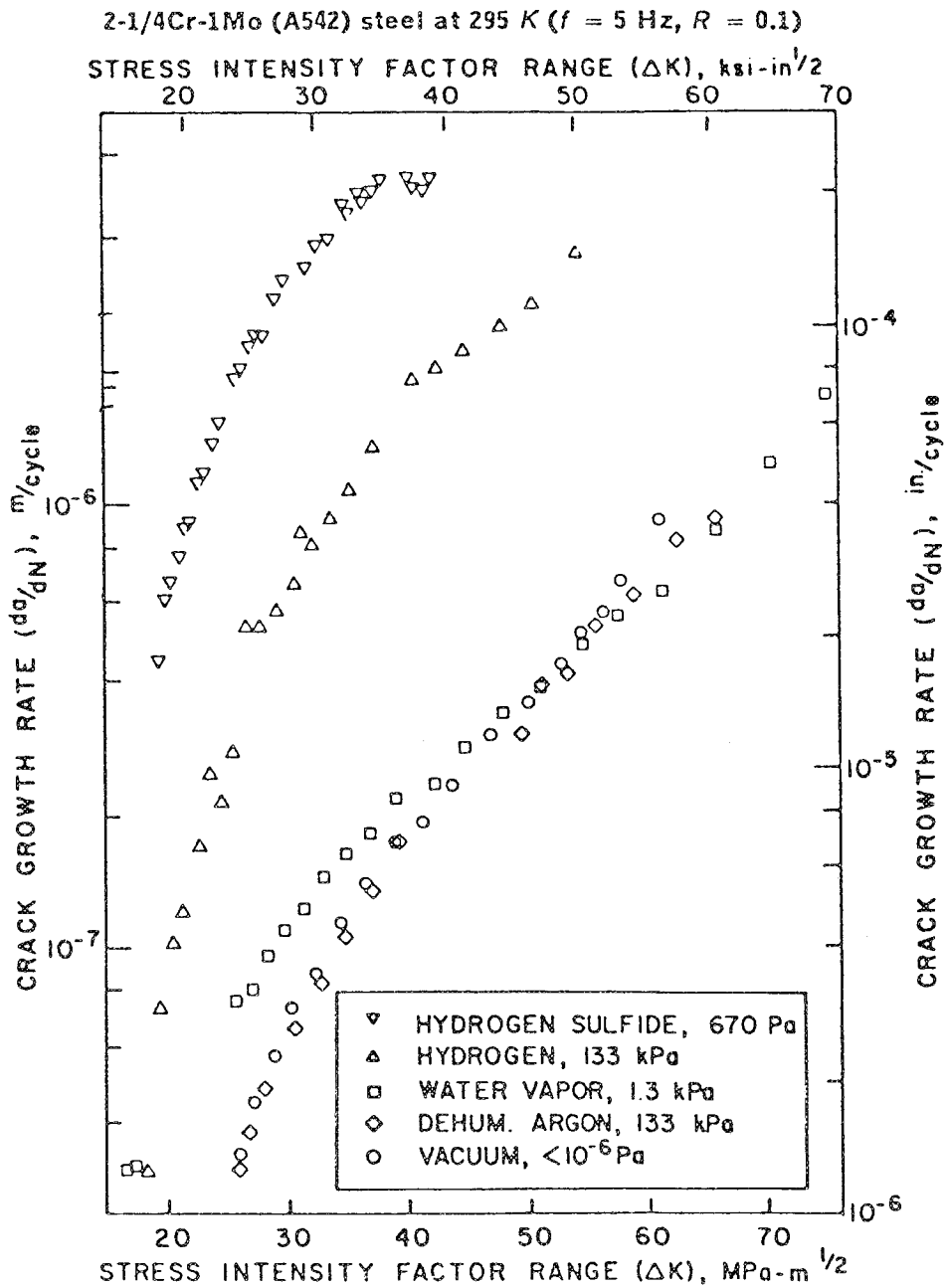
Fig. 47   The effect of gaseous H_2S in promoting EFCP in moderate strength 2¼Cr-1Mo
pressure vessel steel. After Brazill et al. [196].
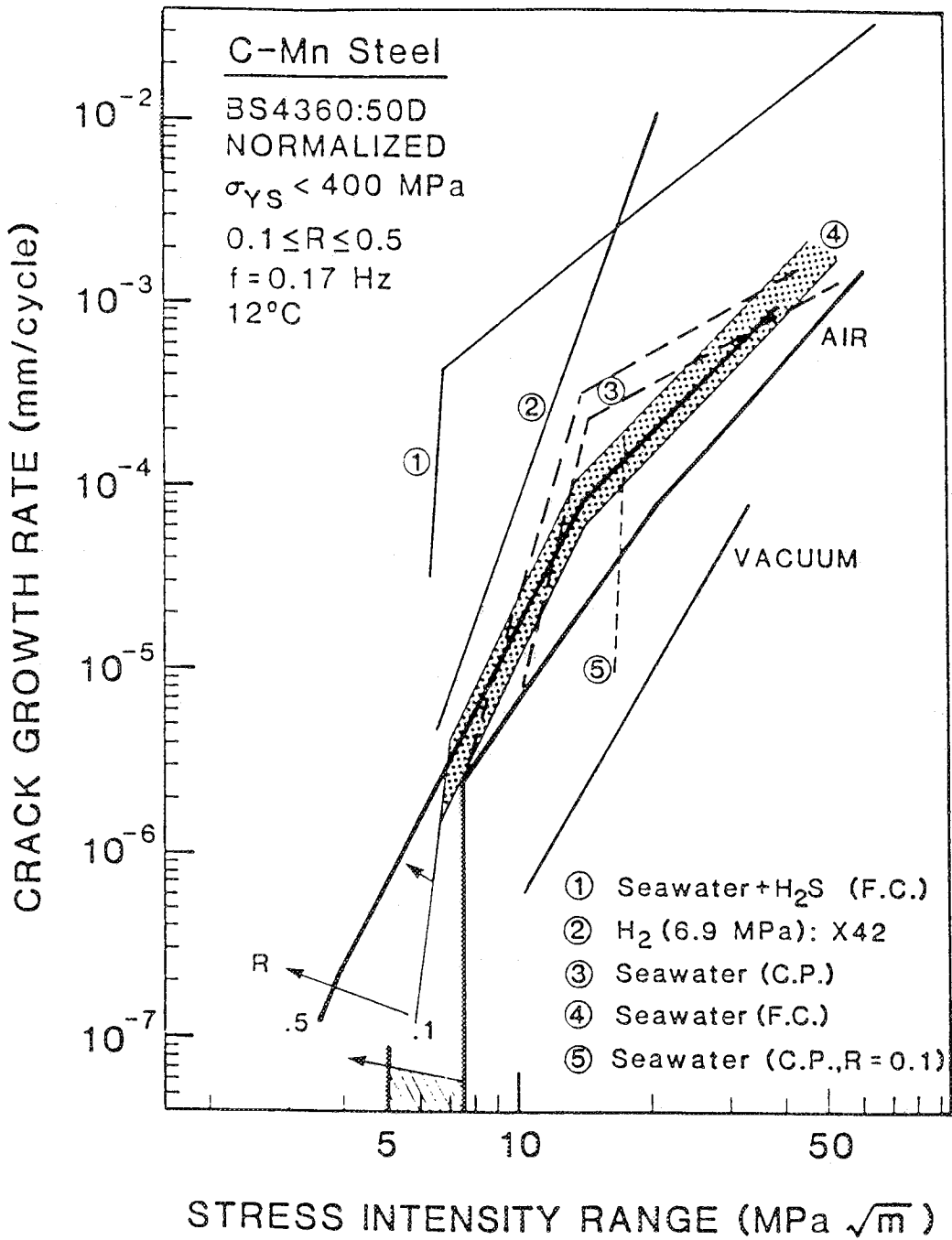
Fig. 48 Corrosion fatigue crack propagation in low strength, normalized carbon-manganese steels in hydrogen-producing environments: 1) Seawater contaminated by H_2S [199], 2) High pressure H_2 [197], 3) Seawater with cathodic polarization [200-203], 4) Seawater at free corrosion [124,200-203] and 5) Seawater with cathodic polarization at low R [121]; Moist air and vacuum [69,204].

91

$C \cdot 2$

reported for low R loading, as illustrated by curve 5 in Fig. 48 [2]. Ritchie and coworkers reported a decrease in ΔK_{th} and a concurrent increase in near-threshold crack growth rates for 2 1/4Cr-1Mo in gaseous hydrogen environment compared to FCP in moist air, as illustrated in Fig. 49 [205,206]. Oxide formed on the steel crack surface during cyclic loading in moist air, but not in dry H_2. Accordingly, corrosion product-induced crack closure enhanced ΔK_{th} for the former environment. The possibility for hydrogen embrittlement in H_2, apart from reduced closure, was not explored.

For many material and environment systems, it is possible to define that threshold stress intensity factor (K_{IEAC}) which is required to produce environmental crack propagation under sustained or monotonically varying load. K_{IEAC} is within the range of the ΔK values typical of fatigue crack propagation for the highest strength steels in the various hydrogen producing environments, Fig. 19. As discussed in Chapter IV on "Monotonic Load Environmental Cracking", this suggests that MECP contributes to the environmental fatigue response for this case. For the lower strength steels represented in Figs. 43 through 49, K_{IEAC} is typically greater than 100 MPa√m and is much larger than the highest stress intensities employed for environmental fatigue. Here, environmental cracking does not occur under monotonic loading; cyclic deformation must uniquely interact with the environment to cause fatigue crack growth.

The carbon steel-hydrogen environment system was reviewed in detail by Gangloff and Krishnamurthy [198] as well as by Jaske et al. [207].

B.   **Precipitation Hardened Aluminum Alloys in Water Vapor and Aqueous Chloride**

Extensive corrosion fatigue data have been produced for high strength 2000 and 7000 series aluminum alloys in aqueous chloride and purified water vapor environments. Several conclusions are drawn from the tabulation of typical results presented in Fig. 50 [14,74,75,91,136,173,208-214].

Both gaseous and aqueous environments produce significant corrosion fatigue crack propagation in aluminum alloys, and relative to helium or vacuum for a wide range of stress intensities. Hydrogen production and embrittlement (Fig. 5) are implicated for these systems,

---

[2]   Cathodic polarization produces calcium and magnesium hydroxide precipitates within the fatigue crack, causing corrosion product induced crack surface closure contact and increased ΔK_{th}.
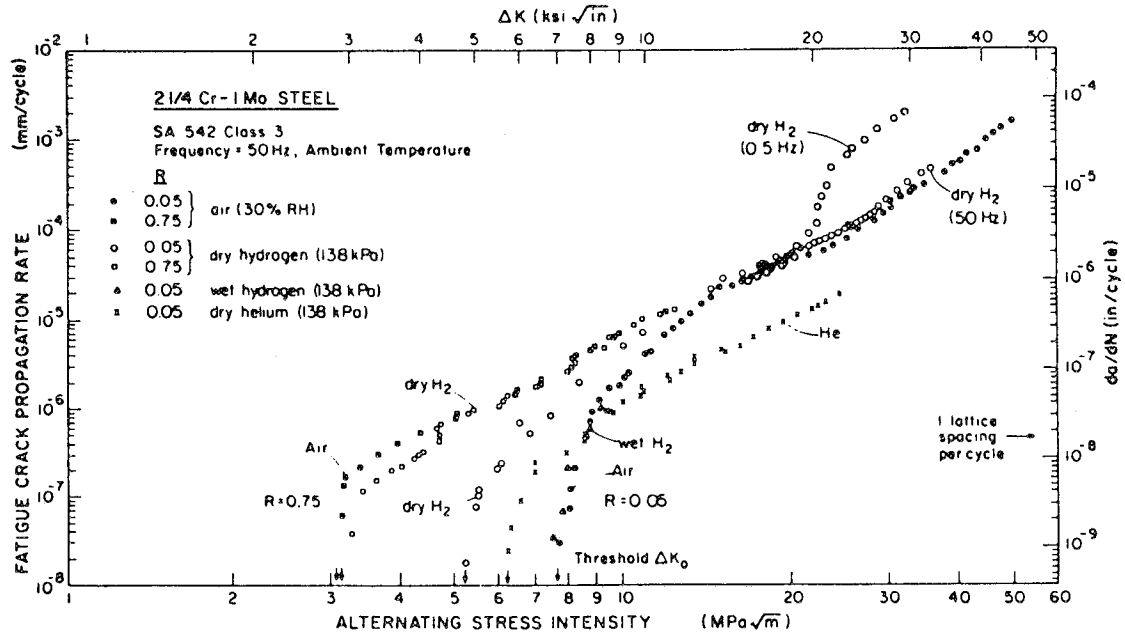
Fig. 49   Environmental fatigue crack propagation in 2¼Cr-1Mo steel in low-pressure gaseous hydrogen at room temperature. After Suresh and Ritchie [205,206].

93
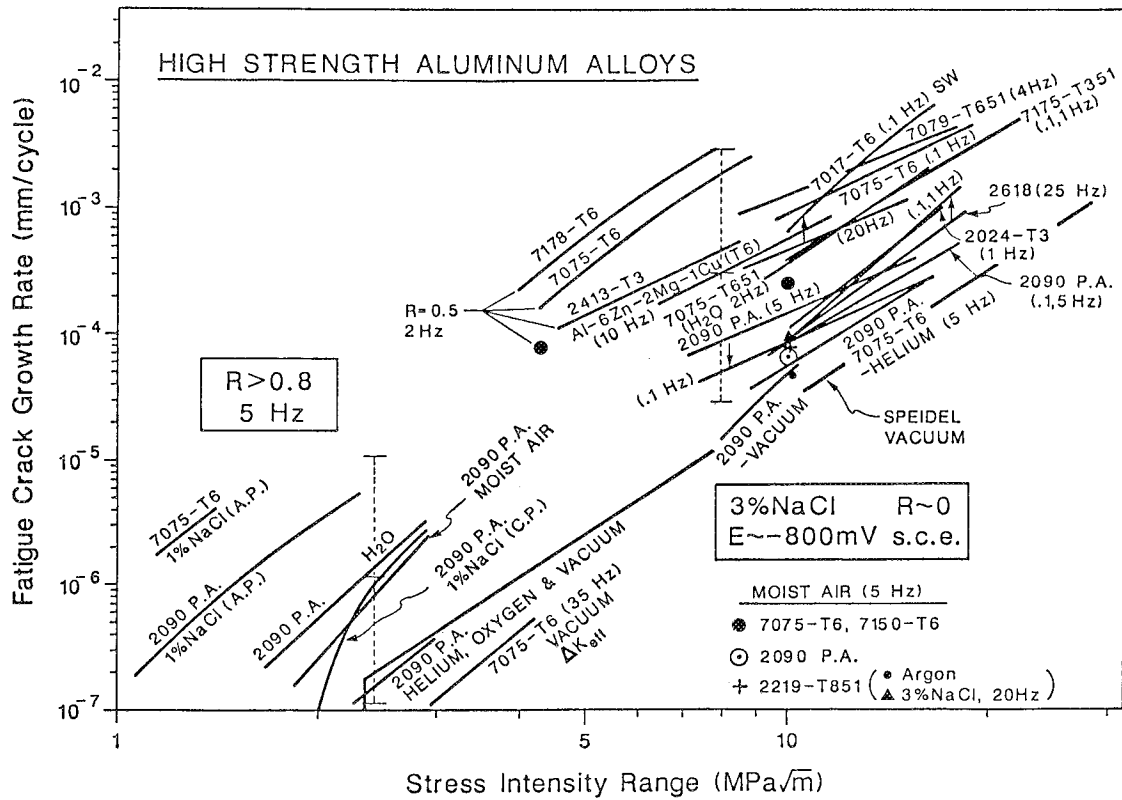
Fig. 50   Environmental fatigue crack propagation in high strength 2000 and 7000 aluminum alloys for: 1) Case A; High ΔK, low R; aqueous 3% NaCl near free corrosion [14,59,75,136,208-213,215], and 2) Case B; Near-threshold at high mean stress with aqueous chloride and gaseous environments [74,136,209].

however, the concurrent actions of anodic dissolution and passive film formation obscure the mechanism for EFCP which may be either above or below K_{IEAC}. The results presented in Fig. 48 were obtained for continuous immersion of the cracking specimen. Here, aqueous chloride at typical free corrosion potentials (about -800 mV, SCE) increases da/dN by between 4 and 100-fold relative to helium. Alternate immersion and salt spray environments are important to aerospace applications, however, fracture mechanics fatigue crack growth rate data are limited. Distilled water also promotes EFCP in aluminum alloys; Cl^- exacerbates, but is not a requisite for cracking. As stress corrosion cracking resistant aluminum alloys have been developed, sub-K_{IEAC} environmental fatigue behavior has become of paramount importance. Specific sub-K_{IEAC} environmental fatigue crack growth behavior for the advanced aerospace Al-Li-Cu alloy 2090 is presented in Fig. 51 [135]. For the alloy, LT crack orientation and environments represented in Fig. 51, K_{IEAC} is above K_{max} (17 MPa$\sqrt{}$/m) and environmental fatigue cracking is by transgranular processes.

Moist air is an embrittling environment compared to helium, particularly for the 7000 series alloys, and with water vapor as the likely embrittling culprit through a hydrogen mechanism. Wei and colleagues conducted extensive studies on the deleterious effect of pure water vapor on 7000 and 2000 series alloys at moderate stress intensity levels [75,212]. The range of rates varies between an upper bound somewhat higher than growth rates for humid air and a lower bound given by data for inert environments.

Only limited data have been obtained to describe near-threshold corrosion fatigue crack propagation in aluminum alloys [74,136,209,216,217]. Here, only high stress ratio results are reasonably interpreted because the complicating extrinsic effects of crack closure are minimal. Enhanced crack closure mechanisms in highly corrosive environments can lead to increased nominal ΔK_{th} at low stress ratios. As shown in Fig. 50, the intrinsic effect of water vapor, moist air and aqueous chloride (either free corrosion or cathodically polarized) is to reduce threshold stress intensity value relative to helium. The mechanism for this effect is speculative, with both hydrogen environment embrittlement and film rupture/dissolution processes possible. Notably, similar da/dN are reported for FCP in the helium and oxygen environments, suggesting a minimal effect of surface oxide films.

7000 series Al alloys are more prone to EFCP than 2000 series Al alloys, including the Mg + Cu and Li + Cu classes, in both the low and intermediate stress intensity ranges.

95
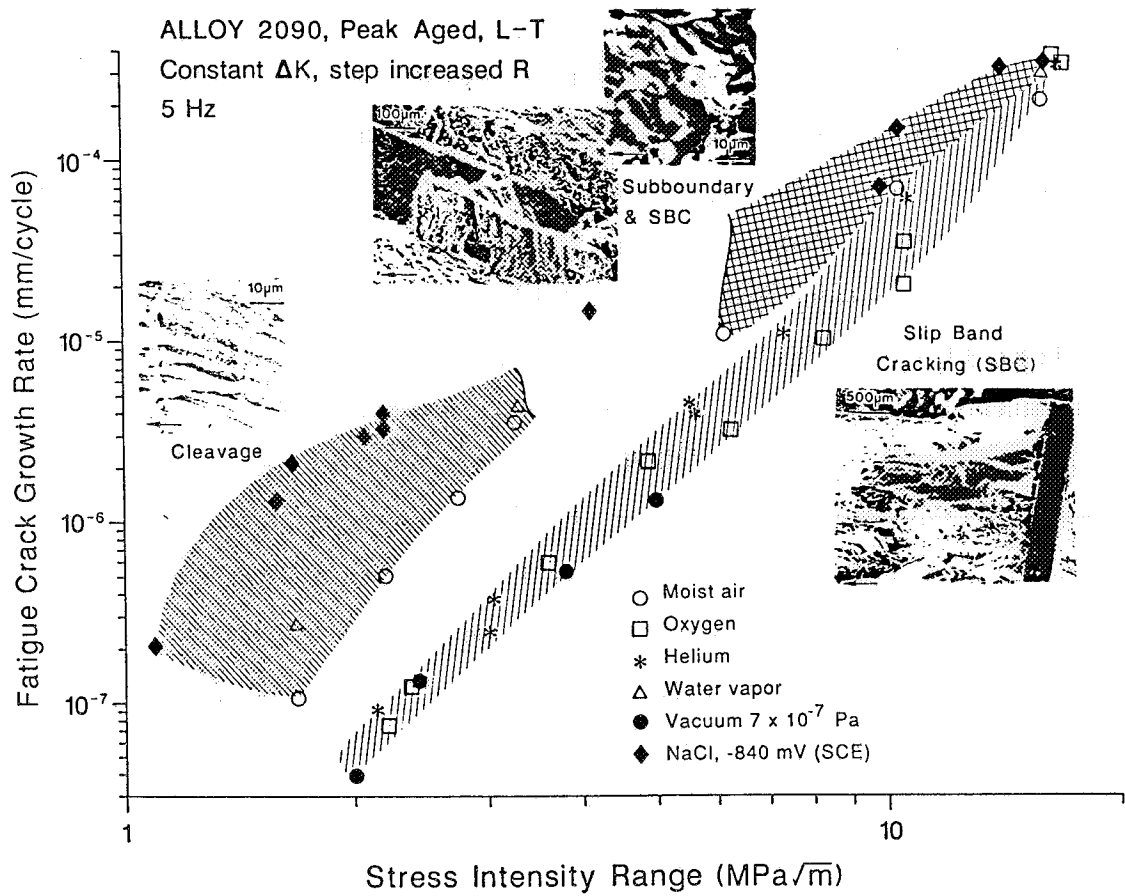
Fig. 51 Environmental effects on fatigue crack growth kinetics and microscopic cracking modes for Al-Li-Cu alloy 2090. After Piascik [135].

The transgranular environmental fatigue sensitivity of 7000 series alloys parallels the well known differences in intergranular SCC and hydrogen embrittlement resistance for these alloy classes [147]. The fundamental mechanism for the effect of alloy composition is, however, unclear.

The systems represented in Fig. 50 were reviewed by Speidel and Duquette [76,173].

C. Titanium Alloys in Halogen Bearing Electrolytes.

Since the pioneering stress corrosion cracking work of Brown, which showed the sensitivity of precracked titanium alloys to aqueous chloride solutions [149], many studies have investigated the corrosion fatigue behavior of this structural material [173]. Typical data are presented in Fig. 52 for Ti-6Al-4V [138,173]. Environmental fatigue crack growth rates are enhanced by up to 10-fold by cyclic loading in several halogen-bearing solutions, including 0.6M KCl and 5M KI, at the free corrosion potential. The resemblance between stress corrosion cracking and EFCP behaviors in titanium alloys is apparent; that is, the same ions increase subcritical crack growth rates.

Studies by Dawson and Pelloux demonstrated that the environmental fatigue crack growth behavior of both Ti-6Al-4V and Ti-6Al-6V-2Sn alloys in such halogen-bearing solutions is largely governed by ΔK and loading frequency, with the forms of the dependencies specific to fatigue above or below K_{IEAC} [72]. Fig. 53 summarizes the effects of frequency and bulk solution pH on the EFCP behavior of Ti-6Al-6V-2Sn in aqueous 0.6 M NaCl. Note the complex dependence of da/dN on ΔK and frequency. At higher ΔK, for either solution and where K_{max} is above K_{IEAC}, da/dN values increase with decreasing loading frequency and exceed growth rates for vacuum by up to two orders of magnitude. At low ΔK, the reverse frequency dependence is observed; faster loading rates favor increased da/dN. These two regimes of frequency response are bounded by a specific ΔK level, defined as ΔK_{SCC} by Dawson and Pelloux, where the fatigue crack growth rate versus ΔK relationship shows a sudden increase with increasing ΔK. This critical stress intensity range marks the onset of a strong environmental effect that Dawson and Pelloux referred to as "cyclic stress corrosion cracking". ΔK_{scc} is markedly lower than K_{IEAC} for static or monotonic loading of these alloys in the same solutions. Furthermore, ΔK_{scc} is a strong function of frequency, as illustrated in Fig. 54 [72]. ΔK_{scc} increases with decreasing frequency, approaching 0.9 K_{IEAC}

Legend (inside plot):

□ DRY ARGON
● DISTILLED WATER
○ 3.6M $(NH_4)_2 SO_4$
▲ 0.6M KCl
■ 5M KI

Ti-6Al-4V (MA) - ALLOY B

DCB
R = 0
F = 240 cpm
24°C

Axis labels:

FATIGUE CRACK GROWTH RATE   (cm/cycle)

CYCLIC STRESS INTENSITY   (Ksi $\sqrt{in.}$)
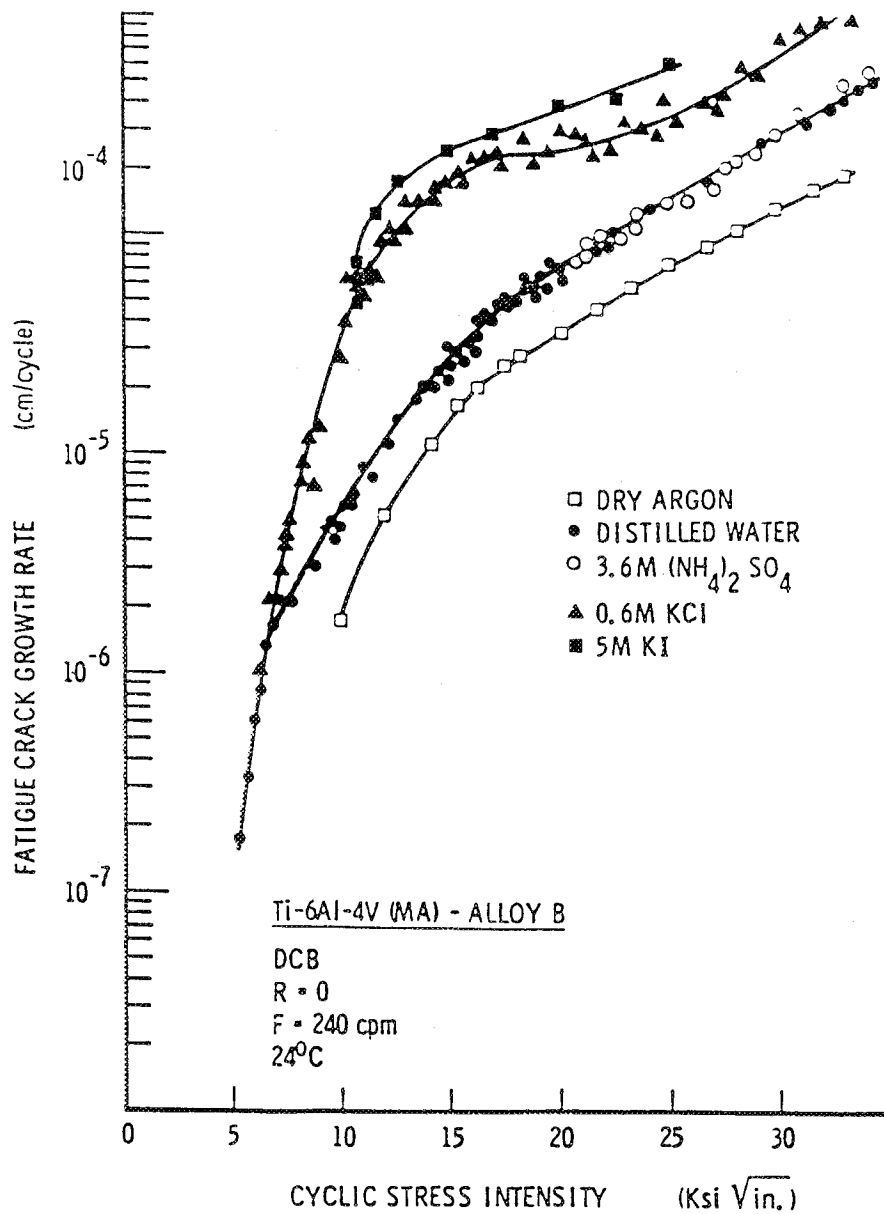
Fig. 52   Corrosion fatigue crack propagation data for a high strength titanium alloy in aqueous halide solutions. After Speidel et al. [173].
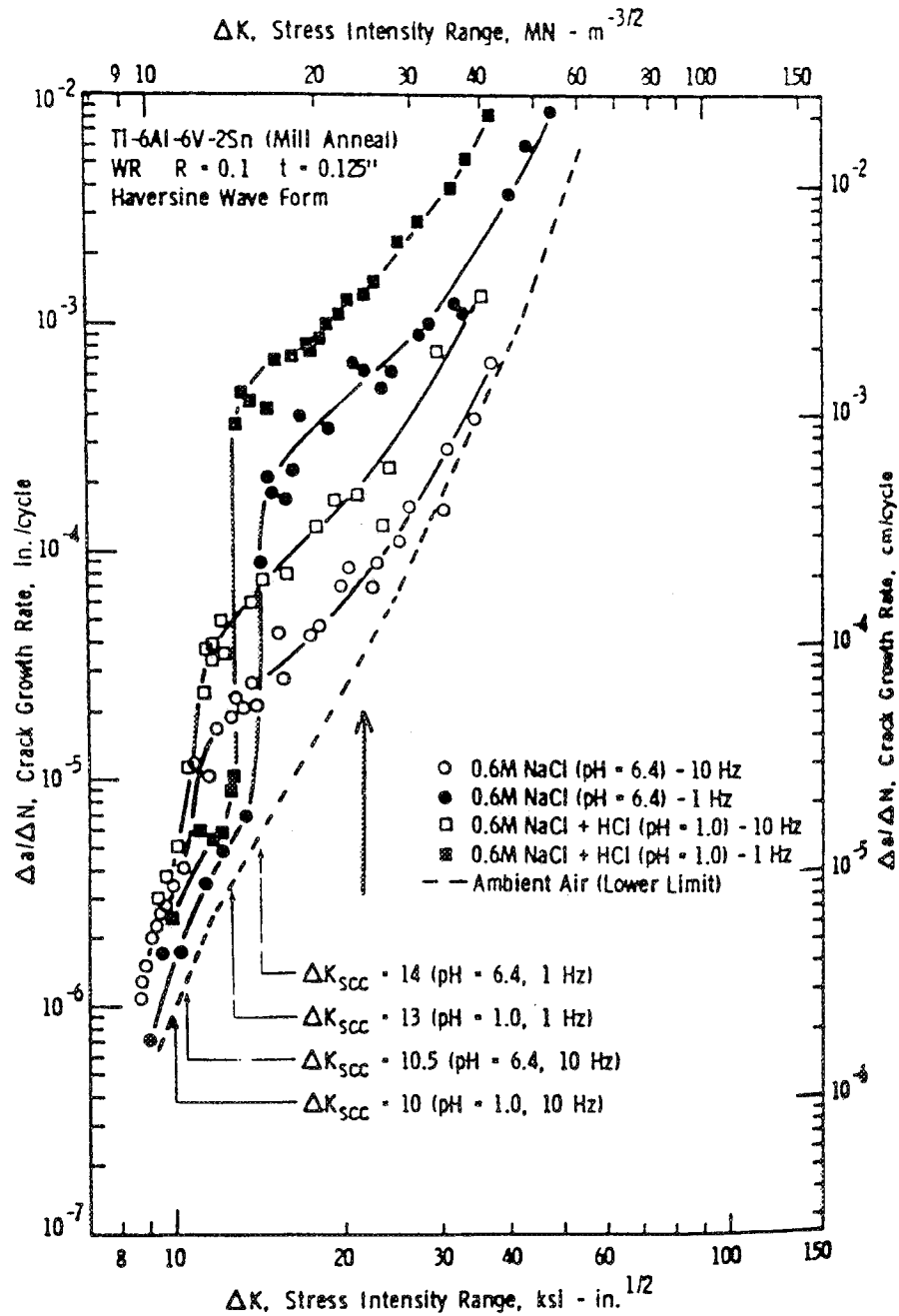
Fig. 53   Effect of loading frequency and bulk solution pH on the corrosion fatigue crack growth behavior of Ti-6Al-6V-2Sn in aqueous 0.6 M NaCl (pH 6.4) and 0.6 M NaCl + HCl (pH 1.0) at 1 and 10 Hz. After Dawson and Pelloux [72].

99
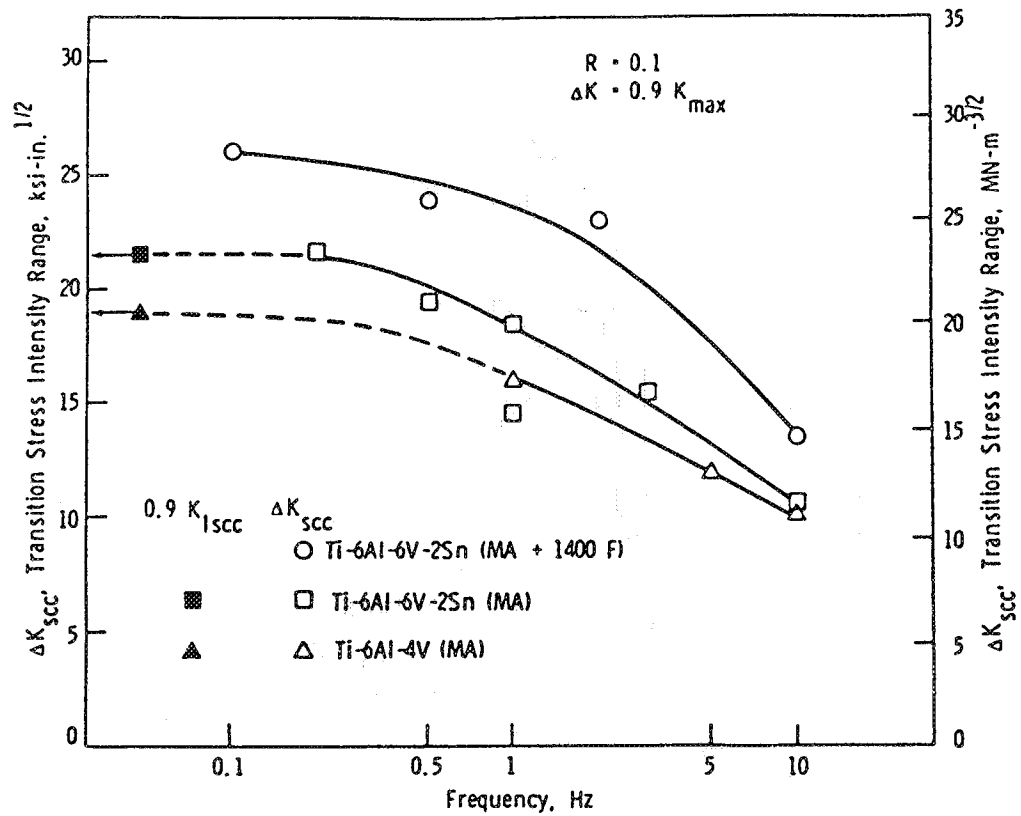
Fig. 54   Effect of frequency on ΔK_{SCC}, the transition stress intensity range for cyclic SCC. The ΔK level for which $K_{max} = K_{IEAC}$ shown for reference. After Dawson and Pelloux [72].

(where $K_{max} = K_{IEAC}$ for $R = 0.1$) as frequency decreases to the static load condition. The enhancement in ΔK_{scc} with increasing loading rate, or crack tip strain rate, is attributed to the repeated rupture of the passive film at the crack tip due to cyclic loading. Environmental fatigue crack growth rates above ΔK_{scc}, but below K_{IEAC}, cannot be accurately predicted by a simple linear superposition model. Indeed, proportional increases in da/dN with decreasing f for ΔK levels above K_{IEAC} are not observed, indicating that EFCP is not predictable by linear superposition of monotonic or static load da/dt versus K data. The fatigue crack growth rate is rather determined by both cyclic and time component of fatigue cycles for titanium alloys in electrolytes.

D.   Precipitation Hardened Nickel Based Superalloys in Hydrogen Gas

Limited data demonstrate strong gaseous hydrogen environment effects on fatigue crack growth rates in nickel based superalloys stressed at ambient temperature. The most notable work in this regard was conducted over the past 25 years by Walter, Chandler, Jewett and Frandsen at Rocketdyne and in support of materials applications in aerospace systems such as the Space Shuttle Main Engine. While a large amount of data were reported on high pressure hydrogen effects on uniaxial tensile and precracked fracture mechanics specimens subjected to monotonically increasing or constant load, only limited data are available for fatigue crack growth.

Data contained in Fig. 55 demonstrate that high strength ($\sigma_{ys} = 1120$ MPa) precipitation hardened Inconel 718 is prone to gaseous hydrogen enhanced fatigue crack propagation for a range of loading frequencies and H_2 pressures at 23°C [78]. Similar slow crack growth rates are observed for high pressure He and low pressure (69 kPa) hydrogen, with both sets of data in good agreement with Speidel's prediction from Equation 8 (E = 207 GPa). Substantial increases in crack growth rate, up to a factor of 10, were produced by higher hydrogen gas pressures and by reduced loading frequency including the long time load cycle based on the Space Shuttle Main Engine application[3]. The shaded band in Fig. 55 indicates typical values of the threshold (K_{IEAC} or K_{TH} in Fig. 55) for monotonic load environmental cracking of IN 718 in high pressure H_2. Data in Fig. 56 further demonstrate

---

[3]   (1.75 second ramp to P_{max}, 255 second hold period at P_{max}, 1.0 second ramp to 0.92 P_{max}, 235 second hold period at 0.92 P_{max}, 1.2 second ramp to P_{min}, and a 30 second hold period at P_{min}).

Inconel 718

$\sigma_{YS} = 1100$ MPa

69 MPa H_2
23°C

SSME HOLD
34.5 MPa H_2

0.1 Hz

34.5 MPa He

1 Hz

VACUUM

MOIST AIR

K_{th}

6 to 34.5 MPa H_2
−75 to 23°C

FATIGUE CRACK GROWTH RATE (mm/cycle)

STRESS INTENSITY RANGE (MPa√m̄)
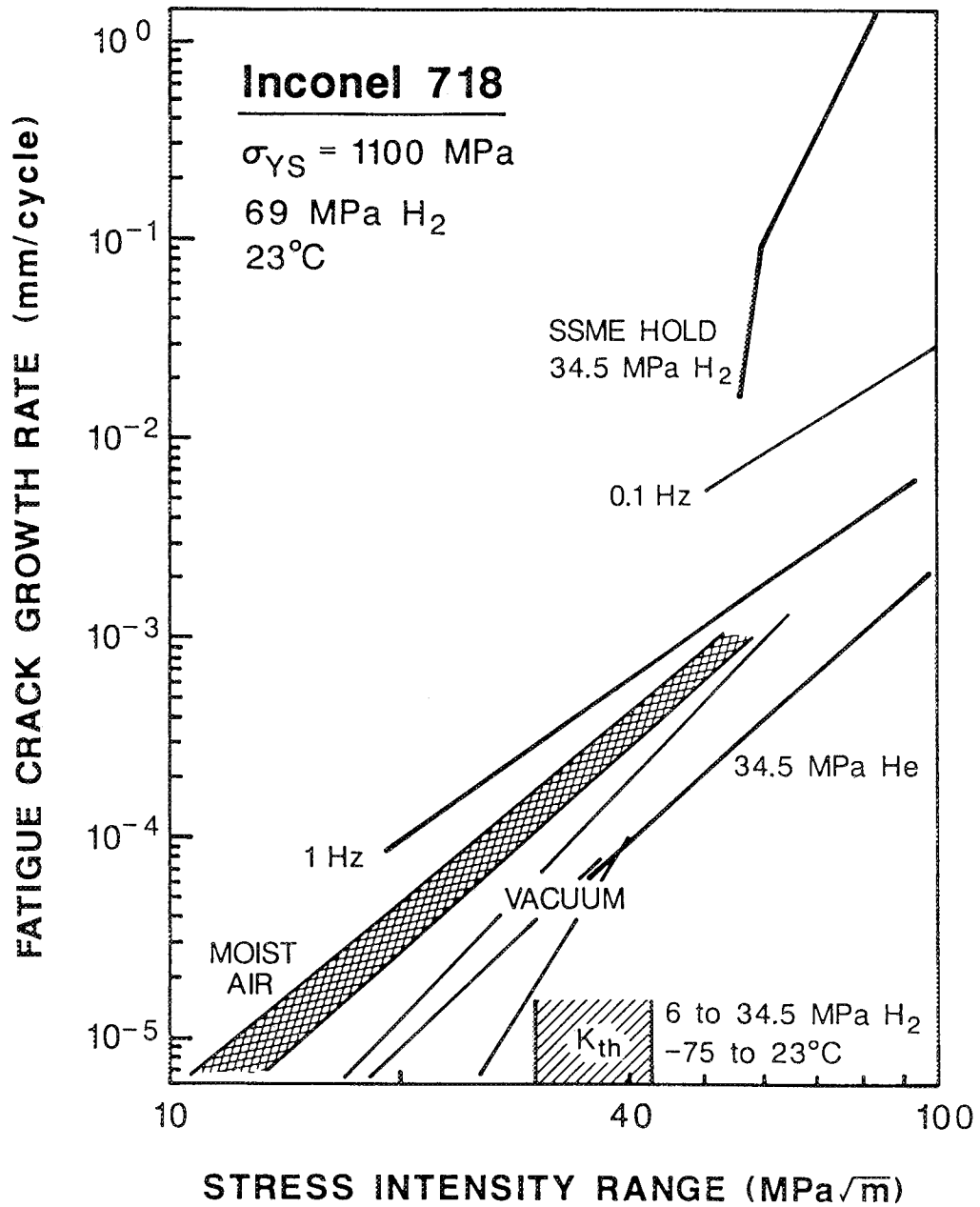
Fig. 55   Effect of high pressure gaseous hydrogen on fatigue crack propagation in IN 718 at 23°C and for several frequencies [78,80,218], compared to cracking in vacuum [112,119] and moist air [110].

Fig. 56   Frequency dependent fatigue crack propagation in IN 718 exposed to high pressure (7.5 MPa) gaseous hydrogen at 25°C. After Dodelin et al. [219].

frequency dependent EFCP in IN 718 exposed to high pressure (7.5 MPa) H_2 at 25°C [219]. Growth rates in H_2 are up to 40-fold faster than reference levels for FCP in moist air and arereasonably described by simple Paris power-law behavior. EFCP rates in hydrogen increase by a factor of 10 with a 100-fold decrease in frequency.

Data in Fig. 57 further indicate that high pressure H_2 (35 to 50 MPa) at 23°C accelerates fatigue crack growth rates in several high strength (900 MPa < σ_{ys} < 1300 MPa) nickel, cobalt and iron based superalloys[4] [218]. Compared to the Speidel vacuum result (Equation 8), da/dN values are enhanced up to five orders of magnitude by hydrogen for the very slow frequency fatigue cycle simulating a Space Shuttle Main Engine mission. These data indicate large effects of alloy composition and, for IN 718, of the microstructure of the precipitated phases. The fastest crack growth rates correlate with cracking of the interfaces between precipitates and the matrix, while somewhat slower growth rates were produced by intergranular cracking. Modes of cracking in hydrogen were different from those produced by fatigue in inert gas.

The stress intensity levels of the environmental fatigue results in Figs. 55 through 57 are notable for two reasons. Firstly, strong environmental effects on fatigue occur for cyclic stress intensities above K_{IEAC} for several of the microstructures. Considering Fig. 55, K_{IEAC} equals 30 to 40 MPa√m for hydrogen pressures greater than 5 MPa. The environmental fatigue data for 0.1 Hz and for the SSME cycle, and 68.9 MPa H_2, were obtained for maximum stress intensities above this monotonic load threshold. As a second example, data in Fig. 57 for IN 718 were obtained at stress intensity levels above sustained load thresholds of 14 MPa√m for STA 2 and 42 MPa√m for STA 1. The rapid environmental fatigue indicated here is consistent with these relatively low monotonic threshold values and with the prolonged hold periods of the fatigue cycle.

As a second point, much of the data in Figs. 55, 56 and 57 are of limited use because they were obtained at extremely high levels of ΔK. Hydrogen effects on FCP in IN 718 are not well characterized for important ΔK levels below about 18 MPa√m. The data for steels, aluminum and titanium alloys in various environments were for ΔK levels well below 40 to 50 MPa√m, and as low as ΔK = 2 MPa√m, while the bulk of the da/dN data in Figs. 55

---

[4] Haynes 188 is a single phase cobalt based superalloy, while IN 903 is an iron based alloy.
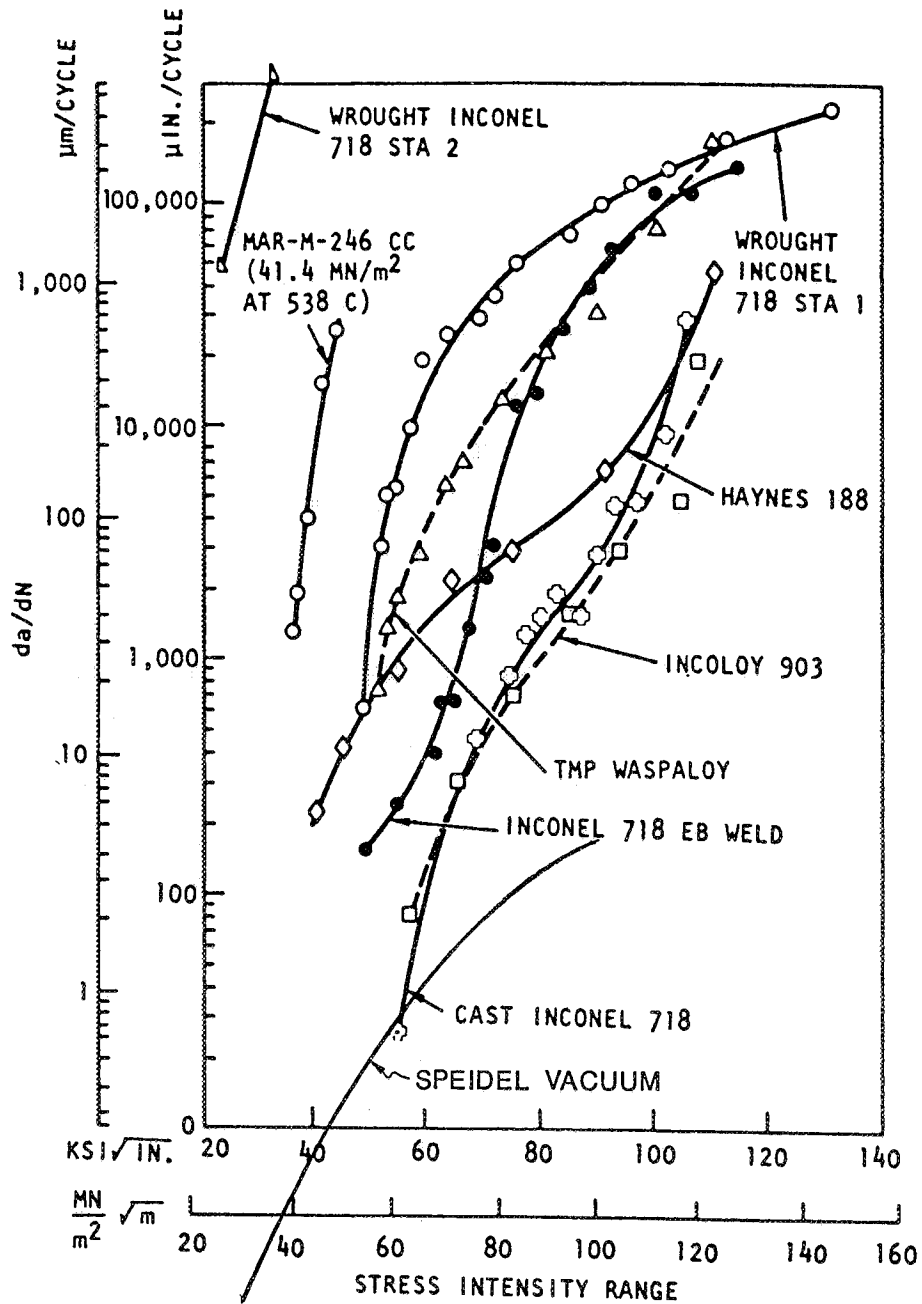
Fig. 57   Crack growth rate versus ΔK for various superalloys exposed to 34.5 to 48.3 MPa hydrogen gas at ambient temperature. After Walter et al. [218].

through 57 were obtained at ΔK levels between 40 and 140 MPa$\sqrt{m}$. Such high stress intensities are unlikely to be relevant to typical structural applications where applied stresses and existing flaw sizes are small to moderate. ΔK_{th} for nickel based superalloys in vacuum is about 5 MPa$\sqrt{m}$ based on Equation 9, and the fracture toughness levels of the superalloys in Figs. 55 and 57 are between 80 and 120 MPa$\sqrt{m}$. The results in Figs. 55, 56 and 57 are far from the important threshold regime and approach K_{IC}.

Crack growth rate data in Fig. 58 show that the chemistry of the H_2 environment critically affects EFCP, analogous to the behavior of steels [219]. While high pressure pure H_2 promotes EFCP in IN 718, the presence of KOH poisons the otherwise deleterious environmental effect. Crack growth rates for the H_2/KOH case are reduced by up to an order of magnitude compared to EFCP in pure H_2. Fatigue crack growth in the former environment is, however, up to 3-fold faster than da/dN for IN 718 in moist air.

Additional environmental fatigue crack growth rate data are required for nickel based superalloys in gaseous hydrogen. Mr. Ken Garr of the Rocketdyne Division of Rockwell International provided a bibliography of internal Rocketdyne work reported to date on the hydrogen compatibility of aerospace materials. Many of these experiments were carried out under contract to the NASA-Marshall Space Flight Center [78-80,220-225].

E.   Precipitation Hardened Nickel Based Superalloys in Elevated Temperature Moist Air

Extensive research over the past ten years has been aimed at the fatigue crack propagation behavior of high strength nickel based superalloys in elevated temperature moist air environments. The application for this work has been the development of damage tolerant alloys and fracture mechanics design methods for turbine disk components in military and commercial aircraft engines.   For high strength disk alloys, elevated temperature environmental effects can be strong, similar to the data presented for structural alloys in room temperature H_2. The fracture mechanics approach is relevant if time dependent plasticity is limited to a tens-of-micron sized process zone at the crack tip. This is the case, at least for typical alloys such as IN 718 at temperatures up to 550°C. The possibility for substantial inelastic creep deformation must be assessed for each set of da/dN-ΔK data; time dependent crack tip field parameters would have to be employed should the basic assumptions of the linear-elastic stress intensity approach be breached.
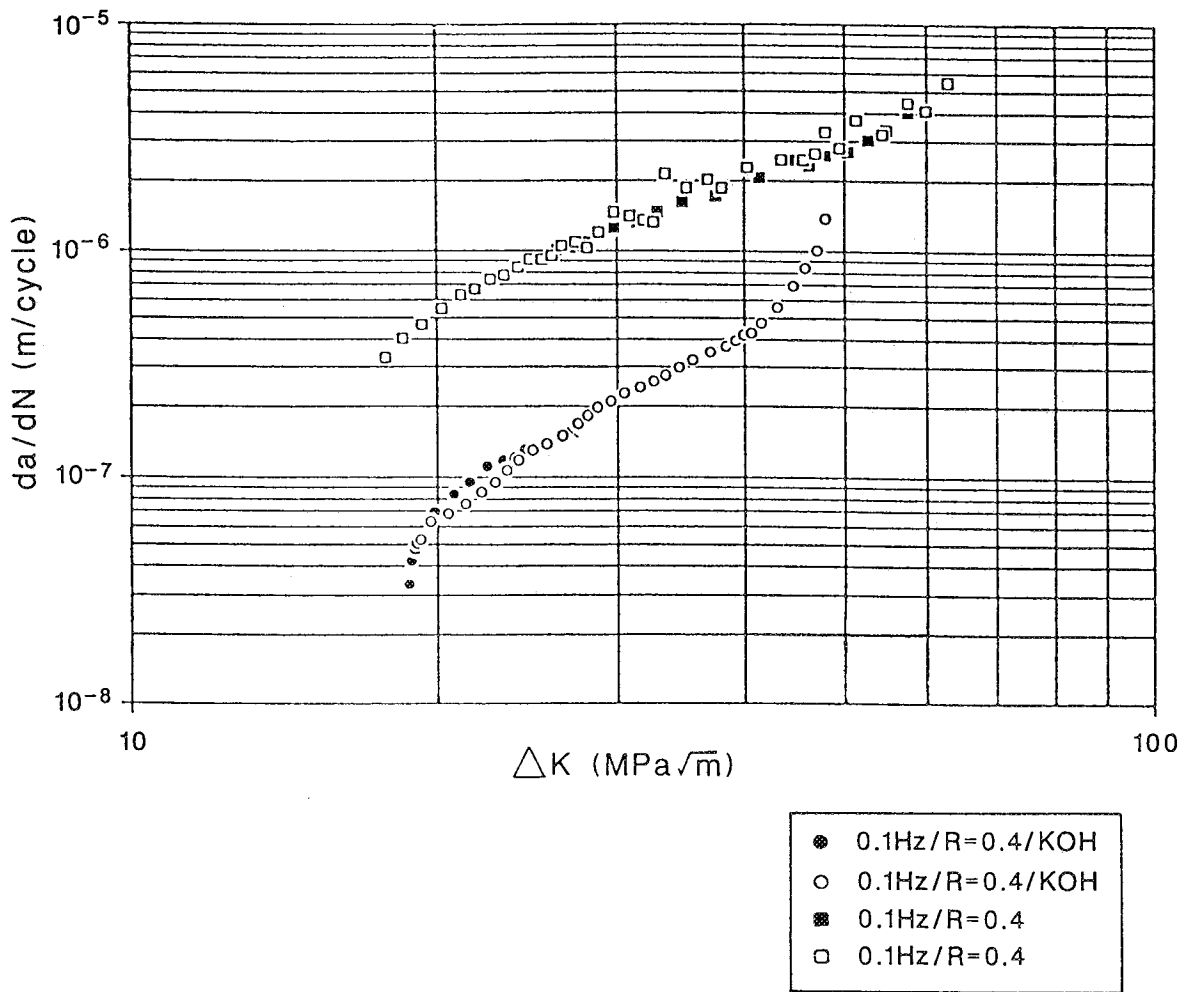
Fig. 58   The poisoning effect of KOH additions on environment enhanced fatigue crack
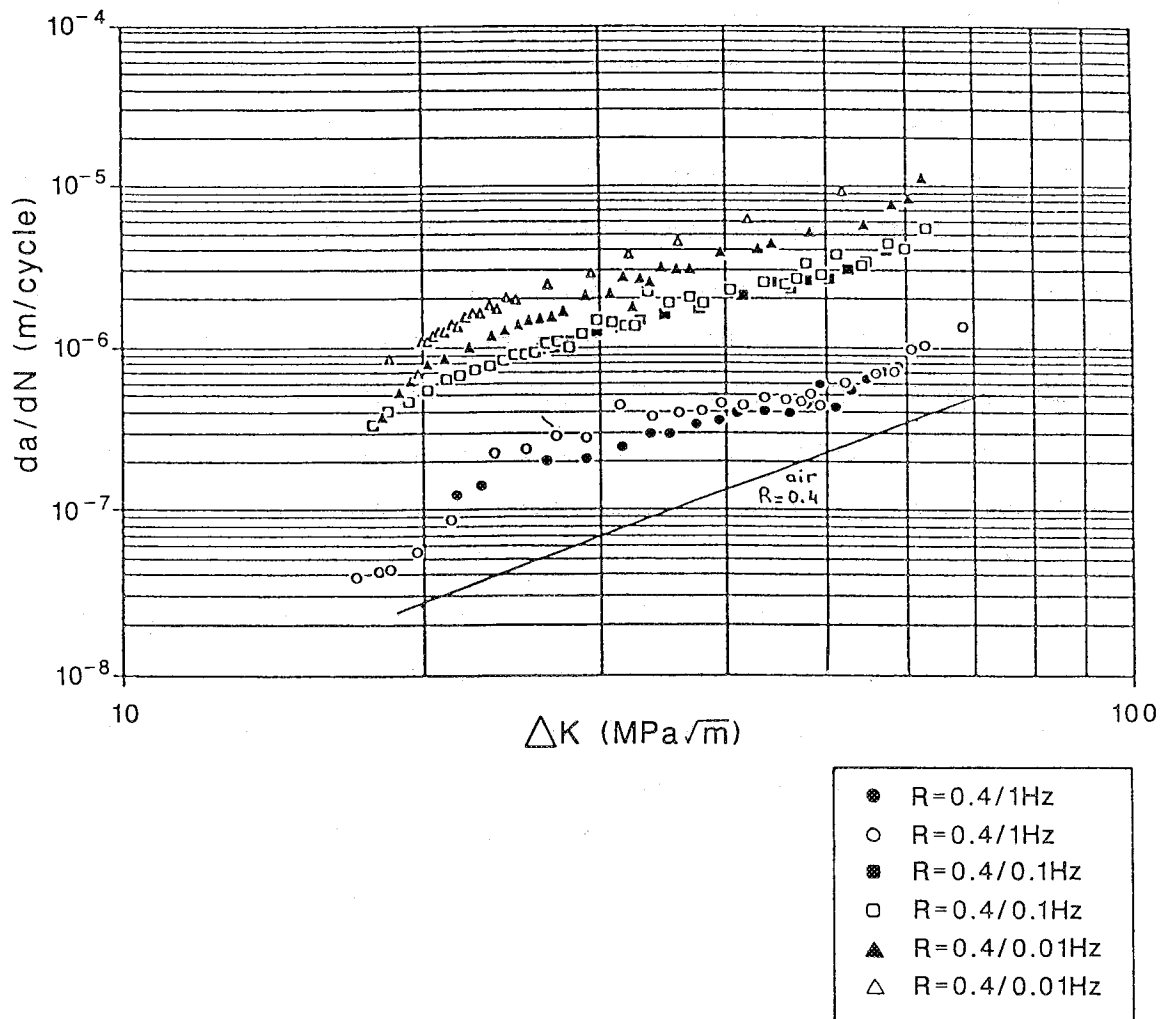propagation in IN 718 exposed to 7.5 MPa gaseous hydrogen at 25°C. After
Dodelin et al. [219].

Oxidizing moist air enhances rates of fatigue crack propagation in high strength nickel based superalloys at elevated temperatures, as illustrated in Fig. 59 [226]. These data were obtained for cast and wrought Rene' 95 (σ_{ys} = 1200 MPa), subjected to either continuous or hold time load cycling at 538°C. Slow crack growth rates are observed for fatigue in vacuum, consistent with the prediction of Equation 8 (E = 207 GPa). Notably, similar da/dN values are reported for fast (1 to 5 Hz by Speidel) and slow (0.1 Hz) loading frequencies in vacuum. This result indicates that time dependent creep-fatigue deformation does not contribute to FCP in this alloy at 538°C. In sharp contrast crack growth is accelerated by loading in moist air, with the effect exacerbated substantially by the 15 minute hold period. Similar results are shown in Figs. 12 and 13 for IN 718. For FCP at 25°C, equivalent da/dN levels are reported for vacuum and moist air. An enhancement in growth rates is seen for elevated temperature, fast (20 Hz) loading; the environmental effect is promoted by slower frequency continuous and hold time loading.

The trends indicated in Fig. 59 are further demonstrated in Fig. 60 for IN 718 cyclically loaded in moist air at 649°C [111]. The slowest rates of crack growth are recorded for the baseline conditions which include a loading frequency of 1 Hz, a hold period of 0 seconds and a stress ratio of 0.1. Increased R to 0.5 only affects a reduction in the threshold stress intensity. Critically, crack growth rates are increased by decreased loading frequency to 0.01 Hz or by the inclusion of a 50 second hold period at K_{max}.
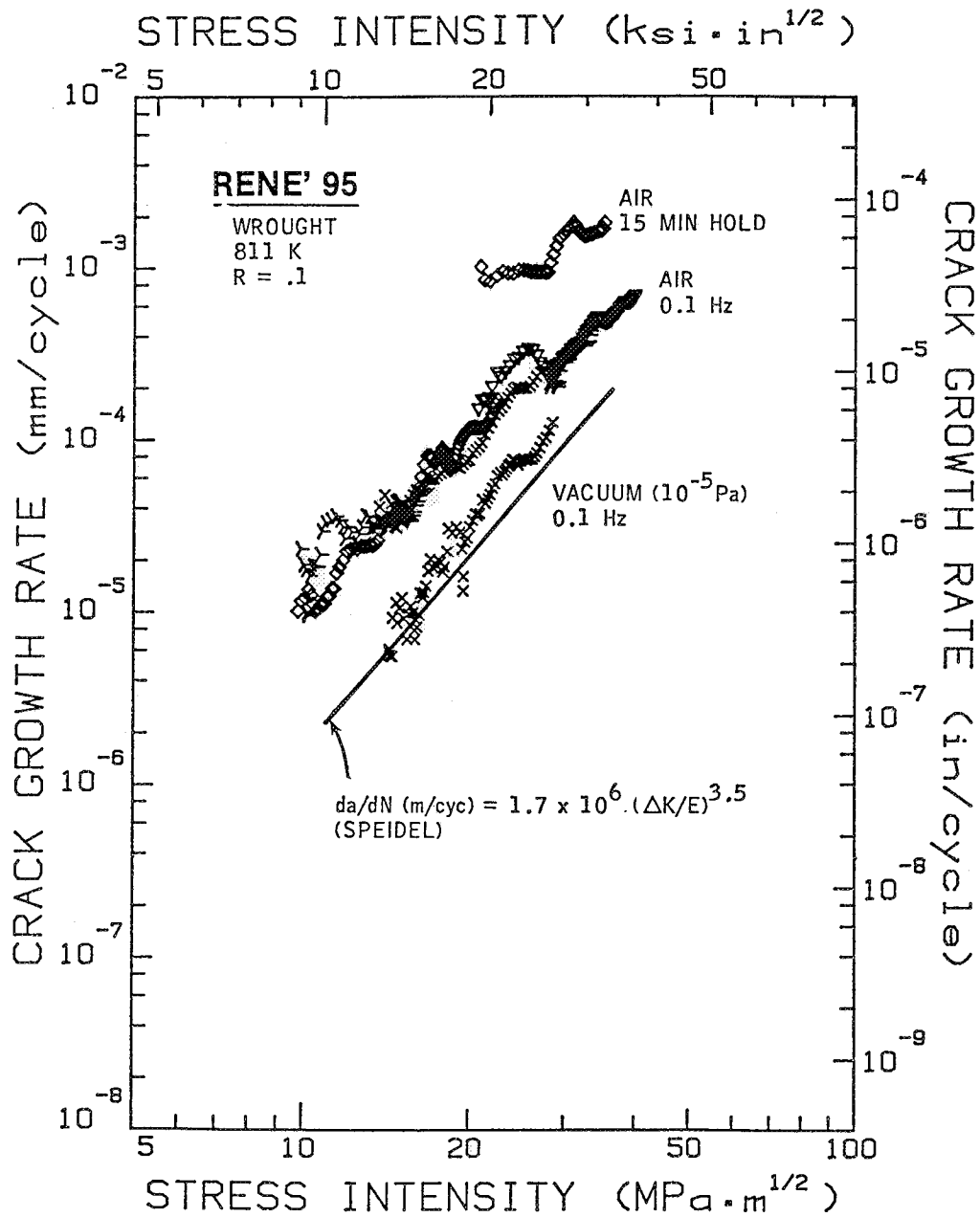
Fig. 59   Effects of moist air and hold time on fatigue crack propagation rates for cast
and wrought Rene' 95 (σ_{ys} = 1200 MPa) at elevated temperature. After
Gangloff [226].

109
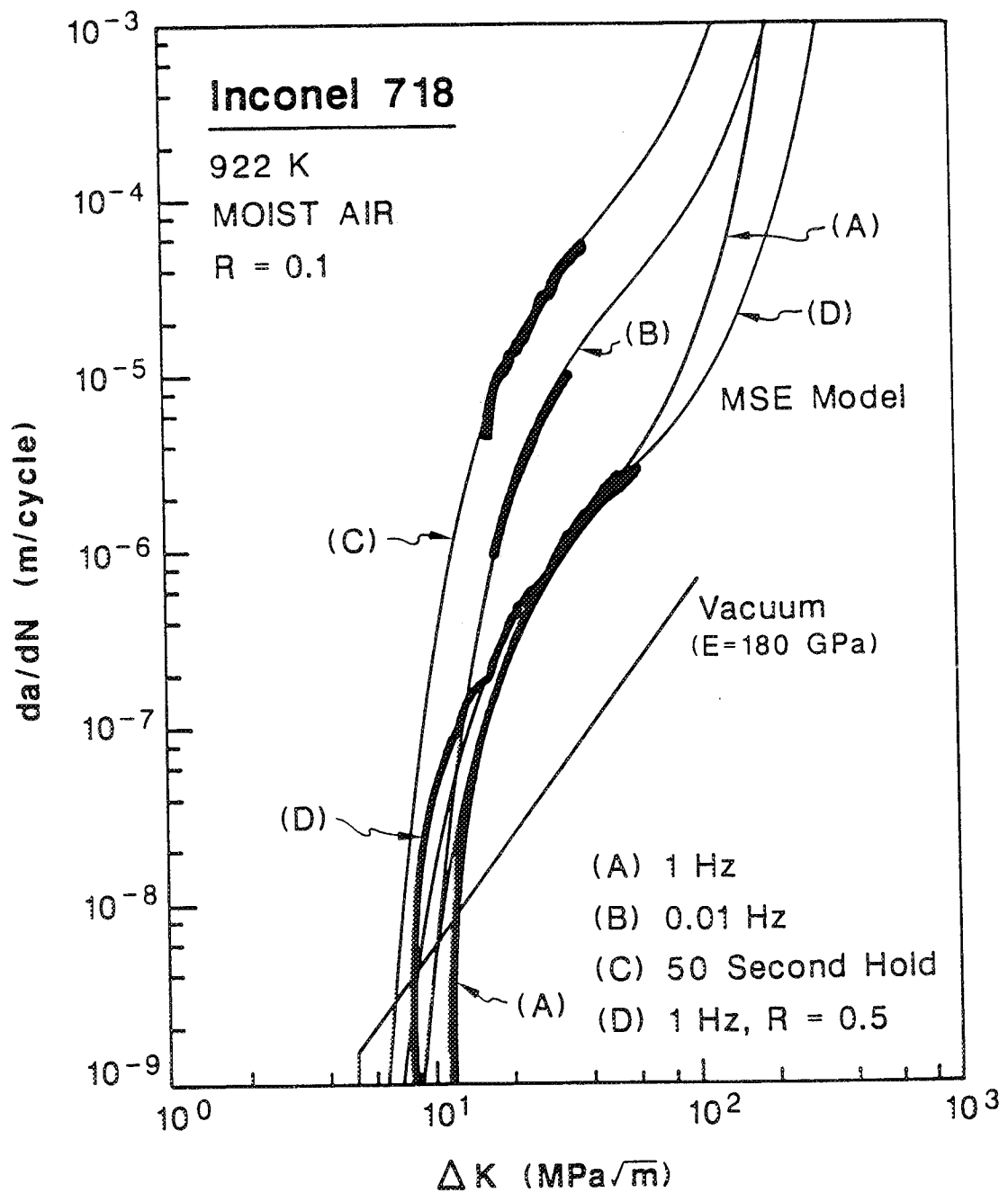
Fig. 60   Effect of moist air environment and loading frequency on elevated temperature
fatigue crack propagation in IN 718. After Haritos et al. [111]

VI. VARIABLES THAT AFFECT ENVIRONMENTAL FATIGUE CRACK PROPAGATION IN STRUCTURAL ALLOYS

Environment enhanced fatigue crack propagation behavior is determined by the interactions of a wide range of mechanical, metallurgical and environment chemical variables, as can be inferred from the typical results presented in Figs. 42 through 60. An example is provided in Table 1 for aluminum alloys in water vapor and aqueous chloride environments. These variables are similarly relevant for steels, Ti and Ni-based alloys. Many of these variables have no influence on FCP in benign environments; for the environmental case, however, these variables interact to complicate fatigue crack growth kinetics. Environmental da/dN versus ΔK data are decidedly more complex to incorporate into life prediction models.

A. Stress Intensity Range

The simple Paris power-law relationship between da/dN and ΔK, to stress intensities approaching ΔK_{TH}, has significance for FCP in benign environments, but is not applicable for aggressive environment cases. That stress intensity range affects environmental fatigue crack propagation in a complex fashion compared to inert environments is schematically illustrated in Figs. 16, 19 and 61 [36,171]. While a power-law response is typical for any limited range of ΔK, a more complex da/dN-ΔK relationship is possible over a broader range of stress intensities, as first suggested by McEvily and Wei in Fig. 16 [171] and amplified by Scott [36]. The complex forms of da/dN-ΔK relationships are exhibited in Fig. 62 for Ti-6Al-4V, X65 controlled rolled microalloyed ferritic steel, and precipitation-hardened aluminum alloy 7017-T651; each in aqueous chloride.

Environmental effects do not simply shift the da/dN-ΔK relationship to increased growth rates. Rather, the magnitude and pattern of EFCP depend on the relative contributions of monotonic load environmental cracking and cyclic strain induced environmental cracking. Such results are expected because inert environment fatigue is driven by crack-tip plasticity, which is uniquely related to ΔK, while environment enhanced fatigue crack growth involves conjoint plastic strain and chemical processes. Predictions of the complex effect of stress intensity require mechanistic models of the environmental effect.

When monotonic load environmental cracking dominates the contribution to environmental fatigue crack growth rates, the da/dN-ΔK relationship clearly indicates this class of behavior and is of the Type B cracking form indicated in Fig. 16, or equivalently of the

111
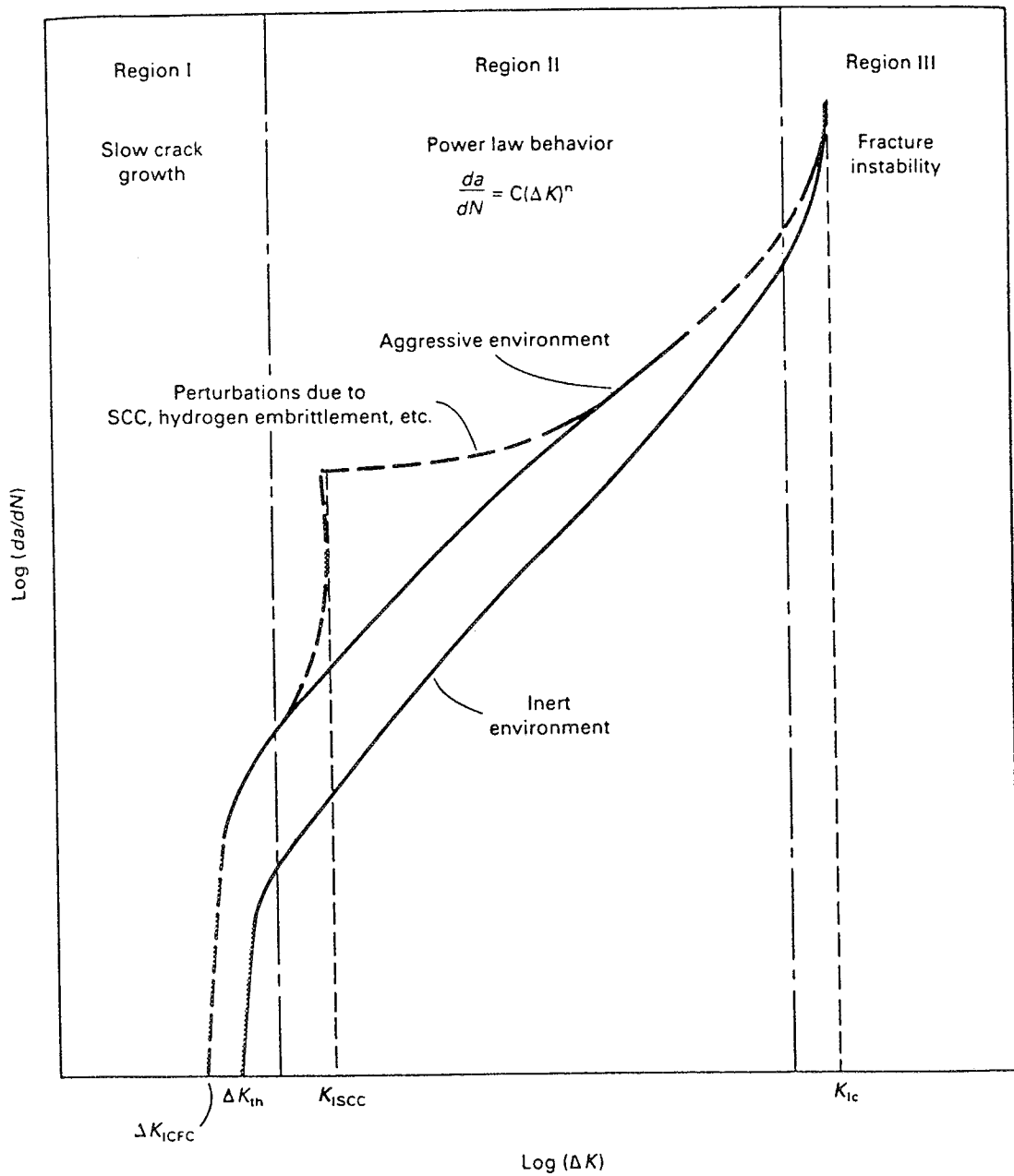
Fig. 61   Schematic illustration of environmental fatigue crack propagation as a function of ΔK. After Scott [36].

112
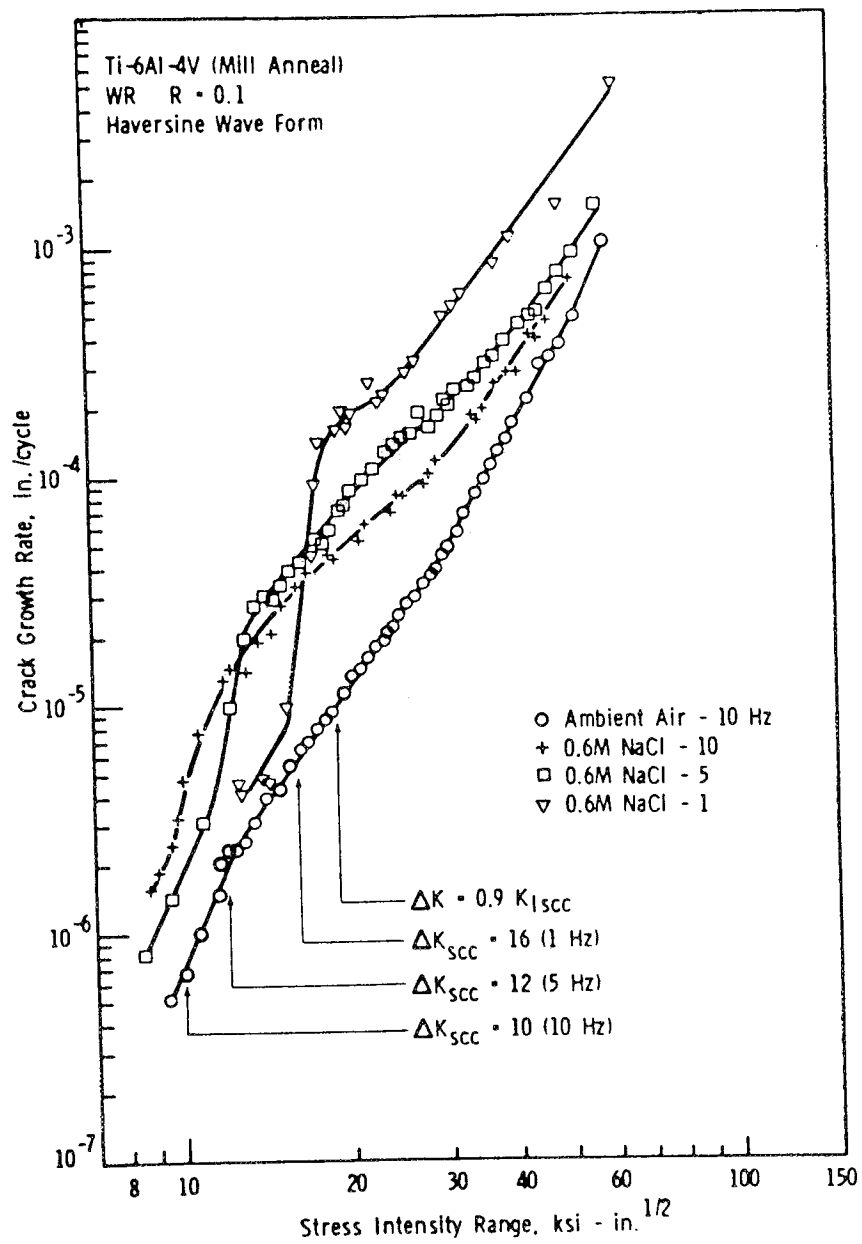
Fig. 62a   Effect of ΔK on corrosion fatigue crack growth rate at several frequencies for Ti-6Al-4V in 0.6 M NaCl. After Dawson and Pelloux [72].

113
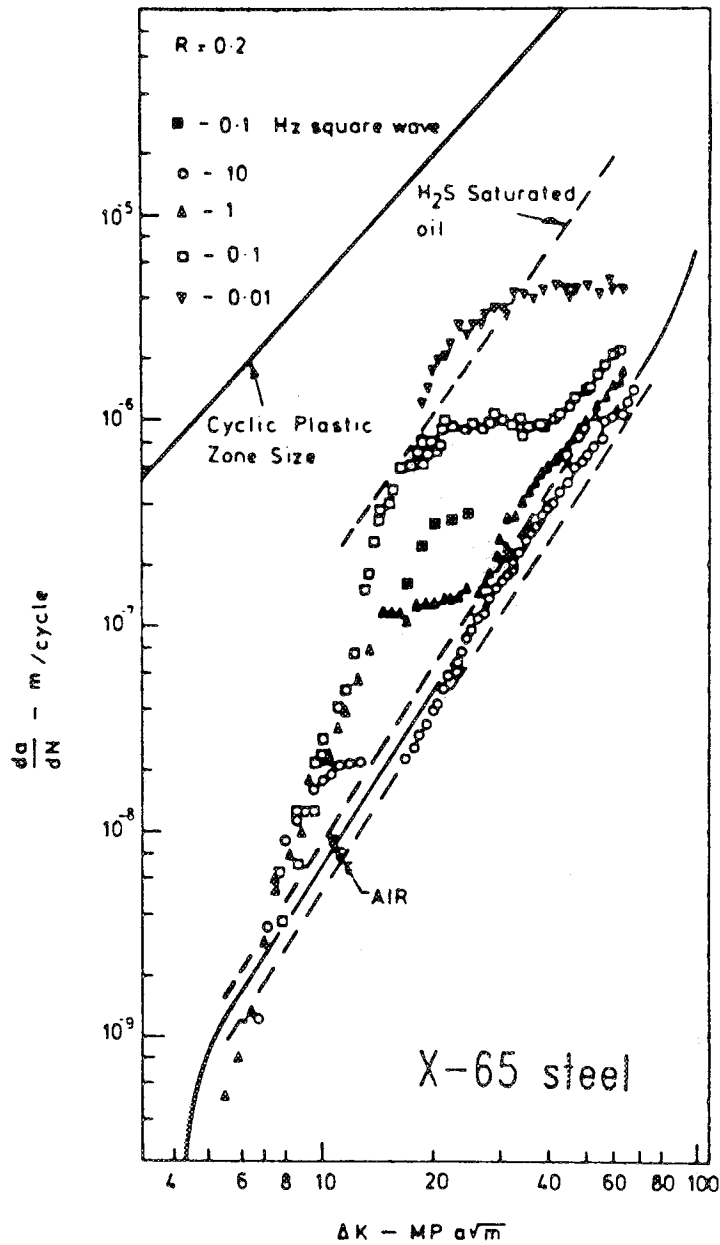
Fig. 62b   Effect of ΔK on corrosion fatigue crack growth rate at several frequencies for X65 C-Mn steel in 3.5% NaCl with cathodic polarization. After Vosikovsky et al. [36,227].

114
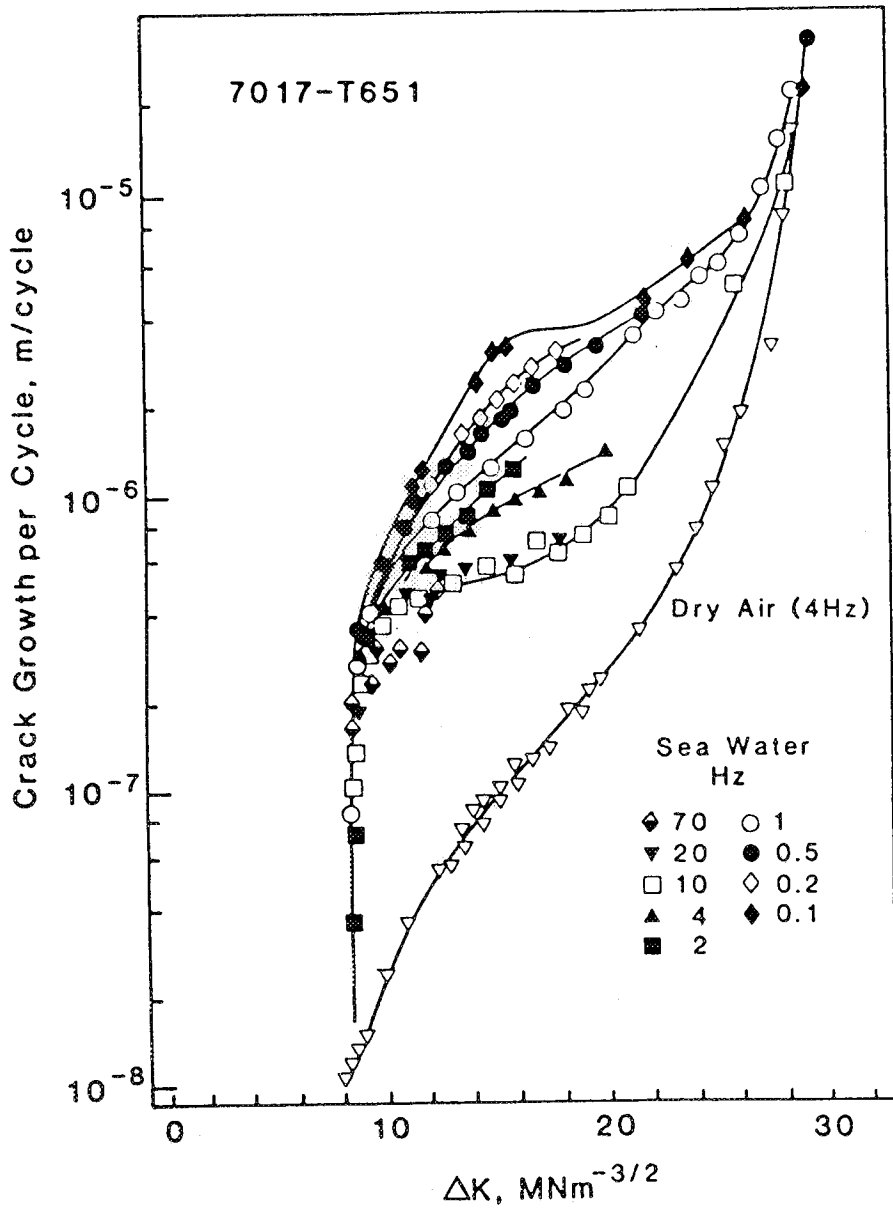
Fig. 62c   Effect of ΔK on corrosion fatigue crack growth rate at several frequencies for 7071-T651 aluminum alloy in seawater. After Holroyd and Hardie [91].

above-K_{TH} (or above K_{IEAC}) type in Fig. 19, and is similarly indicated by the dashed line in the schematic diagram of Fig. 60. Here inert and environmental growth rates are equal for those stress intensity cycles (R and ΔK levels) where K_{max} is less than K_{IEAC}. Environmental fatigue crack growth rates sharply increase with increasing ΔK, when a significant portion of the stress intensity cycle is above K_{IEAC}, and with extremely steep power law behavior often yielding to a shallower rate of increase of da/dN with ΔK due to mass transport and reaction limitations on monotonic load cracking rates. This form of cracking is discussed more fully in Chapter VII on superposition of MECP and FCP, and was introduced in Chapter III. Examples of this stress intensity dependence are given in Figs. 44, 57 and 60.

Environment affects fatigue crack propagation rates at stress intensity levels below K_{IEAC}. For this case, it is useful to consider that three stress intensity regimes of corrosion fatigue crack growth are possible, as represented schematically in Fig. 16 for Type A behavior, in Fig. 19 and by the combined solid and dashed lines in Fig. 57.

Regime 1: Fatigue crack growth rates in this regime are nearly asymptotic to a limiting stress intensity, ΔK_{th}, below which da/dN is practically negligible. Near-threshold (da/dN < 10^{-6} mm/cycle) environmental effects may reduce the apparent crack growth threshold and accelerate da/dN, with the ΔK dependence paralleling benign environment behavior.

In Fig. 62a, rates for the titanium alloy are well above 10^{-6} mm/cycle, however, imaginative extrapolation suggests that the environment could lower ΔK_{th} and raise growth rates relative to moist air. For steels, indications of this effect were reported by Booth et al. [124] and by Bardal [200]; however; little difference is seen for near-threshold cracking in chloride versus moist air in Fig. 62b. In fact near-threshold rates for the former are somewhat less than moist air kinetics and perhaps approach vacuum behavior.

Near-threshold corrosion fatigue in aluminum alloys is largely unexplored; limited data are shown in Fig. 50 [209] which demonstrate a decrease in ΔK_{th} and a concurrent enhancement in near-threshold da/dN for high-strength Al-Li-Cu alloy 2090 in 1% NaCl compared to FCP in either moist air or high-purity helium. A similar trend is likely for other 2000 and 7000 series aluminum alloys when loaded in moist gases and aqueous electrolytes. For nickel based superalloys in elevated temperature moist air, increasing temperature increases ΔK_{th}, while also promoting increased crack growth rates, as demonstrated in Fig.

60. This fatigue crack growth crossover with temperature was first noted by Van Stone and Krueger for Inconel 718 [113]. They speculated that this behavior is due to local crack tip blunting by combinations of creep and cyclic plasticity.

Measurements of crack growth in the near-threshold regime are prohibitively time consuming owing to the low loading frequencies relevant to EFCP [201,228]. As such, environmental effects in this regime are poorly established.

REGIME 2: A second regime of EFCP is often observed for ΔK levels above the fatigue threshold. Here da/dN values increase rapidly relative to the reference environment and with a significantly stronger power-law dependence above a critical stress intensity level. This behavior is shown for steel in Figs. 48 and 62b [36,227], for titanium alloys in Figs. 52 and 62a [72,173] and for an aluminum alloy in Fig. 62c [91]. EFCP in Regime 2 is often interpreted as the intervention of cyclic deformation stimulated "stress corrosion cracking" above a threshold K level [36,70,72].

Many researchers argue that monotonic load values of K_{IEAC} are lowered by cyclic loading, resulting in behavior similar to the Type B response [36]. That is, the threshold K for the onset of the dashed line behavior in Fig. 61 depends on loading mode and decreases from K_{IEAC} with cyclic loading. A counter view is illustrated in Fig. 19 where cycle-time dependent da/dN-ΔK behavior occurs above a critical ΔK and R combination, but below and separate from EFCP above K_{IEAC}. The two-transition response in Fig. 19 has not been observed. Rather single perturbations in the da/dN-ΔK behavior, of the type illustrated in Fig. 61, are more common.

REGIME 3: As ΔK approaches a critical value at the end of Regime 2 for below-K_{IEAC} cracking, the environmental effect is diminished rendering a reduction in the slope of the da/dN-ΔK dependence. In some instances so called "plateau" nearly ΔK-independent behavior is observed. This latter behavior is indicated for the steel-NaCl system in Figs. 48 and 62b, while a reduced power-law relationship is observed for titanium and aluminum alloys, Figs. 14, 62a and 62c. The reduced environmental influence at higher ΔK is often interpreted to result from a ΔK-independent, transport limited "cyclic SCC" rate superimposed on a ΔK-dependent mechanical fatigue process. Stated equivalently, plateau behavior may be a result of chemically rate-limited environmental cracking that cannot respond to increasing mechanical driving force. A dramatic reduction in the slope of the da/dN versus ΔK

relationship is also typically observed for above-K_{IEAC} EFCP behavior.

Corrosion fatigue crack growth rates intersect and equal benign environment values at very high ΔK approaching K_{IC}. This regime is of little significance owing to the high levels of ΔK and fast crack growth rates involved.

Two points are important regarding the stress intensity dependence of environmental cracking. The stress intensity dependence of EFCP rates is typically characterized by a simple constant load, increasing ΔK experiment. To date there have been no extensive studies of the load and crack length history dependence of the da/dN-ΔK relationship for corrosion fatigue. That the results in Fig. 16 are true material property laws which are independent of loading and geometry factors remains to be proven. Secondly, when analyzing the effects of variables on corrosion fatigue crack propagation and when developing crack propagation rate models, it is important to recognize the various ΔK regimes.

B.   Stress Ratio

Increasing mean stress intensity in a fatigue load cycle, as characterized by the stress ratio R (R = K_{min}/K_{max}), generally increases fatigue crack growth rates and decreases ΔK_{TH} values for both inert and aggressive environments. For aggressive environments, dramatic stress ratio effects on fatigue above K_{IEAC} are well described by linear superposition of stress corrosion cracking rates, as discussed in Chapter VII [229].

For benign environments and at temperatures where time-dependent plastic deformation is minimal, the crack closure mechanism is commonly invoked to explain the observed effect of stress ratio on FCP rates, particularly for low growth rates ($<$ 10^{-5} mm/cycle). Fig. 49 shows data for 2¼Cr-1Mo steel fatigued in moist air and dry hydrogen, and that were interpreted based on crack closure [205,206]. The effective stress intensity factor, ΔK_{eff} (ΔK_{eff} = K_{max} - K_{cl}), typically decreases with decreasing R for a given applied ΔK because of the increasingly important effect of crack surface contact at a characteristic stress intensity, K_{cl}. Crack closure often occurs at particularly high values of K_{cl} for EFCP because of environmentally induced crack path tortuosity and resulting crack surface roughness, and because of corrosion product debris within the crack. Mechanical fretting during low-R FCP can enhance chemical reaction rates and increase the volume of corrosion product, and hence promote crack closure. Intrinsic damage mechanisms other than extrinsic crack closure may

also contribute to the effect of stress ratio on environmental FCP rates. For example, the magnitude of K_{max} could influence hydrogen embrittlement damage within the crack tip process zone (Fig. 5) by increasing the volume of material that is subjected to very high stresses. Intrinsic stress ratio effects on da/dN have not been modeled based on particular damage mechanisms. The relative contributions of crack closure and intrinsic mean stress effects are not often separated.

Vosikovsky and coworkers demonstrated the deleterious effect of stress ratio on corrosion fatigue in carbon and heat treated alloy steels exposed to NaCl [127,230]. For a specific frequency, single crack growth rate laws of the type shown in Fig. 62b were produced for FCP in moist air and aqueous NaCl when ΔK was replaced by a function including the stress ratio; viz. $(\Delta K + 4R)$ for X70 C-Mn steel and $(\Delta K + 3R)$ for HY130 steel. The relative contributions of crack closure and intrinsic R-sensitive environmental cracking were not defined. Given that the $(\Delta K + R)$ function equally correlates da/dN data for air and aqueous chloride, and based on the relatively small effect of R on corrosion fatigue, it is likely that mean stress predominantly affected crack closure for this system. Indeed, Ewalds argued that these fatigue data are equally well correlated with an "effective ΔK" equal to $(0.6 + 0.3R)\Delta K$ and based on Elber's physical notion of plasticity induced crack closure [231].

The need in this area is to define the effect of stress ratio on intrinsic corrosion fatigue crack propagation, independent of crack closure. This aim is hindered by the complexity of measuring displacement in aggressive environments and by the lack of understanding of the relationship between such measurements, physical load transfer and the relevant stress intensity range.

C.   Loading Waveform

Apart from overload effects, loading waveform is a secondary variable for fatigue crack growth in moist air [139]. Several studies indicate that loading waveform, including constant amplitude loading wave shape, periodic overloads or underloads, and variable amplitude loading spectra, can substantially influence environmental fatigue crack propagation.

Rates of EFCP are well correlated by the root-mean-square (rms) of the applied stress intensity distribution for the steel/NaCl system under narrow band random loading [232-237].

When evaluating the service life of structural components, however, load interaction effects must be carefully assessed. For example, it is well known that tensile overloads have a strong retarding effect on subsequent subcritical fatigue crack growth [139], as illustrated in Fig. 63 for 2124 and 7150 aluminum alloys [233], and elsewhere for advanced Al-Cu-Li alloy 2090, all in moist air [234]. More recently, it has been found that compressive underloads may also affect subsequent crack growth in aluminum alloys, causing da/dN to increase for a number of subsequent tensile load cycles [234]. These effects are qualitatively related to crack tip shape, stress/strain distributions and crack closure. Over- and underload effects on environmental FCP are not understood, however, such results are beginning to emerge [214].

Loading wave shape effects on environmental fatigue crack propagation above K_{IEAC} are well described by the integrated load-time history for each cycle [229]. Results suggest that crack growth only occurs on the loading portion of the cycle.

Several studies of corrosion fatigue below K_{IEAC} indicate that crack growth rates are substantially influenced by the waveshape. Barsom demonstrated that the NaCl environment has a negligible effect on crack growth rate, over that in air, when the waveform is square or negative sawtooth for 12Ni-5Cr-3Mo steel [51,67]. That is, fast loading with unloading at any rate does not favor environment enhanced FCP. On the other hand, triangular, sinusoidal or positive sawtooth load fluctuations cause noticeable increases in fatigue crack growth rates. Environmental crack growth rates are increased by waveforms which involve slow rising load, which involves sufficient time for chemical interactions, compared to fast rising-slow falling or fast rise-prolonged K_{max} hold periods for constant cyclic frequency. Studies of a 7075 aluminum alloy by Pelloux and Selines [211], of low strength C-Mn steel by Vosikovsky [227], and of low strength carbon steel by Scott et al. [69] confirmed Barsom's hypothesis. In contrast Wei and Hudak reported that varying rise time had no effect on severe corrosion fatigue of 7075-T651 in distilled water [67].

It is reasonable to expect that environmental effects are stimulated by slow strain and surface creation rates during rising loading. None-the-less, the effect of waveform depends on the rate controlling mechanism and will be material-environment specific. Changing rate of loading may have little effect on corrosion fatigue governed by fast surface reactions, but a large effect on systems where hydrogen diffusion in the crack tip plastic zone is rate limiting. The microscopic processes of surface creation on loading and of crack tip shape

120

Fig. 63   Effect of 50, 100 and 150% single tensile overloads on fatigue crack growth
rates in: (a) 2124-T351 and (b) 7150-T651 alloys as a function of crack
extension after the overload. After Venkateswara Rao and Ritchie [233].

change on unloading, and of varying convective mixing may also affect the waveform dependence.

D. Loading Frequency

The strong time dependence of corrosion fatigue is arguably the most important aspect of this fracture mode, since the long term fatigue life of a structural component must be evaluated from relatively short term laboratory data. The main source of the frequency effect on EFCP rates arises from the kinetics of environmental interaction; no influence of frequency is observed for FCP in inert environments at temperatures that are less than 30 to 40% of the alloy melting point. The general notion is that corrosion fatigue crack growth rates increase with decreasing cyclic loading frequency (f) because of increasing time per cycle available for increased chemical reaction and mass transport. This trend may be altered for cases where increased frequency increases the rate of environmental cracking due to: (1) enhanced mass transport by convective mixing, (2) enhanced crack tip strain and surface creation rates, and (3) reduced crack tip blunting by dissolution. At extremely high frequencies (> 500 Hz), fatigue crack propagation may be accelerated with increasing frequencies due to crack tip heating.

To understand frequency effects, it is of paramount importance to identify the rate limiting step in the transport, chemical reaction and fracture sequence for corrosion fatigue crack growth [13,34,35,40]. Additionally, the effect of stress intensity must be considered; the frequency dependence is specific to each of the three ΔK regimes.

1. Above K_{IEAC} Environmental Fatigue

For K_{max} above K_{IEAC}, da/dN always increases with either decreasing frequency or with increasing time ("hold") periods of constant stress intensity within the load cycle and at any constant ΔK; environmental fatigue is purely time dependent. This behavior is modeled by linear superposition integrating monotonic load crack growth rates (da/dt versus K) with the time dependence of the stress intensity cycle above K_{IEAC}. The resulting amount of per cycle environmental cracking is added to da/dN for an inert environment. This approach is amplified in Chapter VII.

In all cases da/dN equals (1/f) times da/dt. For EFCP above K_{IEAC} and when da/dt is independent of stress intensity level as in Stage II MECP (Fig. 15), da/dN varies inversely

122

with frequency (da/dN = 1/f · da/dt). This behavior is indicated by the inclined dashed line and data for aluminum alloy 7079 in NaCl (Fig. 64 [119,238]) and by the results for high strength IN 718 in H_2 at two high pressures (Fig. 65 [78,218]). Here, the measured fatigue crack growth rate in an aggressive environment and at constant ΔK, is plotted as a function of either log frequency or time per the rising portion of the loading cycle (1/2f). The slope of -1 for the former, and the similar linear proportionality between da/dN and time per load cycle for IN 718 at two pressures, demonstrate the pure time dependence of environmental fatigue. (Note that the simple relationship between da/dN and 1/f is not obeyed for the full range of frequencies examined in Fig. 65.) This class of problems is discussed in an ensuing section.

2. Below K_{IEAC} Environmental Fatigue: Near-Threshold Regime 1 and Moderate ΔK Regime 2

Studies on the effect of frequency on ΔKth and on Regime 1 EFCP rates are extremely limited, mainly due to long testing time involved in generating low crack growth rates at low frequencies. Two unique frequency dependencies have been reported for near-threshold environmental fatigue crack propagation; da/dN is constant with increasing f, or alternately, da/dN increases with increasing f. A limited number of papers report decreasing near-threshold corrosion fatigue crack growth rates, or increasing ΔK_{TH}, with decreasing frequency. This latter trend is traced to the extrinsic contribution of exposure-time enhanced, corrosion product induced crack closure.

Frequency independent corrosion fatigue crack growth was reported by Speidel for steels and nickel based alloys [119]. This "true" or cycle-dependent EFCP behavior is illustrated by the horizontal lines in Fig. 66 for Inconel 600 fatigued in both moist air and NaOH environments. A similar frequency independence of near-threshold da/dN was reported by Meyn for Ti-8Al-1Mo-1V in 3.5% NaCl [215], and by Piascik and Gangloff for an aluminum-lithium-copper alloy exposed to 1% NaCl with anodic polarization [209].

Frequency independent near-threshold cracking is well established for the steel-aqueous chloride system. Vosikovsky reported da/dN independent of f for X-65 and HY130 steels at low ΔK levels [127,227], as illustrated in Fig. 62b. This effect was also observed by Gangloff for carbon and heat treated alloy steels in 3% NaCl with cathodic polarization [239]. Specific data in Fig. 67 were obtained for constant ΔK at a level within the steeply rising portion of the da/dN-ΔK relationship for each frequency. Note that crack growth rates in
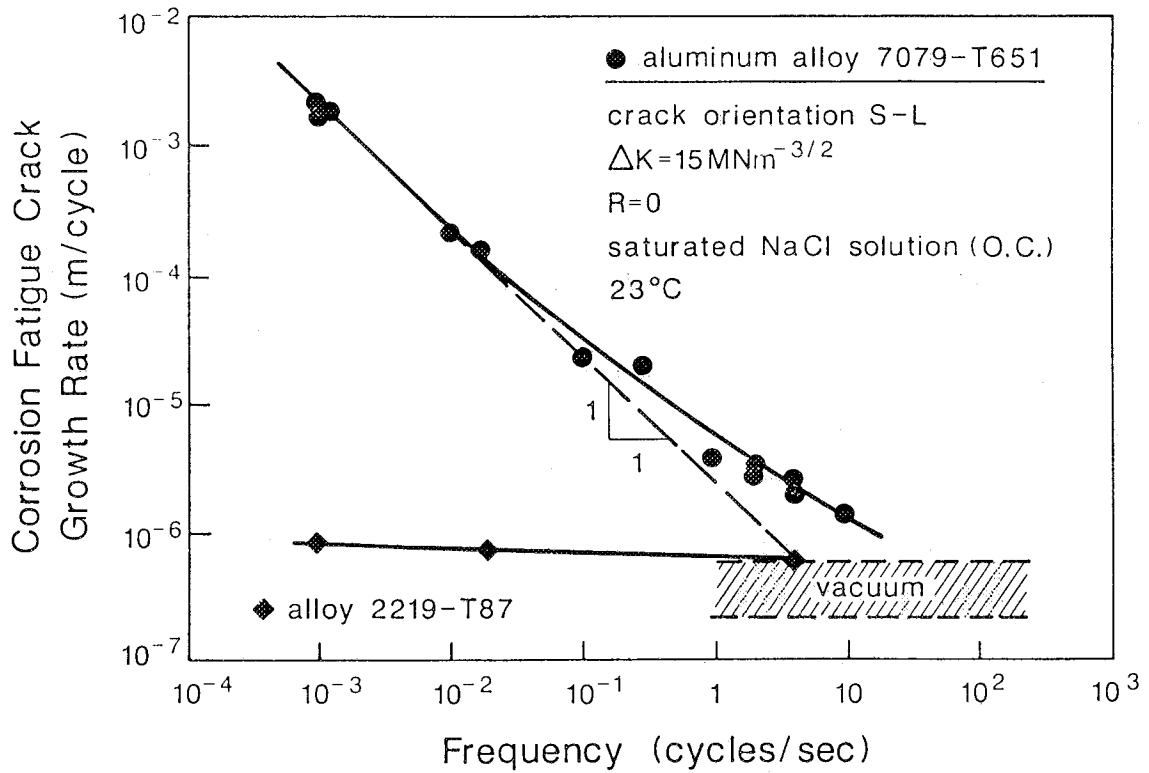
Fig. 64   Frequency dependence of corrosion fatigue crack propagation illustrating time-dependent, cycle-dependent, and cycle-time-dependent behavior for aluminum alloys in NaCl. After Speidel [119,238].

124

FATIGUE CRACK GROWTH RATE (mm/cycle) (y-axis)

Inconel 718

$\Delta K = 55$ MPa$\sqrt{m}$

$23°C$

$$\frac{da}{dN} \alpha (2f)^{-0.67}$$

$\triangle$	34.5 MPa He
$\blacktriangle \blacksquare$	69 MPa H_2
$\bullet$	7.5 MPa H_2

ONE-HALF LOAD PERIOD (1/2f-seconds) (x-axis)
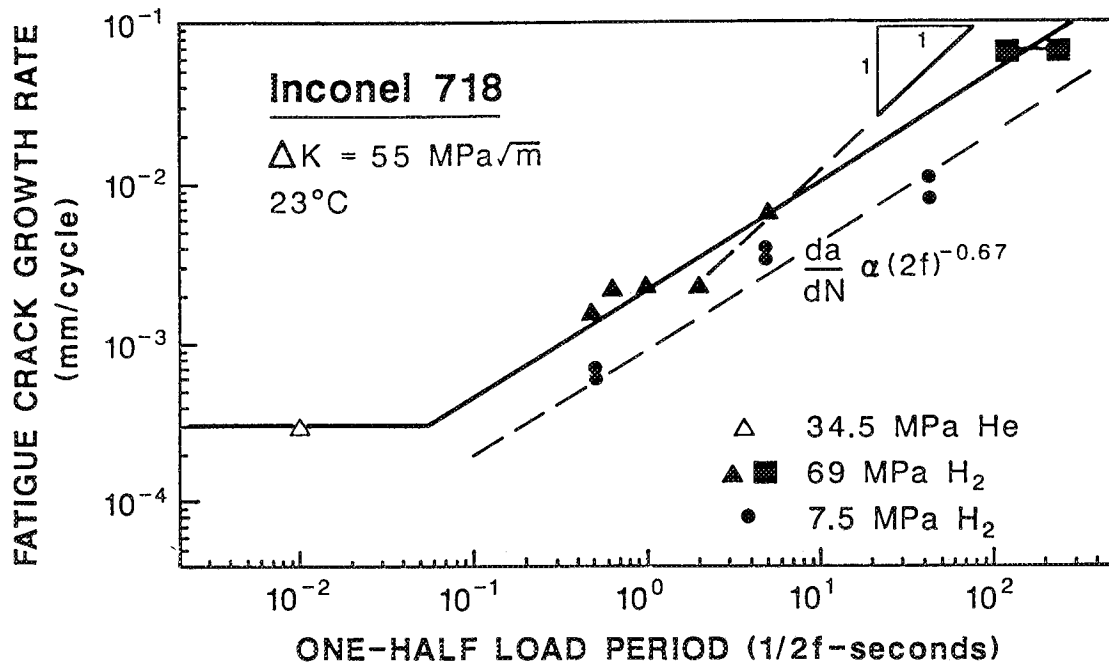
Fig. 65   Effect of the rising load cycle period on fatigue crack growth rate at constant ΔK for Inconel 718 in high pressure gaseous hydrogen [78,80,219].
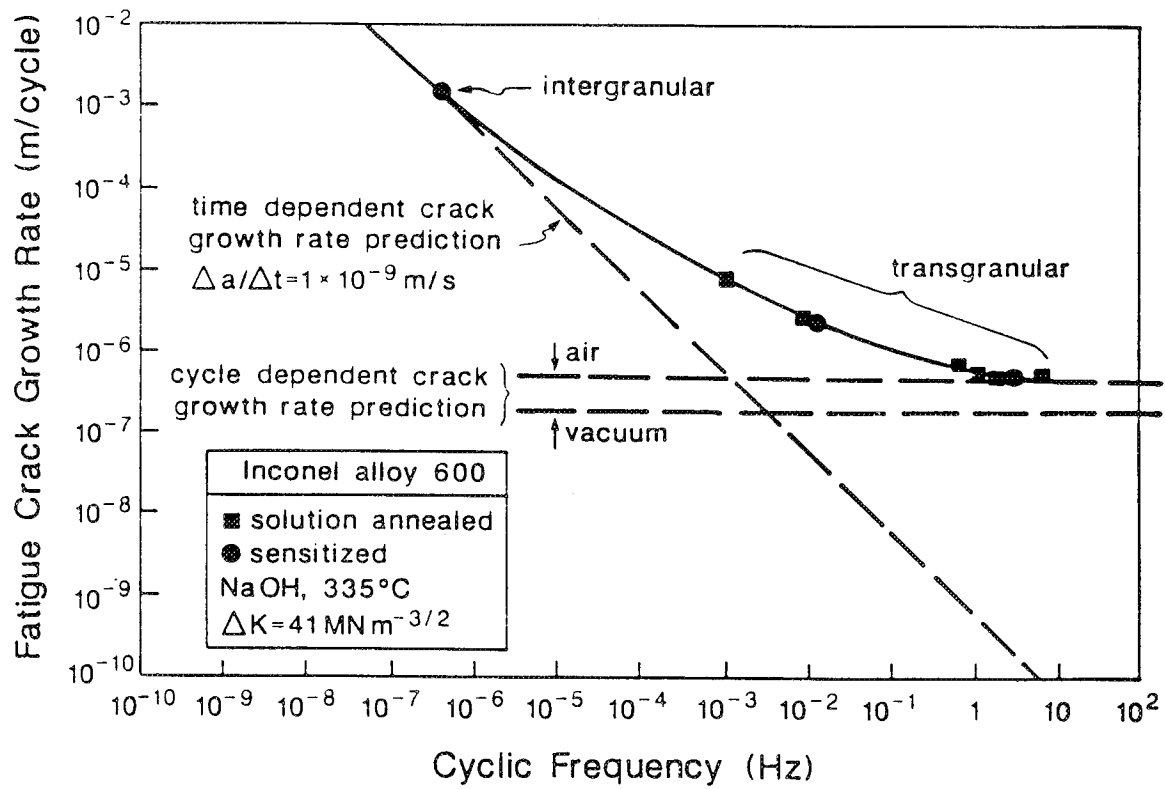
Fig. 66   Frequency dependence of corrosion fatigue crack propagation illustrating time-
dependent, cycle-dependent, and cycle-time-dependent behavior for Inconel 600
(UNS N06600) in hot NaOH.   After Speidel [119,238].
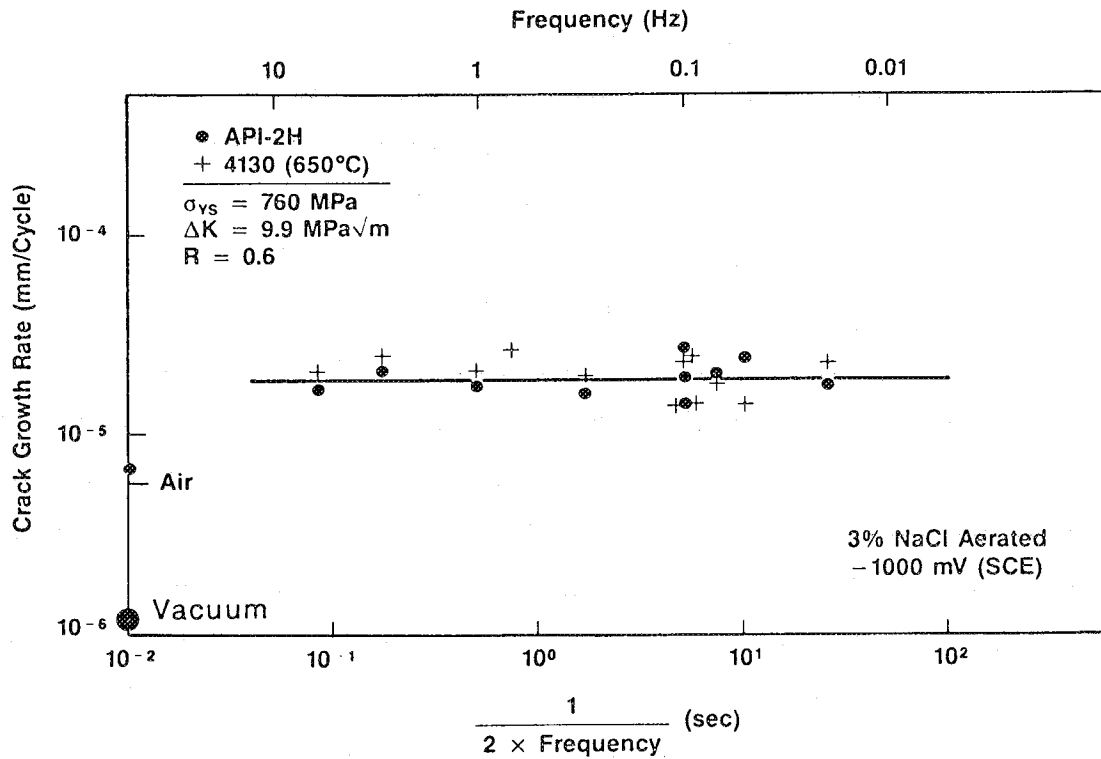
Fig. 67　　　The effect of loading frequency on near-threshold fatigue crack growth rates at constant ΔK and R for quenched and tempered C-Mn and alloys steels in 3% NaCl with cathodic polarization. After Gangloff [239].

127

NaCl are independent of loading frequency, are about 3 to 4-fold greater than the value for moist air, and are 20 times the da/dN for vacuum. At very low ΔK, frequency independent crack growth rates in aqueous chloride and moist air merge, as suggested in Fig. 62.

In selected instances low ΔK corrosion fatigue crack growth rates increase with increasing frequency. This trend was reported for Ti-6Al-4V in NaCl by Dawson and Pelloux, as shown in Figure 62a [72]. They also observed that the critical ΔK for the onset of "cyclic stress corrosion" increases as frequency decreases. An Al-7% Mg alloy cyclically loaded in 1 N Na_2SO_4 with cathodic polarization showed a similar trend [107]. In this case crack growth rates increased by an order of magnitude as f increased from 3 to 33 Hz; all rates were significantly faster than reference values for dry argon.

3. Below K_{IEAC} Environmental Fatigue: Moderate ΔK Plateau

For ΔK levels where the power-law dependence of da/dN is reduced and approaching plateau behavior, sub-K_{IEAC} corrosion fatigue growth rates generally increase with decreasing frequency. A saturation crack growth rate is often observed for low frequencies. Extensive data supporting these trends were reported by Vosikovsky [127,227 and Fig. 23], Scott et al. [69,202], Gallagher [240], Gangloff [13,108,241] and Hinton and Procter [242] for steels in aqueous chloride; by Wei and Shim [13,88] for steels in distilled water and water vapor; by Brazill et al. [196] for an alloy steel in gaseous H_2S; by Holroyd and Hardie [91 and Fig. 22] for 7000 series aluminum alloys in seawater; by Wei and coworkers [75,172,212], and Dicus [243] for 2000 and 7000 series aluminum alloys in purified water vapor; by Chiou and Wei [244], and Dawson and Pelloux [72 and Fig. 23] for Ti-6Al-4V in aqueous NaCl; and by Ford and Andresen [38,245] for austenitic stainless steels in high temperature purified water.

As an example, the frequency dependence of the corrosion fatigue crack propagation rate in API-2H C-Mn steel exposed to 3% NaCl with cathodic polarization is shown in Fig. 68 [241]. These results were obtained by constant stress intensity experimentation, with the specific ΔK level of 23 MPa$\sqrt{m}$ selected to be within the "plateau" region of corrosion fatigue cracking for this steel. The logarithmic plot of environmental crack growth rate versus one-half of the reciprocal frequency is suggested by mechanistic modeling. At frequencies above about 20 Hz, equal rates of fatigue crack propagation are observed for aqueous chloride andmoist air; this value is about three times faster than crack growth in vacuum. Three regimes of behavior are observed with decreasing frequency. Initially, da/dN increases
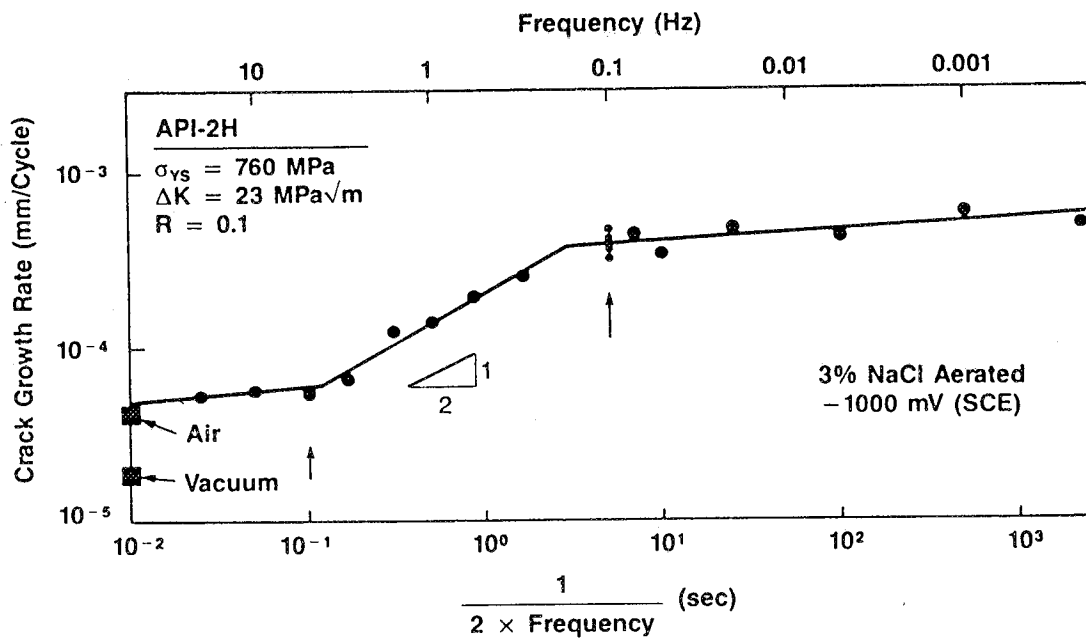
Fig. 68   Effect of frequency on corrosion fatigue crack propagation in the "plateau" regime of ΔK for API-2H steel in 3% NaCl with cathodic polarization. After Gangloff [241].

mildly, followed by a strong acceleration of corrosion fatigue for frequencies between 4 and 0.1 Hz, and leading to a third regime where da/dN is constant or mildly increasing as frequency declines to very small values.[4]

The trend shown in Fig. 68 is general, as indicated by da/dN-ΔK data in Fig. 62 and by the behavior of a variety of additional steels of varying yield strength but similar ΔK, R and electrochemical conditions [13,69,88,127,202,227,240-242,246]. Results indicate similar behavior for the first two stages of the frequency response. Interestingly, the saturation behavior seems to be observed for the high strength quenched and tempered steels (viz, API-2H and HY130 with σ_{ys} = 760 and 900 MPa, respectively), but not for lower strength ferrite-pearlite BS4360 and X-65 steels (σ_{ys} = 450 MPa).

The frequency dependence in Fig. 68 is explained by hydrogen embrittlement modeling reviewed in Chapter VII on "Qualitative Crack Growth Rate Models". The slope of the second regime is suggestive of the mechanism which controls corrosion fatigue, be it 1/2 indicating hydrogen diffusion control or some other value indicating hydrogen production (by surface reaction) rate control. The saturation behavior observed for the higher strength steels at the lower frequencies is also mechanistically significant. Similar results were reported for an aluminum alloy in seawater as indicated in Fig. 62c [91].

E.   Environment Activity.

Environment activity, often specific to each alloy-environment system, can strongly affect rates of fatigue crack propagation. For example, as water vapor pressure reaches a threshold value and further increases, crack growth rates rise rapidly for aluminum alloys. The effect of water vapor pressure is again a strong function of loading frequency. Gaseous hydrogen can cause similar effect for steels. When aluminum alloys and steels are exposed to aqueous chloride solution, applied electrode potential can critically affect the environmental fatigue behavior.

1. Aluminum-water vapor system

Increasing water vapor pressure, promoting increased rates of environmental fatigue

---

[4] For perspective, the data point at a cyclic loading frequency of 0.0002 Hz required 12 days and 250 load cycles to produce a crack growth interval of only 0.10 mm.

for aluminum alloys, at least for ΔK levels well above near-threshold, has been extensively characterized by Wei and coworkers. Several investigations indicate that growth rates uniquely depend on environmental exposure, which is given by the product of load cycle period and water vapor pressure (P_{H2O}) (viz, P_{H2O}/loading frequency) [13,75,212]. Data are presented in Figs. 69 and 70 for two aluminum alloys, 2219-T851 and 7075-T651, in terms of environmental crack growth rate versus $P_{H2O}/2f$ or P_{H2O} at a single frequency. Several constant stress intensity range levels are represented for a single frequency of 5 Hz and variable P_{H2O}. With increasing vapor pressure, da/dN increases and reaches a saturation level. Some aluminum alloys, such as Al 7075-T651, showed an intermediate plateau followed by further increases in da/dN with increasing pressure.

Since frequency was not varied, the data in Figs. 69 and 70 do not unequivocally establish the interchangeable influences of P_{H2O} and frequency. The role of exposure to describe both frequency and water vapor pressure effects on crack propagation needs to be established. Bradshaw and Wheeler examined an Al-Cu-Mg alloy (DTA 5070A) in water vapor at two frequencies (1 and 100 Hz) and a range of P_{H2O} [247]. The pressure dependence at each frequency was equivalent to that shown in Figs. 69 and 70; the levels of P_{H2O} required to produce a given crack growth rate scaled with inverse frequency. Dicus concluded that frequencies between 1 and 10 Hz had no influence on corrosion fatigue rates for 7475-T651; only water vapor pressure controlled da/dN [243]. These results are consistent with the saturation behavior in Figs. 69 and 70, at least for water vapor pressures up to the point of the second rise. Dicus found that this second rate transition occurred at a constant pressure for the two frequencies.

The frequency dependence of corrosion fatigue in the aluminum-water vapor system has not been determined for near-threshold crack growth. Recent results for an Al-Li alloy suggest that the trends presented in Figs. 69 and 70 are also obeyed for the near-threshold stress intensity range regime [136]. Limited data by Niegel and coworkers show that ΔK for the onset of environmental fatigue cracking along high angle grain boundaries in an Al-Zn-Mg alloy is reduced from the level for inert environment Stage II transgranular crack growth according to the reciprocal square root of P_{H2O} [216]. Presumably, the exposure parameter describes the effect of pressure and frequency.

131
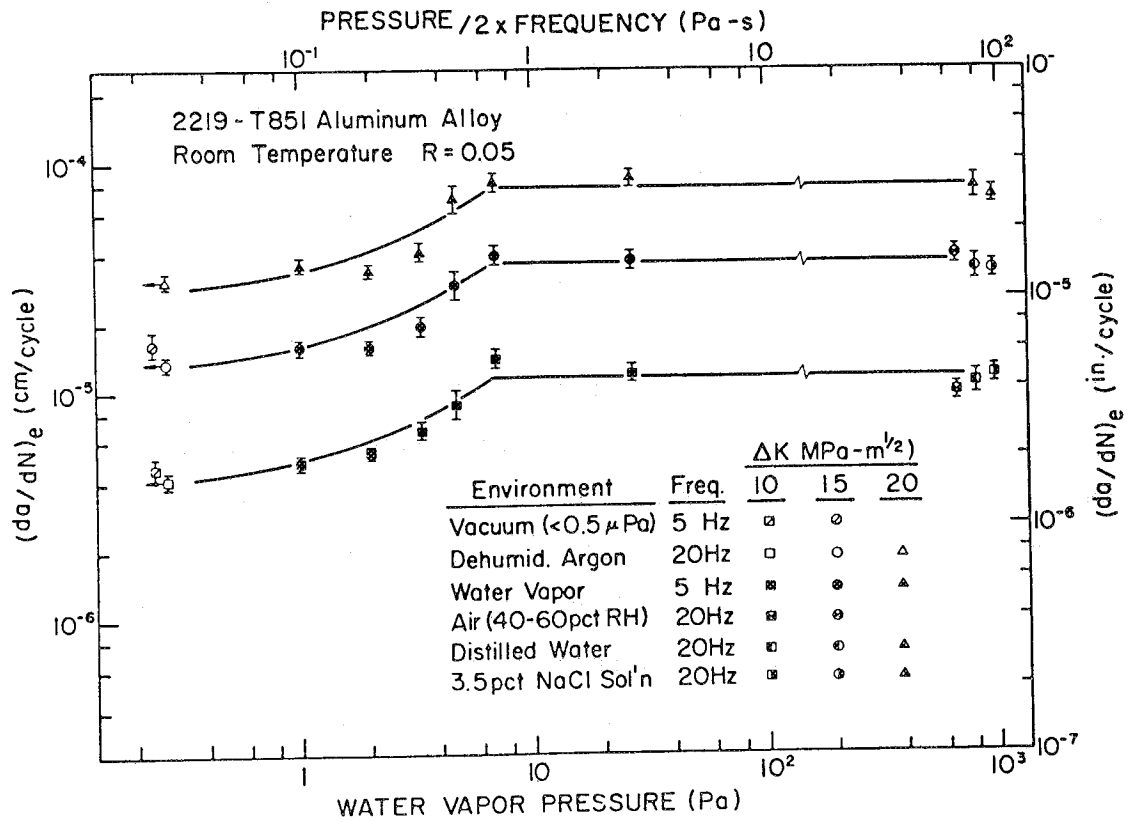
Fig. 69   Effect of environmental exposure (water vapor partial pressure/frequency) on corrosion fatigue crack propagation in a precipitation-hardened aluminum alloy. After Wei et al. [212].
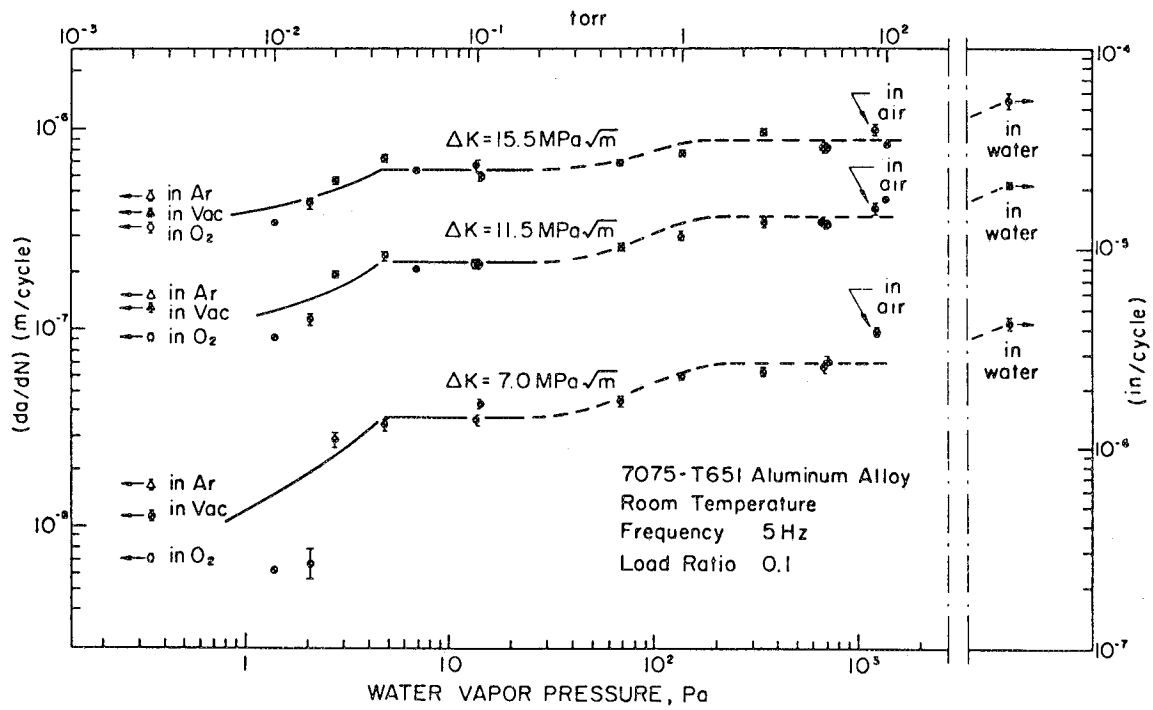
Fig. 70   Effect of water vapor pressure on corrosion fatigue crack propagation in high-strength 7075-T651 at constant frequency. After Gao et al. [75].

133

2. Steel-Hydrogen Gas System

It has been observed that K_{IEAC} decreases and monotonic load time based crack growth rates increase with increasing hydrogen pressure, particularly for high strength steels (e.g., Fig. 23). Studies have shown that the time-based rate of monotonic load hydrogen assisted crack growth varies with hydrogen pressure in accordance with:

$$da/dt \propto (P_{H2})^m \qquad (29)$$

where m ranges from 0.5 to 2.0 [180]. Rates of time-cycle dependent EFCP below K_{IEAC} similarly depend on hydrogen gas pressure.

Fig. 71 demonstrates the deleterious effect of increasing hydrogen pressure on fatigue crack growth in a moderate strength steel stressed at a high, constant ΔK below ΔK_{IEAC} [78]. Data are approximated by a square root pressure dependence, indicated by the dashed line and suggested by the Sievert's Law relationship between pressure and the concentration of chemically adsorbed hydrogen atoms on the metal surface.

Unlike steels, the effects of gaseous hydrogen on fatigue crack propagation in aluminum, titanium and nickel-based alloys are largely unexplored. Limited studies indicate that aluminum alloys are immune to gaseous hydrogen [119]. The minimal effect of H_2 in promoting subcritical MECP and FCP in aluminum alloys is attributed to the low fugacity of atomic hydrogen at the crack tip. Increasing crack growth rate in Ti-5Al-2.5Sn with increasing gaseous hydrogen pressure at intermediate ΔK was reported by Nelson [73]. Limited data in Fig. 65 suggest that, for IN 718 at only two levels of high pressure H_2, da/dN at any frequency increases with P_{H2} raised to the 0.6 power.

3. Steels and Aluminum in Aqueous Chloride: Effect of Electrode Potential

An increase in cathodic polarization generally increases fatigue crack growth rates for steels in aqueous chloride environments. Data in Fig. 72 illustrate this trend for two C-Mn steels in NaCl at fixed ΔK, R and f. Note that "plateau ΔK" crack growth rates exhibit a minimum at about 200 mV cathodic to the free-corrosion potential. The higher growth rates at cathodic potentials indicate that hydrogen embrittlement is a leading mechanism promoting crack growth; crack growth rates are proportional to the amount of hydrogen electrochemically produced at the crack tip. The observed minima is due to competitive hydrogen production from proton and water reduction reactions; the former decreases with increasing cathodic polarization as the crack becomes more alkaline, while the latter increases

134
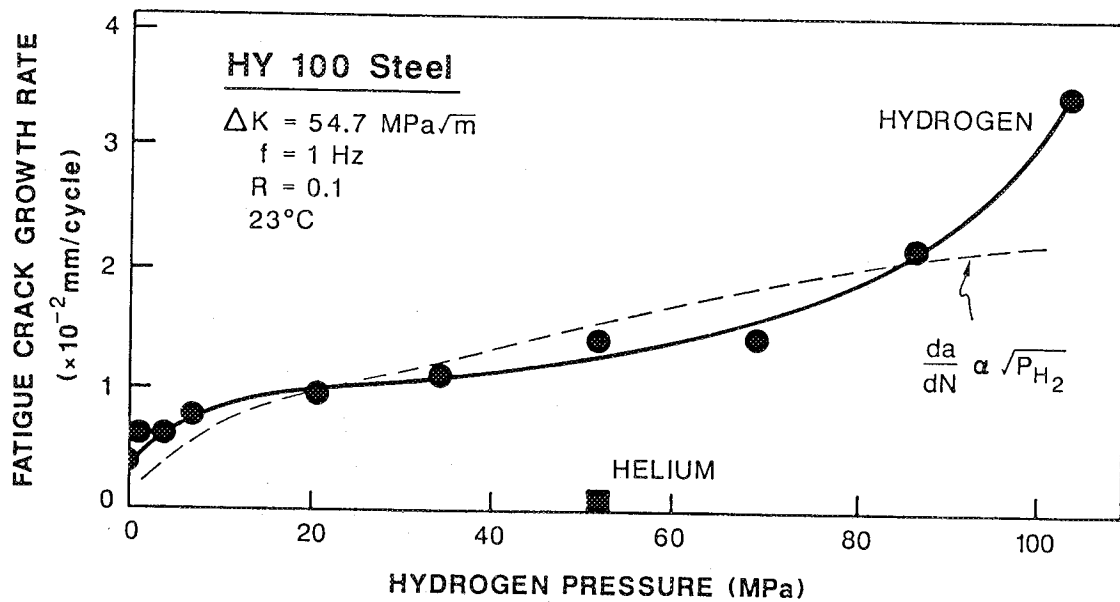
Fig. 71   Effect of hydrogen gas pressure on fatigue crack propagation in HY 100 steel at constant applied ΔK and loading frequency [78].
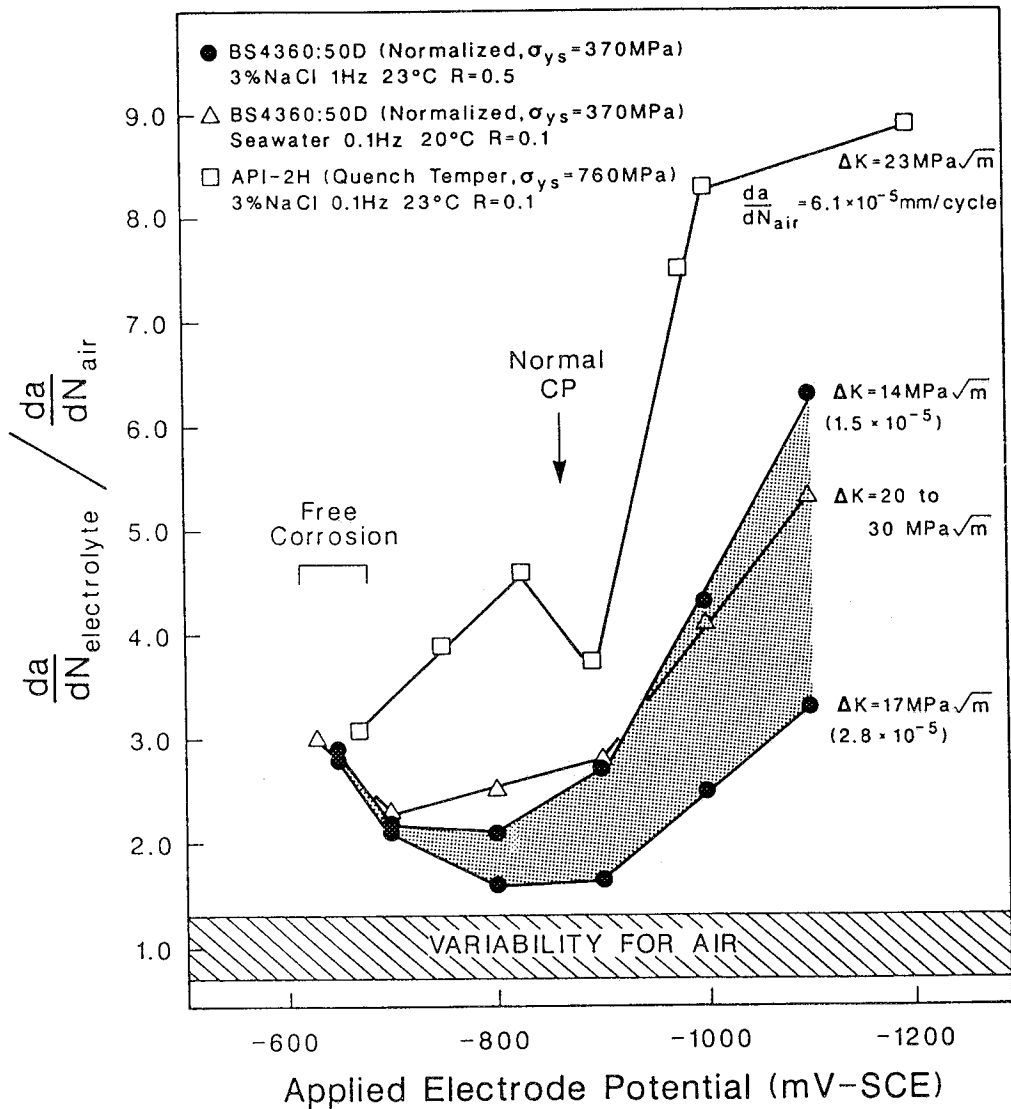
Fig. 72 Effect of applied cathodic potential on corrosion fatigue crack propagation in the C-Mn steel/aqueous chloride system [198], BS4360:50D in 3% NaCl [203] or in seawater [69], API-2H in 3% NaCl [239].

136

in importance for potentials below about -900 mV$_{SCE}$.

The effect of electrode potential is more complex in aluminum alloys. For precipitation-hardened aluminum alloys in aqueous electrolytes rates of EFCP are generally accelerated by either anodic polarization or large cathodic polarization. Environmental FCP is mitigated by mild cathodic polarization. Specific data are presented in Fig. 73 for Al-Li-Cu alloy 2090. Crack propagation is significantly enhanced by loading in 1% NaCl aqueous solution with anodic polarization, compared to cracking in moist air and high-purity helium. Cathodic polarization reduces crack growth rates to levels typical of moist air or lower. The mechanistic interpretation of the effect of electrode potential for aluminum alloys is poorly understood, being associated with the fact that both dissolution and hydrogen evolution can occur over a broad range of electrode potentials.

F.   Temperature

Only limited attention has been given to the effect of temperature on EFCP in metals. Apart from the possible interaction with environment, increasing temperature may promote oxide-induced crack closure, alter alloy yield strength and microstructure, and ultimately cause time-dependent plastic deformation within the crack tip process zone and throughout the uncracked ligament.

Most studies have shown that hydrogen effects are a maximum at or around room temperature. Increasing temperature increases the reaction kinetics responsible for production of atomic hydrogen on clean crack surfaces. As a countering effect, however, increased temperature may reduce hydrogen delivery to the fracture process zone by increasing the rate of atomic hydrogen recombination to innocuous H_2 on the metal surface, by promoting desorption of surface hydrogen, and by overcoming H-trap binding energies to homogenize dissolved hydrogen otherwise segregated within the microstructure. Consistent with these considerations, Wei and coworkers demonstrated that, as temperature increased, da/dN: (1) increased between 23°C to 75°C for an alloy steel in aqueous sodium sulfate [248], (2) mildly increased or was constant between 23°C and 200°C for steel in water vapor [13,39,144], and (3) decreased between 23°C and 127°C for steel in gaseous H_2S [13,35,40,196,212]. Frandsen and Marcus reported that H_2 enhanced fatigue crack propagation in a high strength steel was maximized just below 0°C, and decreased to growth rates typical of vacuum at ±
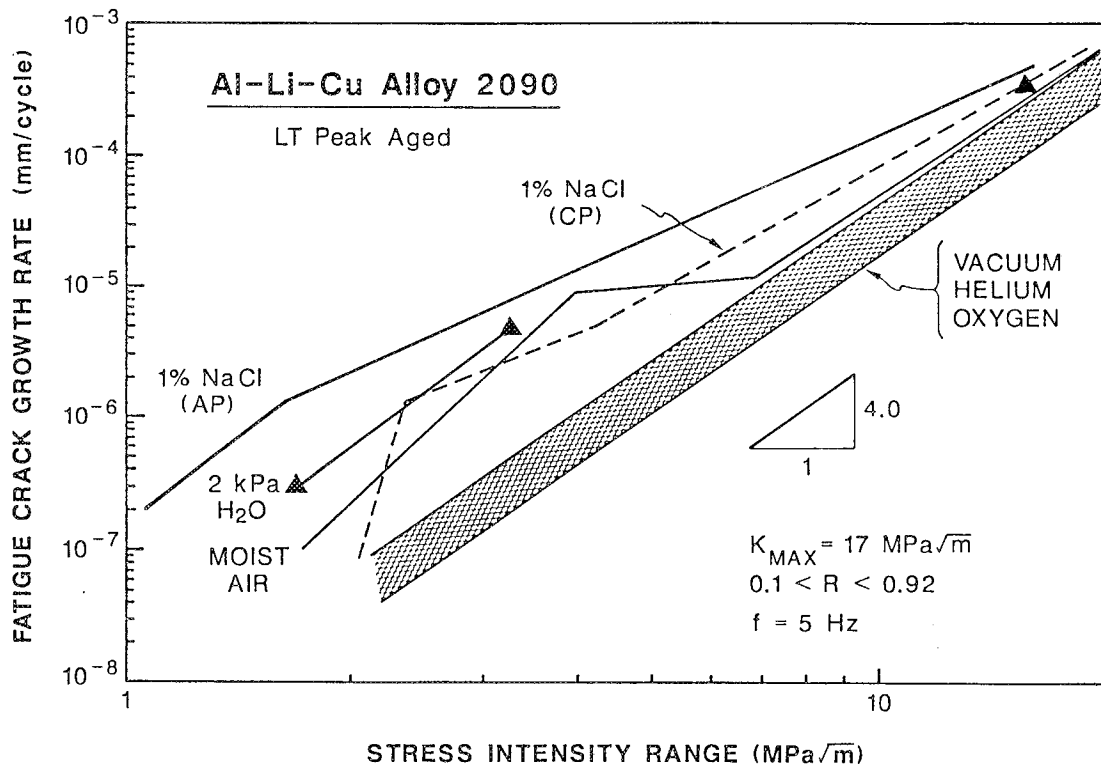
Fig. 73   Effect of electrode potential on corrosion fatigue crack propagation in Al-Li-Cu
alloy 2090 in aqueous chloride at constant ΔK and high mean stress. After
Piascik and Gangloff [209].

100°C, as represented in Fig. 74 [249]. Similar effects were reported for static load hydrogen environment cracking [145,180].

Vosikovsky and coworkers reported that reduced temperature between 300 and 273°K resulted in up to a four-fold increase in EFCP rates for ferritic steel in seawater [250].

G.   Yield Strength, Microstructure and Alloy Composition

For benign environments fatigue crack propagation is generally postulated to be insensitive to yield strength within the Paris regime. However, decreasing ΔK_{TH} and increases in near-threshold da/dN ($< 10^{-6}$ mm/cycle) are often observed with increasing yield strength for ferrous alloys [251]. While the exact mechanism is not established, the decrease in the fatigue process zone size and cyclic plastic strain distribution at the crack-tip have been proposed. Oxide induced crack closure may also be reduced for higher strength steels because of decreased fretting oxidation and less voluminous reaction debris. The effect of strength level on near-threshold crack growth in nonferrous alloys is more complex, in that, there is no marked trend of increasing or decreasing ΔK_{TH} values with a corresponding change in strength for precipitation hardened systems. For these systems, microstructure and slip morphology effects may dominate inert environment FCP.

Yield strength is a primary variable that influences environmental cracking for monotonic loading [145]. For many material-environment systems, K_{IEAC} decreases and da/dt values increase with increasing yield strength. Environmental FCP above K_{IEAC} will be accordingly exacerbated by increasing yield strength, as predicted by linear superposition (see Chapter VII).

A striking example of the lack of a strong yield strength effect on cycle-time-dependent EFCP below K_{IEAC} is shown in Figs. 75 and 76 for ferritic steels in aqueous chloride with applied cathodic polarization and at low loading frequency. Since CF is attributed to hydrogen embrittlement, a yield strength effect could be expected. Rather, data in Fig. 75 show an essentially constant environmental effect for steels that vary in monotonic yield strength from 390 MPa (BS4360:50D) to 1080 MPa (Ni-Cr-Mo) [198]. Crack growth rates at a plateau stress intensity range of 23 MPa√m are plotted in Fig. 76 for each steel in Fig. 75. Corrosion fatigue crack growth rates are five to eight times faster than the yield strength-independent value for moist air, however, no trend is observed for cyclic yield strengths from
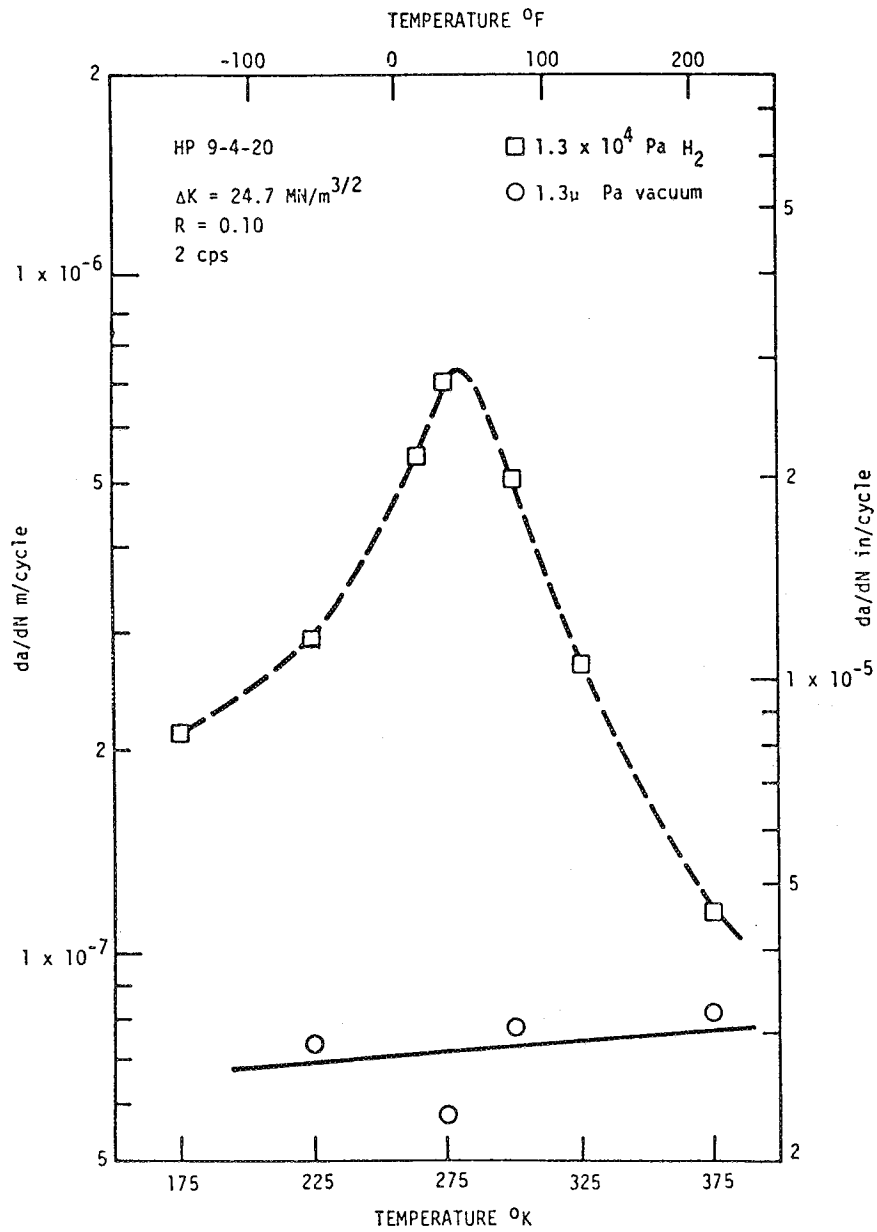
Fig. 74   Temperature dependence of H_2-assisted fatigue crack propagation in high-strength HP-9-4-20 steel at constant ΔK and frequency. After Frandsen and Marcus [249].
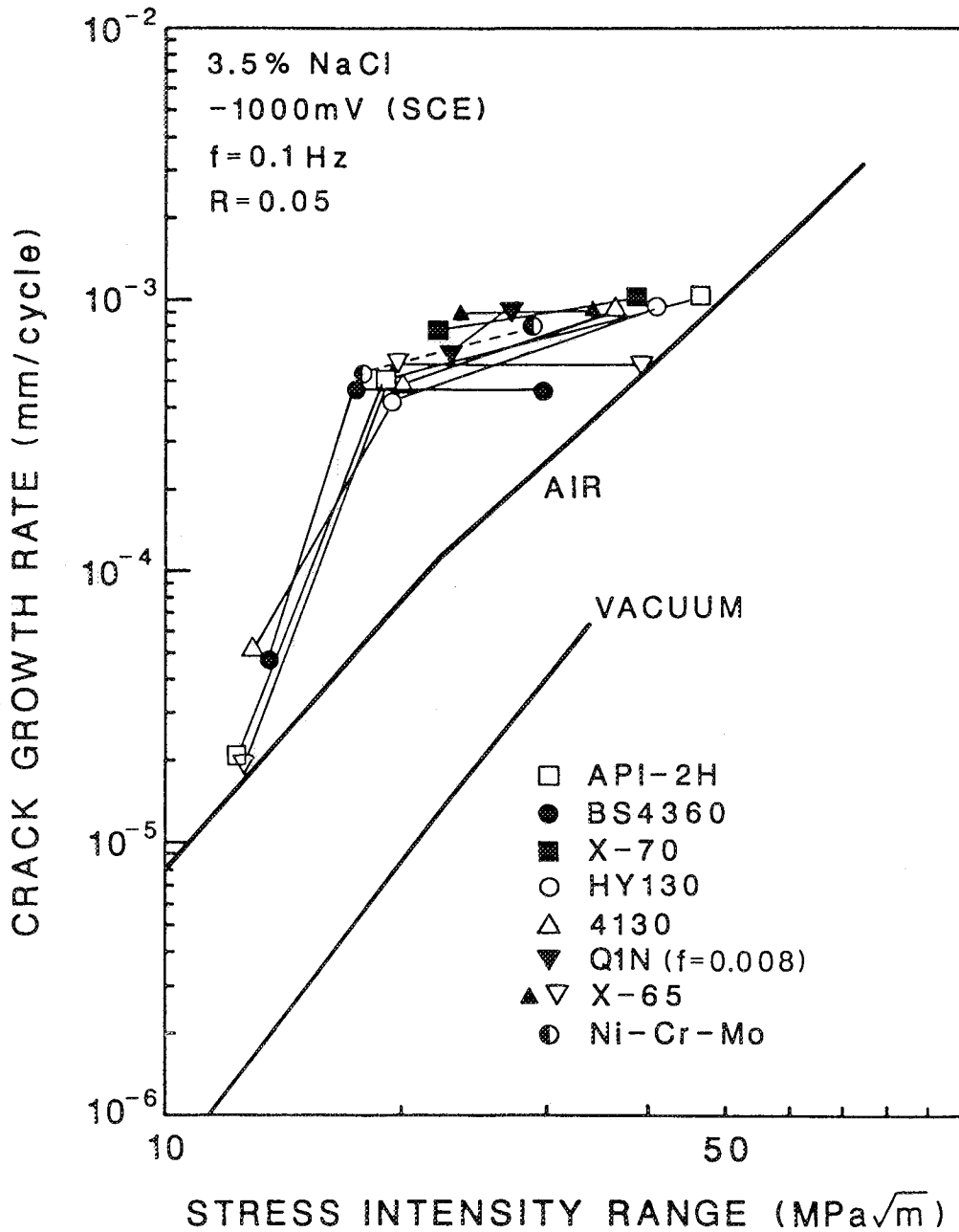
Fig. 75   Corrosion fatigue crack propagation in steels of varying yield strength and microstructure in 3.5% NaCl at constant cathodic potential, R and low loading frequency. After Krishnamurthy et al. [198].

ΔK=23 MPa√m
3.5%NaCl −1000mV(SCE)
f=0.1Hz R=0.05
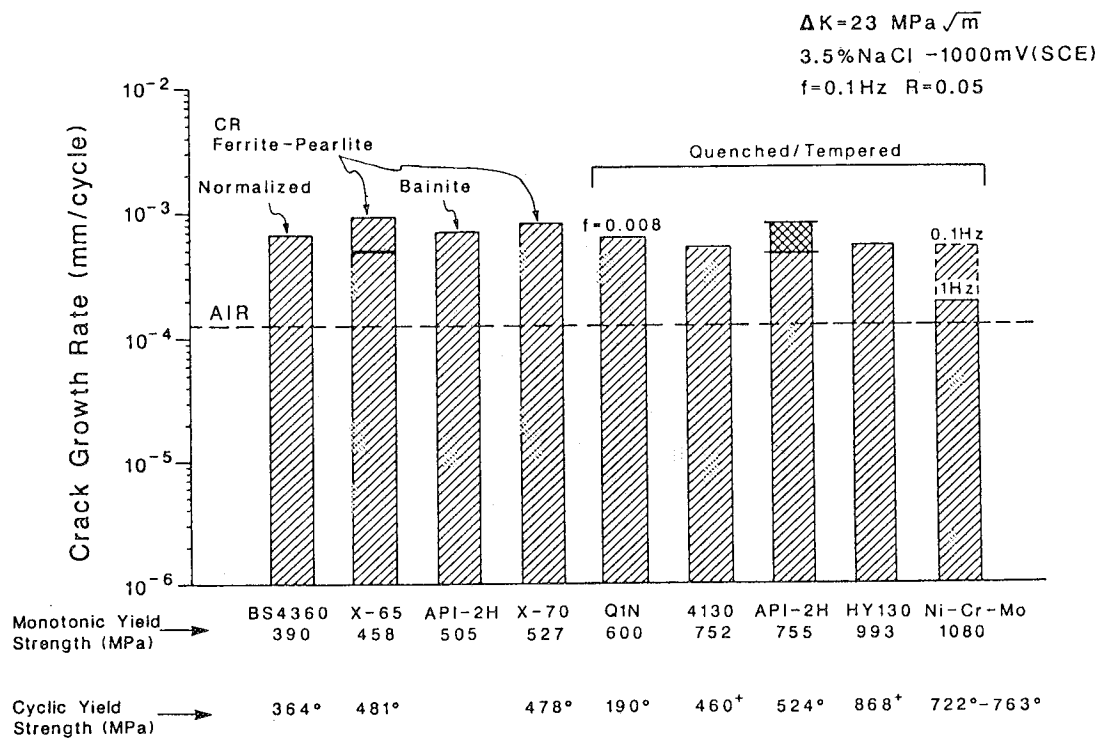
Fig. 76   Effect of steel yield strength and microstructure on corrosion fatigue crack propagation rate at constant cathodic potential, ΔK, R and frequency, from Fig. 75. After Krishnamurthy et al. [198].

190 to 870 MPa. Figs. 75 and 76 demonstrate that plateau regime corrosion fatigue crack growth rate does not systematically vary with yield strength and microstructure for various steels. While the lack of an effect of yield strength and microstructure on the corrosion fatigue crack propagation behavior of steels appears to be conclusive, further confirmation is needed.

Comprehensive studies on the effect of microstructure on the CF crack growth are lacking. Very often, the effect of yield strength and microstructure are not separated and are intertwined with extrinsic factors, particularly crack closure, which makes it extremely difficult to predict the effect of these variables on da/dN. Fig. 77 demonstrates no systematic effect of microstructure on EFCP in ferritic C-Mn and heat-treated alloys steels in aqueous chloride with cathodic polarization [239]. The C-Mn steel was heat treated to produce, in order of heat treatment on the figure, tempered martensite of two prior austenite grain sizes, upper and lower bainite, and dual-phase ferrite + martensite with two martensite volume fractions. These heat treatments produced a constant monotonic yield strength of 760 MPa, based on measured hardness. These variations in microstructure have no effect on environmental fatigue crack propagation for constant applied cathodic potential and low loading frequency.

Similar to aqueous chloride, only limited studies have been conducted on fatigue crack propagation in carbon or alloy steels exposed to gaseous hydrogen. Wachob and Nelson observed that ΔK_{TH} increases with increasing yield strength and grain size for A516 steel in both moist air and high-pressure hydrogen [252]. This effect of microstructure is attributed to extrinsic crack closure; the contribution of microstructure and strength-sensitive mechanisms for intrinsic EFCP damage is unclear for the steel/H_2 system.

Despite extensive work on microstructural effects on MECP in precipitation-hardened aluminum alloys [146,147], microstructure-EFCP properties relationships have received limited attention. Lin and Starke demonstrated that normalized EFCP rate decreased with increasing copper content for four differently heat-treated Al-6Zn-2Mg-Cu alloys in distilled water [253]. Specific data are shown in Fig. 78. Fatigue crack propagation experiments were conducted in distilled water at a frequency of 10 Hz and R=0.1. The reduction in fatigue crack growth rate with increasing copper content is most prominent for the peak age condition and intermediate ΔK. Lin and Starke argued that a damaging interaction between absorbed

The plot shows:

Y-axis: CRACK GROWTH RATE (mm/CYCLE), ranging from 10^{-7} to 10^{-1}

X-axis: STRESS INTENSITY RANGE (MPa$\sqrt{m}$), ranging from 5 to 100

Plot annotations:
- 3% NaCl
- −1000 mV (SCE)
- AERATED
- 0.1 Hz   R = 0.1
- ▼,I CONSTANT ΔK ALL HEAT TREATMENTS
- CHLORIDE
- MOIST AIR

API–2H Steel (σ_{ys}=760 MPa)

1200°C/30 min + 1200°C/5min +

- □ 600°C/ 1 hr
- + 600°C/ 1 hr (1200°C/3.5min)
- △ SP 285°C/ 5 min
- × SP 227°C/ 5 min
- ○ 780°C/12 min
- ● 810°C/12 min
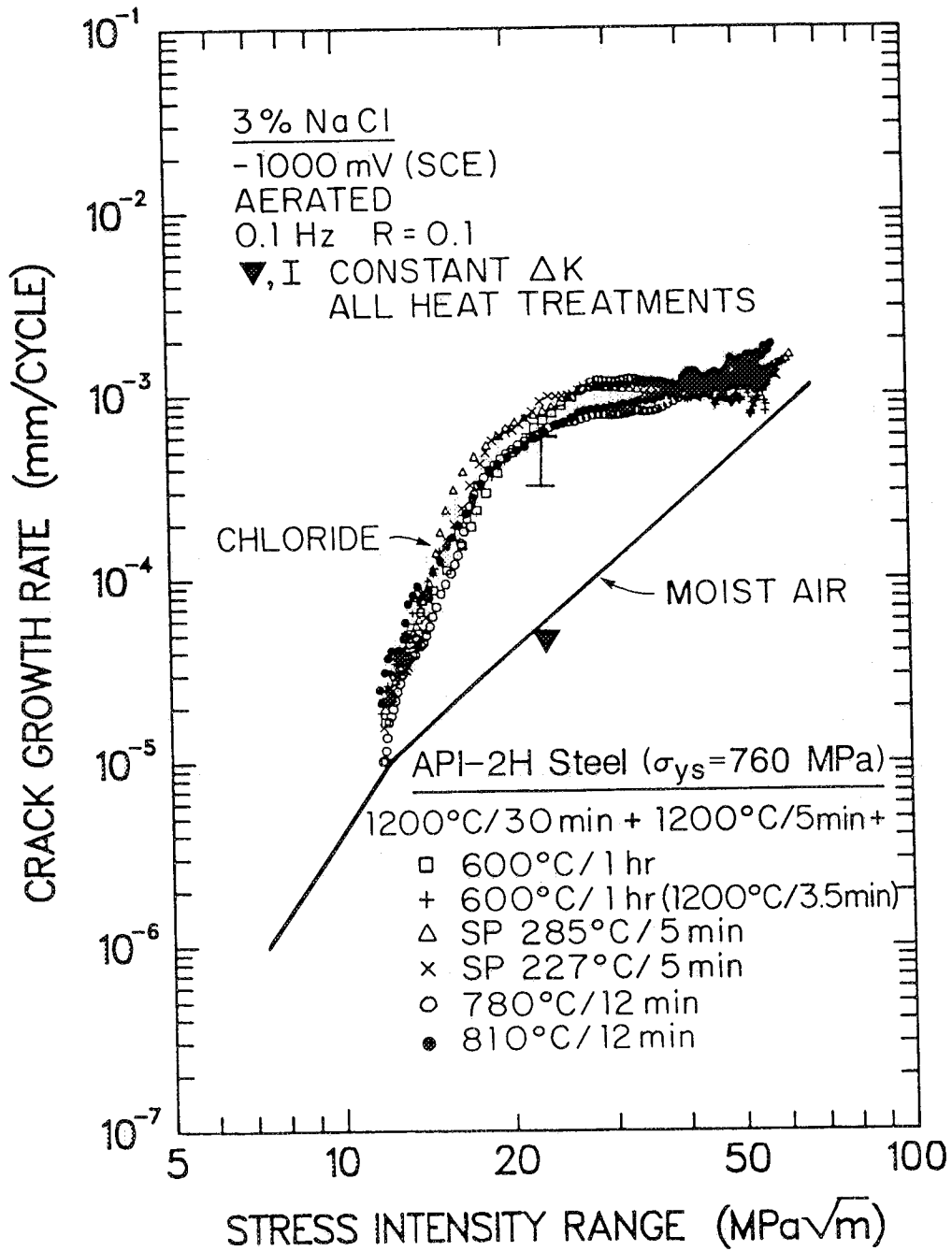
Fig. 77   Effect of microstructure on corrosion fatigue in C-Mn steel heat treated for constant yield strength (760 MPa) and stressed at either constant ΔK or constant load in aqueous 3% NaCl with cathodic polarization. After Gangloff, Koo, and Marzinsky [239].
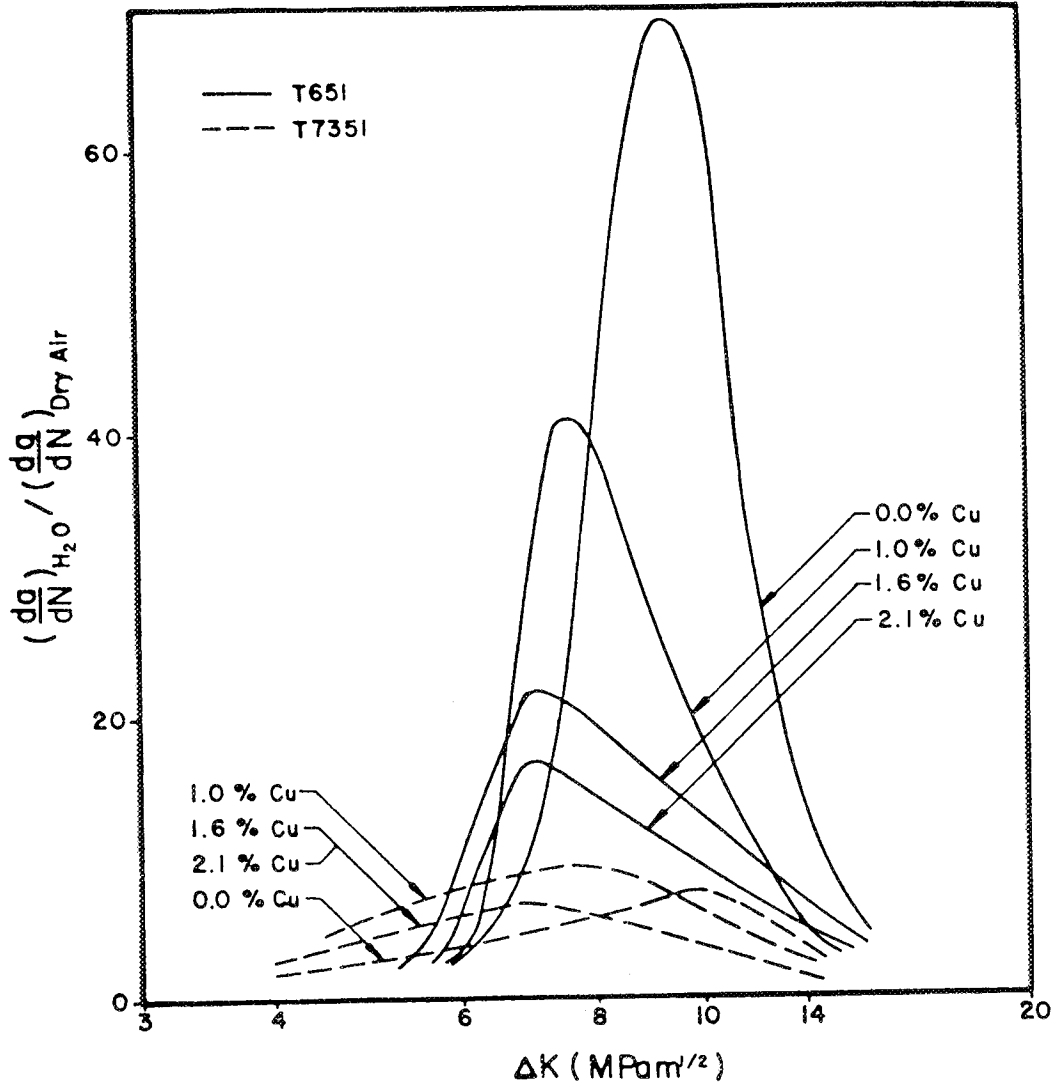
Fig. 78   Effect of copper content and aging treatment on corrosion fatigue crack propagation in Al-6Zn-2Mg exposed to distilled water (10 Hz, R = 0.10). After Lin and Starke [253].

145

environmental hydrogen and localized planar slip within the crack-tip cyclic plastic zone is responsible for the effect shown in Fig. 78.

VII. QUANTITATIVE CRACK GROWTH RATE MODELS

The challenges to incorporating environmental effects into component fatigue life prediction codes such as NASA-FLAGRO are apparent from the data presented in Chapters IV, V and VI.

The primary challenge stems from the fact that environmental damage generally increases with prolonged exposure time; that is, da/dN increases with decreasing loading frequency at fixed ΔK. The long term EFCP behavior of alloys in components is, therefore, difficult to predict based on short term laboratory data. For example, it is important to predict the 40 year life of marine structures at the wave-action loading frequency of interest, 0.2 Hz. While Paris regime crack growth rates are easily measured for loading frequencies as low as 10^{-4} Hz (e.g., see Fig. 68), a fracture mechanics characterization of near-threshold response requires long times (of order 6 months) for loading frequencies of 1 Hz. Application life is often dominated by low growth rate crack propagation. Since fracture mechanics methods characterize the kinetics of fatigue crack propagation, models can in principle be developed to predict the effect of frequency, thus providing a means of expanding short term laboratory data to predict long term component performance.

As a second challenge, a wide range of variables affect environmental fatigue crack propagation, as illustrated in Table 1 for aerospace aluminum alloys. Interactions of these variables are widespread. Generally a given material will be sensitive to EFCP for specific conditions of alloy composition, microstructure and chemical environment. Compared to moist air, identification of the pertinent environmental fatigue crack growth rate law for use in a life prediction codes is greatly complicated. The need in this regard is to develop predictive models based on the fundamental embrittling mechanism, which is hydrogen embrittlement for many structural alloys in gases and electrolytes near 300°K.

There are several approaches to incorporating environmental effects into fatigue crack propagation life prediction codes, as summarized in Table 3 for fracture control in several technologies. Here, the success of the approach is qualitatively graded from "A" to "F", with the grade largely determined by the complexity of the particular environmental cracking problem (and not the quality of the research and engineering). In two cases, K_{IEAC} is sufficiently high to preclude the linear superposition approach.

	Linear Superposition	Empirical -Bounds or -Curvefit	Mechanism -Reaction + -Damage
Offshore Structures	$K_{th} > 80$ (MPa√m)	A	B
Nuclear Reactor Piping	$K_{th} > 80$ (MPa√m)	B	A
Jet Engine Disk *(ACDCYCLE)*	A	A	D

Table 3   A summary of fracture control methodologies that have reasonably incorporated environmental effects on crack propagation into component life prediction for major technologies including: (a) offshore structures [36,108,254], (b) pressure vessels and piping in light water nuclear reactors [38,108,109,245,255], and (c) jet engine turbine disks [110,113,114,115].

The simplest approach to life prediction is to measure the crack growth rate behavior for those material, environment, loading and frequency conditions which are exactly selected to reproduce a specific application. Vosikovsky and Cooke provide an example of this approach for environmental fatigue crack propagation in a welded carbon steel pipeline carrying H_2S contaminated oil [256].

A second approach involves a detailed literature search to define the upper bound on environment sensitive crack growth rate behavior for a specific material/environment system, from a broad data base and for those chemical, frequency and material conditions which represent a worst case scenario. Hudak, Burnside and Chan employed this approach for welded carbon steel tubular components of oil and gas production platforms which operate in aggressive marine environments [254].

Ford, Wei, Nicholas, Van Stone and coworkers advocate the development of crack growth rate models which enable prediction of the effects of important variables; particularly ΔK, environment chemistry and frequency [13,38,89,108,111,245,257]. These models are based on: (1) empirical curve fitting, (2) linear superposition of mechanical fatigue and monotonic load environmental cracking data, or (3) first principles mechanistic models of the plastic deformation-chemical reaction production of damage at the crack tip. Andresen et al. describe the application of this approach, particularly employing mechanism-based models, to monotonic load and fatigue crack propagation in ferritic and austenitic steels exposed to elevated temperature pure water environments typical of commercial nuclear reactor systems [108,257]. Van Stone et al. and Nicholas et al. applied this approach, specifically employing linear superposition, to elevated temperature crack growth in nickel based superalloy jet engine turbine disks [110,113,114].

The state of the art in environmental fatigue crack growth rate models is summarized and assessed in this Chapter. Here, three types of model are considered: (1) linear superposition model for time-dependent fatigue crack growth, (2) empirical curve fitting, and (3) mechanism-based models of cycle-time-dependent crack growth. Once fully developed, such modeling approaches will be suitable for incorporation into fatigue life prediction codes such as NASA-FLAGRO.

A. Linear Superposition

An early approach to predict environmental fatigue crack growth rate versus stress intensity range relationships involved a linear superposition concept first proposed by Wei, Landes, Gallagher and Bucci [138,229,257]. Linear superposition predicts environment enhanced crack growth rate (da/dN_E) by combining inert environment fatigue crack growth rate, da/dN_M, with time dependent monotonic load time-based environmental crack growth rate, da/dN_{SCC}:

$$da/dN_E = da/dN_M + da/dN_{SCC} \tag{30}$$

Da/dN_{SCC} is computed by integrating sustained-load crack growth data and the applied time-dependent stress intensity factor in a single fatigue load cycle K(t). Mathematically, da/dN_{SCC} is given by:

$$da/dN_{SCC} = \int_0^{1/f} [da/dt(K)] \, [K(t)] \, dt \tag{31}$$

Figure 79 schematically illustrates the concepts involved in the linear superposition approach, and the elements of Equation 31 [229]. K(t) for the fatigue cycle is stated as a function of time, employing the loading parameters ΔK and R (or K_{min} and K_{max}). An example of a sinusoidal load cycle, with frequency f, is:

$$K(t) = K_{min} + \Delta K/[2 - \cos(2\pi ft)] \tag{32}$$

K(t) describes the effects of R, f, and waveform that are unique to a specific environmental fatigue case. Monotonic load environmental crack growth rate is measured as a function of applied K for the alloy of interest exposed to the aggressive environment relevant to the fatigue problem. Specific examples of such data are presented in Chapter IV.

The linear superposition model reasonably predicts environmental FCP rates; as a function of ΔK, R, f and waveform; if two conditions are met. K_{MAX} during the fatigue cycle must be above K_{IEAC} and the increment of crack advance for a single load cycle and from da/dt must be substantial compared to that from purely mechanical fatigue, da/dN_M. That is, linear superposition should accurately predict EFCP kinetics for material/environment systems that are particularly prone to MECP. Wei, Landes and Gallagher demonstrated the accuracy of linear superposition by predicting the frequency and stress ratio dependencies of corrosion fatigue crack growth in several high strength steels exposed to water vapor, H_2 and

150

$$\left(\frac{da}{dN}\right)_T = \left(\frac{da}{dN}\right)_{fat} + \int \frac{da}{dt} K(t)\,dt$$

Resultant environment enhanced behavior

Sustained loading component for specified ΔK

Reference environment

log da/dn

log ΔK

Area = sustained loading component for specified ΔK

da/dt

Time

K

K_{IEAC}

log $\frac{da}{dt}$

K_{max}

ΔK

K_{min}

K

Time
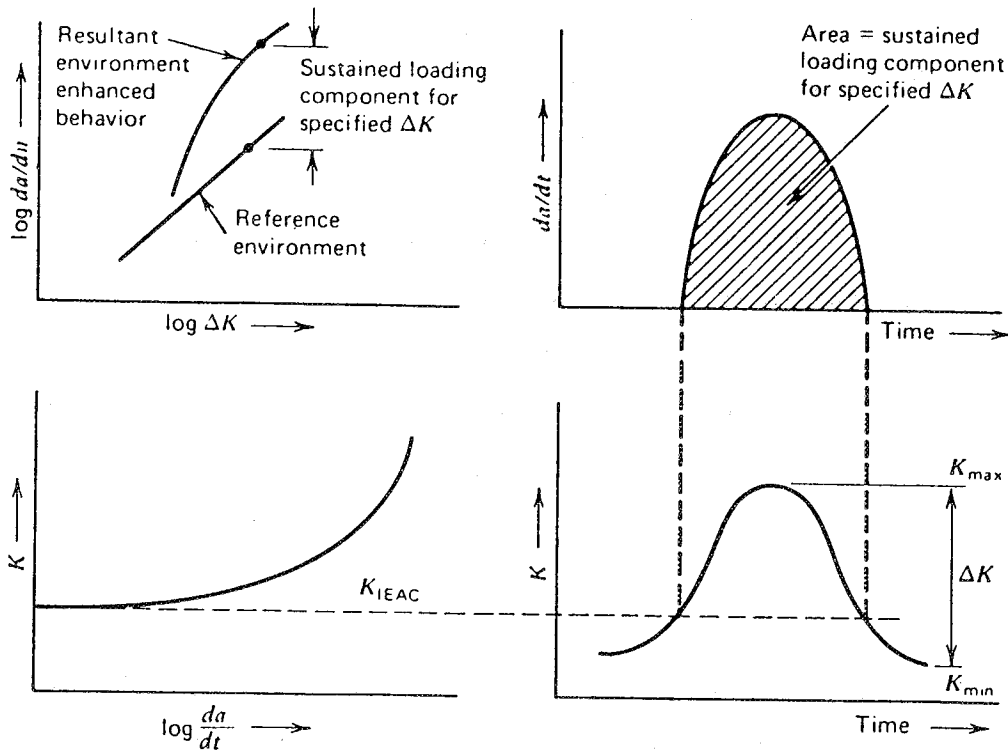
Fig. 79   Schematic diagram illustrating the linear superposition approach to predicting environmental fatigue crack growth rates through Equation 31.   (a) The increments of FCP rates due to mechanical fatigue and environment, (b) MECP rate versus applied K, (c) the applied stress intensity cycle in fatigue, and (d) the integrated fatigue crack growth from the relationships in b and c. After Landes and Wei [229].

NaCl [138,229]. A specific example is given in Fig. 80 for AISI 4340 steel fatigued in distilled water [39,229]. Predicted EFCP kinetics for several waveforms (solid and dashed lines) are in good agreement with measured growth rates (filled symbols).

Several specific cases of Equation 31 are important. Materials that are sensitive to monotonic load environmental cracking (e.g., high strength steels or nickel based superalloys in H_2, water vapor or electrolytes, and some aluminum and titanium alloys; Chapter IV) are likely to exhibit MECP above a sharply defined K_{IEAC} and at a constant or plateau velocity, da/dt_P [145]. Equation 31 then reduces to:

$$da/dN_{SCC} = (da/dt_P) \, \Delta t \tag{33}$$

where Δt is the time during fatigue loading where stress intensities are above K_{IEAC}. For some material/environment systems, Δt is more properly taken as the time where K in the fatigue cycle is both above K_{IEAC} and in the rising load portion of the cycle. If K_{IEAC} is small compared to K_{max}, or if the load cycle is a square wave, then Δt is approximated by $1/f$ and:

$$da/dN_{SCC} = (da/dt_P) \, (1/f) \tag{34}$$

$$= (da/dN_E - da/dN_M)$$

Accordingly:

$$da/dN_E = da/dN_M + (da/dt_P) \, (1/f) \tag{35}$$

Equation 35 describes purely time-dependent EFCP behavior; the logarithm of da/dN_E linearly depends on the logarithm of f, with a slope of -1, as demonstrated by the data contained in Fig. 64. Equation 34 indicates that, by measuring both da/dN_M (frequency independent) and da/dN_E as a function of frequency at one or more constant ΔK levels, da/dt_P can be calculated for the corresponding K_{max} level(s). The resulting da/dt_P can then be employed with Equations 33 and 35 to predict da/dN_E for a wider range of frequency, hold time, stress ratio and load waveform conditions.

For nickel base superalloys in moist air at elevated temperatures, time-dependent crack growth rate depends on applied K according to:

$$da/dt = CK^n \tag{36}$$

where C and n are materials constants [113]. This equation can be combined with Equation 31 to yield:

$$da/dN_E = da/dN_M + C(\Delta K)^n t_{eff} \tag{37}$$

where t_{eff} equals $1/f$ for a square wave hold-time cycle and can be expressed as:
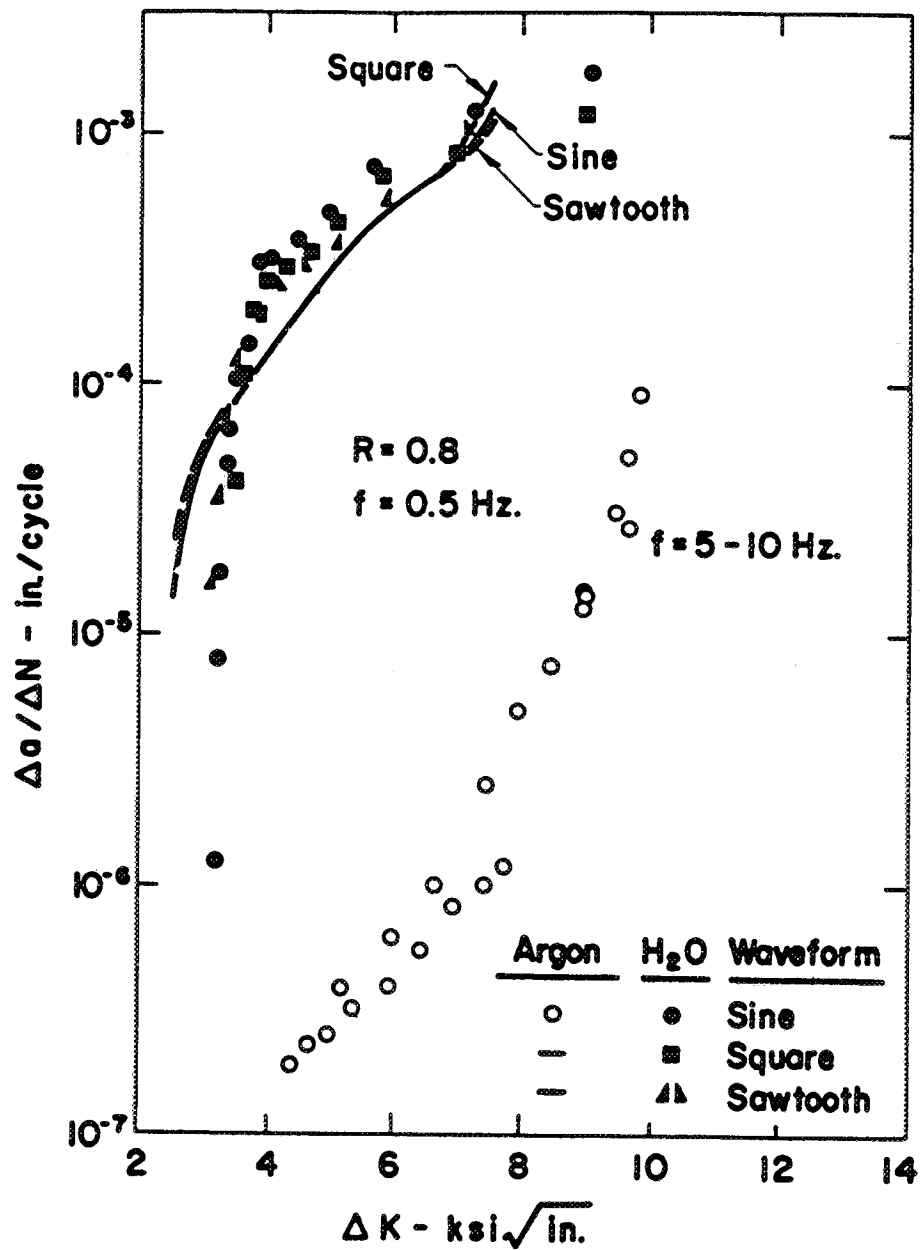
Fig. 80   Time-dependent corrosion fatigue above K_{IEAC} for high-strength type 4340 (UNS G43400) steel in water vapor, modeled by linear superposition. After Wei et al. [39,229].

153

$$t_{eff} = \{(1-R)^{n+1}/(n+1)\}(1/f) \qquad (38)$$

for a symmetric and linearly increasing/decreasing stress intensity versus time cycle.

Data indicate that monotonic load environmental cracking may only contribute to da/dN_E during the loading portion of the fatigue cycle, introducing the term $(1/2f)$ in Equations 34, 35 and 38 [119,258]. ($1/2f$ is only strictly applicable for a symmetric load cycle.)

Equations 37 and 38 were employed to predict time dependent crack growth in high-strength nickel base superalloys at elevated temperatures, as illustrated in Fig. 81 [111,259,260]. Nicholas and coworkers demonstrated that this approach is reasonably successful in predicting sustained-load crack growth for Inconel 718 at 649°C at low stress ratios. At high stress ratios and high frequencies, however, the linear superposition model was proven to have a limited predictive capability. This application of linear superposition is amplified in Chapter IX on "Case Study: Fatigue Crack Growth Rate Modeling for Nickel-Based Superalloys in Moist Air".

Linear superposition is an effective approach to predict the kinetics of EFCP, but only for those material-environment systems where the MECP kinetics make a substantial contribution to da/dN_E. Additionally, da/dt must be known as a function of applied stress intensity. Apart from high strength steels in hydrogen producing environments and nickel-based superalloys in elevated temperature moist air, such data are neither commonly available nor easily determined. Examples are provided in Chapter IV. For many materials, K_{IEAC} is high relative to typical flawed component stress intensity levels and environmental fatigue crack growth is substantial below K_{IEAC}. For these cases, more sophisticated models must be developed to predict da/dN_E as a function of ΔK and the other pertinent variables.

B. Empirical Curve Fitting

The empirical curve fitting approach requires a systematic regression analysis of relatively extensive experimental FCP data to determine the functional relationships between da/dN and ΔK, as well as other associated variables such as f, R and hold time. A notable example is provided by the analysis of corrosion fatigue cracking in welded steel tubular joints for oil and gas platforms in marine environments [108]. Many man-years of effort were expended to develop extensive da/dN-ΔK data for the application-relevant conditions of steel
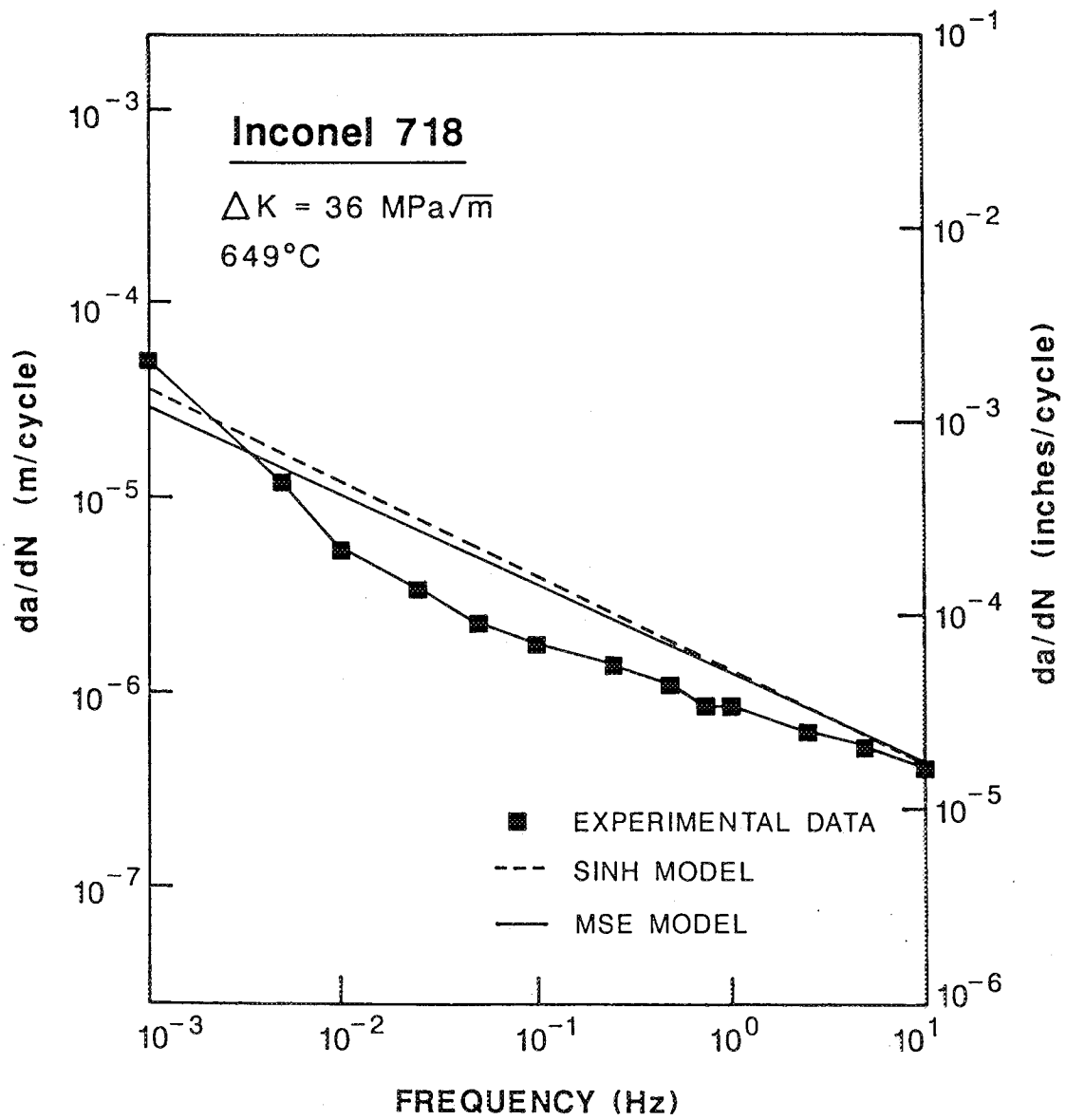
Fig. 81   Effect of loading frequency on fatigue crack propagation in IN 718 exposed to moist air at elevated temperature and constant ΔK. After Haritos et al. [111].

composition and microstructure, loading frequency, stress ratio, wave loading spectra, and seawater/cathodic polarization. As input to a similitude-based life prediction code, Hudak and coworkers empirically described upper bounds on these data sets with a four-variable model describing three commonly observed crack growth regions as follows [254]:

$$1/(da/dN) = A_1/\Delta K^{n1} + A_2/\Delta K^{n2} - A/[(1-R)K_c]^{n2} \tag{39}$$

where A_1, n_1, A_2, n_2 are empirical constants and K_c represents the onset of final fracture. Reasonably good agreement was demonstrated between predicted fatigue lives, from the fracture mechanics approach illustrated in Fig. 1, and measured life for large scale welded tubular components. Life prediction was particularly accurate for the air environment case where extensive FCP data were available and where the effect of loading frequency is unimportant.

Interpolative models based on regression analysis of da/dN-ΔK data have been intensively employed to describe fatigue crack propagation in nickel base superalloys at elevated temperatures [111,113]. Two curve fitting approaches, the so-called MSE and SINH models, were developed. Here, the constants in the complex da/dN-ΔK relationships were stated as functions of those variables; frequency, hold time and R; which are relevant to elevated temperature environmental fatigue cracking. This sophistication departs from simple empirical FCP relationships for the ambient temperature moist air case [22].

1. MSE Model

The modified sigmoidal equation (MSE) model was proposed to represent FCP data for the superalloy alloy, AF115 [261]. This growth rate relationship is of the form:

$$da/dN = \exp(B) \{(\Delta K/\Delta K^*)^P [\ln(\Delta K/\Delta K^*)]^Q [\ln(\Delta K_c/\Delta K)]^D\} \tag{40}$$

This equation represents a sigmoidal shape with the lower asymptote, ΔK^*, representing the threshold value of ΔK and the upper asymptote, ΔK_c, representing the critical or maximum value of ΔK for overload fracture. The remaining four coefficients (B, P, Q and D) depend on the test parameters: T, f, R and τ_H. These coefficients, however, interact in a complex manner in controlling the shape and location of the sigmoidal curve; it is difficult to determine B, P, Q and D as functions of T, f, R and τ_H. To alleviate this difficulty, alternate coefficients were introduced as [186,262]:

$$da/dN = \exp(B') \{(\Delta K/\Delta K_i)^P [\ln(\Delta K/\Delta K^*)]^Q [\ln(\Delta K_c/\Delta K)]^D\} \tag{41}$$

where:

156

$$P = (da/dN_i)' - Q/\ln(\Delta K_i/\Delta K^*) + D/\ln(\Delta K_c/\Delta K_i) \qquad (42)$$

$$B' = \ln(da/dN_i) - Q\ln[\ln(\Delta K_i/\Delta K^*)] - D\ln[\ln(\Delta K_c/\Delta K_i)] \qquad (43)$$

The new parameters, ΔK_i, da/dN_i and $(da/dN_i)'$ represent the horizontal and vertical locations of the inflection point, as well as the slope at the inflection point, respectively. Q and D are shaping parameters such that the da/dN versus ΔK relationship is symmetric when $Q = -D$.

2. SINH Model

A second curve fitting approach, utilizing a hyperbolic sine function, was developed for interpolating elevated temperature fatigue crack growth data for nickel base superalloys [111,113]. This SINH model is expressed as:

$$\log(da/dN) = C_1 \sinh[C_2(\log\Delta K + C_3)] + C_4 \qquad (44)$$

where C_1 and C_2 are shape factors, and C_3 and C_4 control the horizontal and vertical location of the inflection point, respectively. Through regression analysis of a large body of FCP data for several nickel-based superalloys, the following general functional form was established for the SINH model:

$$C_j = C_{base} + b_{1j}\log(f) + b_{2j}\log(\tau_H + 1) + b_{3j}\log[(1-R)/0.9]; \quad j=2,3,4 \qquad (45)$$

Where C_{base} refers to a specific frequency, R and hold time (τ_H) condition, and the 12 constants $(b_{1j}, b_{2j}, \ldots, f)$ are determined by multiple variable regression analysis for a given material. Here, FCP rate changes due to each variable are assumed to be independent.

Both the MSE and SINH models were evaluated for interpolative and extrapolative capabilities by comparing predicted growth rates to FCP data for IN 718 and Rene'95 at 649°C [111,113]. These models provided excellent interpolative capabilities when coupled with time-dependent material constants, b_{ij}. For example, the effects of the changes in f and τ_H indicated in Fig. 60 were satisfactorily described with these models. When f, R, and τ_H vary outside of the data based that is employed to define the constants in the SINH law and MSE laws, then both models exhibit substantial deviation between predicted and experimental values of crack growth rates. While of secondary importance to modeling FCP for benign environment conditions [22], critical effects of loading time and waveform critically compromise the empirical approach to modeling rates of environmental fatigue crack propagation.

Predictions of da/dN_E based on empirical curve fitting are particularly flawed when the damage mechanism for environmental fatigue changes, either within or outside of the

establishing data base. Fig. 81 provides an example where da/dN_E exhibits a bilinear dependence on frequency. Fatigue crack growth is purely time-dependent and intergranular for loading frequencies below 0.01 Hz, but is cycle-time-dependent and transgranular at frequencies between 0.01 and 10 Hz. Both the hyperbolic sine and sigmoidal models predicted linear behavior. Furthermore, these approaches are not able to predict the effects of variables which are not included in the data base; for example superalloy yield strength, microstructure or test temperature. Finally, important low frequency data are not typically obtained to describe near-threshold environmental fatigue; a regime critical to most applications. These limitations are apparent in the empirical treatment of environmental effects on fatigue crack propagation in steels exposed to nuclear reactor water environments at elevated temperature [108]. As operating experience and the laboratory data base broaden, the empirical relationship between da/dN and ΔK has been adjusted to higher growth rates. Ford and coworkers propose a mechanism-based approach to predict da/dN-ΔK in order to improve life prediction capabilities [38,108].

While weaknesses in the interpolative and linear superposition models provide important research challenges, these approaches provide a reasonable basis for state-of-the art life prediction to control environmental fatigue. For example, a PC-based program known as ACDCYCLE (Advanced Cumulative Damage Cycle) predicts flawed component life based on da/dN-ΔK derived from linear superposition, interpolation, Walker modeling of R for crack closure and a Willenborg model for delay retardation [ ]. This program was developed and evaluated for nickel-based superalloys in the jet aircra   'ine disk application.

C.   Mechanism-Based

The simple linear superposition statement of the environmental FCP rate (da/dN_E) is generalized to define both time-dependent (above K_{IEAC}) and time-cycle-dependent (below K_{IEAC}) crack propagation according to [34,185]:

$$da/dN_E = da/dN_M + da/dN_{CF} + da/dN_{SCC} \qquad (46)$$

where da/dN_E, da/dN_M and da/dN_{SCC} were defined with regard to Equation 30, and da/dN_{CF} is the increment of da/dN_E that is attributed to time-cycle dependent damage driven by the interaction between environment chemical and cyclic plasticity processes. Since plasticity-driven pure mechanical fatigue and time-cycle dependent environmental fatigue can proceed

by different micromechanisms and occur concurrently or in parallel, da/dN_E is equivalent described by [263]:

$$da/dN_E = da/dN_M \, (\Theta) + da/dN_C \, (\Phi) \tag{47}$$

where Θ is the fraction of the crack surface formed by mechanical fatigue, Φ is the fractional surface area formed by "pure" environmental fatigue, and da/dN_C is the rate of "pure" EFCP. The FCP rate contribution derived from monotonic load environmental cracking is a sequential contribution and, for simplicity, is not included in Equation 47. Θ and Φ are measured by fractographic analysis. For two parallel processes when $\Theta = (1-\Phi)$, Equation 47 may be rewritten in the following form:

$$da/dN_E - da/dN_M = (da/dN_C - da/dN_M) \, (\Phi) = da/dN_{CF} \tag{48}$$

This equation indicates that the phenomenological difference between inert and aggressive environment fatigue rates from the da/dN-ΔK relationship (da/dN_{CF}) is equivalent to the difference between the rates of chemical-mechanical (da/dN_C) and mechanical (da/dN_M) fatigue times the fractional occurrence of the former. Model predictions of da/dN_C are discussed in the ensuing section.

Austen and Walker argued that corrosion and mechanical fatigue processes are competitive rather than superposable [264]. They assume that environmental crack growth rates are controlled by the dominant of two processes, be it mechanical fatigue or cycle-time-dependent EFCP, and can be expressed as:

$$da/dN_E = C(\Delta K + d\Delta K)^n \tag{49}$$

where $d\Delta K$ is an adjustable parameter representative of the corrosion fatigue contribution, and C and n are material constants that bear the same significance as in the Paris law description of FCP. This competition model is a special case of Equation 48, in that $\Phi = 1$ and $da/dN_M \ll da/dN_C$. This model is weak when environmental crack growth involves a significant amount of mechanical fatigue at relatively high rates. Studies indicate that this model overestimates environmental crack growth rates at K levels below K_{IEAC} for high-strength aluminum alloys in electrolytes and for steels in gaseous hydrogen.

In order to rigorously model EFCP kinetics, it is necessary to derive da/dN_C and Φ in Equation 48 as a function of the pertinent chemical and metallurgical variables, and particularly as a function of loading time. Several hypotheses have been proposed in this regard. In hydrogen embrittlement modeling, da/dN_C is assumed to be proportional to the

amount of hydrogen produced at the crack tip. Two limiting cases, transport-controlled and surface reaction-controlled, have been considered depending on the alloy-environment system. The film rupture model, on the other hand, assumes that da/dN_C (more precisely, da/dN_{CF}) is controlled by the change in oxidation charge density with time and the frequency of oxide rupture at the strained crack tip. Each proposed mechanism-based corrosion fatigue model is assessed in this section.

1. Environmental Fatigue Crack Propagation by Hydrogen Environment Embrittlement

Model predictions of da/dN_C and the fraction of the crack front progressing by pure EFCP (or equivalently da/dN_{CF}) have been developed from the hydrogen environment embrittlement perspective. This approach is based on chemical modeling and experimental verification of the roles of: (a) mass transport within the occluded crack environment, (b) surface reactions, including the rate and amount of hydrogen produced by the reaction sequence for gases or electrolytes, and (c) atomic hydrogen diffusion within the crack tip process zone; combined with the local crack-tip field, most probably the cyclic plastic strain and the hydrostatic normal stress distributions. Microstructure determines the diffusion kinetics and distribution of segregated hydrogen through trapping processes. Local fracture will be determined by a damage criteria. These processes are illustrated in Fig. 5. The successful model will incorporate these complex processes to predict EFCP kinetics as a function of ΔK, R, loading time, σ_{ys} and alloy microstructure.

A variety of HEE models for predicting EFCP kinetics have been developed and are summarized in Table 4 [31]. These models are classed as either hydrogen production limited (Scott, Gangloff, and Wei et al.) or hydrogen diffusion limited (Holroyd and Hardie, Austin and Walker, and Kim et al.).

Scott et al. hypothesize that EFCP rates are controlled by the rate of supply of atomic hydrogen to the process zone for the case of plateau crack growth rates for steels in seawater and 3.5% NaCl at cathodic potentials [69]. The model assumes that the time-based plateau crack growth rate a in hydrogen producing environment, da/dt_e, is proportional to the rate of cathodic hydrogen evolution given by the reduction reaction current density, i_H, i.e:

$$da/dt_e = Bi_H \qquad (50)$$

where B is a constant and i_H is related by the Tafel equation to the more useful term of cathodic overpotential. Scott's original correlation with data was primitive and predicted that

	CONTROL PROCESS	da/dN ASSUMPTION	GROWTH RATE PREDICTION
Scott	Crack Tip Cathodic Hydrogen Production	$\dfrac{da}{dN}_{e,\,PLATEAU} \propto i_H$	$A(1/f)\,(exp(-E/RT))$
Gangloff	Competition Between O_2 and H^+ Reduction	$\dfrac{da}{dN}_{cf} \propto C_H$	$A'\,(V_{max})^{1/2}\,exp(\alpha a_0/fV_{max})$
Wei et al.	Molecular Flow Gas Transport	$\dfrac{da}{dN}_{cf} \propto C_H \propto \theta$	$\dfrac{da}{dN}_{cf,SAT}\left(\dfrac{P_0}{f}\right)\Big/\left(\dfrac{P_0}{f}\right)_{SAT}$
	Gas-Metal Reaction	$\dfrac{da}{dN}_{cf} \propto C_H \propto \theta$	$\dfrac{da}{dN}_{cf,SAT}\,(1-exp(-kP_0/f))$
	Charge Transfer by Transient Reaction	$\dfrac{da}{dN}_{cf} \propto C_H \propto q$	$\dfrac{da}{dN}_{cf,SAT}\,(1-exp(-\tau/f))$
Holroyd and Hardie	Hydrogen Diffusion in Plastic Zone	$\dfrac{da}{dN}_{e} \propto \dfrac{\Delta x}{cycle}$	$4(\sqrt{D_H/f})$
Kim et al.	Hydrogen Diffusion in Plastic Zone	$\dfrac{da}{dN}_{cf} \propto \dfrac{\Delta x}{cycle}$	$A''\,(\sqrt{P_0 D_H/f})\,(exp(-\Delta H/RT))\Delta K^2$
Austin and Walker	Hydrogen Diffusion in Plastic Zone	$\dfrac{da}{dN}_{e} = \dfrac{da}{dN}_{m}\,\chi$	$\dfrac{(\Delta x - s)}{(r_p - s)}\,(\delta_{max} - s)$
			$\dfrac{da}{dN}_{e,\,PLATEAU} = 37.7\,\dfrac{\sigma_{ys}}{E}\,(\sqrt{D_H/f})$

E = Modulus

Δx = Hydrogen penetration distance = $4\sqrt{D_H/f}$

C_H = Hydrogen concentration

C_{H^+} = Hydrogen ion concentration

T = Temperature

θ = Fractional surface coverage

χ = Environmental factor

q = Electrochemical charge

σ_{ys} = Yield strength

f = Frequency

i_H = H production rate

a_0, A, A', A'', R = Constants

ΔH = Binding energy of hydrogen to dislocation

s = Striation spacing

τ = Clean surface reaction rate constant

α = Oxygen reduction rate constant

V = Crack mouth opening

P_0 = Nominal gas pressure

D_H = Hydrogen diffusivity

E' = Crack tip electrode potential

k = Reaction rate constant

Table 4   Models for cycle-time-dependent corrosion fatigue crack propagation by hydrogen embrittlement. Scott, et al. [69], Wei, et al. [75,88-90], Gangloff [87], Holroyd and Hardie [91], Austin and Walker [92,93], and Kim, et al. [89].

161

da/dN varied linearly with increasingly cathodic potential; this prediction is not substantiated by measured plateau fatigue crack growth rates. This model is a simple application of crack chemistry concepts and is not based on a specific damage criterion.

Gangloff proposed a HEE model based upon the assumption that the increment in the cycle-time-dependent growth rate for environmental cracking (da/dN$_{CF}$) is proportional to the amount of hydrogen produced per loading cycle by H$^+$ reduction at the crack tip for steel in aqueous chloride [87,131]. Da/dN$_{CF}$ is given by:

$$da/dN_{CF} = \delta \sqrt{C_H} \, \Delta K^2 \qquad (51)$$

where δ is a constant of proportionality. He further argued that dissolved oxygen, supplied to the acidified crack solution by convection during fatigue cycling, reduces the amount of cathodic hydrogen (C$_H$) due to a competing cathodic reduction reaction and, consequently, reduces corrosion fatigue crack growth rates. This notion was modeled to yield:

$$da/dN_{CF} = A' \sqrt{V_{max}} \, \exp(\alpha a_o/fV_{max}) \qquad (52)$$

where V_{max} is the crack mouth opening displacement at maximum load, f is frequency, and α and A' are constants. The concept of O$_2$ inhibition of crack acidification and hydrogen embrittlement successfully predict the influence of V_{max} on corrosion fatigue growth rates for a wide range of crack size, geometry, stress range and stress ratio conditions. The beneficial effect of O$_2$ reduction at constant electrode potential was not, however, experimentally demonstrated.

Wei and coworkers proposed a comprehensive HEE model for EFCP assuming that the environmental enhancement is due to hydrogen embrittlement produced by the reactions of hydrogenous gases (particularly H$_2$O and H$_2$S) with freshly produced crack surfaces [75,88-90,212]. As a first step, they formalized the relationship between crack tip gas-metal reaction kinetics and mass transport, controlled by molecule-wall interactions, as follows:

$$dP/dt = -(SN_okT/V)(d\theta/dt) + (F/V)(P_o-P) \qquad (53)$$

$$(d\theta/dt) = k_c(1-\theta) \qquad (54)$$

where:

P = pressure of gas at the crack tip

P$_o$ = pressure of gas in the surrounding environment

k = Boltzmann's constant

S = effective area of crack tip surfaces that participate in the reactions per cycle

162

T = absolute temperature

V = volume associated with the surface area, S

N_o = density of surface sites

θ = fractional surface coverage, or extent of surface reactions as a fraction of the maximum extent, $θ_s$

F = Knudsen flow parameter

K_c = reaction rate constant

Quantitative relationships for EFCP rates are derived, based on Equations 52 and 53, for the limiting cases of mass transport and surface reaction rate limited crack growth. The former case represents when K_c in Equation 54 is large, such as in highly reactive gas-metal systems (e.g., aluminum alloys in water vapor). Crack growth is controlled by the rate of transport of embrittling gas to the crack tip. On the other hand, when K_c is small, crack growth is controlled by the rate of surface reactions at the crack tip. Expressions for da/dN_{CF}, for each case, are presented in Table 4. Good correlation between predicted and experimentally measured values of da/dN_{CF} has been observed for steels, aluminum alloys, and titanium alloys (see Figs. 69, 70, and 82 and References 75, 88, 90 and 212).

Several environmental fatigue crack growth rate models are based on the assumption that da/dN_E is determined by the extent of hydrogen diffusion (Δx) within the crack tip plastic zone and during the time of a single loading cycle. Holroyd and Hardie assumed that da/dN_{CF} depends on Δx, as characterized by the square root of the time available during each load cycle $(t)^{1/2}$, or equivalently on $(1/f)^{1/2}$, times the hydrogen diffusivity, for the aluminum-seawater system [215]. The inert environment crack growth rate contribution was ignored. Based on these assumptions, da/dN_E is given by:

$$da/dN_E = Δx/1 \text{ cycle} = 4\sqrt{D_H t} = 4\sqrt{D_H/\sqrt{f}} \tag{55}$$

This model reasonably described the frequency dependence of crack growth velocities associated with fracture mode transitions in the aluminum/chloride system, however, there is no direct evidence to support the hypothesis that da/dN_C is controlled by hydrogen diffusion.

Austin and walker postulated that CF crack growth rates are given by an enhancement of the mechanical propagation rate due to hydrogen diffusion within the plastic zone and countered by a reduction due to crack tip blunting by corrosion [92,93,199]. Physically, da/dN_E is equated to the mechanical fatigue rate when the extent of hydrogen diffusion is less

163

High Strength Aluminum Alloys in Water Vapor

▲ 2090   ● 2219   ○ 70XX   ✛ 5070

Stress Ratio: 0.85 ... 0.10

$y = 1.022x - 0.3441$

Saturation Pressure/Frequency (Pa-sec) vs Reciprocal Stress Ratio Function
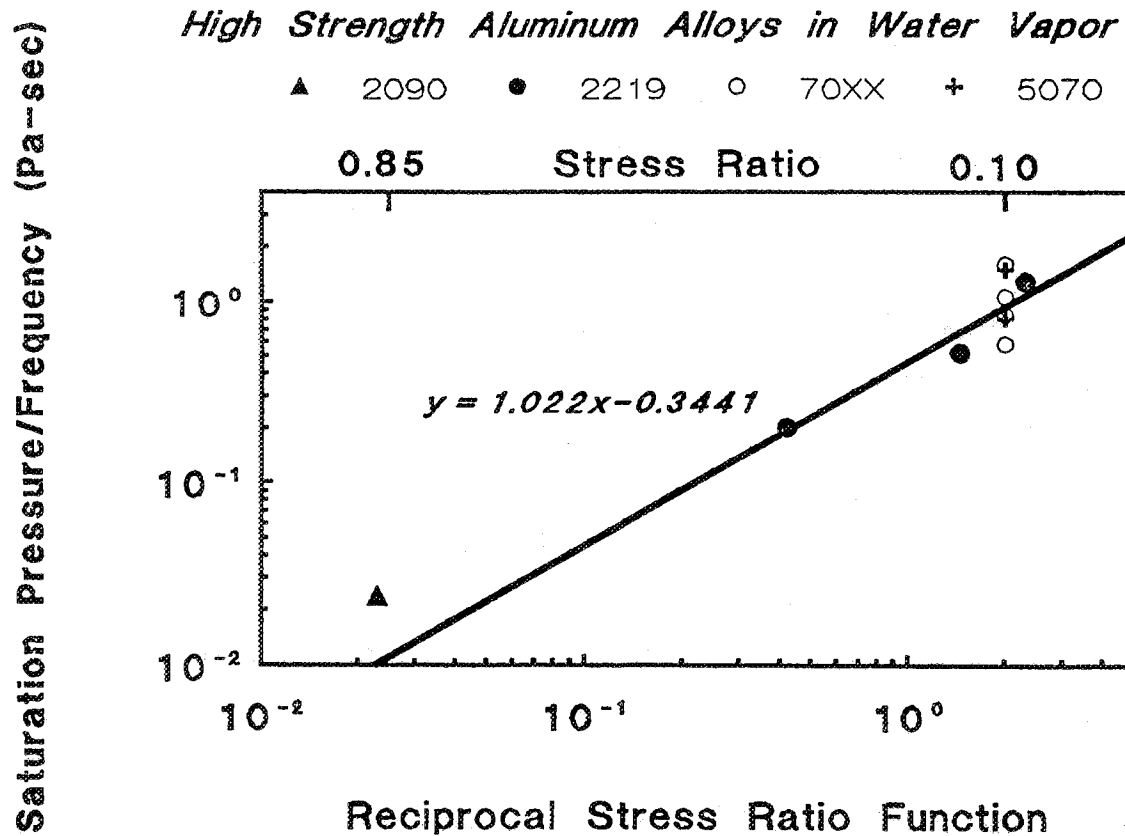
Fig. 82   Effect of mean crack-opening shape, described by a function of R, on the saturation exposure (pressure/frequency) for corrosion fatigue crack propagation in aluminum alloys 2090 [136], 2219 [265], 70xx [75,266], and 5070 [243,247] in water vapor.

164

than one striation spacing. For diffusion distances that exceed the monotonic plastic-zone size, da/dN_E equals the maximum fatigue crack-tip opening displacement per cycle. For intermediate Δx, the governing EFCP rate is given by the equation presented in Table 4. While the Austin and Walker model reasonably predicts some experimental observations of CF for steels in aqueous chloride, the approach is not firmly established.

2. Environmental Fatigue Crack Propagation by Film Rupture and Transient Dissolution

Over several decades, models of environmental cracking have been developed for both monotonic and cyclic loading based on a sequence of passive film rupture at the crack tip, oxidation and progressive repassivation of the exposed metal, and a new rupture of the freshly formed film. The elements of this approach include crack-tip strain rate, transient metal dissolution, film-formation kinetics, and film ductility. This model has been mainly applied to C-Mn and austenite stainless steels in high-temperature water environments [38,105,106,109].

The film rupture approach was discussed in Chapter II, Section C. Recall that da/dN_{CF} is quantitatively related to the oxidation charge density passed between oxide rupture events, Q_f, and the strain rate at the crack tip, $\dot{\epsilon}_{ct}$, by Faraday's Law [38,105,106,109]:

$$da/dN_{CF} = 1/f \ (M/\rho ZF) \ Q_f \ (\dot{\epsilon}_{ct}/\epsilon_f) \tag{56}$$

where M and ρ are the atomic weight and density of the dissolving metal, Z is the number of electrons involved in oxidation, F is Faraday's constant, and ϵ_f is the fracture strain of the oxide at the crack tip. Charge density passed per rupture event is given by:

$$Q_f = \int_0^{t_f = \epsilon_f/\dot{\epsilon}_{ct}} i(t) \ dt \tag{57}$$

where i(t) is the transient current associated with dissolution during reformation of the crack tip passive film.

Ford and Andresen report significant success in predicting the dependencies of da/dt and da/dN_E on pertinent electrochemical variables (viz., temperature, solution conductivity, dissolved oxygen, electrode potential, bulk flow, radiation), on sensitization in type 304 stainless steels, and on soluble sulfide-bearing inclusions in ferritic pressure vessel steels in nuclear reactor environments by this approach [38,105,106,108,109]. Fig. 7 presents the correlation between crack tip strain rate and time-based environmental crack growth rate.

Modeling of the type represented by Equations 56 and 57, and by the results in Fig. 7, is being employed to predict the damage tolerant remaining life of flawed components in commercial nuclear reactor systems.

VIII. FACTORS COMPLICATING FATIGUE LIFE PREDICTION

The fracture mechanics similitude concept, based on a unique geometry independent material relationship between da/dN and ΔK, may be compromised for fatigue crack propagation in aggressive environments. Similitude can be compromised by several mechanisms, including crack closure, small crack mechanics, and crack geometry dependent local environment chemistry. Although these phenomena have been recognized through a wide range of experimental data, modeling to predict complex deviations from simple ΔK-based similitude is limited.

A. Crack Closure

In recent years mechanistic and continuum studies on fatigue crack propagation, particularly in the near-threshold stress intensity range regime, have highlighted crack closure as having a dominant role in influencing crack propagation behavior [2-4,8,251,267,268]. The first crack closure mechanism, proposed by Elber in 1971, involves the idea that premature contact between opposing crack faces can occur during the tensile portion of the fatigue cycle, due to the permanent residual displacements arising from prior plastic zones [15,206]. The consequence of such plasticity-induced crack closure is to reduce the actual stress intensity factor range experienced by the crack tip from a nominal value of ΔK to an effective value defined as $\Delta K_{eff} = K_{max} - K_{cl}$, where K_{cl} represents the stress intensity value at which the two fracture surfaces first come into contact during the unloading portion of the fatigue cycle. Numerous studies on the extrinsic crack closure effect on fatigue crack growth rates clearly demonstrate that there are several mechanisms which can cause crack closure, including:

Crack-wake plasticity [15,268]

Crack surface roughness or deflections with Mode II sliding displacements [206]

Crack corrosion debris [269,270] and

Crack fluid pressure [271].

Several mechanisms for closure are particularly pertinent to EFCP [74,272,273]. Oxide-induced crack closure was invoked to explain the observation that, at low stress ratios, near-threshold FCP rates can be significantly reduced in corrosive environments compared to those in inert environments. It was proposed that the presence of oxide (or more generally,

167

corrosion) debris on the fracture surface provides a mechanism for enhanced crack closure due to the earlier contact between two mating surfaces [205,267,269,274-276]. Oxide-induced crack closure is promoted by several factors including small crack tip opening displacements, highly oxidizing environments, and low stress ratios.

Suresh and Ritchie modeled K_{CL} for oxide induced crack closure under plane strain conditions, while ignoring plasticity and hysteresis effects [206,267]:

$$K_{CL} = dE/[4(\pi l)^{1/2}(1-v^2)] \tag{58}$$

where d is the maximum excess oxide thickness, $2l$ is the location behind the tip corresponding to the thickest oxide formation, and $E/(1-v^2)$ is the effective Young's modulus for plane strain. This model provides an approximate description of the extent of oxide-induced crack closure due to the simplicity of the assumptions and uncertainties in the estimates of d and l.

For steel in aqueous chloride, Todd and coworkers demonstrated that grains, displaced or detached by environment-induced intergranular EFCP, act as wedges to hinder crack closing displacement [277]. The presence of viscous fluid within the pulsating fatigue crack can also promote a closure effect due to the hydrodynamic wedging action of fluid counteracting the closing of the crack [271]. Gangloff and Ritchie speculated that process zone dissolved hydrogen may enhance plasticity and the extent of crack-wake-induced crack closure [205].

Numerous fatigue studies have shown that many of the commonly observed effects of mechanical factors such as stress ratio, microstructural factors and certain environmental conditions, can be traced to the extrinsic influence of crack closure. A substantial amount of controversy exists as to the proper stress intensity range that governs crack growth. The majority of studies have used an effective ΔK value, with K_{CL} determined from compliance measurements. Recent data indicate, however, that the calculated ΔK_{eff} value is too small, implying that fatigue damage continues over a distributed range of loads below K_{cl} [278]. Another problem is the difficulty in the measurement of crack closure in corrosive environments [279]; limited closure data have been published for EFCP.

B. **Small Crack Geometry**

When crack size is below a critical level, fatigue propagation rates are unpredictably

higher than the values predicted by linear elastic fracture mechanics similitude in conjunction with ΔK and conventional long crack specimens. In 1975 Pearson first reported the accelerated growth of a small fatigue crack in a precipitation hardened aluminum alloy in moist air; cracks sized on the order of 100 μm in length grew up to 100 times faster than a long (cm sized) crack at the same applied ΔK and R [280]. Since then, the growth behavior of small fatigue cracks in structural alloys exposed to both benign [6,281-283] and aggressive [6,74,194,205,241,284] environments has been intensely examined. This work demonstrates that the growth of a small crack follows unique mechanisms which differ from those for a long crack. These mechanisms may be based on crack tip mechanics, microstructure or environment chemistry [6].

A crack is defined as "small" if both crack length and the associated plastic zone are wholly contained within 1 to 5 grains. The absolute size of this microstructurally small crack is microstructure dependent and may be quite large for a single crystal. Conventional LEFM is not appropriate for small cracks which are subjected to excessive plasticity over distances comparable to the crack size. Studies have shown that the crack tip strains and openings associated with small cracks are abnormally large compared to those of a long crack at an equivalent applied ΔK [285,286]. This unique behavior of microstructurally small cracks is relevant to FCP in both benign and aggressive environments.

Cracks are generally classified as physically short if they intersect many grains along the crack front, are of limited length dimension, and have a cyclic plastic zone that is much larger than the grain size. Studies have shown that a critical crack size exists below which ΔK_{TH} decreases with decreasing crack length. This behavior is reasonably attributed to crack closure [278,279]. The size of the crack wake, and the importance of associated closure mechanisms, are small for physical short cracks, and growth rates are accordingly not hindered by the levels of crack closure typically encountered for longer cracks at equal applied ΔK levels. As the crack lengthens at constant applied ΔK, the wake increases and closure results in a reduction in the averaged crack growth rate. This mechanism is relevant to FCP in both benign and aggressive environments.

The significance of crack size effects on the chemical driving force for corrosion fatigue, apart from crack size effects on crack tip plasticity and closure, was first recognized by Gangloff. He demonstrated that, for high strength 4130 steel stressed in 3% NaCl, small

(0.1 to 2 mm) surface and edge cracks grew up to 500 times faster than long crack (15 to 40 mm) compact tension data suggested, as shown in Fig. 42b [193,194]. The magnitude of the crack size effect decreases with decreasing maximum crack opening displacement; crack growth rates decrease with increasing maximum applied stress and with increasing R for any ΔK. Gangloff argues that the unpredictably rapid growth of short cracks originates from the influence of crack geometry on localized mass transport and electrochemical processes. Modeling results suggest that uniquely aggressive hydrogen environments develop within the restricted confines of short fatigue cracks due to a complex interplay between convective mixing, ionic diffusion and electrochemical reactions.

Crack size effects on environmental fatigue need to be carefully assessed for life prediction analyses, since a large proportion of component life may be associated with crack growth from 10 μm to 5 mm. Unfortunately, experimental studies and model predictions of the contributions of crack tip plasticity, crack closure and crack environment chemistry are limited [6]. At present, the only recourse is to measure crack growth rate versus applied ΔK for a variety of crack geometries for the material/environment system of interest to a given life prediction problem. The engineer must demonstrate that ΔK-based similitude is reasonably followed before employing the results of conventional LEFM characterizations of da/dN. This suggestion is important for FCP in both benign and aggressive environments.

IX. CASE STUDY: FATIGUE CRACK GROWTH RATE MODELING FOR NICKEL-BASED SUPERALLOYS IN ELEVATED TEMPERATURE MOIST AIR

Elevated temperature fatigue crack growth rates for nickel based superalloys are largely influenced by a number of parameters including frequency (f), temperature (T), stress ratio (R), and sustained load hold time (τ_H) [111-115,259-262]. Of the three approaches to determining fatigue crack growth rates; linear superposition, interpolative models, and mechanism-based models; the former two methods were extensively investigated for nickel based superalloys. Two empirical curve fitting models, the MSE and SINH models discussed in Chapter VII, were developed for describing the constants in the crack growth rate equations as a function of the cycling variables for nickel based superalloys at elevated temperatures [111,113,186,261,262]. Alternately, for this system, linear superposition provides an excellent example of the three methods available to define the time-based crack growth rate response (da/dt versus K) for integration to produce da/dN-ΔK.

A.   Determination of da/dt for Linear Superposition Modeling of da/dN

Nickel based superalloys exhibit sustained load crack growth at elevated temperatures; the purely time-dependent crack growth rate, da/dt, significantly contributes to the total fatigue crack growth rate when K_{max} is above K_{IEAC} [145]. Determination of da/dt versus applied K is a necessary first step to predict da/dN versus ΔK for varying R, f and waveform. Characterization of the sustained crack growth rate as a function of stress intensity level and temperature is approached by using methods based on either curve fitting of directly measured da/dt-K data, or by indirect calculations based on the linear superposition principle and measured da/dN-ΔK data. The following methods are applicable to any material-environment system where crack growth occurs at relatively low sustained stress intensities and at high time-based rates, as previously discussed in Chapter VII.

1. Da/dt-K Measured in Sustained Load Cracking Experiments

In this method da/dt is measured as a function of applied stress intensity with a sustained load experiment for a given temperature and alloy condition. Da/dt-K data are curve fit to either simple power law or more complex equations by regression analysis. Temperature and alloy metallurgical variables will affect da/dt-K and additional experiments are required to define such influences.

Sustained load cracking experiments are conducted similar to room temperature stress

corrosion cracking and hydrogen embrittlement experiments. Generally, a fatigue precracked specimen is subjected to a constant load at a low stress intensity and crack length is monitored by optical or electrical potential methods. If no crack growth is observed after a specific time, then the constant load is incrementally increased until crack extension is resolved. By continuously measuring crack length (a), as a function of time (t), it is possible to calculate da/dt versus K data pairs by the standard secant or incremental polynomial methods described in ASTM E647. Variations of this method are possible, including constant displacement decreasing K loading and computer controlled constant K loading.

In all cases the experimental challenge is to measure crack length for a specimen contained in a furnace. Additionally, it is necessary to guarantee that time-independent small scale yielding is maintained throughout the experiment for accurate usage of standard K equations. Specimen thickness is a variable; there are no simple relationships to guarantee specimen thickness and geometry independent da/dt data. While sustained load cracking experiments have not been specifically standardized by ASTM Committee E-24, emerging standards to define the threshold for stress corrosion cracking (K_{EAC}, or K_{IEAC}), and to characterize creep crack growth (da/dt versus C_T or C^*) provide guidance on experimental methods. Many experimental procedures are also documented in the literature.

A specific example of directly measured sustained load crack growth kinetics is given in Fig. 83 [113]. In this figure da/dt is plotted as a function of ΔK and the da/dt versus K relationship is conveniently represented by a power-law relationship truncated at low K by a threshold value. For nickel based superalloys in moist air at high temperatures, da/dt was found to be well correlated by a power-law function of K. The true threshold was taken to be the lowest value of K at which crack growth approached a vanishingly small rate in the K-shed (or decreasing K) test. The apparent thresholds observed in the constant load experiments are transient artifacts of this testing procedure. Commonly; for stress corrosion, hydrogen and elevated temperature cracking; initial crack growth rates at constant low K accelerate to a steady state value. Such transient effects must be carefully accounted for by conducting a variety of constant load, constant displacement and constant K experiments.

As an alternate approach, Nicholas et al. utilized a modified sigmoidal equation (MSE) to curve-fit directly measured da/dt data as a function of K and temperature [185]. An example of fitted sustained load crack growth data for Inconel 718 is presented in Fig. 36.
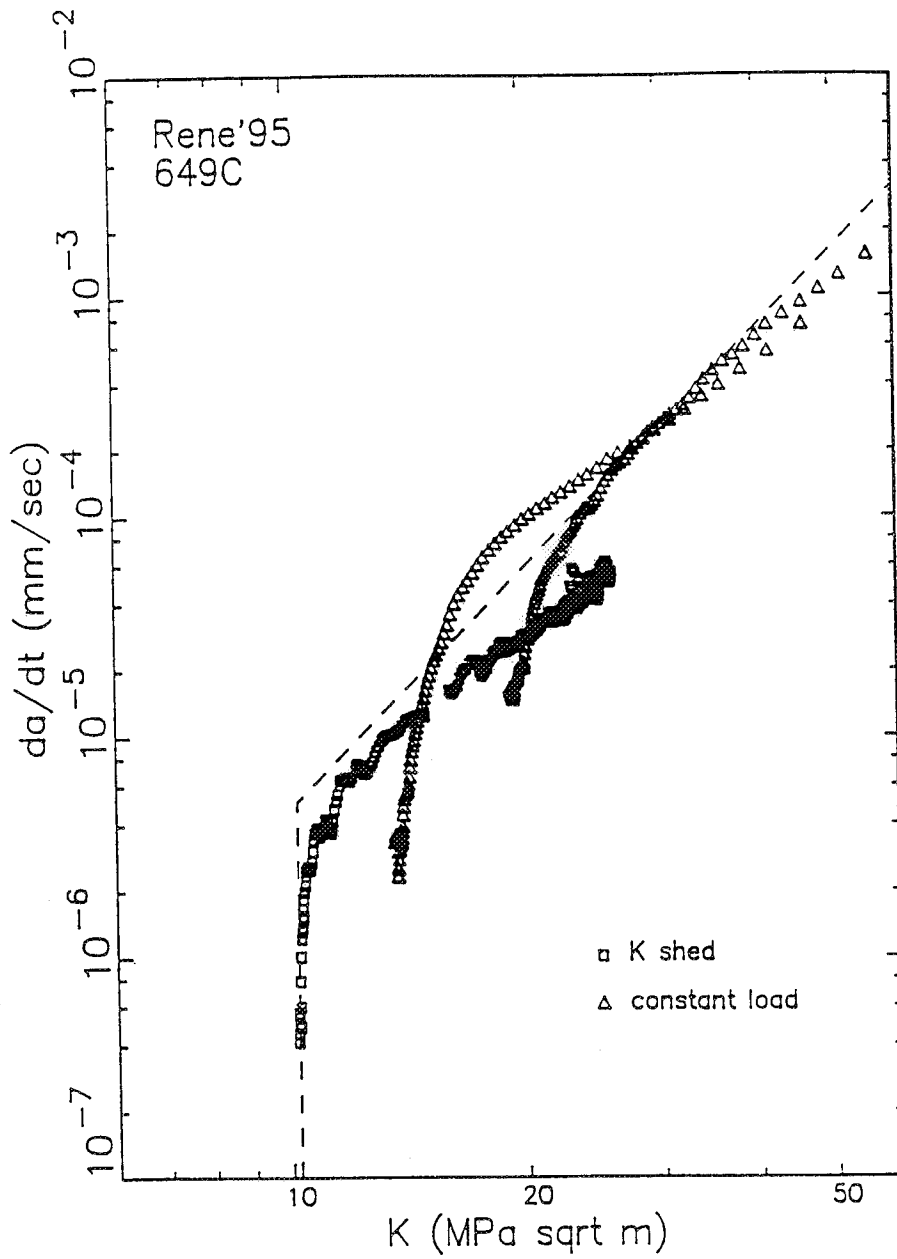
Fig. 83   Sustained load crack growth rate data for Rene'95 at 649°C described by a power law function of applied K, truncated at a threshold stress intensity level. After Van Stone et al. [113].

To analytically define da/dt, da/dN and ΔK in the MSE equation (Equation 41) were replaced by da/dt and K as:

$$da/dt = \exp (B') \{(K/K_i)^P (\ln (K/K^*))^Q (\ln (K_c/K))^D\} \qquad (59)$$

where:

$$K_c = K_i^2/K$$

$$Q = -D = 0.4$$

The constants (B and P) were determined from the data obtained from sustained load crack growth tests at 538°C and 649°C. Since da/dt varies with temperature, the parameters in the model must account for these variations. The interpolative model provides this capability, resulting in a set of temperature-dependent linear relations. As demonstrated in Fig. 36, the MSE equation provides an excellent fitting of the baseline data at 538°C and 649°C. It also provides an excellent prediction of the sustained load crack growth behavior at 593°C.

2. Da/dt-K Measured in Dynamic Rising Load Cracking Experiments

The prolonged times associated with experimental determinations of da/dt versus K and K_{IEAC}, by constant load or crack mouth opening displacement methods, has lead to the development of dynamic rising load procedures [287-290]. These methods, in the initial state of development, are based on the standard rising load K or J-Δa R-curve experiment. The notable departures are that the specimen is loaded to fracture in the aggressive environment of interest, crack growth rates are calculated as a function of K or J, and load line displacement rate (or more precisely, crack tip strain rate) is a primary variable.

Limited comparative experiments with environmental cracking prone alloys indicate that R-curve experiments, conducted on the order of 1 to 5 days, provide similar threshold and da/dt-K data compared to classical constant load or displacement methods [288]. Additional method development and comparative experiments are required for the wide spread use of this important new approach.

3. Da/dt-K Determined from the Measured Effect of Hold Time on FCP Rate

Time-based crack growth rates can be calculated by employing the linear superposition concept in conjunction with measured fatigue crack growth rate data as a function of hold time at varying ΔK, R and temperature for a given alloy. In this approach the fatigue load depends on a simple "square wave" function of time, with the time at maximum load defined as τ_H. The effect of τ_H on da/dN is measured. This approach is particularly attractive because: (a)

the integration of K(t) in Equation 31 is simple, (b) since the loading rate to the hold period is fast, there is no need to arbitrarily define the portion of the load cycle during which sustained load crack growth occurs, and (c) there is no need to assume a value for a crack growth threshold; it is indicated by the experiment and analysis.

The complete linear superposition equation (Equation 31) is simplified for the case of applied square wave loading to any constant K_{max} at any R. That is:

$$da/dN_{SCC} = (da/dt)_{AVG} (t_2 - t_1) \qquad (60)$$

where the difference between t_2 and t_1 is the time during fatigue loading where sustained load crack growth occurs at an average rate, da/dt_{AVG}. If it is assumed that crack growth occurs continuously and at a constant rate between t_1 and t_2, then:

$$da/dN_{SCC} = (da/dt)_{AVG} \tau_H \qquad (62)$$

and by linear superposition:

$$\log da/dN_{SCC} = \log (da/dN_E - da/dN_M) = \log (da/dt)_{AVG} + \log \tau_H \qquad (63)$$

for hold times of duration τ_H at K_{max}.

From Equation 63 and by measuring da/dN_M, a rate that is presumably independent of loading frequency, and da/dN_E as a function of hold time for a square wave load cycle, the average da/dt can be calculated. This experiment can be conducted at one, or ideally more, ΔK and R levels. Da/dt can be correlated with K_{max} (or K) by curve fitting and then used to predict the effects of alternate conditions, such as varying R or high hold time, on da/dN.

Saff and coworkers suggest a simplification of the above method where only two fatigue experiments are employed to obtain da/dt-K for a single temperature and alloy microstructure [291-296]. Specifically, the first experiment defines da/dN as a function of ΔK for any R and at very rapid loading frequencies (10 to 50 Hz sine wave) where time dependent crack growth is assumed to be nil. The second experiment measures da/dN versus ΔK employing a prolonged hold period (for example, τ_H = 300 seconds). For each ΔK and K_{MAX} level, da/dt is calculated from Equation 63 with τ_H equalling 300 seconds, da/dN_M taken from the fast frequency fatigue experiment, and da/dN_E taken from the hold time experiment. Da/dt versus K_{max} (or K) is thus defined over the range of ΔK values characterized. The accuracy of da/dt-K data and the rigor of the limited assumptions can be assessed by defining the effect of τ_H on $(da/dN_E - da/dN_M)$ at fixed ΔK; the logarithmic plot of these two terms should yield a straight line of unit slope and with an intercept given by

$(da/dt)_{avg}$ at this K_{max}; Equation 63.

The schematic in Fig. 84 follows from the original superposition model of Landes and Wei [229], and shows the method of separating the sustained load and cyclic load effects on environmental fatigue crack growth. While Saff has shown that this method produces reasonable results, caution is required. The approach has not been broadly applied to problems in elevated temperature cracking and ambient temperature stress corrosion or hydrogen cracking. While the superposition equation is easily integrated without assumptions for square wave loading, the effects of loading and unloading on da/dt are undefined. For example, unloading may alter crack tip shape relative to constant load. Cyclic loading may alter crack electrochemistry by convective mixing for aqueous environments. These effects are likely to be more important for short hold times. Accordingly, experiments should include long hold times and should examine the effect of τ_H.

4. Da/dt-K Determined from the Measured Effect of Loading Frequency on FCP Rate

Examination of the linear superposition equations discussed in Chapter VII indicates that it should be possible to calculate da/dt based on the measured effect of loading frequency on da/dN_E for loading waveforms based on sinusoidal or triangular functions. This approach is complicated because it is necessary to: (a) assume a value for the threshold, K_{IEAC}, (b) assume the form of the da/dt versus K relationship, and (c) define or assume that portion of the fatigue load cycle that causes time dependent crack growth.

A simple case is represented by the following assumptions:

-- da/dt-K is described by a threshold K of zero and a constant value of da/dt $(da/dt_{constant})$ for all K.

-- sustained load crack growth only occurs during the loading portion of the fatigue load cycle, which can be of any arbitrary but symmetric waveform at a loading frequency, f.

For these conditions, integration of the superposition equation yields:

$$\log (da/dN_E - da/dN_M) = \log (da/dt_{constant}) - \log (2f)$$

$$\text{or} \tag{64}$$

$$\log (da/dN_E - da/dN_M) = \log (da/dt_{constant}) - \log 2 - \log (f)$$

This equation can be experimentally evaluated to yield $da/dt_{constant}$, similar to Equation 63 and for example by Saff's approach. A single ΔK and R condition can be selected. Da/dN_M is

176
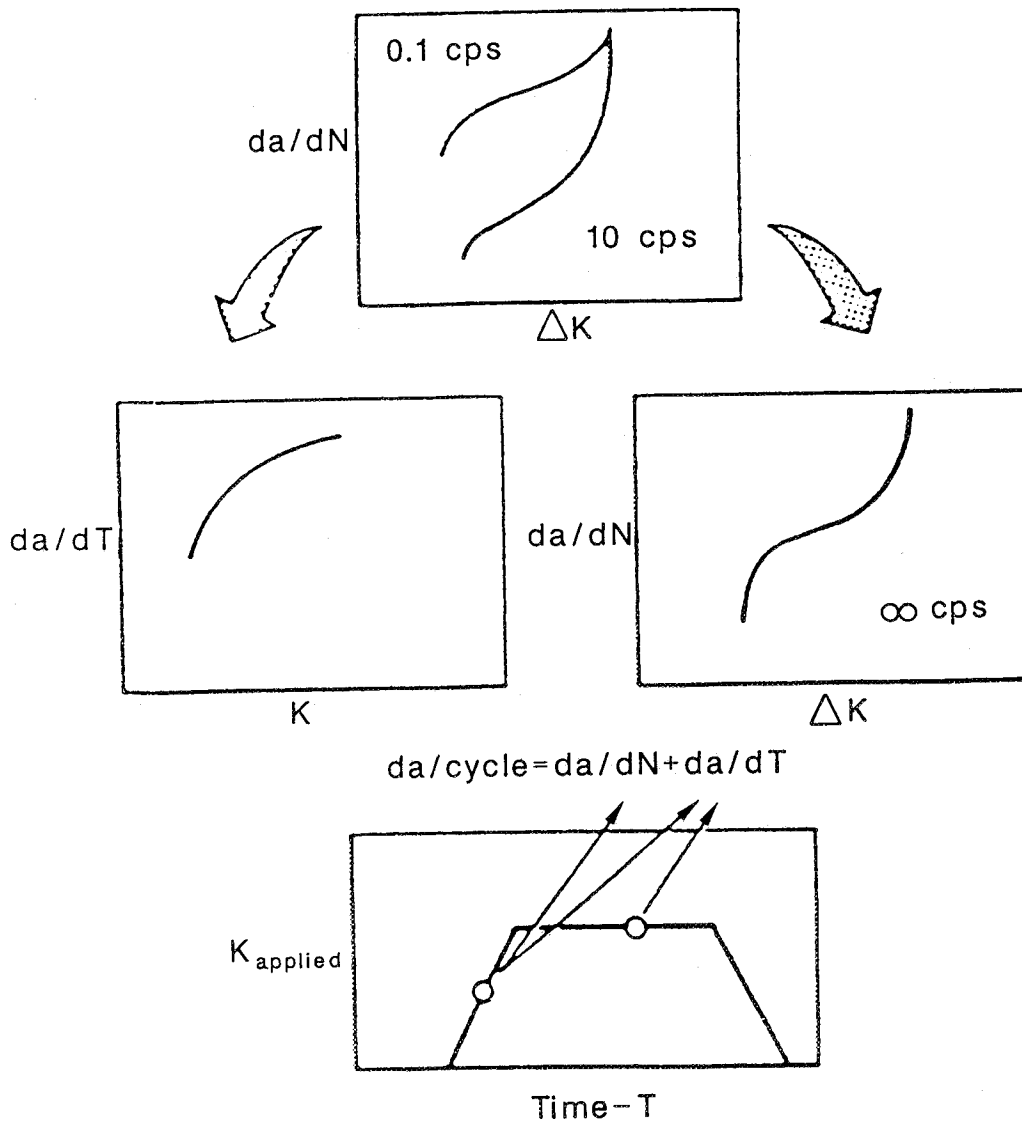
Fig. 84   The simplified linear superposition approach for the determination of da/dt versus K from measured fatigue crack propagation rate data. After Harmon, Saff and Burns [291].

measured by a very high frequency load cycle for the material and environment of interest, by an experiment at any loading frequency in vacuum, or by the previously tabulated data for vacuum. Da/dN_E is measured at one or more loading frequencies and $da/dt_{constant}$ is calculated through Equation 64. The accuracy of the method and the rigor of the assumptions can be assessed by fatigue experiments conducted at a variety of ΔK, R and frequency conditions; a single constant time-based crack growth rate should be determined. Examples of this analysis are represented by the data in Figs. 15, 17, 64, 66 and 81.

A more realistic analysis must address each of the important assumptions for the "damaging" portion (τ_D) of the fatigue load cycle and the form of da/dt versus K. Wei and Landes originally took τ_D to be that portion of the fatigue load cycle where K exceeds the "threshold" level for crack growth including both loading and unloading [229]. Extensive research has shown, however, that time-dependent damage occurs only during the loading (and maximum load hold time) portion of the cycle [113,185]. The most likely physical explanation offered for this phenomenon is that the reduced tensile and eventually compressive stress field at the crack tip during unloading inhibits environmentally-enhanced crack growth. As advocated by Nicholas and coworkers, the sustained-load crack growth rate is best calculated over the loading portion of the mechanical cycle for the superalloy-elevated temperature cracking case.

As mentioned previously, the time-dependent crack growth rate for nickel based superalloys can be correlated with K for a variety of test geometries as:

$$da/dt = C\,K^n \tag{65}$$

where C and n are materials constants that are determined by curve fitting. For simplicity, assume that the threshold K equals 0. Equation 65 can be integrated in conjunction with Equation 31 and simplified forms of K(t), particularly the triangular or square wave forms, to determine da/dN_{SCC} and thus da/dN_E through linear superposition. That is:

$$da/dN_E = da/dN_M + C\,K^n\,t_{eff}$$

$$\text{and} \tag{66}$$

$$\log(da/dN_E - da/dN_M) = \log C + n\log K + \log t_{eff}$$

For the simple constant K_{MAX} square wave hold time case, t_{eff} equals $1/f$ or τ_H, and Equation 66 is equivalent to Equations 62 and 63. For triangular loading ramps at a frequency, f, t_{eff} is given by:

$$t_{eff} = [(1-R)^{(n+1)} / (n+1)] (1/2f) \qquad (67)$$

and Equation 66 can be rewritten as:

$$(da/dN_E - da/dN_M) = (da/dt) ((1-R)^{(n+1)} / (n+1)) (1/2f) \qquad (68)$$

utilizing the relationship between K and da/dt in Equation 65. Employing Equation 68, da/dN_E is measured as a function of ΔK, R and frequency, and da/dN_M is determined as previously discussed. Da/dt is calculated for various K_{max} (or K) levels in the fatigue experiment; that is, C and n are defined in Equation 65.

The quality of the analysis represented by Equation 68 depends on the rigor of the assumptions that there is no threshold value of K below which cracks will not grow, that time dependent cracking only occurs during the loading portion of the fatigue cycle, and that da/dt depends on a simple power law of stress intensity. This approach was used by Nicholas et al. to predict the growth of cracks in nickel based superalloys [114,259,260]. The frequency-based superposition approach did not accurately predict the growth of cracks when the load or K is held at values below the maximum level and overpeak retardation occurs. For superalloys, Van Stone found that da/dt-K, calculated from square wave hold time experiments, more accurately defined frequency effects on specimen and component life for complex loadings [113].

The square wave hold time approach should provide reasonable da/dt-K data for those materials that are particularly sensitive to environmental cracking. However, the uncertainties associated with the assumptions in the frequency-based approach with more complex loading waveforms are those very problems that will limit the application of linear superposition to describe fatigue crack growth rates relevant to components subjected to arbitrary waveforms.

B. Application of Models for Predicting Fatigue Crack Growth Kinetics for Nickel Based Superalloys at Elevated Temperatures

Empirical curve fitting models (both MSE and SINH) and the linear superposition model were employed to predict the elevated temperature fatigue crack growth behavior of nickel based superalloys, including Inconel 718 and Rene'95 [36,114,259,260]. In this section, the specific application and capability of these models to predict FCP behavior, over a reasonable range of operational parameters, are demonstrated.

1. Prediction of da/dN-ΔK for Inconel 718 by MSE and Linear Superposition Models

Nicholas et al. employed the MSE empirical curve-fitting model to interpolatively

179

"predict" cycle-dependent fatigue crack growth rates for IN 718 at elevated temperatures [262]. The linear superposition concept was employed to sum the time-dependent and cycle-dependent contributions to the total environment sensitive fatigue crack growth rate, paralleling Equation 30:

$$da/dN_{Total} = da/dN_{Cycle\ Dependent} + da/dN_{Time\ Dependent} \qquad (68)$$

The cycle-dependent contribution to crack growth is independent of test temperature and loading frequency. Since mechanical fatigue is the dominant mechanism in IN 718 for temperatures below 538°C, at least for cycle periods less than several hundred seconds, the cycle-dependent damage contribution to crack growth for a mechanical cycle was determined from a fatigue crack growth test at 538°C or below. These crack growth rate data for the cycle-dependent contribution for any ΔK or stress ratio were analytically expressed in the form of a modified sigmoidal equation as:

$$da/dN_{Cycle\ Dependent} = (exp\ B')\ (\Delta K/\Delta K_i)^P\ (\ln\ (\Delta K/\Delta K^*))^Q\ (\ln\ (\Delta K_c/\Delta K))^D \qquad (69)$$

where:

$$P = (da/dN_i)' - (Q/\ln(\Delta K_i/\Delta K^*)) + (D/\ln(\Delta K_c/\Delta K_i))$$

$$B' = \ln(da/dN_i) - (Q\ \ln[\ln(\Delta K_i/\Delta K^*)]) - (D\ \ln[\ln(\Delta K_c/\Delta K_i)])$$

In the above equations, ΔK^* and ΔK_c represent the threshold and critical stress intensity factor range, respectively, while Q and D are shaping parameters such that when Q = -D, the curve is symmetric. The other parameters, ΔK_i, da/dN_i, and $(da/dN_i)'$, represent the horizontal and vertical locations of the inflection point, and the slope of the inflection point, respectively. The constants in Equation 69 were determined from a best fit to the experimental crack growth curves obtained at several stress ratios. Specifically, values were determined from data at R = 0.1 and R = 0.5 at 427°C as:

$$\Delta K_c = \Delta K_i^2/\Delta K \quad and \quad Q = -D = 0.4 \qquad (70)$$

which provides a symmetric curve and a shaping parameter which is independent of R. The remaining constants which allow interpolation for any value of R were obtained as follows:

$$
\begin{array}{lllll}
\log \Delta K^* & & 1.0866 & & 1.0312 \\
\log \Delta K_i & = & 1.6299 & + & 0.6068 \quad \log (1-R) \qquad (71) \\
\log (da/dN_i) & & -6.2244 & & 0.7690 \\
(da/dN_i)' & & 3.586 & & 1.9587 \\
\end{array}
$$

The time based crack growth rate, for use in the linear superposition model, was obtained by the method described in Section IX.A.1. These da/dt versus K data were employed in conjunction with Equation 31 to calculate $da/dN_{Time\ Dependent}$.

Results are presented for R = 0.1 and 0.5 at 649°C in Fig. 85 [262]. The loading frequency was 0.01 Hz in all cases. The time-dependent term in the model was obtained by integrating da/dt only during the rising load portion of the cycle. The MSE plus linear superposition model adequately describes environment sensitive fatigue crack growth behavior at this temperature.

2. Prediction of da/dN-ΔK in Rene'95 by Interpolation and Superposition Models

Van Stone et al. modeled elevated temperature fatigue crack growth in Rene'95 with a combined interpolative and linear superposition approach [113]. Specifically, the sigmoidal interpolative model was utilized to describe the constants in the crack growth rate equations as a function of the cycling variables (R, frequency, hold time, etc.). Again, the cycle-dependent and time-dependent contributions to da/dN_{Total} were separately accounted for through the linear superposition concept. The near-threshold crack growth rate was modeled using an interpolative model to predict the influence of R ratio, frequency and hold time. This approach included the Walker model to account for the influence of R on cycle-dependent crack growth rates.

The baseline experiments to establish this modeling include frequency variations, with cycle periods of 3, 30, or 300 seconds, and hold time tests with a 1.5 second loading ramp, a hold time at maximum load, and a 1.5 second unloading ramp. The durations of the hold times were 4, 30, and 300 seconds. Sustained load crack growth tests were performed using either a K-shed or load control modes. The sustained load cracking behavior was defined by linear superposition from measured fatigue crack growth results, as described in Section IX.A.3.

Fig. 86 compares experimental da/dN-ΔK data with predictions from the interpolation model (I), and the interpolation plus superposition model (I + S) for Rene'95 at 649°C [113]. It is clear that both methods predict the general trends in the crack growth response. Predictions of crack growth behavior, outside of the range of conditions over which the model was calibrated, may, however, be unreliable.
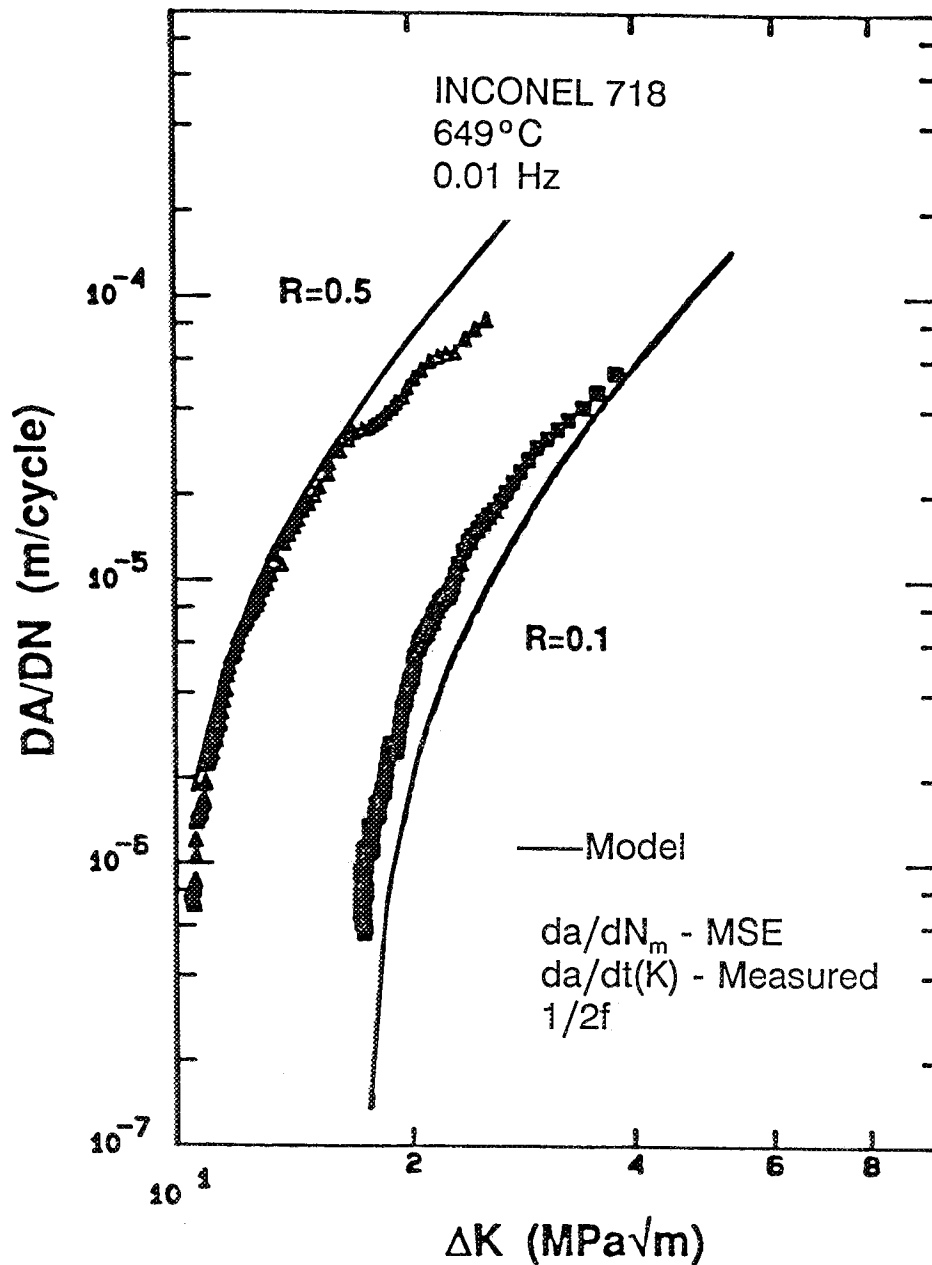
Fig. 85   Measured da/dN versus ΔK for Inconel 718 at 649°C for R=0.1 and 0.5, compared to predictions from the MSE plus linear superposition models. After Nicholas et al. [262].
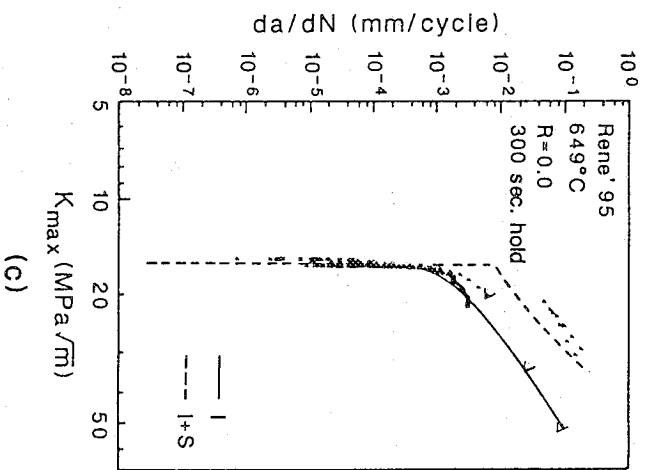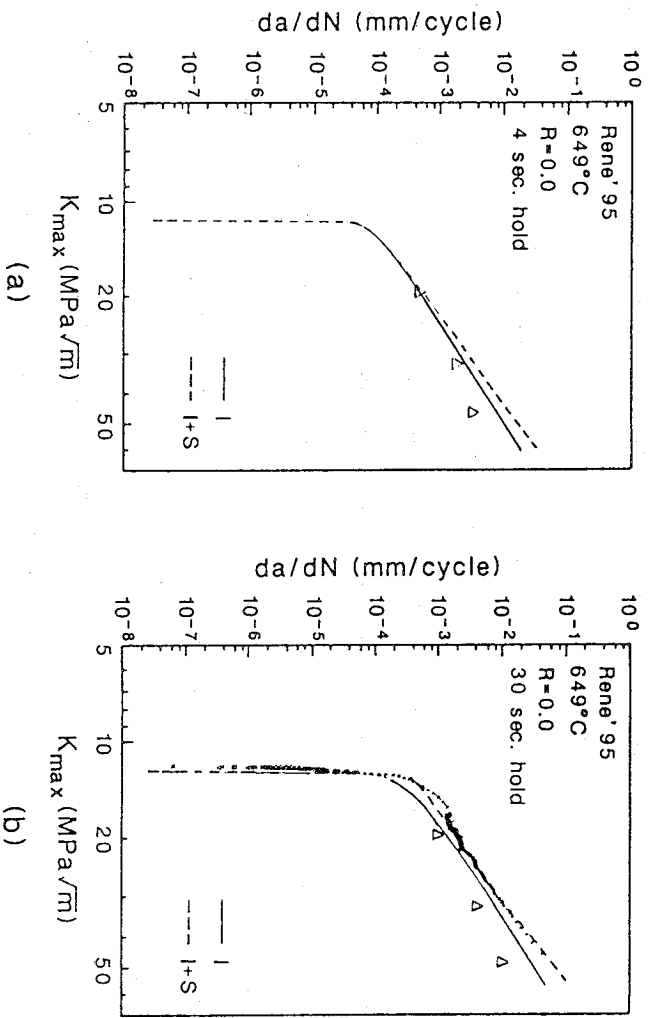
Fig. 86   Measured da/dN versus K_{max} compared to predictions from the interpolation model (I) and the interpolation + superposition models (I+S) for Rene'95 tested at 649°C with R = 0 and hold times of: (a) 4 seconds, (b) 30 seconds, and (c) 300 seconds. After Van Stone et al. [113].

183

3. Comparison of the MSE and SINH Models for Predicting da/dN-ΔK forIN718

Haritos et al. studied the ability of the MSE and SINH models to predict the time-dependent crack growth behavior of Inconel 718 at 649°C [111]. First, fatigue crack growth rate data were generated at the test temperature of 649°C under a baseline condition of frequency (1 Hz), stress ratio (0.1) and hold time (0 seconds). Additional data were then generated under varying conditions of lower frequency, higher stress ratio and longer hold time. This limited set of data was used to determine the coefficients of the functional relationships between the model constants and the test variables. Additional sets of experimental data were generated to evaluate the interpolative and predictive characteristics of each model.

The data sets used to establish the coefficients for the functional relationships between the model constants and the test parameters are plotted along with the best-fit SINH and MSE curves in Figs. 87a and b, respectively. A comparison of these two figures reveals that these two models provide essentially the same fit to the experimental data, except possibly in the near-threshold regime of the stress intensity factor range. Here, the MSE model, through the incorporation of the functional relationship for ΔK^*, exhibits additional flexibility in predicting the experimental data.

The ability of the models to predict trends in da/dN with changing hold time duration and frequency was also studied. Fig. 88 shows the measured effect of hold time duration on crack growth rate compared to the SINH and MSE predictions. The two models yield essentially the same prediction and both predict the trend of the experimental data very well. Fig. 75 compares model predictions with experimental data on the effect of loading frequency on crack growth rate at constant ΔK and R. The predicted frequency dependence is essentially linear and identical for the two models. Over the range of frequencies studied, however, the behavior of da/dN on a log-log scale is bilinear. Clearly, the SINH and MSE models are not able to predict this bilinear behavior.

184
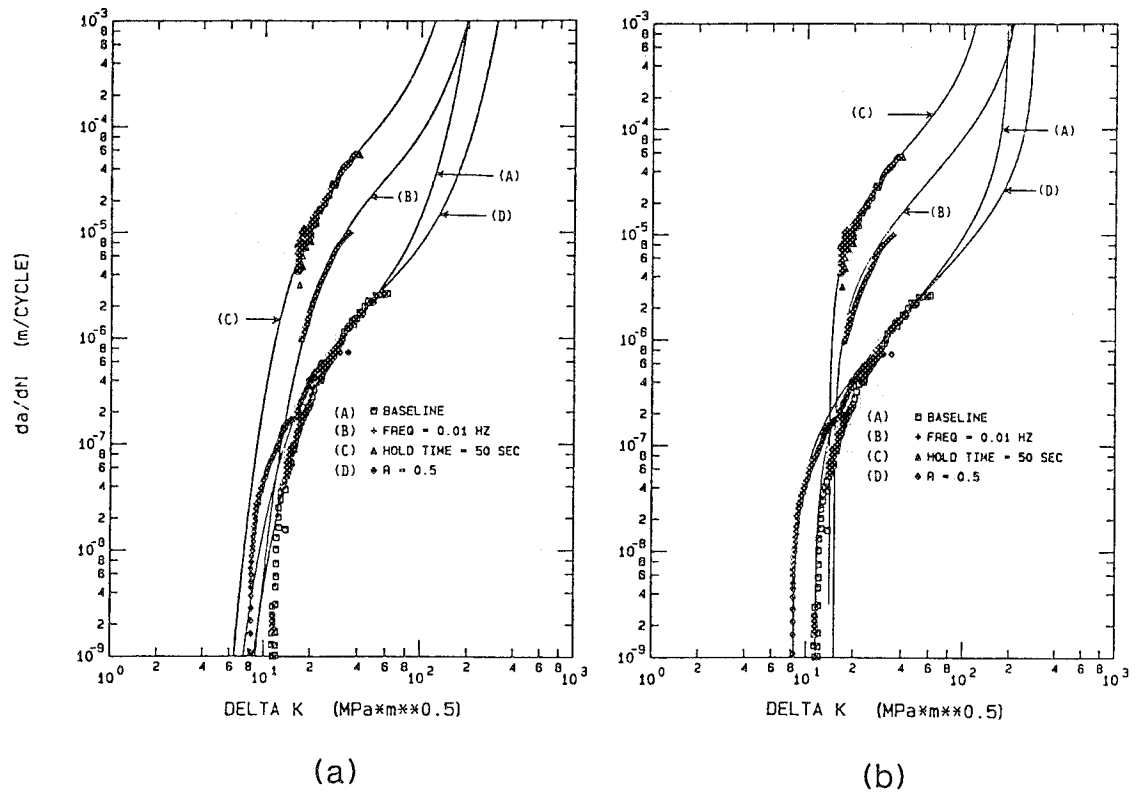
Fig. 87   Measured da/dN versus ΔK for baseline conditions and compared with: (a) SINH and (b) MSE model fits. After Haritos et al. [111].
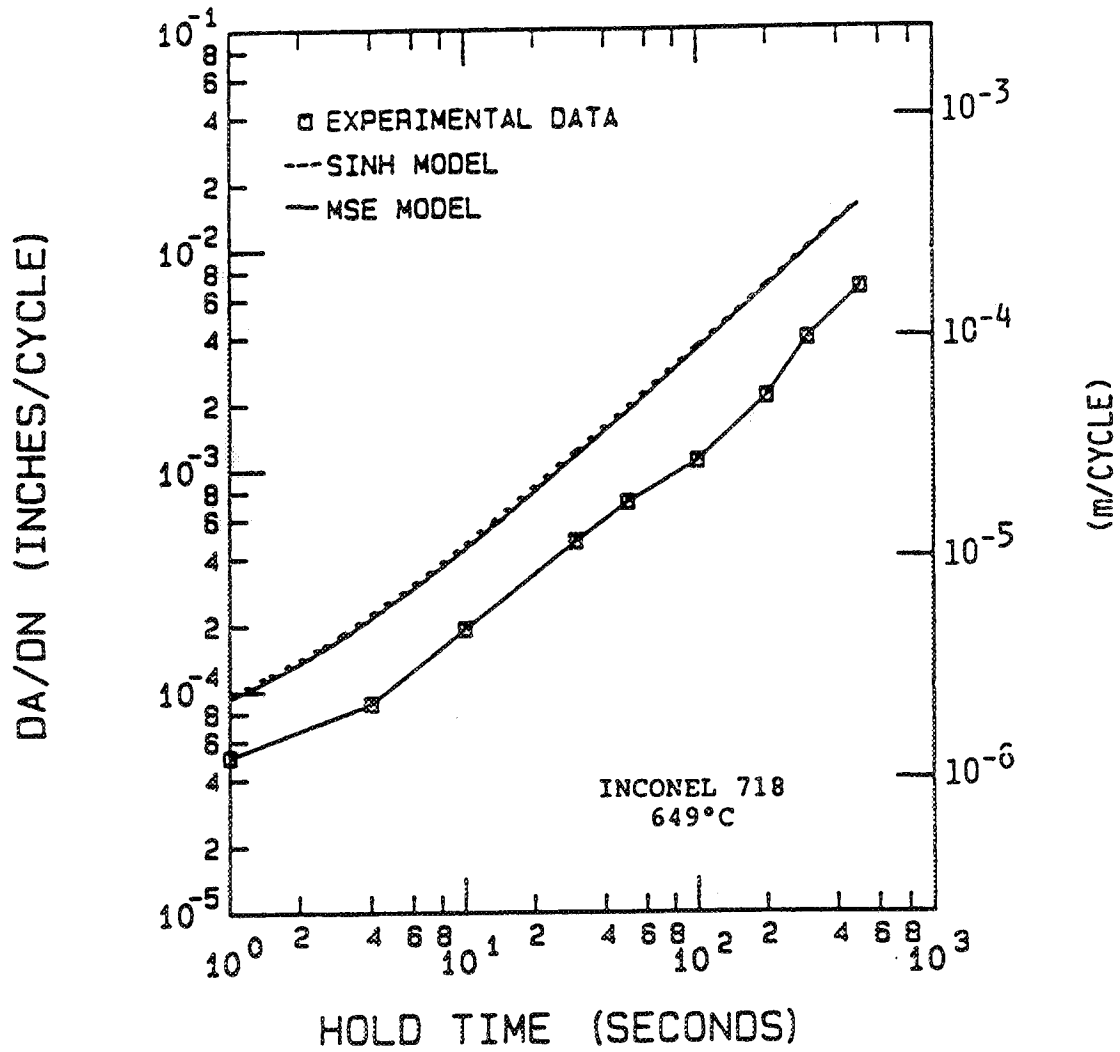
Fig. 88   Comparison of predicted and experimental results for the effect of K_{max} hold time on da/dN at constant ΔK for IN718 at 649°C. After Haritos et al. [111].

186

X. UNCERTAINTIES HINDERING COMPONENT FATIGUE LIFE PREDICTION

A substantial amount of research and engineering work is required to implement descriptions of environmental effects into fracture mechanics-based damage tolerant fatigue life prediction codes for structural aerospace alloys. The challenge is particularly acute for aerospace applications because of the wide range of material/environment systems that can be encountered in such components. Successes have been recorded when substantial efforts are directed towards environmental cracking in a single system (e.g., offshore platforms, light water reactor piping and pressure vessels, or jet engine turbine disks). This progress has been substantial, as reviewed in this report, and encourages continued work in this area.

Specific needs include:

A. Crack Growth Rate Data

Experiments must be conducted on alloy-hydrogen gas or electrolyte systems relevant to aerospace applications and in order to determine:

(1) Sustained load threshold (K_{IEAC}) and crack propagation kinetics to define the extent to which linear superposition modeling can be employed.

(2) Environmental effects on "sub-K_{IEAC}" Paris regime and near-threshold fatigue cracking, particularly as a function of loading frequency and temperature, and identifying the contributions of extrinsic closure and intrinsic fatigue damage.

(3) Environmental fatigue crack propagation under complex spectrum loading, including the effects of single and multiple over/under-loads and load history.

(4) Fatigue crack propagation behavior of advanced light alloys and composites.

(5) A model material-environment system which simulates high pressure hydrogen effects on da/dN and which is amenable to simple experimentation with precise monitoring of crack length and closure behavior.

B. Experimental Methods

New experimental methods are required for:

(6) Accelerated measurement of near-threshold da/dN, particularly at low frequencies relevant to environmental effects.

187

(7)   *In situ* measurement of defect-based fatigue crack initiation, early growth, coalescence and closure evolution for microstructurally small cracks in various environments and without loading interruptions.

C.   **Fracture Mechanics Similitude**

Work in this area is required for:

(8)   Measurement and modeling of crack closure in aggressive environments and under complex loading histories. Models must be developed for roughness and corrosion product mechanisms.

(9)   Measurement and modeling of the growth kinetics of short and small fatigue cracks, with chemical and mechanical mechanisms to extend ΔK-similitude.

D.   **Micromechanical-Chemical Mechanism Modeling**

Modeling and associated experimentation must be expanded to:

(10)   Identify the physical mechanisms for electrochemical and hydrogen enhanced fatigue damage within the crack tip process zone.

(11)   Develop mechanism based models for intrinsic da/dN as a function of ΔK, R, f, environment activity and alloy variables such as σ_{ys}.

E.   **Life Prediction**

Applications of the fracture mechanics approach must emphasize:

(12)   Life prediction codes which incorporate cycle-time-dependent environmental effects on fatigue crack growth, extrapolated from short term laboratory data.

(13)   Incorporation of small/short crack and closure phenomena in residual life predictions.

(14)   Comparisons of code predictions with damage sensor data and full scale component fatigue life experiments.

F.   **Recommendations**

Based on these uncertainties, and the scope of the environmental fatigue problem, recommendations for the next steps to incorporate environmental effects into NASA-FLAGRO are summarized in Table 5.

C-3

- ⊛⊛ Catalog material-environment systems where chemical effects on FCP are known.

- ⊛⊛ If IN718 + 500-650°C air is relevant, implement GE-ACDCYCLE as a module in NASA-FLAGRO.

  - + Conduct evaluation experiments; improve model if necessary (eg., load interactions).

  - + Consider temperatures below 400°C.

- ⊛⊛ If environment-sensitive systems (300M, Ti-8-1-1, AA 7079 in water or NaCl; IN718 in H_2) are relevant, select most important and implement ACDCYCLE superposition approach in FLAGRO.

  - + Develop crack growth rate data base: Wide range da/dN-ΔK; Da/dt-K from sustained load and hold time FCP.

  - + Conduct evaluation experiments; improve model.

- ⊛⊛ Critically focus on sub-K_{th} FCP; usefulness of superposition.

- ⊛⊛ If important material-environment systems (Ti-6-4, AA 2XXX or 7XXX, moderate σ_{ys} alloy steels in electrolyte or H_2) exhibit cycle-time dependent FCP below K_{th}, then select an important case:

  - + Accumulate literature FCP data.

  - + Experimentally characterize FCP rate data for controlled alloy and chemical conditions; as function of ΔK, R, f, τ_H.

  - + Empirically formulate upper bounds or interpolative da/dN-ΔK relationships.

  - + Support development of fundamental mechanism and associated predictive da/dN model.

Table 5   Recommendations for the next steps to incorporate environmental effects in NASA-FLAGRO.

The data and references cited in this report provide a starting point to incorporate specific environmental fatigue crack propagation data into FLAGRO. Additionally, material/environment systems that are likely to be susceptible to MECP and EFCP can be noted in the materials properties library. If a specific system is of sufficient importance to NASA applications, then empirical curve-fitting or upper bound approaches can be employed to determine specific da/dN versus ΔK relationships. Additional data can be generated to test and improve the accuracy of such growth rate models.

If elevated temperature FCP in nickel-based superalloys (particularly IN718, IN100 and Rene'95) is relevant to NASA applications, then the work summarized in Chapter IX can be incorporated into FLAGRO. Specifically, the General Electric Aircraft Engine computer program, ACDCYCLE, could be modified where necessary and adapted as a FLAGRO module to predict EFCP growth rate laws. Specific laboratory experiments would need to be conducted to develop material properties data relevant to NASA alloys, and to test the predictions of ACDCYCLE for load, time and temperature cycles that are relevant to NASA applications. This methodology is particularly powerful for fatigue crack growth at temperatures above about 500°C, however, substantial work is required to confirm the accuracy of the modeling for FCP at lower temperatures. Data are limited for this temperature regime.

If material/environment systems that are particularly prone to MECP are relevant to NASA applications, then the linear superposition approach embodied in the Wei-Landes model and ACDCYCLE could be implemented into FLAGRO. Examples of possible systems are high strength landing gear and fastener steels in ambient temperature water vapor and chloride spray, Ti-8Al-1Mo-1V in NaCl, AA7079 in moist gases and electrolytes, and high strength superalloys in gaseous hydrogen. Pertinent MECP rate data, in terms of da/dt versus K, and wide range da/dN versus ΔK EFCP data must be determined. Experiments must be conducted to test model predictions for a variety of time and stress ratio conditions.

Most environmental effects on FCP occur at stress intensities that are below K_{IEAC} for monotonic load environmental cracking. MECP prone alloys are typically identified during materials selection and are not employed in applications. Aerospace alloy systems that are influenced by important environmental effects "below K_{IEAC}" include Ti-6Al-4V, AA2XXX

190

and AA7XXX alloys, low to moderate strength C-Mn and alloy steels in various electrolytes and hydrogen gas, and nickel-based superalloys in H_2. A system that is relevant to NASA applications must be identified and the data contained in this report must be augmented by additional literature review. Literature results must be supplemented by laboratory experiments that define da/dN as a function of ΔK, R, f, hold time, environment activity and pertinent metallurgical variables. The empirical curve-fitting and upper bound expressions can be determined for use in FLAGRO. Fundamental research must be conducted on intrinsic crack tip damage mechanisms and growth rate models, as well as on extrinsic environment sensitive crack closure mechanisms.

XI. CONCLUSIONS

Extensive fatigue data from the literature were reviewed with emphasis on environmental effects on linear elastic fracture mechanics-based crack propagation kinetics for alloys that are relevant to aerospace component applications. The many variables that affect da/dN versus ΔK material property laws are cited. Models for describing environment sensitive fatigue crack growth kinetics are analyzed. The following conclusions are established by this literature analysis.

(1) Literature data indicate that fatigue crack propagation rates in most aerospace structural alloys are significantly accelerated by the presence of aggressive environments, compared to vacuum and moist air, and particularly those that are capable of electrochemically reacting with straining crack surfaces and of producing atomic hydrogen at crack tips.

(2) Environment assisted fatigue crack propagation is severe at stress intensities above the threshold level, K_{IEAC}, for monotonic load environmental cracking. Notably, however, strong and deleterious environmental effects on fatigue persist at stress intensities well below K_{IEAC}. Materials that are not susceptible to "stress corrosion cracking" are often deleteriously affected by environment under cyclic loading in both gases and electrolytes.

(3) While mechanistic understanding is qualitative, environmental effects on FCP can be rationalized based on either an environmental hydrogen production/embrittlement mechanism, or on electrochemical film formation with repeated rupture and transient anodic dissolution. These models are useful for hypothesizing the nature of environmental effects, but have not been quantitatively developed.

(4) The fracture mechanics stress intensity range can correlate environmental fatigue crack propagation rates independent of load magnitude, crack size and geometry. Stress intensity-based similitude is, however, complicated by the effects of crack closure (including several mechanisms unique to external environments), small crack size as well as loading history and spectra. These complications must be considered in life prediction.

(5)   Fatigue crack growth rates for alloys in aggressive environments are governed by the synergistic interaction of a plethora of variables including ΔK, stress ratio, frequency, environmental activity, loading waveform, alloy yield strength and microstructure.

(6)   Two variables particularly affect rates of environmental fatigue crack propagation; stress intensity range and loading frequency. Compared to simple Paris power-law behavior for FCP in benign environments, complex-shaped da/dN versus ΔK relationships are typical of an environmental effect. For any ΔK level, da/dN generally increases with decreasing loading frequency (or increasing hold time), with the functional dependence specific to the stress intensity regime under consideration, be it above or below K_{IEAC}.

(7)   Fatigue crack propagation rates for nickel based superalloys are substantially increased at elevated temperatures by moist air exposure, and depend on stress ratio, frequency and hold time. Phenomenological similarities exist between elevated temperature fatigue cracking in nickel based superalloys and FCP in Fe, Al, Ni and Ti-based alloys in low temperature hydrogen producing gases and electrolytes.

(8)   Environment assisted crack growth rate data, for monotonic and cyclic loading, are limited for many alloys and environments relevant to aerospace applications. These environments are often complex to contain and control in laboratory experimentation.

(9)   Stress intensity-based FCP laws can be developed from three perspectives: (a) linear superposition of mechanical fatigue and monotonic load environmental cracking, (b) empirical curve fitting of a broad range of crack growth rate data, and (c) mechanistic modeling of crack tip chemo-mechanical fatigue damage. Models of this sort are required for incorporation into NASA FLAGRO.

(10)   Each approach to modeling da/dN versus ΔK has been employed to quantitatively describe environmental effects on fatigue crack propagation, relevant to several technologies including offshore structures, pressure vessels and pipes in nuclear reactors and jet engine disks.

(11)   There is currently no rigorous and quantitative method to broadly predict environment enhanced FCP rates, outside of an existing data base and for a given material and environment system.

194

(12) Further research is required in the areas of near-threshold environmental fatigue behavior, advanced alloy and composite cracking, fundamental damage mechanism models, da/dN-ΔK modeling, crack closure and small crack effects on similitude.

(13) Specific recommendations for incorporating environmental effects on FCP in NASA FLAGRO include cataloging the MECP and FCP data contained in this report, adapting a linear superposition computer program (e.g., ACDCYCLE) as a FLAGRO module, testing the linear superposition approach for a relevant material/environment system, experimentally defining the "below K_{IEAC}" behavior of a relevant material/environment system, and continuing to develop fundamental models of environment sensitive crack closure and intrinsic damage mechanisms.

XII. REFERENCES

1. Fatigue Mechanisms, ASTM STP 675, J.T. Fong, ed., ASTM, Philadelphia, PA (1979).

2. Fatigue Crack Growth Threshold Concepts, D.L. Davidson and S. Suresh, eds., TMS-AIME, Warrendale, PA (1984).

3. Current Research on Fatigue Cracks, T. Tanaka, M. Jono and K. Komai, eds., Society of Materials Science, Japan, Kyoto, Japan (1985).

4. Fatigue 84, C.J. Beevers, ed., EMAS, West Midlands, UK (1984).

5. Fatigue Crack Growth, 30 Years of Progress, R.A. Smith, ed., Pergamon Press, Oxford, UK (1986).

6. Small Fatigue Cracks, R.O. Ritchie and J. Lankford, eds., TMS-AIME, Warrendale, PA (1986).

7. Fatigue and Life Analysis and Prediction, V.S. Goel, ed., ASM, Metals Park, Ohio (1986).

8. Fatigue 87, R.O. Ritchie and E.A. Starke, Jr., eds., EMAS, West Midlands, UK (1987).

9. Basic Questions in Fatigue, ASTM STP 924, Vol. 2, R.P. Wei and R.P. Gangloff, eds., ASTM, Philadelphia, PA (1988).

10. Fatigue and Microstructure, ASM International, Metals Park, OH (1979).

11. P.C. Paris, M.P. Gomez and W.E. Anderson, The Trend in Engineering, Washington State Univ., Vol. 13, No. 1, pp. 9-14 (1961).

12. "Standard Test Method for Measurement of Fatigue Crack Growth Rates", Designation E647-91, Annual Book of ASTM Standards, Vol. 03.01, ASTM, Philadelphia, PA, pp. 674-701 (1992).

13. R.P. Wei and R.P. Gangloff, in Fracture Mechanics: Perspectives and Directions, ASTM STP 1020, R.P. Wei and R.P. Gangloff, eds., ASTM, Philadelphia, PA, pp. 233-264 (1989).

14. J.A. Feeney, J.C. McMillan and R.P. Wei, Met. Trans., Vol. 1, pp. 1741-1757 (1970).

15. Mechanics of Fatigue Crack Closure, ASTM STP 982, J.C. Newman and W. Elber, eds., ASTM, Philadelphia, PA (1988).

16. Methods and Models for Predicting Fatigue Crack Growth Under Random Loading, ASTM STP 748, J.B. Chang and C.M. Hudson, eds., ASTM, Philadelphia, PA (1981).

17. R.P. Gangloff, R.S. Piascik, D.L. Dicus and J.C. Newman, "Fatigue Crack Propagation in Aerospace Aluminum Alloys", Journal of Aircraft, in review (1992).

18. J.B. Chang, M. Szamossi and K.W. Liu, "User's Manual for a Detailed Level Fatigue Crack Growth Analysis Computer Code - CRKGRO", AFWAL-TR-3093, November (1981).

19. R.G. Forman, V. Shivakumar, J.C. Newman, Jr., S.M. Piotrowski and L.C. Williams, in Fracture Mechanics: Eighteenth Symposium, ASTM STP 945, ASTM, Philadelphia, PA, pp. 781-803 (1988).

20. NASCRAC--NASA Crack Analysis Code User's Manual, Failure Analysis Associates, Inc., Palo Alto, CA (1989).

21. FASTRAN--Fatigue Crack Growth Analysis--A Closure Model, Computer Software Management and Information Center, University of Georgia, Athens, Georgia, December (1984).

22. M.S. Miller and J.P. Gallagher, in Fatigue Crack Growth Rate Measurement and Data Analysis, ASTM STP 738, S.J. Hudak, Jr. and R.J. Bucci, ASTM, Philadelphia, PA, pp. 205-251 (1981).

23. Environment Induced Cracking of Metals, R.P. Gangloff and M.B. Ives, eds., NACE, Houston, TX (1990).

24. Atlas of Stress-Corrosion and Corrosion Fatigue Curves, A.J. McEvily, ed., ASM International, Metals Park, OH (1990).

25. Corrosion Fatigue Technology, ASTM STP 642, H.L. Craig, Jr., T.W. Crooker and D.W. Hoeppner, eds., ASTM, Philadelphia, PA (1978).

26. Proceedings, Conference on the Influence of Environment on Fatigue, Inst. Mech. Engr., London (1978).

27. Fatigue: Environment and Temperature Effects, J.J. Burke and V. Weiss, eds., U.S. Army Materials Technology Laboratory, Watertown, MA (1984).

28. Corrosion Fatigue: Mechanics, Metallurgy, Electrochemistry and Engineering, ASTM STP 801, T.W. Crooker and B.N. Leis, eds., ASTM, Philadelphia, PA (1984).

29. Environment Sensitive Fracture of Metals and Alloys, Office of Naval Research, Arlington, VA (1987).

30. Environmentally Assisted Cracking: Science and Engineering, ASTM STP 1049, W.B. Lisagor, T.W. Crooker and B.N. Leis, eds., ASTM, Philadelphia, PA (1990).

31. R.P. Gangloff, in Environment Induced Cracking of Metals, R.P. Gangloff and M.B. Ives, eds., NACE, Houston, TX, pp. 55-109 (1990).

32. Corrosion Fatigue, Chemistry, Mechanics and Microstructure, O. Devereux, A.J. McEvily and R.W. Staehle, eds., NACE, Houston, TX (1972).

33. Stress Corrosion Cracking and Hydrogen Embrittlement of Iron Based Alloys, J. Hochmann, J. Slater, R.D. McCright and R.W. Staehle, eds., NACE, Houston, TX (1977).

34. R.P. Wei, in Fatigue Mechanisms, ASTM STP 675, J.T. Fong, ed., ASTM, Philadelphia, PA, pp. 816-840 (1979).

35. R.P. Wei and G. Shim, in Corrosion Fatigue: Mechanics, Metallurgy, Electrochemistry and Engineering, ASTM STP 801, T.W. Crooker and B.N. Leis, eds., ASTM, Philadelphia, PA, pp. 5-25 (1983).

36. P.M. Scott, in Corrosion Fatigue: Mechanics, Metallurgy, Electrochemistry and Engineering, ASTM STP 801, T.W. Crooker and B.N. Leis, eds., ASTM, Philadelphia, PA, pp. 319-350 (1983).

37. R.P. Gangloff and D.J. Duquette, in Chemistry and Physics of Fracture, R.M. Latanision and R.H. Jones, eds., Martinus Nijhoff Publishers BV, Netherlands, pp. 612-645 (1987).

38. F.P. Ford, J. Press. Ves. Tech., Trans. ASME, Vol. 110, pp. 113-128 (1988).

39. Mechanics and Physics of Crack Growth:Application to Life Prediction, R.B. Thompson, R.O. Ritchie, J.L. Bassani and R.H. Jones, eds., Elsevier, London (1988).

40. R.P. Wei and G.W. Simmons, Int. J. Fract., Vol. 17, pp. 235-247 (1981).

41. P.J.E. Forsyth, The Physical Basis of Metal Fatigue, Clarendon Press, Oxford, U.K. (1969).

42. S. Purushothaman and J.K. Tien, Matl. Sci. and Eng., Vol. 34, p. 241 (1978).

43. D. Taylor, Fatigue Thresholds, EMAS, Warley Heath, U.K. (1982).

44. A.T. Yokobori and T. Yokobori, in Advances in Fracture Research (ICF5), Pergamon Press, Oxford, p. 1373 (1981).

45. T. Mura and J. Weertman, in Fatigue Crack Growth Threshold Concepts, TMS-AIME, Warrendale, PA, p. 513 (1984).

46. G.R. Yoder, L.A. Cooley and T.W. Crooker, in Fracture Mechanics, Fourteenth Symposium - Vol. I: Theory and Analysis, ASTM STP 791, ASTM, Philadelphia, PA, p. 348 (1983).

47. C.J. Beevers, in Fatigue Thresholds, EMAS, Warley, U.K., p. 17 (1981).

48. E.A. Starke, Jr., F.S. Lin, R.T. Chen and H.C. Heikkenen, in Fatigue Crack Growth Threshold Concepts, D. Davidson and S. Suresh, eds., TMS-AIME, Warrendale, PA, pp. 43-61 (1984).

49. C. Laird and G. Thomas, Int. J. of Frac. Mech., Vol. 3, pp. 81-97 (1967).

50. R. W. Lardner, Phil. Mag., Vol. 17, pp. 71-82 (1967).

51. R.M.N. Pelloux, Trans. of ASM, Vol. 62, pp. 281-285 (1969).

52. F.A. McClintock, in Fracture of Solids, D.C. Drucker and J.J. Gilman eds., Vol. 20, New York, Wiley, pp. 65-102 (1963).

53. J. Weertman, Int. J. of Frac., Vol. 2, pp. 460-467 (1966).

54. S. Majumdar and J.D. Morrow in Fracture Toughness and Slow Stable Cracking, ASTM STP 559, ASTM, Philadelphia, PA, pp. 159-169 (1974).

55. S.B. Chakrabortty, Fat. Engr. Matls. Struc., Vol. 2, pp. 331-344 (1979).

56. J.R. Rice, in Fatigue Crack Propagation, ASTM STP 415, ASTM, Philadelphia, PA, pp. 247-309 (1967).

57. J. Weertman, in Fatigue and Microstructure, ASM, Metals Park, OH, pp. 279-306 (1979).

58. R.G. Forman, V.E. Kearney and R.M. Engle, Trans. AIME, J. Basic Eng., Vol. D89, pp. 459-464 (1967).

59. Environmental Degradation of Engineering Materials-III, M.R. Louthan, R.P. McNitt and R.D. Sisson, eds., Pennsylvania State University, University Park, PA (1987).

60. Hydrogen Embrittlement and Stress Corrosion Cracking, R. Gibala and R.F. Hehemann, eds., ASM, Metals Park, OH (1984).

61. Hydrogen in Metals, I.M. Bernstein and A.W. Thompson, eds., ASM, Metals Park, OH (1974).

62. Effect of Hydrogen on the Behavior of Materials, A.W. Thompson and I.M. Bernstein, eds., TMS-AIME, Warrendale, PA (1976).

63. Hydrogen Effects in Metals, I.M. Bernstein and A.W. Thompson, eds., TMS-AIME, Warrendale, PA (1981).

64. Environmental Degradation of Engineering Materials in Hydrogen, M.R. Louthan, R.P. McNitt and R.D. Sisson, eds., VPI Press, Blacksburg, VA (1981).

65. Hydrogen Degradation of Ferrous Alloys, R.A. Oriani, J.P. Hirth and M. Smialowski, eds., Noyes Publications, Park Ridge, NJ (1985).

66. Hydrogen Effects on Material Behavior, N.R. Moody and A.W. Thompson, eds., TMS-AIME, Warrendale, PA (1990).

67. J.M. Barsom, in Corrosion Fatigue, Chemistry, Mechanics and Microstructure, O. Devereux, A.J. McEvily and R.W. Staehle, eds., NACE, Houston, TX, pp. 424-436 (1972).

68. R.P. Gangloff, Matls. Sci. Engr., Vol. A103, pp. 157-166 (1988).

69. P.M. Scott, T.W. Thorpe and D.R.V. Silvester, Corrosion Science, Vol. 23., pp. 559-575 (1983).

70. B.R.W. Hinton and R.P.M. Procter, Metals Forum, Vol. 5, pp. 80-91 (1982).

71. P.S. Pao and R.P. Wei, in Titanium: Science and Technology", Vol. 4, pp. 2503-2510 (1984).

72. D.B. Dawson and R.M. Pelloux, Metall. Trans. A, Vol. 5A, pp. 723-731 (1974).

73. H.G. Nelson, in Hydrogen in Metals, I.M. Bernstein and A.W. Thompson, eds., ASM International, Metals Park, OH, pp. 445-464 (1974).

74. J. Petit and A. Zeghloul, in Environmentally Assisted Cracking: Science and Engineering, ASTM STP 1049, W.B. Lisagor, T.W. Crooker and B.N. Leis, eds., ASTM, Philadelphia, PA, pp. 334-346 (1990).

75. M. Gao, P.S. Pao and R.P. Wei, Metall. Trans. A, Vol. 19A, pp. 1739-1750 (1988).

76. D.J. Duquette, "Mechanisms of Corrosion Fatigue of Aluminum Alloys", AGARD Report No. AGARD-CP-316 (1981).

77. W. Gruhl, Z. Metallknde, Vol. 75, pp. 819-826 (1984).

78. R.J. Walter and W.T. Chandler, "Influence of Gaseous Hydrogen on Metals", Final Report, Contract NAS8-25579, NASA CR-124410 (1973).

79. R.J. Walter and W.T. Chandler, "Effect of High Pressure Hydrogen on IN 718 at -260°F", Rocketdyne Report No. RR-70-3/QNO79953 (1970).

80. R.J. Walter and W.T. Chandler, in Environmental Degradation of Engineering Materials, M.R. Louthan and R.P. McNitt, eds., VPI Press, Blacksburg, VA, pp. 513-522 (1977).

81. N.R. Moody, S.L. Robinson and W.M. Garrison, Jr., "Hydrogen Effects on the Properties and Fracture Modes of Iron-Based Alloys", Res Mechanica, in press (1990).

82. R.G. Forman, "Environmental Crack Growth Behavior of High Strength Pressure Vessel Alloys", NASA TN D-7952 (1975).

83. B. Ladna and H.K. Birnbaum, Acta Metall., Vol. 35, pp. 1775-1778 (1987).

84. J.K. Tien, A.W. Thompson, I.M. Bernstein and R.J. Richards, Metall. Trans. A, Vol. 7A, pp. 821-829 (1976).

85. G.M. Pressouyre and I.M. Bernstein, Metall. Trans. A, Vol. 12A, p. 835 (1981).

86. J.P. Hirth, Metall. Trans. A, Vol. 11A, pp. 861-890 (1980).

87. R.P. Gangloff, in Embrittlement by the Localized Crack Environment, R.P. Gangloff, ed., TMS-AIME, Warrendale, PA, pp. 265-290 (1984).

88. G. Shim, Y. Nakai and R.P. Wei, in Basic Questions in Fatigue, Vol. II, ASTM STP 924, R.P. Wei and R.P. Gangloff, eds., ASTM, Philadelphia, PA, pp. 211-229 (1987).

89. R.P. Wei, in Fatigue 87, R.O. Ritchie and E.A. Starke, Jr., eds., EMAS, West Midlands, UK, pp. 1541-1560 (1987).

90. R.P. Wei, "Corrosion Fatigue Crack Growth and Reactions with Bare Steel Surfaces", Corrosion 89, Paper No. 569, NACE, Houston, TX (1989).

91.   N.J.H. Holroyd and D. Hardie, Corrosion Science, Vol. 23, pp. 527-546 (1983).

92.   I.M. Austin, W.J. Rudd and E.F. Walker, in Proceedings of the International Conference on Steel in Marine Structures, Comptoir des produits Siderurgiques, Paris, Paper ST 5.4 (1981).

93.   I.M. Austin, "Quantitative Assessment of Corrosion Fatigue Crack Growth Under Variable Amplitude Loading", British Steel Company Report BSC FR S132-8/862, Swinden Laboratories, Rotherham, England (1987).

94.   E.A. Steigerwald, F.W. Schuller and A.R. Troiano, Trans. Metall. Soc. AIME, Vol. 218, p. 832 (1960).

95.   R.A. Oriani and P.H. Josephic, Acta Metall., Vol. 22, p. 1065 (1974).

96.   R.A. Oriani and P.H. Josephic, Acta Metall., Vol. 25, p. 979 (1977).

97.   D.H. Sherman, C.V. Owen and T.E. Scott, Trans. AIME, Vol. 242, p. 1775 (1968).

98.   D.G. Westlake, Trans ASM, Vol. 62, p. 1000 (1969).

99.   D. Hardie and P. McIntyre, Metall. Trans. A, Vol. 4A, p. 1247 (1973).

100.   C.D. Beachem, Met. Trans., Vol. 3, p. 437 (1972).

101.   G. Bond, I.M. Robertson and H.K. Birnbaum, Acta Metall., Vol. 36, p. 2193 (1988).

102.   S.P. Lynch, in Atomistics of Fracture, R.M. Latanision and J.R. Pickens, eds., Plenum Press, New York, pp. 955-963 (1983).

103.   H.K. Birnbaum, in Environment Induced Cracking of Metals, R.P. Gangloff and M.B. Ives, eds., NACE, Houston, TX, pp. 21-30 (1990).

104.   G.H. Koch, A.J. Bursle and E.N. Pugh, in Proc. of 2nd Int. Cong. on Hydrogen in Metals, Pergamon, New York, NY (1977).

105.   F.P. Ford, in Embrittlement by the Localized Crack Environment, R.P. Gangloff, ed., TMS-AIME, Warrendale, PA, pp. 117-147 (1984).

106. F.P. Ford and P.L. Andresen, "Corrosion Fatigue of Pressure Boundary Materials", Advances in Fracture Research, M. Salema, K. Ravi-Chandar, D.M.R. Taplin and P. Ramo Rao, eds., Pergamon Press, Oxford, UK, in press (1989).

107. F.P. Ford, Corrosion, Vol. 35, pp. 281-287 (1979).

108. P.L. Andresen, R.P. Gangloff, L.F. Coffin and F.P. Ford, in Fatigue 87, R.O. Ritchie and E.A. Starke, Jr., eds., EMAS, West Midlands, England, pp. 1723-1751 (1987).

109. F.P. Ford, in Environment Induced Cracking of Metals, R.P. Gangloff and M.B. Ives, eds., NACE, Houston, TX, pp. 139-166 (1990).

110. R.H. Van Stone, Matls. Sci. and Engr., Vol. A103, pp. 49-61 (1988).

111. G.K. Haritos, T. Nicholas and G.O. Painter, in Fracture Mechanics, Eighteenth Symposium, ASTM STP 945, D.T. Read and R.P. Reed, eds., ASTM, Philadelphia, PA, pp. 206-220 (1988).

112. P. Woollin and J.F. Knott, in Advances in Fracture Research, K. Salema, K. Ravi-Chandar, D.M.R. Taplin and P. Ramo Rao, eds., Pergamon Press, London, pp. 1859-1868 (1989).

113. R.H. Van Stone, O.C. Gooden and D.D. Krueger, "Advanced Cumulative Damage Modeling", Final Report, AFWAL-TR-88-4146, Wright-Patterson Air Force Base, OH (1988).

114. J.M. Larsen and T. Nicholas, "Cumulative Damage Modeling of Fatigue Crack Growth", AGARD Advisory Group for Aerospace Research and Development, Conference Proceedings No. 368, NATO (1987).

115. M.F. Henry, "Time Dependent Crack Propagation in Gaseous Environments", presented at NACE Research Symposium, Corrosion '90, Las Vegas, NV (1990).

116. S. Floreen and R.H. Kane, Metall. Trans. A, Vol. 10A, pp. 1745-1751 (1979).

117. H.H. Smith and D.J. Michel, Metall. Trans. A, Vol. 17A, pp. 370-374 (1986).

118. T. Weerasooriya, in <u>Fracture Mechanics: Nineteenth Symposium, ASTM STP 969</u>, T.A. Cruse, ed., ASTM, Philadelphia, PA, pp. 907-923 (1988).

119. M.O. Speidel, in <u>Stress Corrosion Cracking and Hydrogen Embrittlement of Iron Based Alloys</u>, J. Hochmann, J. Slater, R.D. McCright and R.W. Staehle, eds., NACE, Houston, TX, pp. 1071-1094 (1977).

120. D.C. Slavik, C.P. Blankenship, Jr., E.A. Starke, Jr. and R.P. Gangloff, "Intrinsic Fatigue Crack Growth Rates for Al-Li-Cu-Mg Alloys in Vacuum", <u>Metall. Trans. A</u>, in review (1992).

121. L. Bertini, "Characterization of Corrosion Fatigue Properties from a Statistical Viewpoint by a Material Data Base", presented at ASTM Conference on Environment Assisted Cracking: Science and Engineering, Bal Harbour, FL, not published (1987).

122. N. Yazdani and P. Albrecht, <u>J. Struct. Engr.</u>, Vol. 113, pp. 483-500 (1987).

123. Rolfe, S.T. and J. M. Barsom, in <u>Fracture and Fatigue Control in Structures</u>, Prentice-Hall, Inc., Englewood Cliffs, NJ, pp. 278-302 (1977).

124. G.S. Booth, J.G. Wylde and T. Iwasaki, in <u>Fatigue 84</u>, C.J. Beevers, ed., EMAS, West Midlands, UK, pp. 1471-1484 (1984).

125. J.K. Shang, J.-L. Tzou and R.O. Ritchie, <u>Metall. Trans. A</u>, Vol. 18A, pp. 1613-1627 (1987).

126. E. Bardal and P.J. Haagensen, "Corrosion Fatigue - Offshore II, Project 1", SINTEF Report No. STF-16 A86156, Foundation for Scientific and Industrial Research, Norwegian Institute of Technology, Trondheim (1986).

127. O. Vosikovsky, <u>J. Test. Eval.</u>, Vol. 6, pp. 175-182 (1978).

128. M. Klesnil and P. Lukas, <u>Matls. Sci. J.</u>, Vol. 9, pp. 131-143 (1972).

129. H.G. Nelson, in <u>Effect of Hydrogen on the Behavior of Materials</u>, A.W. Thompson and I.M. Bernstein, eds., TMS-AIME, Warrendale, PA, pp. 602-611 (1976).

130. F.H. Heubaum, "Propagation Kinetics of Short Fatigue Cracks in Low Alloy Steels", PhD Dissertation, Northwestern University, Evanston, ILL (1986).

131. R.P. Gangloff, in Basic Questions in Fatigue, Vol. II, ASTM STP 924, R.P. Wei and R.P. Gangloff, eds., ASTM, Philadelphia, PA, pp. 230-251 (1988).

132. M.N. James and J.F. Knott, Scripta Met., Vol. 19, pp. 189-194 (1985).

133. J.M. Kendall and J.F. Knott, in Fatigue 84, C.J. Beevers, ed., EMAS, West Midlands, UK, pp. 307-317 (1985).

134. W.G. Clark, Jr., Metals Engr. Quart., pp. 16-28, August (1977).

135. R.S. Piascik, "Mechanisms of Intrinsic Damage Localization During Corrosion Fatigue: Al-Li-Cu System", PhD Dissertation, University of Virginia (1989).

136. R.S. Piascik and R.P. Gangloff, in Advances in Fracture Research, K. Salema, K. Ravi-Chandar, D.M.R. Taplin and P. Ramo Rao, eds., Pergamon Press, London, pp. 907-918 (1989).

137. S.D. Antolovich and J.E. Campbell, in Application of Fracture Mechanics for Selection of Metallic Structural Materials, J.E. Campbell, W.W. Gerberich and J.H. Underwood, eds., ASM International, Metals Park, OH, p. 290 and p. 300 (1982).

138. R.J. Bucci, PhD Dissertation, Lehigh University, Bethlehem, PA (1970).

139. R. W. Hertzberg, in Deformation and Fracture Mechanics of Engineering Materials, Ch. 13, 2nd Ed., John Wiley and Sons, New York, NY (1983).

140. Fundamental Aspects of Stress Corrosion Cracking, R.W. Staehle, A.J. Forty, and D. Van Rooyen, eds., NACE, Houston, TX (1969).

141. The Theory of Stress Corrosion Cracking in Alloys, J.C. Scully, ed., NATO, Brussels (1971).

142. Environment Sensitive Fracture of Engineering Materials, Z.A. Foroulis, ed., TMS-AIME, Warrendale, PA (1979).

143. H.G. Nelson and D.P. Williams in Stress Corrosion Cracking and Hydrogen Embrittlement of Iron Base Alloys, NACE, Houston, TX, pp. 390-404 (1977).

144. G.W. Simmons, P.S. Pao and R.P. Wei, <u>Metall. Trans. A</u>, Vol. 9A, pp. 1147-1158 (1978).

145. R.P. Gangloff, in <u>Corrosion Prevention and Control, Proc. Sagamore Army Materials Research Conference</u>, Vol. 33, M. Levy and S. Isserow, eds., U.S. Army Materials Technology Laboratory, Watertown, MA, pp. 64-111 (1987).

146. M.O. Speidel, <u>Metall. Trans. A</u>, Vol. 6A, pp. 631-651 (1975).

147. N.J.H. Holroyd, in <u>Environment Induced Cracking of Metals</u>, R.P. Gangloff and M.B. Ives, eds., NACE, Houston, TX, pp. 311-346 (1990).

148. G.P. Airey, in <u>Environment-Sensitive Fracture of Engineering Materials</u>, Z.A. Foroulis, ed., TMS-AIME, Warrendale, PA, pp. 205-216 (1979).

149. B.F. Brown, <u>Matl. Res. and Stands.</u>, Vol. 6, p. 129-133 (1966).

150. E.G. Haney and W.R. Wearmouth, <u>Corrosion</u>, Vol. 25, p. 87 (1969).

151. M. Levy and D. Seitz, <u>Corrosion Sci.</u>, Vol. 9, pp. 341-351 (1969).

152. B.F. Brown and C.D. Beachem, <u>Corrosion Sci.</u>, Vol. 5, pp. 745-750 (1965).

153. B.F. Brown, in <u>Stress Corrosion Cracking and Hydrogen Embrittlement of Iron Base Alloys</u>, NACE, Houston, TX, pp. 747-750 (1977).

154. S.R. Novak and S.T. Rolfe, <u>Corrosion</u>, Vol. 26, pp. 121-130 (1970).

155. B.F. Brown, <u>Metall. Rev.</u>, Vol. 129, pp. 171-183 (1965).

156. D.P. Williams, <u>Int. J. of Frac.</u>, Vol. 9, pp. 63-74 (1973).

157. "Standard Test Method for Determining Threshold Stress Intensity Factor for Environment Assisted Cracking of Metallic Materials Under Constant Load", 11th Draft of a Proposed Standard, ASTM Committee E24.04 on Subcritical Crack Growth (1992).

158. R.N. Parkins, in <u>Environment Induced Cracking of Metals</u>, R.P. Gangloff and M.B. Ives, eds., NACE, Houston, TX, pp. 1-20 (1990).

159. E.N. Pugh in <u>Stress Corrosion Cracking and Hydrogen Embrittlement of Iron Base Alloys</u>, NACE, Houston, TX, pp. 37-51 (1977).

160. E.N. Pugh in <u>The Theory of Stress Corrosion Cracking in Alloys</u>, J.C. Scully, ed., NATO, Brussels, pp. 418-441 (1971).

161. R.W. Staehle, in <u>Stress Corrosion Cracking and Hydrogen Embrittlement of Iron-Based Alloys</u>, NACE, Houston, p. 180 (1977).

162. R.W. Staehle, in <u>The Theory of Stress Corrosion Cracking in Alloys</u>, J.C. Scully, ed., NATO, Brussels, p. 223 (1971).

163. J.C. Scully in <u>Environment-Sensitive Fracture of Engineering Materials</u>, Z.A. Foroulis, ed., TMS-AIME, Warrendale, PA, pp. 71-90 (1979).

164. N.J. Petch, <u>Phil. Mag.</u>, Vol. 1, p. 331 (1956).

165. H.H. Uhlig, <u>J. Res. NBS.</u>, Vol. 48, p. 1 (1952).

166. A.W. Thompson and I.M. Bernstein in <u>Advances in Corrosion Science and Technology</u>, Vol. 7, R.W. Staehle and M.G. Fontana, eds., Plenum Press, New York, NY, p. 53 (1980).

167. W.W. Gerberich and S. Chen, in <u>Environment Induced Cracking of Metals</u>, R.P. Gangloff and M.B. Ives, eds., NACE, Houston, TX, pp. 167-188 (1990).

168. R.A. Oriani, <u>Ann. Rev. Matl. Sci.</u>, Vol. 8, pp. 327-357 (1978).

169. R.A. Oriani, in <u>Environment Induced Cracking of Metals</u>, R.P. Gangloff and M.B. Ives, eds., NACE, Houston, TX, pp. 439-448 (1990).

170. K.N. Akhurst and T.J. Baker, <u>Metall. Trans. A.</u>, Vol. 12A, pp. 1059-1070 (1981).

171. A.J. McEvily and R.P.Wei, in <u>Corrosion Fatigue: Chemistry, Mechanics and Microstructure</u>, O. Devereux, A.J. McEvily and R.W. Staehle, eds., NACE, Houston, TX, pp. 381-395 (1972).

172. R.P. Wei, M. Gao and P.S. Pao, <u>Scripta Metall.</u>, Vol. 18, pp. 1195-1198 (1984).

173. M.O. Speidel, M.J. Blackburn, T.R. Beck and J.A. Feeney, in Corrosion Fatigue, Chemistry, Mechanics and Microstructure, O. Devereux, A.J. McEvily and R.W. Staehle, eds., NACE, Houston, TX, pp. 324-345 (1972).

174. R.O. Ritchie, M.H. Catro Cedeno, V.F. Zackay and E.R. Parker, Metall. Trans. A, Vol. 9A, pp. 35-40 (1978).

175. W.W. Gerberich, R.H. Van Stone and A.W. Gunderson in Application of Fracture Mechanics for Selection of Metallic Structural Materials, J.E. Campbell, W.W. Gerberich and J.H. Underwood, eds., ASM International, Metals Park, OH, pp. 41-103 (1982).

176. R.P. Gangloff and A. Turnbull, in Modeling Environmental Effects on Crack Initiation and Propagation, R.H. Jones and W.W. Gerberich, eds., TMS-AIME, Warrendale, Pa., pp. 55-81 (1986).

177. R.P. Gangloff, "Critical Assessment of Hydrogen Embrittlement in Pressure Vessel Steels: An Executive Summary", Report to Southwest Research Institute and the American Petroleum Institute, June (1991). (Compiled in SWRI Interim Report on Project No. 06-3966, "Fitness-for-Service Requirements for Thick-Walled Petroleum Processing Vessels, S.J. Hudak, Jr., ed., June (1991).)

178. V.J. Colangelo and M.S. Ferguson, Corrosion, Vol. 25, pp. 509-514 (1969).

179. D.P. Williams and H.G. Nelson, Met. Trans., Vol. 1, pp. 63-68 (1970).

180. R.P. Gangloff and R.P. Wei, Metall. Trans. A, Vol. 8A, pp. 1043-1053 (1977).

181. M.O. Speidel and M.V. Hyatt in Advances in Corrosion Science and Technology, Vol. 2, Plenum Press, New York (1972).

182. R.J. Walter and W.T. Chandler in Environment-Sensitive Fracture of Engineering Materials, Z.A. Foroulis, ed., TMS-AIME, Warrendale, PA, pp. 513-522 (1979).

183. N.R. Moody, S.L. Robinson and W.M. Garrison, Jr., "Hydrogen Effects on the Properties and Fracture Modes of Iron-Based Alloys", Sandia National Lab. Report, SAND88-8860, Livermore, CA (1989).

184. P.D. Hicks and C.J. Altstetter in Hydrogen Effects on Material Behavior, N.R. Moody and A.W. Thompson, eds., TMS, Warrendale, PA, p. 613-623 (1990).

185. M.L. Heil, T. Nicholas, and G.K. Haritos, in Thermal Stress, Material Deformation and Thermomechanical Fatigue, PVP Vol. 123, H. Sehitoglu and S.Y. Zamrik, eds., ASME, New York, NY pp. 23-29 (1987).

186. M.L. Heil, "Crack Growth in Alloy 718 Under Thermal-Mechanical Cycling", Ph.D. Dissertation, Air Force Institute of Technology, Wright-Patterson AFB, OH, (1986).

187. J.A. Feeney and M.J. Blackburn in The Theory of Stress Corrosion Cracking in Alloys, J.C. Scully, ed., NATO, Brussels, pp. 355-398 (1971).

188. W.F. Czyrklis in Environment-Sensitive Fracture of Engineering Materials, Z.A. Foroulis, ed., TMS-AIME, Warrendale, PA, pp. 303-313 (1979).

189. M.J. Blackburn, J.A. Feeney, and T.R. Beck, Boeing Scientific Research Laboratories Document, D1-82-105x, Seattle, WA (1970).

190. Seawater Corrosion Handbook, M. Schumacher, ed., Noyes Data Corporation, Park Ridge, NJ (1979).

191. D. Hardie, in Environment Induced Cracking of Metals, R.P. Gangloff and M.B. Ives, eds., NACE, Houston, TX, pp. 347-364 (1990).

192. Metallurgical Aspects of Environmental Failures, C.L. Briant, Elsevier, Amsterdam, Netherlands (1985).

193. R.P. Gangloff, Res. Mech. Let., Vol. 1, pp. 299-306 (1981).

194. R.P. Gangloff, Metall. Trans. A., Vol. 16A., pp. 953-969 (1985).

195. H.H. Johnson, in Stress Corrosion Cracking and Hydrogen Embrittlement of Iron Based Alloys, J. Hochmann, J. Slater, R.D. McCright and R.W. Staehle, eds., NACE, Houston, TX, pp. 382-389 (1977).

196. R. Brazill, G.W. Simmons and R.P. Wei, J. Engr. Matls. Tech., Trans. ASME, Vol. 101, pp. 199-204 (1979).

211

197. H.J. Cialone and J.H. Holbrook, Metall. Trans. A., Vol. 16A., pp. 115-122 (1985).

198. R. Krishnamurthy, C.N. Marzinsky and R.P. Gangloff, in Effects of Hydrogen on Material Behavior, N.R. Moody and A.W. Thompson, eds., TMS-AIME, Warrendale, PA, pp. 807-825 (1990).

199. I.M. Austen and E.F. Walker, in Fatigue 84, C.J. Beevers, ed., EMAS, West Midlands, England, pp. 1457-1469 (1984).

200. E. Bardal, in Fatigue Handbook, A.A. Naess, ed., Tapir, pp. 291-312 (1985).

201. E Bardal, P.J. Haagensen, M. Grovlen and F. Saether, in Fatigue, '84, C.J. Beevers, ed., EMAS, West Midlands, UK, pp. 1541-1551 (1984).

202. T.W. Thorpe, P.M. Scott, A. Rance and D. Silvester, Intl. J. Fatigue, Vol. 5., pp. 123-133 (1983).

203. M.J. Cowling and R.J. Appleton, in Proceedings Institute of Mechanical Engineers Conference on Fatigue and Crack Growth in Offshore Structures, Inst. Mech. Engr., London, pp. 77-92 (1986).

204. L. Bertini, in Managing Engineering Data: The Competitive Edge, ASME, New York, N.Y., pp. 113-119 (1987).

205. R.P. Gangloff and R.O. Ritchie, in Fundamentals of Deformation and Fracture, B.A. Bilby, K.J. Miller and J.R. Willis, eds., Cambridge University Press, Cambridge, UK, pp. 529-558 (1985).

206. S. Suresh and R.O. Ritchie, Metall. Trans. A., Vol. 13A, pp. 1627-1631 (1982).

207. C.E. Jaske, J. H. Payer and V.S. Balint, in Corrosion Fatigue of Metals in Marine Environments, Metals and Ceramics Information Center, MCIC-81-42 (1981).

208. K. Jata and E.A. Starke, Jr., Metall. Trans. A., Vol. 17A, pp. 1011-1026 (1986).

209. R.S. Piascik and R.P. Gangloff, in Environment Induced Cracking of Metals, R.P. Gangloff and M.B. Ives, eds., NACE, Houston, TX, pp. 233-239 (1990).

210. D. Aliaga and E. Budillon, "Corrosion Fatigue Behavior of Some Aluminum Alloys", AGARD Report No. AGARD-CP-316 (1981).

211. R.J. Selines and R.M. Pelloux, Met. Trans., Vol. 3, pp. 2525-2531 (1972).

212. R.P. Wei, P.S. Pao, R.G. Hart, T.W. Weir and G.W. Simmons, Metall. Trans. A, Vol. 11A, pp. 151-158 (1980).

213. P.S. Pao, M.A. Imam, L.A. Cooley and G.R. Yoder, Corrosion, Vol. 45, pp. 530-535 (1989).

214. N. Ranganathan, M. Quintard and J. Petit, in Environmentally Assisted Cracking: Science and Engineering, ASTM STP 1049, W.B. Lisagor, T.W. Crooker and B.N. Leis, eds., ASTM, Philadelphia, PA, pp. 374-391 (1990).

215. D.A. Meyn, Met. Trans., Vol. 2, pp. 853-865 (1971).

216. A. Niegel, H.-J. Gudladt and V. Gerold, in Fatigue 87, R.O. Ritchie and E.A. Starke, Jr., eds., EMAS, West Midlands, UK, pp. 1229-1238 (1987).

217. R.J.H. Wanhill and L. Schra, "Corrosion Fatigue Crack Arrest in Aluminum Alloys", NLR-TR-87128-U, National Aerospace Laboratory, The Netherlands (1987).

218. R.J. Walter, J.D. Frandsen and R.P. Jewett, in Hydrogen Effects in Metals, I.M. Bernstein and A.W. Thompson, eds., TMS-AIME, Warrendale, PA, pp. 819-827 (1981).

219. J.L. Dudelin, B. Journet, M. Kornmann, D. Paugam and L. Perret, in Ni/H_2 Battery Cells", Proc. Conf. Space Craft Structures and Mechanical Testing, Nourdwijk, Netherlands, pp. 749-753 (1991).

220. L.G. Fritzemeir and W.T. Chandler, "Hydrogen Embrittlement-Rocket Engine Applications", Rocketdyne Report No. CCC01079, Canoga Park, CA (1986).

221. G.A. Vroman, R.P. Jewett, D.E. Peterson and A. Nathan, "Fracture Properties for SSME Life Prediction", Rocketdyne Report No. RSS-8637/CCC01079, Canoga Park, CA (1980).

222. R.J. Walter, R.P. Jewett and J.D. Frandsen, "Da/dN Test Results for Conventionally Cast MAR-M-246 Exposed to 6000 psi Hydrogen at 1000°F", Rocketdyne Report No. R76-161/CCC01079, Canoga Park, CA (1976).

223. D. Peterson and G.A. Vroman, "The Interaction Between Hydrogen Pressure and Crack Growth Rate in IN 718", Rocketdyne Report No. R-9408/CCC01079, Canoga Park, CA (1975).

224. W.T. Chandler, "Crack Growth in ASME AS-105 Steel in Hydrogen at Ambient Temperature", Rocketdyne Report No. RSS-8601/CCC01079, Canoga Park, CA (1975).

225. G.A. Vroman, "Fracture Mechanics Analysis of a High-Pressure Hydrogen Facility Compressor", Rocketdyne Report No. RSS-8597/CCC01079, Canoga Park, CA (1974).

226. Advances in Crack Length Measurement, C.J. Beevers, ed., EMAS, West Midlands, UK (1982).

227. O. Vosikovsky, Trans. ASME, J. Engr. Matls. Tech., Vol. 97, pp. 298-304 (1975).

228. E. Bardal, T. Berge, M. Grovlen, P.J. Haagensen and B.M. Forre, in Advances in Crack Length Measurement, C.J. Beevers, ed., EMAS, West Midlands, UK, pp. 139-158 (1982).

229. R.P. Wei and J.D. Landes, Matls. Res. Stds., Vol. 9, pp. 25-28 (1969).

230. O. Vosikovsky, J. Test. Eval., Vol. 8, pp. 68-73 (1980).

231. H.L. Ewalds, J. Test. Eval., Vol. 9, pp. 158-161 (1981).

232. W.D. Dover and S. Dharmavasan, in Fatigue 84, C.J. Beevers, ed., EMAS, West Midlands, England, pp. 1417-1434 (1984).

233. K.T. Venkateswara Rao and R.O. Ritchie, Acta Metall., Vol. 36, No. 10, pp. 2849-2862, 1988.

234. K.T. Venkateswara Rao and R.O. Ritchie, Intl. Matls. Rev., Vol. 37, pp. 153-185 (1992).

235. I.M. Austin and E.F. Walker, in <u>Steel in Marine Structures</u>, Elsevier, Amsterdam, pp. 859-870 (1987).

236. O. Orjasaeter and A. Dragen, in <u>Fatigue 84</u>, C.J. Beevers, ed., EMAS, West Midlands, UK, pp. 1553-1564 (1984).

237. J.M. Barsom and S.R. Novak, "Subcritical Crack Growth and Fracture of Bridge Steels", National Cooperative Highway Research Program Report 181, National Research Council, Washington, DC (1977).

238. M.O. Speidel, Unpublished research (1975), reported in: J.C. Scully, in <u>Environment Sensitive Fracture of Engineering Materials</u>, Z.A. Foroulis, ed., TMS-AIME, Warrendale, PA, pp. 71-90 (1979).

239. R.P. Gangloff, "The Environmental Effect on Fatigue Crack Propagation", Report No. CR. 13BV.85, Exxon Research and Engineering Company, Annandale, N.J. (1985).

240. J.P. Gallagher, "Corrosion Fatigue Crack Growth Behavior Above and Below K_{ISCC}", Report No. NRL-7064, AD708377, Naval Research Laboratory, Washington, DC (1970).

241. R.P. Gangloff and R.P. Wei, in <u>Small Fatigue Cracks</u>, R.O. Ritchie and J. Lankford, eds., TMS-AIME, Warrendale, PA, pp. 239-264 (1986).

242. B.R.W. Hinton and R.P.M. Procter, in <u>Hydrogen Effects in Metals</u>, I.M. Bernstein and A.W. Thompson, eds., TMS-AIME, Warrendale, PA, pp. 1005-1015 (1981).

243. D.L. Dicus, in <u>Environment Sensitive Fracture: Evaluation and Comparison of Test Methods, ASTM STP 821</u>, S.W. Dean, E.N. Pugh and G.M. Ugiansky, eds., ASTM, Philadelphia, PA, pp. 513-533 (1984).

244. S. Chiou and R.P. Wei, "Corrosion Fatigue Cracking Response of Beta-Annealed Ti-6Al-4V in 3.5% NaCl Solution", Report No. NADC-83126-60, U.S. Naval Air Development Center, Warminster, PA (1984).

245. F.P. Ford, D.F. Taylor, P.L. Andresen and R.G. Ballinger, "Environmentally Controlled Cracking of Stainless and Low-Alloy Steels in Light Water Reactor Environments", EPRI Report No. NP-5064M, EPRI, Palo Alto, CA (1987).

246. B.F. Jones, in Embrittlement by the Localized Crack Environment, R.P. Gangloff, ed., TMS-AIME, Warrendale, PA, pp. 453-469 (1984).

247. F.J. Bradshaw and C. Wheeler, Intl. J. Frac. Mech., Vol. 5, pp. 255-268 (1969).

248. R. Nakai, A. Alavi and R.P. Wei, Metall. Trans. A., Vol. 19A, pp. 543-548 (1988).

249. J.D. Frandsen and H.L. Marcus, Metall. Trans. A, Vol. 8A, pp. 265-272 (1977).

250. O. Vosikovsky, W.R. Neill, D.A. Carlyle and A. Rivard, Canadian Metall. Quart., Vol. 26, pp. 251-257 (1987).

251. R.O. Ritchie, Intl. Metall. Rev., Vol. 20, pp. 205-230 (1979).

252. H.F. Wachob and H.G. Nelson, in Hydrogen in Metals, I.M. Bernstein and A.W. Thompson, eds., TMS-AIME, Warrendale, PA, pp. 703-711 (1980).

253. F.S. Lin and E.A. Starke, Jr., in Hydrogen Effects in Metals, I.M. Bernstein and A.W. Thompson, eds., TMS-AIME, Warrendale, PA, pp. 485-492 (1981).

254. S.J. Hudak, O.H. Burnside and K.S. Chan, J. Energy Resources Tech., ASME Trans., Vol. 107., pp. 212-219 (1985).

255. P.L Andresen and F.P. Ford, Matls. Sci. Engr., Vol. A103, pp. 167-184 (1988).

256. O. Vosikovsky and R.J. Cooke, Intl. J. Pres. Ves. & Piping, Vol. 6, pp. 113-129 (1978).

257. J.P. Gallagher and R.P. Wei, in Corrosion Fatigue, Chemistry, Mechanics and Microstructure, O. Devereux, A.J. McEvily and R.W. Staehle, eds., NACE, Houston, TX, pp. 409-423 (1972).

258. M.O. Speidel, in High Temperature Materials in Gas Turbines, P.R. Sahm and M.O. Speidel, eds., Elsevier, Amsterdam, Netherlands, pp. 207-251 (1974).

259. T. Nicholas, T. Weerasooriya and N.E. Ashbaugh, in Fracture Mechanics, ASTM STP 905, J.H. Underwood, et al., eds., ASTM, Philadelphia, PA, pp. 167-180 (1986).

260. T. Nicholas and T. Weerasooriya, in Fracture Mechanics, ASTM STP 905, J.H. Underwood, et al., eds., ASTM, Philadelphia, PA, pp. 155-168 (1986).

261. D.A. Utah, Air Force Wright Aeronautical Laboratories Report AFWAL-TR-80-4098, Accession No. ADA093992 (1980).

262. T. Nicholas, G.T. Haritos and J.R. Christoff, AIAA Jour. Propulsion and Power, Vol. 1, pp. 131-136 (1985).

263. R.P. Wei and M. Gao, Scripta Met., Vol. 17, pp. 959-962 (1983).

264. I.M. Austin and E.F. Walker, in Proc. Intl. Conf. Influence of Environment on Fatigue, I. Mech. Engr., London, UK, pp. 1-16 (1977).

265. True-Hwa Shih and R.P. Wei, Engr. Frac. Mech., Vol. 18, pp. 827-837 (1983).

266. P.S. Pao, Ming Gao and R.P. Wei, in Basic Questions in Fatigue, ASTM STP 924, Vol. 2, R.P. Wei and R.P. Gangloff, eds., ASTM, Philadelphia, PA, pp. 182-195 (1988).

267. S. Suresh and R.O. Ritchie, in Fatigue Crack Growth Threshold Concepts, D. Davidson and S. Suresh, eds., TMS-AIME, Warrendale, PA, pp. 227-261 (1984).

268. W. Elber, in Damage Tolerance in Aircraft Structures, ASTM STP 486, ASTM, Philadelphia, PA, pp. 230-243 (1971).

269. S. Suresh, G.F. Zaminski and R.O. Ritchie, Metall. Trans. A., Vol. 12A, pp. 1435-1443 (1981).

270. S. Suresh and R.O. Ritchie, Scripta Metall., Vol. 17, pp. 575-580 (1983).

271. J.-L. Tzou, C.H. Hsueh, A.G. Evans and R.O. Ritchie, Acta Metall., Vol. 33, pp. 117-127 (1985).

272. K. Komai, in Current Research on Fatigue Cracks, T. Tanaka, M. Jono and K. Komai, eds., Japan Society of Materials Science, Kyoto, Japan, pp. 235-253 (1985).

273. S.S. Rajpathak and W.H. Hartt, in <u>Environmentally Assisted Cracking: Science and Engineering, ASTM STP</u>, W.B. Lisagor, T.W. Crooker and B.N. Leis, eds., ASTM, Philadelphia, PA, pp. 425-446 (1990).

274. R.O. Ritchie, S. Suresh and P.K. Liaw, in <u>Ultrasonic Fatigue</u>, J.M. Wells, O. Buck, L.K. Roth and J.K. Tien, eds., TMS-AIME, Warrendale, PA, pp. 443-460 (1982).

275. S. Suresh and R.O. Ritchie, <u>Metal Science</u>, Vol. 16, pp. 529-538 (1982).

276. R.O. Ritchie, S. Suresh and C.M. Moss, <u>J. Engr. Matls. Tech., Trans. ASME</u>, Vol. 102, pp. 293-299 (1980).

277. J.A. Todd, P. Li, G. Liu and V. Raman, in <u>Environmental Degradation of Engineering Materials</u>, M.R. Louthan, R.P. McNitt and R.D. Sisson, Jr., eds., Pennsylvania State University, University Park, PA, pp. 533-541 (1987).

278. K.T. Venkateswara Rao, R.S. Piascik, R.P. Gangloff and R.O. Ritchie, in <u>Proc. Fifth Intl. Al-Li Conf.</u>, T.H. Sanders, Jr. and E.A. Starke, Jr., eds., Materials and Component Engineering Publications Ltd., Birmingham, UK, pp. 955-971 (1989).

279. W.A. Herman, R.W. Hertzberg and R. Jaccard, <u>J. Fat. and Frac. of Engr. Matls. and Struc.</u>, Vol. 11, pp. 303-320 (1988).

280. H. Pearson, <u>Engr. Frac. Mech.</u>, Vol. 7, pp. 235-244 (1975).

281. S. Suresh and R.O. Ritchie, <u>Int. Metall. Rev.</u>, Vol. 29, pp. 445-476 (1984).

282. R.O. Ritchie and J. Lankford, <u>Matls. Sci. Engr.</u>, Vol. 84, pp. 11-16 (1986).

283. S.J. Hudak, <u>J. Engr. Matls. Tech.</u>, Vol. 103, pp. 26-35 (1981).

284. A. Zeghloul and J. Petit, in <u>Small Fatigue Cracks</u>, R.O. Ritchie and J. Lankford, eds., TMS-AIME, Warrendale, PA, pp. 225-235 (1986).

285. S.J. Hudak, "Corrosion Fatigue Crack Growth: The Role of Crack-Tip Deformation and Film Formation Kinetics", PhD Dissertation, Lehigh University, Bethlehem, PA (1988).

286. S.J. Hudak, D.L. Davidson and R.A. Page, in <u>Embrittlement by the Localized Crack Environment</u>, R.P. Gangloff, ed., TMS-AIME, Warrendale, PA, pp. 173-198 (1984).

287. W. Dietzel, et al., "Recommendations for Stress Corrosion Testing Using Precracked Specimens", Document EISI P4-92D, First Draft, Committee 10, European Structural Integrity Society, April (1992).

288. W. Dietzel, K.H. Schwalbe and D. Wu, <u>Fatigue and Fracture of Engineering Materials and Structures</u>, Vol. 12, pp. 495-510 (1989).

289. R.A. Mayville, T.J. Warren and P.D. Hilton, in <u>Fracture Mechanics: Perspectives and Directions, ASTM STP 1020</u>, R.P. Wei and R.P. Gangloff, eds., ASTM, Philadelphia, PA, pp. 605-614 (1989).

290. L.M. Hartman and R.P. Gangloff, "Hydrogen Environment Embrittlement of Beta Titanium Alloys", in <u>Seventh World Conference on Titanium</u>, F.H. Froes, ed., TMS-AIME, Warrendale, PA, in press (1992).

291. D.M. Harman, C.R. Saff and J.G. Burns, "Development of an Elevated Temperature Crack Growth Routine", American Institute of Aeronautics and Astronautics, Inc. (1988).

292. C.R. Saff et al., "Damage Tolerance Analysis for Manned Hypervelocity Vehicles", First through Fifth Interim Technical Reports, Contract No. F33615-86-^C-3208, continued McDonnell Aircraft Company, St. Louis, MO, 1986 through 1988.

293. H.D. Dill and C.R. Saff, "Environment-Load Interaction Effects on Crack Growth", Final Report AFFDL-TR-78-137, McDonnell Douglas Corporation, St. Louis, MO (1978).

294. C.R. Saff, "Environment-Load Interaction Effects on Crack Growth in Landing Gear Steels", Report to VSN Naval Air Development Center, McDonnell Douglas Corporation, St. Louis, MO, December (1980).

295. C.R. Saff and M.S. Rosenfeld, in <u>Design of Fatigue and Fracture Resistant Structures, ASTM STP 761</u>, ASTM, Philadelphia, PA, pp. 242-266 (1980).

296. H.D. Dill, C.R. Saff, M.E. Artley, "Environment-Load Interaction Effects on Crack Growth-Correlation of Center Crack and Surface Flaw Results", presented at ASCE Convention and Exposition, Chicago, ILL, October (1978).

REPORT DOCUMENTATION PAGE

1. AGENCY USE ONLY (Leave blank)	2. REPORT DATE September 1993	3. REPORT TYPE AND DATES COVERED Contractor Report

4. TITLE AND SUBTITLE

Environment Enhanced Fatigue Crack Propagation in Metals: Input to Fracture Mechanics Life Prediction Models

5. FUNDING NUMBERS

NAG1-745
WU 510-02-12-10

6. AUTHOR(S)

Richard P. Gangloff and Sang-Shik Kim

7. PERFORMING ORGANIZATION NAME(S) AND ADDRESS(ES)

University of Virginia
School of Engineering and Applied Science
Charlottesville, VA 22903

8. PERFORMING ORGANIZATION REPORT NUMBER

9. SPONSORING/MONITORING AGENCY NAME(S) AND ADDRESS(ES)

National Aeronautics and Space Administration
Langley Research Center
Hampton, VA 23681-0001

10. SPONSORING/MONITORING AGENCY REPORT NUMBER

NASA CR-191538

11. SUPPLEMENTARY NOTES

Langley Technical Monitor: Robert S. Piascik
Final Report

12a. DISTRIBUTION/AVAILABILITY STATEMENT

Unclassified - Unlimited

Subject Category 24

12b. DISTRIBUTION CODE

13. ABSTRACT (Maximum 200 words)

This report is a critical review of both environment-enhanced fatigue crack propagation data and the predictive capabilities of crack growth rate models. This information provides the necessary foundation for incorporating environmental effects in NASA FLAGRO and will better enable predictions of aerospace component fatigue lives. The review presents extensive literature data on "stress corrosion cracking and corrosion fatigue." The linear elastic fracture mechanics approach, based on stress intensity range (ΔK) similitude with microscopic crack propagation threshold and growth rates provides a basis for these data. Results are presented showing enhanced growth rates for gases (viz., H_2 and H_2O) and electrolytes (e.g. NaCl and H_2O) in aerospace alloys including: C-Mn and heat treated alloy steels, aluminum alloys, nickel-based superalloys, and titanium alloys. Environment causes purely time-dependent accelerated fatigue crack growth above the monotonic load cracking threshold (K_{IEAC}) and promotes cycle-time dependent cracking below (K_{IEAC}). These phenomenon are discussed in terms of hydrogen embrittlement, dissolution, and film rupture crack tip damage mechanisms.

14. SUBJECT TERMS

Fatigue crack growth; Environment; FLAGRO; Corrosion fatigue; Time-dependent cracking; Aluminum; Titanium; Steels

15. NUMBER OF PAGES

228

16. PRICE CODE

A11

17. SECURITY CLASSIFICATION OF REPORT Unclassified	18. SECURITY CLASSIFICATION OF THIS PAGE Unclassified	19. SECURITY CLASSIFICATION OF ABSTRACT	20. LIMITATION OF ABSTRACT